Microstructural Evolution and Arrest in a Silver Nanoparticle Based Die Attach Material for Extreme Environments

Paknejad, Seyed Amir

Awarding institution:
King's College London

Microstructural Evolution and Arrest in a Silver Nanoparticle Based Die Attach Material for Extreme Environments

by

Seyed Amir Paknejad

Thesis Submitted to the Physics Department of King's College London for Fulfilment of the Requirements for the degree of PhD in Physics

December 2017

بسم الله الرحمن الرحيم

Abstract: Utilisation of silver nanoparticle paste as high temperature die attach has been investigated. The examinations of high temperature behaviour of sintered silver have indicated massive grain growth and microstructural evolution at 250 °C. The rate of evolution of the microstructure has been found to increase substantially above 350 °C. This high temperature behaviour can undermine the reliability of sintered silver nanoparticles at high operating temperatures if no modifications are applied to the pure form of this material. In addition to the microstructural evolution of the silver in isolation, silver atoms inside the die attach undergo massive migration towards any gold interfaces contacting the die attach. This behaviour can result in reduction of the mechanical performance of the die attach and undermine the thermal reliability as well. Here two new techniques are introduced addressing these two concerns, both of which produce joint structures with improved thermal stabilities. In one technique oxidation of sintered silver's internal surfaces has been able to stop microstructural evolution of sintered silver up to 400 °C, increasing the thermal stability of sintered silver from 200 °C to this new limit. The other technique has combined sintered silver with a gold mesh interposer to use the mass migration of silver and gold atoms to obtain extreme thermal stability. The samples produced with this technique could withstand testing at 600 °C. Furthermore, a review of literature on this field has uncovered the result that while applying sintering pressure on the die results in improved mechanical strength, without this pressure the higher porosity allows better thermal cycling resistance of sintered silver. This indicates another important advantage of the second thermal stabilization technique, namely that using a mesh interposer allows control over the amount of porosity, helping to achieve the desired properties.

Acknowledgements

I would like to thank my wife and parents for their support during my studies and encouraging me to follow my interests. Words cannot express how grateful I am to my parents for their financial support during my studies. I would like to thank my brother as well for his moral support and advices whenever I needed them.

I would like to express my gratitude and appreciation to my first supervisor Professor Samjid H. Mannan for his unreserved support and aid throughout my research and studies. He has been most supportive and encouraging of me and his guidance and assistance has been most invaluable. In addition, I would like to extend my appreciation for Dr Chris Lorenz, my second supervisor, for his help.

I am also grateful to my colleagues and friends Ali Mansourian, Khalid Khtatba, and Yohan Noh for their help and collaboration on my project, especially Ali Mansourian for bringing up interesting ideas helping to speed up the progress in my project.

Special thanks to Julian Greenberg and Julia Kilpatrick for their help and support during my project as well.

I would like to thank everybody else who helped me during my PhD but are not mentioned here.

Table of Contents

1 Introduction

To improve the efficiency of aeroplanes and vehicles there is a need for a suitable and reliable high temperature die attach material. Such material can enable electronics comprising wide-bandgap semiconductors and high temperature tolerant passive components to control actuators and sensors needed to improve efficiency and reduce pollution. Not only might aerospace and automotive industries benefit from such die attach material, but also oil and gas industry can benefit by extraction of oil from deeper oil wells [1]. While a high temperature die attach normally refers to the material utilised for mechanical attachment of electronic chips to electronic boards operating beyond 125 °C, the current targeted temperature range for future applications is 300 °C and more [2], which is also the temperature range targeted in this project.

The main aim of this project is to investigate the suitability of a promising high temperature die attach material and understand the underlying physical mechanism of its high temperature behaviour to recommend potential routes and techniques towards utilisation of that potential solution. The particular material technology selected is based on sintering of silver nanoparticles. In this chapter firstly a brief overview will be provided on the necessity of performing these investigations. Then, all the currently available technologies will be investigated along with their shortcomings. Following the review of currently available solutions, there will be an introduction to the material selected in this project. Next, the author will state the aim and objectives of the project and the areas that have been targeted. Finally, the contributions of the author will be outlined.

Chapter 2 will describe the background information on the particular implementation of the technology selected for this project. In Chapter 3, the thermal behaviour and reliability of that solution is investigated. Next, in Chapter 4, a novel technique for stabilisation of the solution's microstructural changes to increase its reliability is proposed. In Chapter 5 the behaviour of the solution when utilised on two common substrates will be studied. Chapter 6 will illustrate a new technique for production of a high temperature die attach material, showing very promising extreme thermal stability. In Chapter 7, the key points will be summarized and some recommendations for future work will be introduced.

1.1 Background on the need for development of a suitable die attach material for high temperature applications

High temperature die attach materials generally fall into two main categories. The first category corresponds to the die attach that is used for high temperature environments. Applications for this category are normally sensors and electronics for oil and gas extraction, monitoring aerospace or automotive engines, and space exploration [1]. The second category is related to applications, in which the high temperature is generated by the electronics, most important example being power electronics. One important requirement of the die attach of the latter category is heat dissipation from the electronic chip into the substrate. Therefore, the thermal conductivity of the die attach would be a crucial aspect for consideration. However, for the former category the thermal conductivity would not be of particular importance. On the other hand, the mechanical properties of the joint would be of much more significance, especially as most of the applications, such as oil/gas extraction involving oil/gas well drilling and engine monitoring for aeroplanes and automotive, would require higher vibrational endurances. There are also many shared properties required to be in possession of die attach for both categories. Some important examples of these common properties are thermal stability, thermal cycle resistant, and suitable flexibility to prevent die fracture as a result of difference in coefficient of thermal expansions of the die and the substrate.

The category of die attach materials targeted in this research is based on applications subjected to high temperatures from their environments. Therefore, the main requirements of the suitable die attach for this research would then be mechanical reliability, thermal stability, resistance to thermal cycles, and flexibility. The thermal stability and flexibility requirements are implicit in the requirements to resist thermal cycles as well. Therefore, the thermal stability, flexibility, and mechanical reliability aspects will be under further considerations in this project. Some of these requirements are more significant in some applications, as it will become clearer in later sections.

For applications such as aerospace and automotive, especially hybrid and electric vehicles, the need for a suitable die attach comes from the fact that the electronic equipment, especially the sensors, should get as close as possible to the engine to increase their accuracy, and therefore, improving the efficiency of the engine [3], while this can reach up to 300 °C in case of automotive [4] and even higher for aerospace industry. In addition to improved

efficiency as a result of improved accuracy of electronics, reducing the distance to the engine would reduce the cabling of the electronic connections and increase the engine efficiency by reducing the weight of the aeroplane [3]. For these two applications the resistance to thermal cycles is of more importance, as a result of engine on and off cycles, while long operating times are also important, which can be sometimes as long as 10 to 30 years [1].

In addition, as the Si technology is approaching the theoretical limit of its capabilities and the maximum operational temperature for Si is 150 °C [5] with break-down temperature of beyond 350 °C [6], wide-bandgap semiconductors have been considered for future electronic, especially for high temperature applications. This is due to the fact that the wide-bandgap semiconductors, such as silicon carbide (SiC), gallium nitride (GaN), and Diamond, can operate at extreme operating temperatures. For instance, the predictions of silicon carbide (SiC) semiconductors from their intrinsic carrier concentrations indicated potential operating temperature of even more than 800 °C [7], while more than 500 °C has been experimentally confirmed [7]. In addition to their capability of operating at extreme temperatures, they can operate with higher frequencies, for example, in case of diamond semiconductors it can be possibly 81,000 times of Si semiconductors [5], and also SiC can have high energy efficiency [8]. As a result of these potentials, the market value of these wide-bandgap semiconductors is estimated to reach about $1 billion by 2020 for only SiC and GaNi [9]. However, to achieve this potential and easily present these semiconductors into the high temperature electronics market, there is a need for a suitable die attach material to handle the high operating temperatures.

Other driving forces for this research are the EU regulations to remove the lead (Pb) contents from the electronic equipment [10], but lead based solders are normally used for applications of only up to maximum 250 °C [11], which is below the aim of this research. However, the solution investigated in this research may also be used for lower temperatures to potentially fulfil the need for lead-free electronic equipment.

In addition to the requirements on the capabilities of the die attach itself, the processing steps are also very important. For example, to ease the processing of the materials, the processing temperature should not be higher than the maximum operating temperature. This becomes more significant for the operating temperatures targeted for this research. If the processing temperature is higher than the operating temperature, similar to the case of solders, the processing temperature would have to be extremely high. This would complicate

manufacturing and potentially damage other electronics on the circuit. Another important processing criterion would be pressure-less processing, as the pressure on the die during the processing steps may cause cracks on it, while it will also make the manufacturing processes more difficult.

1.2 Current high temperature die attach materials and their limitations

At the moment, there exist many different types of die attach materials, such as conductive adhesives, many different solders alloys, Low Temperature Transient Liquid Phase (LTTP) bonding, also called Solid-Liquid Inter-Diffusion (SLID) bonding, liquid interconnects, and sintering micro and nanoparticles. However, this section will only concentrate on the solutions already known as die attach materials for temperature ranges of 300 °C or more, which in most cases do not require processing pressure. The mentioned criteria would exclude conductive adhesives and many solder alloys, as they cannot operate at such temperatures. Also, sintering micro-scale particles would in many cases require processing pressure, excluding them from the current high temperature die attach materials considered in this section [12].

High gold content solders are one type of currently available die attach materials for the targeted high operating temperatures [13, 14]. The gold based solders are basically an alloy of gold with a lower melting point metal such as tin, indium or gallium. One example of concerns about these materials is that as the solders are required to melt during processing, there can be residual stresses left inside the joint, reducing the mechanical reliability especially at high operating temperatures [15]. In addition to high residual stresses inside the joint, as the solder needs to be molten during processing, the operating temperature cannot exceed about 75% of the processing temperature, so that for high operating temperatures the processing temperatures needs to be extremely high. This issue can complicate the manufacturing and even damage the semiconductors on the electronic board. Furthermore, the high percentage of gold makes the processing of these solders difficult because of the reflow temperatures being higher than other alternatives [16], and also this high gold content is more expensive relative to other solutions, making this solution less favourable for some applications. Moreover, these solders are not very flexible and their hardness can transfer stresses into the die and cause fracture [17].

On the other hand, there are alternative materials, which have decoupled the processing temperature from the operating temperature, resolving issues related to high processing temperatures. Some of these solutions are liquid interconnects [18, 19], SLID interconnects [20 - 22], and nanoparticle sintering of metals such as copper or silver [1, 2, 12, 15, 16, 23 - 29].

Liquid interconnects appear to be another interesting approach to produce the high temperature joint. However, due to the liquid nature of the material at high operating temperatures and lack of a suitable solution for resolving the issues associated with encapsulation of the liquid interconnect for large die, this system has not been much investigated in the literature and requires further examinations and reliability tests for high temperature applications.

SLID based materials are another group of high temperature die attach materials currently in industry for applications up to 300 °C. In a SLID system, there are mainly two metals utilised for production of the bond, in which one metal has a higher melting point than the operating temperature, such as gold, silver or copper, and the other with melting point at the processing temperature, such as indium or tin. Therefore, during processing by reaching the melting point of the metal with the lower melting point the metal liquefies and diffusion occurs between the two metals. This reaction establishes the bond by producing an alloy with melting point higher than the operating temperature, see Figure 1.1 below.
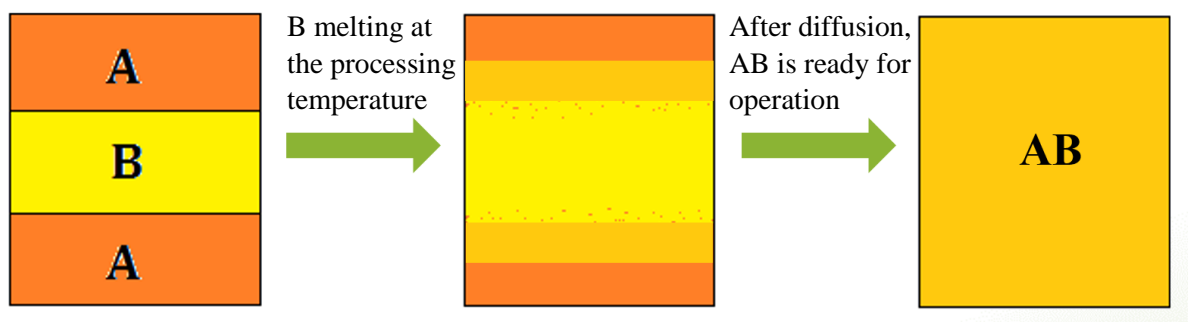
Figure 1.1: Schematic representation of processing of SLID systems, in which "A" represents the metal with higher melting point and "B" represents the metal with lower melting point.

This technique cannot be used for higher temperatures than 300 °C due to many shortcomings [30, 31]. Some disadvantages of SLID technique that prevent it from being

used at higher temperatures are, for example, sharp reduction to their mechanical strength at high temperatures even much lower than their melting point [30, 31]. In addition, they undergo brittle fracture and delamination at high operating temperatures [31].

The remaining technique, which is the subject of this thesis, is based on sintering of nanoparticles, which normally consist of silver [12, 15, 16, 24 - 26, 28, 29], copper [32, 33], or a mixture of metals [23, 34]. In this case the processing temperature can be much lower than their potential operating temperatures. This is due to reduction of sintering temperature as a result of lowering the particle size to nanoscale [25]. The reduction of particle size results in increase of the ratio between surface area and volume, which increases the total surface energy of the particles. This increased surface energy raises the tendency of the particle to join with others and lower its total energy. In addition, this increase to the particle's total energy would also result in a reduction to the temperature required to liquefy the particle and can even result in surface premelting [35], and therefore, reducing the potential sintering temperature even further [25, 36]. Figure 1.2 below shows an example of reduction to the particle's melting point as a function of its size for gold. This phenomenon enables relatively low processing temperatures for the die attach materials, which can then potentially function at extremely higher temperatures close to the material's melting temperature. For example, sintering temperature of copper nanoparticles to produce the die attach can be about 300 °C [37], while its potential operating temperature could be almost as high as the melting point of copper. However, the shortcomings of this technique normally are related to the unknowns of the sintering process and its behaviour during long term operation, especially at high temperature and/or high mechanical vibrations. These unknowns make doubts about their long-term reliability and as a result is delaying their implementation into industry [24].
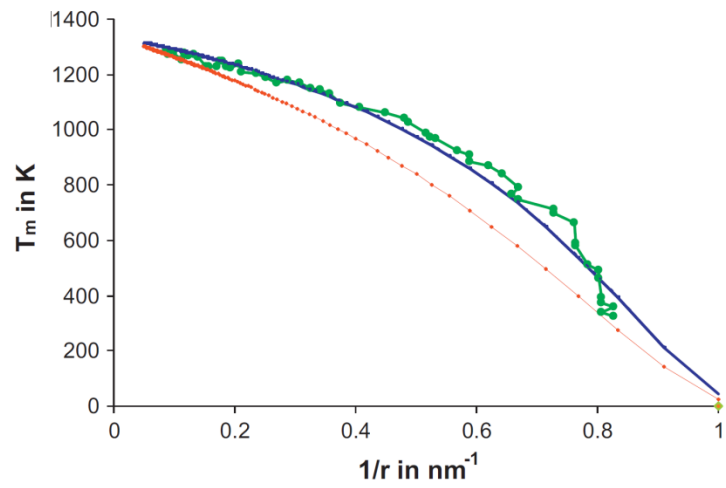
Figure 1.2: *Melting point of gold particles against their size [38]. Here two different theoretical models are compared with experimental data indicated by the uneven dotted line.*

1.3   Selection of silver nanoparticle paste as a potential high temperature die attach

Among the mentioned die attach materials for high temperature applications, sintering nanoparticles appears to have the highest potential to overcome the challenges of high temperature environments. While the other die attach techniques have issues related to their inherent properties, sintered silver nanoparticles have not yet shown any fundamental problems that can completely prevent this material from becoming a potential high temperature die attach. While there exist some inherent issues with the sintered silver such as silver migration [27], this issue has not yet shown any significant concern on practicality of sintered silver as high temperature die attach. Therefore, it has been selected for further investigations to examine its practicality more. The following subsections will explain benefits of silver nanoparticles in more detail.

1.3.1   Benefits of silver

To produce a reasonable die attach with acceptable mechanical capabilities the utilised material should have acceptable properties. Silver fundamentally has good mechanical performance when compared with other materials [2]. In addition, silver based solutions have a much lower price than gold, which can be an advantage for some applications. Moreover, higher resistance of silver to oxidation compared to other alternatives, such as copper, which is one of the most important alternatives, has been another important argument for selection of silver. In addition, while sintering copper normally requires a reducing gas atmosphere, applied pressure on the die, or UV light for successful sintering [15], silver nanoparticles can be sintered without these requirements [15]. Therefore, silver has promising properties, which have contributed to selection of this element as the potential die attach material to be further investigated. Indeed, there are also many other researchers, who have selected this material as their potential solution for such applications as well, see Section 2.4.

Nevertheless, the issues related to silver should also be considered for particular applications. Two of the most important of these issues could be named as silver migration, such as electromigration or ionic migration, or tarnish of silver in presence of sulphur. While the main aim of this research is mechanical attachment of die to the substrate with no electrical current going through the die attach or any voltages being applied across it, it would remain a concern for applications under such conditions. Therefore, while silver migration is

noted as an issue for some applications, it would not be a concern for the applications targeted in this project. However, the stabilisation explained in Chapter 4 for stopping surface diffusion of sintered silver atoms can be potentially used to increase the reliability of sintered silver for those applications. In addition, the intrinsic problem of silver tarnish in presence of sulphur could cause concerns for deep oil and gas exploration, but again it would not be investigated further and additional protection will be required, for example, by insulation of the electronics from the oil and gas wells' environment. Nevertheless, the stabilisation technique might be used to prevent the issues related to silver tarnish as well, and therefore, it would be recommended for future research to further investigate this benefit.

1.3.2   Benefits of nano-size

The benefit of nanoparticles for this type of application is mainly reduction to melting temperature and sintering temperatures [25]. This reduction results from an increase to surface energy and vapour pressure of nanoparticles, empowering sintering of nanoparticles at lower temperatures to decrease their total energy [25]. One example of this reduction to melting point is melting point of 2.4 nm silver particles, which is around 350 °C [39], but the bulk silver melts at around 961 °C. An interesting point of this lowered sintering temperature is that it decouples the processing temperature from operating temperature, as the sintered structure has the melting point of bulk material. Another benefit of nano-size, in addition to lowering the processing temperature, is removing the need for applied pressure during processing [12], again as a result of increased driving force.

Another important aspect of sintering nanoparticles is the final porous structure. The porosity of sintered silver can be controlled by the silver nanoparticle size, the degree of homogeneity of the particle sizes, the organic materials inside the silver nanoparticle paste, and sintering profile. Indeed, these kinds of porosities can be very beneficial for the die attach application, as it can increase the flexibility of the die attach and avoid possible fracture of the die at high temperatures, through plastic deformation of the porous structure [40]. The die fracture can be caused as a result of difference in thermal expansion coefficients of the die and substrate. Furthermore, this kind of porosity has also been considered even required for improving the elastic modulus and mechanical performance of the sintered structures [12].

While the nano-size has such advantages, its drawbacks should be considered as well. The main issue with nanoparticles is the safety concerns in handling and processing them,

which will be resolved after the sintering process and formation of bulk silver. There are two risks associated with handling of nanoparticles, one is inhalation of nanoparticles and the other is dermal exposure. Firstly, inhalation of silver nanoparticles can cause deposition of the particles inside the human lung [41], which can then be absorbed into the circulation system. This effect can result in "silver ion elimination mechanisms", which may damage sensitive human tissues [41]. Secondly, the dermal absorption is another potential route of absorbing silver nanoparticles, which can then be transferred into the circulation system and reach sensitive organs [42]. Due to presence of such risks, the processing of nano-sized materials is more complicated than other available techniques. However, by following some easy safety rules these hazards should be eliminated. For example, after using the paste, the equipment, especially for printing the paste, such as stencil printer and squeegee, should be washed from excess paste, and the excess should then be placed in designated bins. This process should be performed right after the assembling procedure, as the organics inside the silver nanoparticle paste may evaporate and allow transfer of the nanoparticles into the atmosphere and their inhalation. In addition, it would be wise to store the silver paste inside a cool place to avoid dry-up of the paste and prevent easier desiccation of the paste during processing.

1.4   Objectives of the research

As mentioned previously, the main aim of this project is to investigate the suitability of a promising high temperature die attach material; silver nanoparticle paste. The approach towards addressing this objective is organised according to the following subsection and the main contributions of the author are mentioned in the subsequent subsections.

1.4.1   Organisation of thesis

Chapter 2 will include some background information surrounding the silver nanoparticle paste, which is selected as the material for further investigations. In this chapter information on synthesis of silver nanoparticles and the paste will be included. In addition, sintering mechanisms of the nanoparticles leading to fabrication of the micro-scale die attach from the sintering process will be investigated. Finally, the fourth section of the second chapter will include research and state of the art developments on silver nanoparticle paste as a high temperature die attach material, which is a standalone review accepted in Microelectronics Reliability [46].

Chapter 3: This chapter has been published as [43]. It will investigate high temperature behaviour of the sintered silver structure, focusing on its reliability and physical mechanisms associated to its thermal behaviour. This chapter investigates the high temperature behaviour of exposed and unexposed sintered silver to atmosphere prior to the high temperature. The investigations of the microstructural behaviour are performed in a fairly continuous manner at high temperature storage. The results obtained will be used to investigate physical mechanisms of this high temperature behaviour in more detail.

Chapter 4: This chapter has been published as [44]. Here novel oxidising treatments were introduced to the porous sintered silver structure to increase its thermal stability. The microstructural stability was increased to 400 °C for 24 h and 300 °C for 600 h, awaiting longer duration tests through future experiments.

Chapter 5: This chapter has been published as [15]. After the investigations of the mechanisms of solitary sintered silver evolution, described in the previous chapter, its behaviour and interactions with its surroundings is investigated in this chapter. In Chapter 5, behaviour of sintered silver as a die attach will be examined when utilised on substrates with

either gold or silver coatings. The long-term reliability and mechanical strength of this material on those substrates has also been investigated.

Chapter 6: This chapter has been published as [45]. An innovative technique is explained in this chapter which results in die attach materials with extreme thermal stability. This chapter investigates thermal stability of this die attach up to 600 °C, and the lack of any reduction to shear strength shows high potential of this material for utilisation in extreme temperature applications.

Chapter 7 will be covering the conclusions for this thesis and also will recommend some potential routes for future work on this area.

Please refer to Appendix A6 for a summary of the project in a confined format.

1.4.2   Author's primary contributions

The author has been the primary contributor of the following journal papers:

Microstructure evolution during 300 °C storage of sintered Ag nanoparticles on Ag and Au substrates, Journal of Alloys and Compounds, 2014, Authors: S. A. Paknejad, G. Dumas, G. West, G. Lewis, S. H. Mannan [15]

An important aspect of die attach materials is their interactions with their surroundings, such as substrate and die's metallization. In this paper the inter-diffusion resulting in certain types of sintered silver behaviour and its consequences on its mechanical properties and underlying structural evolution have been investigated. Further studies on grain structure and formation of sintered silver has also been performed using Transmission Electron Microscope (TEM) and Electron Back-Scatter Diffraction (EBSD).

Thermally stable high temperature die attach solution, Materials & Design, 2016, Authors: S. A. Paknejad, A. Mansourian, Y. Noh, K. Khtatba, S. H. Mannan [45]

By utilising sintered silver's interactions with gold metallization, a new technique for production of a new thermally stable die attach has been proposed and examined in this paper. Tests on this new material indicated a thermally stable shear strength of the die attach at 600 °C for 100 h storage compared to 450 °C storage after 75 h and 1000 h. The SEM images of samples stored for 24 h at 450 °C compared with 1000 h at 450 °C have also

confirmed this thermal stability. The author has filed a patent on the ideas presented in this paper.

Microstructural evolution of sintered silver at elevated temperatures, Microelectronics Reliability, 2016, Authors: S. A. Paknejad, A. Mansourian, J. Greenberg, K. Khtatba1, L. Van Parijs, S. H. Mannan [43]

This paper investigates the microstructural behaviour of silver at high temperatures continuously using a new in-house made equipment. This technique allowed detailed understanding of sintered silver high temperature behaviour. In this work, physical mechanisms of sintered silver's grain size evolution have also been investigated. Finally, a new idea is also proposed in this paper, which could enable production of a stable sintered silver structure up to 400 °C, which has been tested and confirmed in a different route in Chapter 4.

Review of silver nanoparticle based die attach materials for high power/temperature applications, Microelectronics Reliability, 2017, Authors: S. A. Paknejad, S. H. Mannan [46]

This paper covers scientific publications on utilisation of silver nanoparticles in die attach materials. By considering all the research found in one place, some interesting conclusions are drawn on processing steps and properties of sintered silver. One important example of such conclusions is about the relationship between the processing pressure, mechanical performance, and thermal stability of sintered silver.

Ultra-Stable Sintered Silver Die Attach for Demanding High-Power/Temperature Applications, IEEE Transactions on Device and Materials Reliability, 2017, Authors: S. A. Paknejad, K. Khtatba, A. Mansourian, S. H. Mannan [44]

After observations of massive grain growth inside sintered silver at high temperatures of 250 °C and beyond, a simple technique of steaming the silver structure at 150 °C was utilised here to stabilise sintered silver up to 400 °C. Here it has been shown that sintered silver could withstand 400 °C for 24 h and 600 h at 300 °C.

The author has been the primary contributor of the following conference paper:

Factors influencing microstructural evolution in nanoparticle sintered Ag die attach, HiTEN Conference in Cambridge, 2015, Authors: S. A. Paknejad, A. Mansourian, Y. Noh, K. Khtatba1, L. Van Parijs, S. H. Mannan [47]

In this paper, high temperature storage of sintered silver is investigated after being exposed to air (on its free surface) and after no exposure to atmosphere (sintered under cover slip). The study includes analysis on the grain sizes of the sintered silver grains after thermal storage. For grain size investigations, a computational technique using ImageJ and Matlab is described and utilised. The main finding of this paper has been the difference between microstructural evolution of exposed and not exposed surfaces of the silver to atmosphere. To fully understand this process Differential Scanning Calorimetry (DSC) and acid cleaning of the sintered silver have also been performed. See section A1 inside Appendices for the published paper.

The author has also filed patents on his ideas, which have been partially investigated in Chapters 4 and 6 respectively:

Method and apparatus for creating a bond between objects based on formation of inter-diffusion layers, Inventor: S. A. Paknejad**, Number:** 15/176,567

Increasing stability of porous silver to at least 400 °C, **Inventor**: S. A. Paknejad, **Number:** 62/448,240

1.4.3 Author's secondary contributions

In addition, the same silver nanoparticle paste has been investigated in another project as interconnect for high current density applications, such as power electronics, where the author has also substantially contributed. However, those studies have not been included in this thesis to keep the aim focused on the primary aim of the high temperature die attach project, but part of these studies has improved understanding of sintered silver properties and performance as a die attach in power electronics.

The contributions of author on the related project has been published in journal papers mentioned below:

Tunable Ultra-high Aspect Ratio Nanorod Architectures grown on Porous Substrate via Electromigration, Scientific Reports, 2016, Authors: A. Mansourian, S. A. Paknejad, Q. Wen, G. Vizcay-Barrena, R. A. Fleck, A. V. Zayats, S. H. Mannan [48]

The effect of high current density on nanorod growth on sintered silver is investigated here. In particular, the effects of current density, temperature and location of nanorod growth have been studied in detail. It was found that electromigration in a porous medium differs from that in a non-porous medium, and that the location of nanorod growth is not confined only to the anode. The author has again contributed in designing the experimental setup, setting up the experiments, analysing and understanding the acquired data, and preparing the manuscript for publication. See section A2 inside Appendices for the published paper.

Stereoscopic Nanoscale-Precision Growth of Free-Standing Silver Nanorods by Electron Beam Irradiation, The Journal of Physical Chemistry C, 2016, Authors: A. Mansourian, S. A. Paknejad, A. V. Zayats, S. H. Mannan [49]

In this paper a new technique for fabrication of nanorods using electron beam is explained. The nanorods could be fabricated with precision at the point of electron beam contact. The author contributed in understanding the results. See section A3 inside Appendices for the published paper.

Some other secondary contributions of the author have been published in conference papers mentioned below:

Electromigration Phenomena in Sintered Nanoparticle Ag Systems under High Current Density, HiTEN Conference in Cambridge, 2015, Authors: A. Mansourian, S. A. Paknejad, Q. Wen, K. Khtatba, A. Zayats, S. H. Mannan [50]

This paper investigates the effects of high current density through sintered silver nanoparticles. In this paper, growth of nanorods on sintered silver as a result of electromigration has been reported. This effect increases the concerns for potential short circuits by growth of nanorods. However, it has been confirmed in this paper that these nanorods only grow under high current densities and do not otherwise present a potential issue for high temperature applications. For this study, the author has contributed in setting up the experiments, analysing the acquired data, and providing help in preparation of the manuscript. See section A4 inside Appendices for the published paper.

Internal Structure Refinement of Porous Sintered Silver via Electromigration, HiTEC in Albuquerque, 2016, Authors: A. Mansourian, S. A. Paknejad, Q. Wen, K. Khtatba, A. V. Zayats, S. H. Mannan [51]

It has been observed that electromigration inside sintered silver has refined its grain structures. This effect has been studied in this paper and also additional information on production of the nanorods, mentioned in the previous papers, is also provided, and some potential applications for the nanorods are suggested. The author has contributed in understanding the experimental results. See section A5 inside Appendices for the published paper.

References

[1] Buttay, C., Planson, D., Allard, B., Bergogne, D., Bevilacqua, P., Joubert, C., Lazar, M., Martin, C., Mqorel, H., Tournier, D. and Raynaud, C., 2011. State of the art of high temperature power electronics. *Materials Science and Engineering: B*, *176*(4), pp.283-288.

[2] Manikam, V.R. and Cheong, K.Y., 2011. Die attach materials for high temperature applications: a review. *IEEE Transactions on Components, Packaging and Manufacturing Technology*, *1*(4), pp.457-478.

[3] Riches, S.T., Doyle, K., Tebbit, N., Jia, Y. and Seshia, A., 2015. Assessment of MEMS Vibration Energy Harvesting for High Temperature Sensing Applications. *Additional Papers and Presentations*, *2015*(HiTEN), pp.261-265.

[4] Shashkov, P., Curtis, S. and Humpston, G., 2015. Inorganic Insulated Metal Substrates. *Additional Papers and Presentations*, *2015*(HiTEN), pp.219-226.

[5] Ozpineci, B. and Tolbert, L.M., 2004. *Comparison of wide-bandgap semiconductors for power electronics applications*. United States. Department of Energy.

[6] Gupta, K.M. and Gupta, N., 2016. *Advanced Semiconducting Materials and Devices*. Springer.

[7] Horsfall, A.B., Chan, H.K., Vassilevski, K.V., Wood, N.G. and Wright, N.G., 2015. Silicon Carbide Functional Primitives for Wireless Sensor Nodes. *Additional Papers and Presentations*, *2015*(HiTEN), pp.244-250.

[8] Hamilton, D., Mills, L., Riches, S. and Mawby, P., 2015. Performance and Reliability of SiC dies, Die attach and Substrates for High Temperature Power Applications up to 300° C. *Additional Papers and Presentations*, *2015*(HiTEN), pp.200-207.

[9] Roberts, J., Mizan, A. and Yushyna, L., 2015. Optimized High Power GaN Transistors. *Additional Papers and Presentations*, *2015*(HiTEN), pp.195-199.

[10] Menon, S., George, E., Osterman, M. and Pecht, M., 2015. High lead solder (over 85%) solder in the electronics industry: RoHS exemptions and alternatives. *Journal of Materials Science: Materials in Electronics*, *26*(6), pp.4021-4030.

[11] Tremlett, P.R., 2015. "Turning ceramic on its head"-a polymer based packaging system for operation over 175° C. *Additional Papers and Presentations*, *2015*(HiTEN), pp.111-115.

[12] Bai, J.G. and Lu, G.Q., 2006. Thermomechanical reliability of low-temperature sintered silver die attached SiC power device assembly. *IEEE Transactions on device and materials reliability*, *6*(3), pp.436-441.

[13] Chidambaram, V., Hattel, J. and Hald, J., 2010. Design of lead-free candidate alloys for high-temperature soldering based on the Au–Sn system. *Materials & Design*, *31*(10), pp.4638-4645.

[14] Du, Y., Li, C., Huang, B., Tang, M. and Du, C., 2015. Research and prospect of binary high-temperature Pb-free solders. *Soldering & Surface Mount Technology*, *27*(1), pp.7-12.

[15] Paknejad, S.A., Dumas, G., West, G., Lewis, G. and Mannan, S.H., 2014. Microstructure evolution during 300° C storage of sintered Ag nanoparticles on Ag and Au substrates. *Journal of Alloys and Compounds*, *617*, pp.994-1001.

[16] Zhang, Z., 2005. *Processing and Characterization of Micro-scale and Nanscale Silver Paste for Power Semiconductor Device Attachment* (Doctoral dissertation, Virginia Polytechnic Institute and State University).

[17] McCluskey, P., Das, D. and Jordan, J., Package of Power Electronics for High Temperature Applications. *CPES Power Electronics Semina*, p.T2.

[18] Mannan, S.H. and Clode, M.P., 2004. Materials and processes for implementing high-temperature liquid interconnects. *IEEE transactions on advanced packaging*, *27*(3), pp.508-514.

[19] Li, J.F., Mannan, S.H., Clode, M.P., Johnston, C. and Crossley, A., 2007. Dissolution and interfacial reaction of Nb in contact with the molten 52In–48Sn solder. *Acta Materialia*, *55*(15), pp.5057-5071.

[20] Rodriguez, R.I., Ibitayo, D. and Quintero, P.O., 2013. Kinetics of Dissolution and Isothermal Solidification for Gold-Enriched Solid–Liquid Interdiffusion (SLID) Bonding. *Journal of electronic materials*, *42*(8), pp.2677-2685.

[21] Hou, M.M. and Eagar, T.W., 1992. Low temperature transient liquid phase (LTTLP) bonding for Au/Cu and Cu/Cu interconnections. *Journal of Electronic Packaging*, *114*(4), pp.443-447.

[22] Shieu, F.S., Chang, Z.C., Sheen, J.G. and Chen, C.F., 2000. Microstructure and shear strength of a Au–In microjoint. *Intermetallics*, *8*(5), pp.623-627.

[23] Tan, K.S. and Cheong, K.Y., 2014. Mechanical properties of sintered Ag–Cu die-attach nanopaste for application on SiC device. *Materials & Design*, *64*, pp.166-176.

[24] Siow, K.S., 2014. Are sintered silver joints ready for use as interconnect material in microelectronic packaging?. *Journal of electronic materials*, *43*(4), pp.947-961.

[25] Ide, E., Angata, S., Hirose, A. and Kobayashi, K.F., 2005. Metal–metal bonding process using Ag metallo-organic nanoparticles. *Acta Materialia*, *53*(8), pp.2385-2393.

[26] Siow, K.S., 2012. Mechanical properties of nano-silver joints as die attach materials. *Journal of alloys and compounds*, *514*, pp.6-19.

[27] Khazaka, R., Mendizabal, L., Henry, D. and Hanna, R., 2015. Survey of high-temperature reliability of power electronics packaging components. *IEEE Transactions on Power Electronics*, *30*(5), pp.2456-2464.

[28] Siow, K.S. and Lin, Y.T., 2016. Identifying the Development State of Sintered Silver (Ag) as a Bonding Material in the Microelectronic Packaging Via a Patent Landscape Study. *Journal of Electronic Packaging*, *138*(2), p.020804.

[29] Wang, T., Chen, X., Lu, G.Q. and Lei, G.Y., 2007. Low-temperature sintering with nano-silver paste in die-attached interconnection. *journal of electronic materials*, *36*(10), pp.1333-1340.

[30] Tollefsen, T.A., Løvvik, O.M., Aasmundtveit, K. and Larsson, A., 2013. Effect of Temperature on the Die Shear Strength of a Au-Sn SLID Bond. *Metallurgical and Materials Transactions A*, *44*(7), pp.2914-2916.

[31] Rodriguez, R.I., Ibitayo, D. and Quintero, P.O., 2013. Thermal stability characterization of the Au–Sn bonding for high-temperature applications. *IEEE Transactions on Components, Packaging and Manufacturing Technology*, *3*(4), pp.549-557.

[32] Ryu, J., Kim, H.S. and Hahn, H.T., 2011. Reactive sintering of copper nanoparticles using intense pulsed light for printed electronics. *Journal of Electronic Materials*, *40*(1), pp.42-50.

[33] Yamakawa, T., Takemoto, T., Shimoda, M., Nishikawa, H., Shiokawa, K. and Terada, N., 2013. Influence of joining conditions on bonding strength of joints: efficacy of low-temperature bonding using Cu nanoparticle paste. *Journal of electronic materials*, *42*(6), pp.1260-1267.

[34] Manikam, V.R., Razak, K.A. and Cheong, K.Y., 2012. Sintering of silver–aluminum nanopaste with varying aluminum weight percent for use as a high-temperature die-attach material. *IEEE Transactions on Components, Packaging and Manufacturing Technology*, *2*(12), pp.1940-1948.

[35] Couchman, P.R. and Jesser, W.A., 1977. Thermodynamic theory of size dependence of melting temperature in metals.

[36] Lu, K., 2012. *Nanoparticulate materials: synthesis, characterization, and processing*. John Wiley & Sons.

[37] Ishizaki, T. and Watanabe, R., 2012. A new one-pot method for the synthesis of Cu nanoparticles for low temperature bonding. *Journal of Materials Chemistry*, *22*(48), pp.25198-25206.

[38] Omar, M.S., 2012. Models for mean bonding length, melting point and lattice thermal expansion of nanoparticle materials. *Materials Research Bulletin*, *47*(11), pp.3518-3522.

[39] Maruyama, M., Matsubayashi, R., Iwakuro, H., Isoda, S. and Komatsu, T., 2008. Silver nanosintering: a lead-free alternative to soldering. *Applied Physics A*, *93*(2), pp.467-470.

[40] Li, J., 2010. Thermo-mechanical reliability of sintered silver joint versus lead-free solder for attaching large area devices. *M. Sc. thesis, Virginia Polytechnic Institute and State University*.

[41] Christensen, F.M., Johnston, H.J., Stone, V., Aitken, R.J., Hankin, S., Peters, S. and Aschberger, K., 2010. Nano-silver–feasibility and challenges for human health risk assessment based on open literature. *Nanotoxicology*, *4*(3), pp.284-295.

[42] Wijnhoven, S.W., Peijnenburg, W.J., Herberts, C.A., Hagens, W.I., Oomen, A.G., Heugens, E.H., Roszek, B., Bisschops, J., Gosens, I., Van De Meent, D. and Dekkers, S., 2009. Nano-silver–a review of available data and knowledge gaps in human and environmental risk assessment. *Nanotoxicology*, *3*(2), pp.109-138.

[43] Paknejad, S.A., Mansourian, A., Greenberg, J., Khtatba, K., Van Parijs, L. and Mannan, S.H., 2016. Microstructural evolution of sintered silver at elevated temperatures. *Microelectronics Reliability*, *63*, pp.125-133.

[44] Paknejad, S.A., Khtatba, K., Mansourian, A. and Mannan, S.H., 2017. Ultra-Stable Sintered Silver Die Attach for Demanding High Power/Temperature Applications. *IEEE Transactions on Device and Materials Reliability*, *17(4)*, pp.795-798.

[45] Paknejad, S.A., Mansourian, A., Noh, Y., Khtatba, K. and Mannan, S.H., 2016. Thermally stable high temperature die attach solution. *Materials & Design*, *89*, pp.1310-1314.

[46] Paknejad, S.A. and Mannan, S.H., 2017. Review of silver nanoparticle based die attach materials for high power/temperature applications. *Microelectronics Reliability*, *70*, pp.1-11.

[47] Paknejad, S.A., Mansourian, A., Noh, Y., Khtatba, K., Van Parijs, L. and Mannan, S.H., 2015. Factors influencing microstructural evolution in nanoparticle sintered Ag die attach. *Additional Papers and Presentations*, *2015*(HiTEN), pp. 50-58.

[48] Mansourian, A., Paknejad, S.A., Wen, Q., Vizcay-Barrena, G., Fleck, R.A., Zayats, A.V. and Mannan, S.H., 2016. Tunable Ultra-high Aspect Ratio Nanorod Architectures grown on Porous Substrate via Electromigration. *Scientific reports*, *6*.

[49] Mansourian, A., Paknejad, S.A., Zayats, A.V. and Mannan, S.H., 2016. Stereoscopic Nanoscale-Precision Growth of Free-Standing Silver Nanorods by Electron Beam Irradiation. *The Journal of Physical Chemistry C*, *120*(36), pp.20310-20314.

[50] Mansourian, A., Paknejad, S.A., Wen, Q., Khtatba, K., Zayats, A. and Mannan, S.H., 2015. Electromigration Phenomena in Sintered Nanoparticle Ag Systems Under High Current Density. *Additional Papers and Presentations*, *2015*(HiTEN), pp.000059-000063.

[51] Mansourian, A., Paknejad, S.A., Wen, Q., Khtatba, K., Zayats, A.V. and Mannan, S.H., 2016. Internal Structure Refinement of Porous Sintered Silver via Electromigration. *Additional Papers and Presentations*, *2016*(HiTEC), pp.000190-000195.

2 Background on sintered silver nanoparticles as a high temperature die attach solution

This chapter will concentrate on understanding the fundamental science surrounding the utilisation of silver nanoparticle paste as a high temperature die attach material. The points under investigations are mainly concentrated on production of the silver nanoparticle paste including silver nanoparticle synthesis in particular, the mechanisms of sintering in establishing the bulk structure of the die attach from the silver nanoparticles, mechanism of sintered silver's high temperature behaviour, and finally understanding the achievements and shortcomings of state of the art.

2.1   Silver nanoparticle paste

In this section the general requirements for preparation of silver nanoparticle pastes and the common technique used for synthesis of silver nanoparticles for this type of research will be explained. While utilisation of home-made silver nanoparticle pastes is common amongst researchers in this field [1 - 10], the work in this project is based on pastes available commercially. Therefore, the research here will be aimed at increasing understanding of state of the art. While few companies exist offering silver nanoparticle pastes for die attachment, such as Henkel, Heraeus, Alpha® Aromax®, and NBE Tech LLC, there has been limited research performed on comparing the applicability and performance of the commercial silver nanoparticle pastes in the market, especially at temperatures over 250 °C. Therefore, pastes from NBE Tech LLC, a well-known manufacturer in this field, have been selected, which have also been selected by some other researchers in this field [11 - 18].

Two silver nanoparticle pastes from NBE Tech LLC, NanoTach® N-paste and NanoTach® X-paste have been utilised. N-paste is suitable for die with maximum 3 mm^2 size, while X-paste is a newer version for die with maximum dimension of 10 mm^2. The range of nanoparticle sizes has not been investigated in this project, but others using silver nanoparticle paste from NBE have reported values of 8 - 12 nm [15, 17], 30 - 50 nm [18], and <50 nm [16]. In addition, while the exact processing and characteristics of the pastes remain a knowhow secret of NBE Tech, some general information has been obtained. For example, some general information on their paste's composition can be found on their datasheets, shown in Table 2.1 below. The role of X-paste's compositions will be clearer in the following subsection. In addition, a general description of their processing steps can also been found on some of their patents [19, 20].

Table 2.1: NanoTach® X-paste composition.	
Components	**Weight Percentage**
Silver	70-85
Silver Oxide	0-10
Cellulose	1-8
Alpha Terpineol	5-20
Menhaden Fish Oil	0-2
Isopropanol	<1
Ethanol	<1

2.1.1 Synthesis of silver nanoparticles and preparation of the paste

There exist different procedures for production of nanoparticles [21], especially silver nanoparticles [22]. However, the most common techniques utilised by researchers in the field of high temperature joints is chemical reduction [2, 23 - 25], which is also the simplest method [26].

To produce the required metal nanoparticles, its metal salt needs to go through the chemical reduction, which can be expressed by the equation below [21]:

$$M^{x+} + xe^- \rightarrow M \qquad\qquad 2.1$$
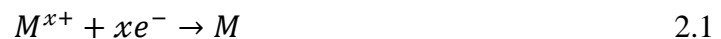
where M is the required metal. This reaction requires loss of electron or oxidation of species α according to the equation below [21]:

$$\alpha^y - xe^- \rightarrow \alpha^{y+x} \qquad\qquad 2.2$$

These two processes together enable production of metal M nanoparticles by release of the M atoms from the metal salt, providing the corresponding standard electrode potential of the oxidation process is lower than that of the reduction [21]. The general term used to describe these two reactions together is "redox reaction".

For the redox reaction, the main precursor used by the researchers in this field is silver nitrate [2, 23 - 25], while the reducing agents used differ. Some examples of the utilised reducing agents, containing α species, are ethylene glycol [25], sodium citrate [2], and sodium borohydride [24].

Production of silver nanoparticles from the redox reaction is then followed by other processes to form a silver nanoparticle paste for ease of handling for example stencil printing or syringe dispensing. These processing normally include centrifugation for thickening the samples, and addition of organic materials for control of particle dispersion and prevention of premature aggregation, and preparing the paste for easy printability [27]. There are three main categories for the added organic materials to form the paste. These are binders, solvents and ligands. The ligands are added for preventing premature sintering or aggregation of nanoparticles. The benefits and functionality of ligands will be described in more detail in the next subsection. Binders are included to avoid crack formation on printed silver paste during

handling, and solvents are required for improved printability by correcting the viscosity [28]. Some examples of these three types of added organics are listed in Table 2.2.

Table 2.2: Main organic additives for silver nanoparticle paste [28] (Materials in Bold are used inside the utilised X-paste, see Table 2.1)	
Component	**Examples**
Ligands	**Menhaden fish oils**, myristyl alcohol, polyacrylic acid, triethylene glycol, oleic acid, methyloctylamine, hexadecylamine, 1-decanol stearic acid, dodecylamine, and palmitic acid
Solvents	**Terpineol, ethanol**, butyl carbitol, toluene, xylene, phenol, isobornyl cyclohexanol, and texanol,
Binders	**Cellulose**, polyvinyl alcohol, and polyvinyl butyral

This type of silver nanoparticle processing can result in formation of nanoparticles with different shapes and sizes, which can be controlled during the synthesis process. One example of this control is synthesis of nanoparticles with wire shapes [29, 30], which were then utilised to strengthen the sintered silver structure [2]. The techniques for improving sintered silver structure are investigated further in Section 2.4. For a comprehensive review on synthesis of nanoparticles and techniques for control of their shapes and sizes the readers may refer elsewhere [22].

2.1.2   Particular need for ligands and prevention of premature sintering

The most important beneficial properties of nanoparticles can also result in problems. The very high surface area to volume ratio of nanoparticles, results in very high surface energies, which provides the critical advantage of low sintering temperature and pressure for nanoparticles. However, this high surface energy can also cause aggregation and premature sintering at room temperature before the intended sintering process inside an oven [31]. In addition to the higher surface energy, the increase in surface interaction of smaller particles can also cause adhesion and agglomeration among them [21, 27, 31].

This aggregation and premature sintering can result in formation of larger particles before the intended sintering process, and therefore, reduce the high driving force of nanoparticle towards densification, which is the main advantage of nanoparticles [6], in

addition to their low sintering temperature. Moreover, this premature sintering can reduce the shelf life of nanoparticle paste, which is another processing issue for the industry.

To prevent the premature sintering, different approaches have been investigated by researchers [6]. However, the most commonly used technique is addition of organic ligands into the silver nanoparticle paste [27, 32]. In this technique, the ligands normally have a polar acid function at one end and at the other a hydrocarbon chain [27]. In this scenario, the polar acid can attach to the hydrated silver nanoparticles and result in surrounding of nanoparticles by the hydrocarbon chain, which can then prevent the premature sintering [27], see Figure 2.1 below.
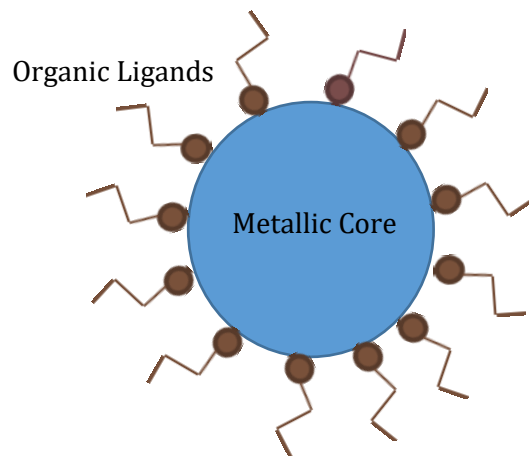

Figure 2.1: *Schematic representation of a nanoparticle coated with organic ligands for prevention of premature sintering.*

2.2   Sintering mechanism of nanoparticles

The general definition of sintering refers to the process in which smaller particles are heated to enable their bonding by atomic movements at their interfaces, which will result in formation of a coherent and mainly solid assembly [21]. This definition mainly relates to the process at macroscopic level, where solid structures are produced by application of heat and sometimes pressure on powdered materials. However, at the microscopic level sintering refers to bonding of two similarly sized particles by neck formation at their contact point, while the general term referring to formation of larger particles at the expense of smaller particles at microscopic scale is called coarsening. Therefore, only in this section the process of producing larger particles by heat treatment of initially smaller ones will be refer to as coarsening, and sintering will refer to its microscopic meaning.

Coarsening at the microscale includes coalescence, sintering and grain growth [31]. During a heat treatment of particles, e.g. micro or nanoparticles, all of these processes can be present at any particular time and contribute to the formation of the larger particles. However, although the main driving forces of these mechanisms differ, the contribution and influence of each of them is predictable [31]. Therefore, by control of their individual driving forces one might be able to achieve production of desired structures through the coarsening of finer particles [31]. Each of these three mechanisms will be described in more detail in the following subsections. Furthermore, as the densification and shrinkage of the bulk structures can be dependent on each of the three main mechanisms, there will be a separate subsection dedicated to the shrinkage and densification as a result of all mechanisms of coarsening combined.

Investigating the coarsening mechanisms requires extra attention for this project, as the current theories normally explain behaviour of microscale particles, and in some cases the behaviours at nanoscale can vary [31]. Therefore, efforts have been made here to highlight the expandability of each mechanism into nanoscale, and also provide examples of mechanisms where such differences exist.

Furthermore, it should also be considered during the studies on coarsening mechanism that the final structures produced by the silver nanoparticle pastes will be dependent on many factors. Some of these factors include formulation of the paste, size of the particles and their purity, processing temperature, applied pressure, treatment technique, joint thickness,

metallization, and metallization roughness, which would all complicate the sintering process. Therefore, current theories may not be able to fully explain the full practical behaviour, but by understanding the key available theories of the coarsening mechanism, the performance of the investigated materials can be better understood and examined, which has been attempted in Chapter 3.

2.2.1 Coalescence

Coalescence can be defined as absorption of smaller particles by larger ones without formation of a neck between them, see Figure 2.2 below. While it can be argued that inside a normal sintered silver paste the small size range of silver nanoparticles may reduce the possibility of coalescence, depending on the manufacturing process, inhomogeneous heat distribution inside the paste during a heating process can result in formation of larger particles, which can then absorb the smaller nanoparticles. Therefore, understanding coalescence can still provide a better view of the whole coarsening mechanism.
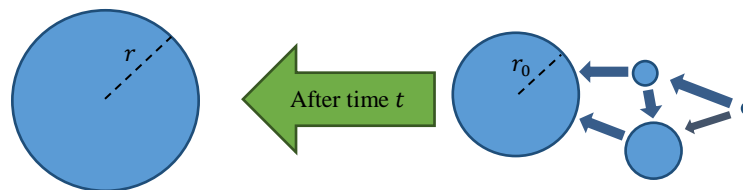

Figure 2.2: Coalescence process, where the smaller particles are condensed onto the larger ones.

The main driving forces for coalescence are reduction of surface energy by increasing the volume to surface ratio and elimination of high curvatures of the smaller particles, where atoms have higher energy relative to flatter surfaces of larger particles.

A simple equation for coalescence can be derived by making the assumption that the only contributor to change in size of particles is mass diffusion into them. As a result of this assumption and by postulating that solubility of the particles would obey Kelvin equation [33], Equation 2.3 can be derived by solving the Fick's first law for describing the coalescence's mechanism [31]. This equation is the same as the Ostwald ripening model [34].

$$r^3 - r_0^3 = \frac{Dp_0\gamma M}{\rho^2 RT}t \qquad\qquad 2.3$$

where r is the particle's radius, p_0 is the vapour pressure of a particle on a flat surface, M is molar weight, D is the diffusion coefficient, ρ is the density, T is the temperature, γ is surface energy, and R is the gas constant.

The equation above describes how larger particles undergo enlargement at the expense of smaller particles, where the original radius of the larger particle, r_0, will expand to r after period of time t has elapsed, see Figure 2.2. One important attribute of coalescence, unlike the other two mechanisms of coarsening, is its insignificant contribution to densification, while it results in reduction of dissimilarities amongst particles sizes, allowing further sintering to occur. These two points will be clearer in Subsections 2.2.2 and 2.2.4 respectably.

2.2.2 Sintering

The basic driving force of sintering is the same as that of coalescence, while the main differences between them are the source of material and the mass transportation's sinks [31]. The most important feature of sintering is formation of a neck between the two particles sintering together, which will act as the sink for mass transportation. That is why sintering normally occurs between two similarly sized particles.

Moreover, the neck formation is the main local driving force for sintering, which is a consequence of the convex curvature of the neck, where the radius of the curvature is negative and atoms inside a convex curvature have more neighbours and are more stable compared with atoms on a concave curvature. Therefore, atoms of the two particles will travel through their volume and surface towards the negative radius of the neck enabling further sintering between the two particle, see Figure 2.3 below. This behaviour can also expand to movement of grain boundary at the neck between the two particles towards relatively higher curvature. This is again due to faster movement of atoms on the smaller particle, having higher curvature, towards the neck, where the atoms are more stable.
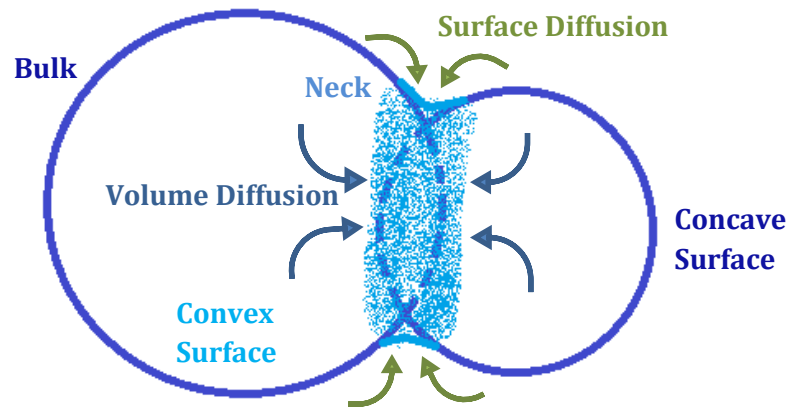
Figure 2.3: *Schematic representation of sintering between two particles and formation of a neck, which acts as a sink for material's transfer.*

This sintering mechanism has been studied at micro- and nano-scales and the comparison showed very interesting results [35]. The facts mentioned above on the sintering mechanism has been experimentally observed and widely accepted at micro-scale scenarios, but in some special circumstances at the nanoscale there exist new phenomena. One interesting example showing that the sintering behaviour does not obey the classical theories at the nanoscale is shown in Figure 2.4 below. In this arrangement the grain boundary travels towards convex curvature instead of concave. However, in the same study in a two particle system the nanoscale particles did obey the classical rules [35].
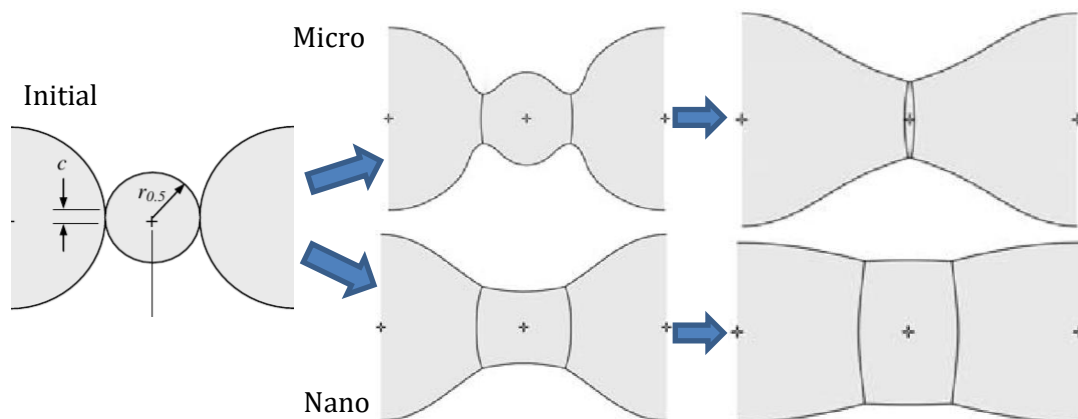
Figure 2.4: *Comparison between sintering at micro- and nano-scales at progressing stages. The middle particle has half the radius of the others. Adapted from [35].*

Another interesting point related to sintering of nanoparticles is their dependency on the lattice alignment between the two sintering particles. If the two particles have aligned lattice interfaces the diffusion routes contributing to neck growth can be reduced [36]. In this

scenario, the volume and surface diffusion mechanisms can be slowed significantly and the main mechanism of sintering can only be condensation of atoms in vapour form. Therefore, the sintered particles with aligned interfaces will not be strongly sintered [36]. Figure 2.5 below compares the sintering of two nanoparticles with and without aligned interfaces.
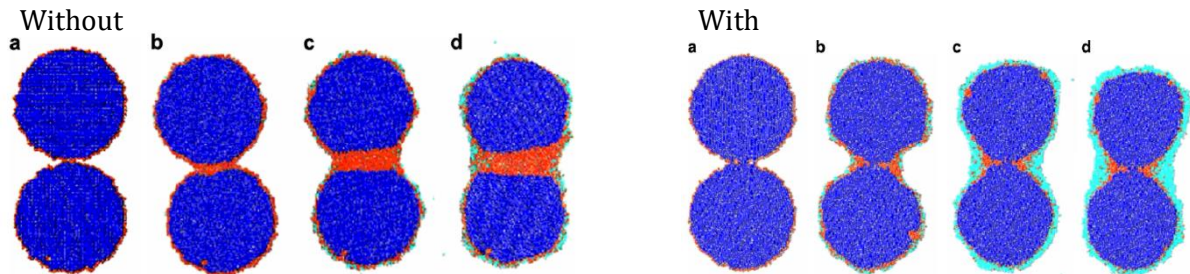

Figure 2.5: Comparison between sintering of two nanoparticles with and without aligned interfaces at progressing stages. Orange indicates diffusing atoms, while light blue indicates condensed atoms. Adapted from [36].

2.2.3   Grain growth

Grains are formed after groups of particles are aligned into a single body. There are different mechanisms contributing into growth of grains, but the main contributors are evaporation-condensation, surface diffusion, and volume diffusion [21], see Figure 2.3 above with interpretation of particles as grains). An important difference between sintering and grain growth are the sink of materials, while their main driving forces still remain the same as coalescence [31]. For grain growth the sink of materials are the grains themselves, unlike the formed necks for sintering.

It is now generally accepted and also experimentally proven that classical theories do not apply to grain growth at nanoscale scenarios [21, 31, 34]. In addition, at nanoscale even small external factors can have significant effects on the grain growth mechanism. For example, impurities inside nanoparticles can have a significant effect on grain growth [37]. Furthermore, some researchers have also stated that the grain growth mechanism should be divided into different segments in order to produce a more accurate model of each segment separately [31]. As a result of all these factors, presenting a complete model for the utilised silver nanoparticle paste would be complicated and not particularly illuminating. Therefore, here two important models describing the mechanism of grain growth will be mentioned to produce a general understanding of the grain growth mechanism. In one technique the rate of

change of grain size has been modelled, and in the other model, the actual grain size can be predicted after a specific period of time.

To investigate the rate of grain growth, it can be assumed that there exist three main contributors to grain growth [21]. These three main parts correspond to the same three main mechanisms of grain growth. By assuming that their contributions are independent of each other, they can be added linearly in this model, shown in Equation 2.4 below [21]. The three main contributing mechanisms are signified in the equation using subscripts of "E-C" for evaporation-condensation, "S" for surface diffusion, and "V" for volume diffusion. In this technique the difference between curved and flat surface pressures have been assumed minimal, which can potentially make the model imprecise for nanoscale particles, for which one of their important characteristics is their high surface curvatures. However, after the initial sintering process and formation of silver grains, this equation might apply to the grain growth mechanisms.

$$\frac{dr}{dt} = (K_{E-C}.S_{E-C} + K_S.S_S + K_V.S_V)H \qquad\qquad 2.4$$

where $\frac{dr}{dt}$ represents the grain growth rate, $S's$ are system related constants, K_{E-C} is another constant representing the mobility of grain boundary in a "E – C" diffusion mechanism, K_S and K_V are constants representing the surface mobility of the grain as a result of surface diffusion and volume diffusion mechanisms respectively, and H is the mean curvature of the grain surface. As this model requires much background information about the system and its diffusion mechanisms, integration of this model into experimental studies, especially the complicated scenario of sintered silver, remains very time consuming and difficult.

The second model is known as the "generalised parabolic grain growth model", and can be used for both micro- and nano-scale scenarios. The model is expressed in Equation 2.5 below, which predicts the grain radius r at time t [31, 37], and has been utilised in Chapter 3 for understanding the mechanism of sintered silver's grain growth at high temperatures.

$$r_{(t)}{}^n - r_0{}^n = kt \qquad\qquad 2.5$$

where t is the elapsed time, $r_{(t)}$ is grain radius at time t, r_0 is initial grain radius, and n is a variable, which can be adjusted to improve the model for each particular scenario. For instance, for nanocrystaline silver it has been estimated as 3 [38], and also for diffusion based

grain growth, which appears to apply to grain growth of sintered silver nanoparticles in this research, the mechanism can be generally best fitted by the same value [37]. Finally, k is a constant for grain growth, and the proportionality relation below can be applied to it [38]:

$$k \propto e^{-Q/RT} \qquad 2.6$$

where R is the ideal gas constant, Q is the activation energy for grain growth, and T is the temperature. In addition, by plotting the natural logarithm of k against $1/T$, the value of Q can be calculated from the slope of the graph. This equation has also been used in Chapter 3, where deviations from these classical sintering models are discussed.

2.2.4 Shrinkage and densification

The mechanism of shrinkage and densification can be dependent on many different factors. Some examples of processing conditions, which can affect the rate of shrinkage and densification, are constraint or free sintering [21, 18, 39, 40], sintering temperature profile [18, 39], especially in presence of organics [18], external pressure [41, 42], interface alignment of the particles [31, 36], and presence of confined vapours, normally from decomposed organics inside the structure [43].

Because of presence of many different factors affecting the densification and shrinkage mechanism, producing a complete model of the whole process is challenging. Therefore, some researchers have attempted to produce mathematical models of these phenomena by simplification of the problem by considering only one or two contributing factors at a time. Therefore, a complete model to fully predict the behaviour of a complicated process, such as the process studied here, is not available currently. However, some researchers in the studied field have tried to investigate the densification and shrinkage of the silver nanoparticle paste by empirical routes, which will be described later in this subsection.

One important example of a simplified model is the general classical densification mechanism of two sintering particles with the same sizes. This model is shown in equation 2.8 below and has been found to be in good agreement with sintering of nanoparticles [31]:

$$\left(\frac{\Delta L}{L}\right)^3 = 3\frac{D_{GB}\gamma_s h\Omega}{kTr^4}t \qquad 2.8$$

where L is the distance between the centres of the two particles, r is the particles' radius, D_{GB} is the grain boundary diffusion coefficient, γ_s is the particles' surface energy, h is the thickness of the diffusion volume, Ω is the atomic volume, k is the Boltzmann constant, T is temperature, and t is time.

To provide practical information for understanding the densification and shrinkage of the silver nanoparticle paste, the empirical techniques appear to provide the most direct and potentially more beneficial contributions.

In one interesting study, the effects of pressure and temperature on densification of silver nanoparticles have been investigated [41]. It has been observed that densification during the sintering process does not depend strongly on the applied pressure, but by rapid heating to the desired processing temperature densification can be promoted. This point only applies to "very fine grains" according to the author, who utilised 2 - 40 nm particles. It should also be noted that no ligands were used for their nanoparticles. Therefore, their observation may not entirely apply to silver nanoparticle pastes utilised for the research here.

In another study the effect of organics and densification after removal of their vapours has been investigated in more depth [18]. It has been observed in their study that thickness of silver paste, which has been acquired from the same company, NBE Tech LLC, shrinks by 40% during evacuation of the organics vapours from the systems. Subsequently, after combustion of some ligands, the nanoparticles start to sinter and densify, resulting in a further 10% shrinkage of the original thickness. This interesting study has been considered for preparation of the samples in Chapter 6, where the shrinkage of the initial paste had a crucial role on the final die attach properties. Another interesting finding of this paper provides insight into preparation of improved processing temperature profiles. They argued that the removal of ligands at early stages of the heat treatment can allow surface diffusion amongst the nanoparticles and prevent densification. To prevent this, the ligands should be removed at temperatures higher than 150 °C, which would then enable further shrinkage of the thickness by the mentioned 10%.

Another exciting technique used for establishment of denser sintered silver structures has been utilisation of a "trimodal mixture system" [1]. In their silver paste system, the researchers have utilised three difference size ranges with average diameters at 20.2, 58.5, and 168.0 nm. In this scenario, the smaller nanoparticles would fill the pores between the

larger particles and help to densify the structure. This study will be mentioned in more detail in Section 2.4.

2.3 High temperature behaviour of sintered silver nanoparticles

After the sintering and establishment of the die attach structure, it is important to understand the behaviour of the sintered structure during operation at high temperatures. The sintered silver behaviour and interactions at high temperatures can determine its suitability and long-term reliability. Therefore, the active mechanisms at high temperatures should be investigated for better understanding of the sintered silver behaviour.

An important active mechanism at high temperatures is diffusion of atoms inside a material. The diffusion mechanism after the sintering process can result in many different effects on the sintered structure. For example, the diffusion can change the shape of the sintered structure, known as microstructural evolution, and it can result in mixture of silver atoms from the die attach with the materials from the metallization. Any of these diffusions inside a die attach structure can change its mechanical properties, so it is very important to understand their effects on long-term reliability of the die attach materials. These effects can be much more severe in sintered silver nanoparticles, due to presence of many grain and twin boundaries inside them [44], see Figure 2.6 below. The high concentration of grain and twin boundaries can increase the speed of diffusion and enhance its effects. The main diffusion paths are lattice, surface, grain boundary, and twin boundary. Contributions and mechanism of each of these diffusion routes will be further investigated in the next subsection.
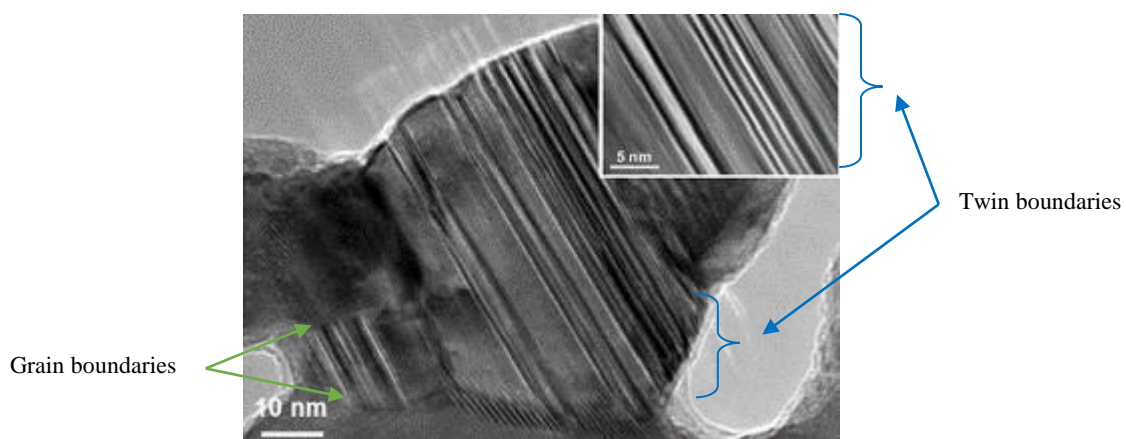

Figure 2.6: *High-resolution transmission electron microscopic images of grains inside sintered silver nanoparticles, showing grain and twin boundaries inside the structure. Adopted from [44].*

After investigating the diffusion inside sintered silver, understanding its particular contribution to high temperature microstructural evolution of sintered structure could be beneficial. By studying the grain growth mechanism inside the sintered silver structure, an important part of the microstructural evolution was investigated in Subsection 2.2.3. However, another important aspect of microstructural evolution is that at high temperatures silver grains can evolve into more energetically favourable shapes by minimising their surface energy through reducing their surface to volume ratios, see Figure 2.7 below. This shape evolution of silver grains is another aspect of microstructural evolution at high temperatures, and it might provide useful information on the predictability of its high temperature behaviour. Therefore, the high temperature shape evolution of sintered silver grains may provide useful information regarding its stability and reliability as a high temperature die attach. While empirical investigations of the microstructural evolution and high temperature reliabilities can be very time consuming and costly, understanding and modelling the underlying mechanism surrounding the microstructural evolution can be an easy and cheap technique. Therefore, in Subsection 2.3.2, the high temperature shape evolution of silver grains will be investigated theoretically.
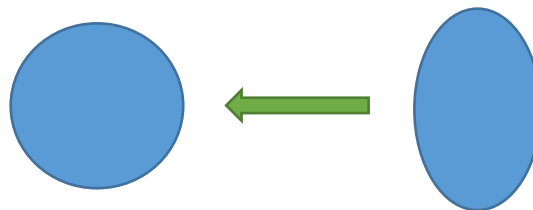

Figure 2.7: Example of shape evolution at high temperatures for reducing the surface to volume ratio.

2.3.1 Diffusion inside sintered silver

An important objective of this research is to understand the suitability of sintered silver nanoparticles as high temperatures die attach materials. Therefore, two important aspects of a die attach material operating at high temperatures should be investigated. One characteristic is its behaviour at high temperatures, and the other is the interaction with its surroundings. The behaviour of sintered silver at high temperatures would rely mainly on its self-diffusivity, and its interference with its surrounding will be strongly dependent on its diffusivity inside the die and substrate's metallization and vice versa. Therefore, it is very important to understand diffusion inside sintered silver.

Diffusing atoms inside structures of materials can mainly go through three routes, lattice, grain or twin boundaries, and surface. Inside a sintered silver structure, due to presence of many grain and twin boundaries [44] and extensive external surfaces, the contribution of grain and twin boundaries, and surface diffusions is considerable, see Figures 2.6 and 2.8, where presence of much twin and grain boundaries and internal free surfaces are shown. The speed of the diffusion along such routes are much faster than the diffusion through the silver lattice. For example, diffusion of gold atoms through the silver lattice is about 1.9×10^{-22} m^2/s [45], which is slower than diffusion along the grain boundaries and surface by 5 [46] and 14 [47] orders of magnitude respectively. In addition, while there is not much information on the effects of twin boundaries on the diffusion of materials inside sintered silver structures, there have been examples of diffusion along twin boundaries being faster than lattice diffusion as well [48].
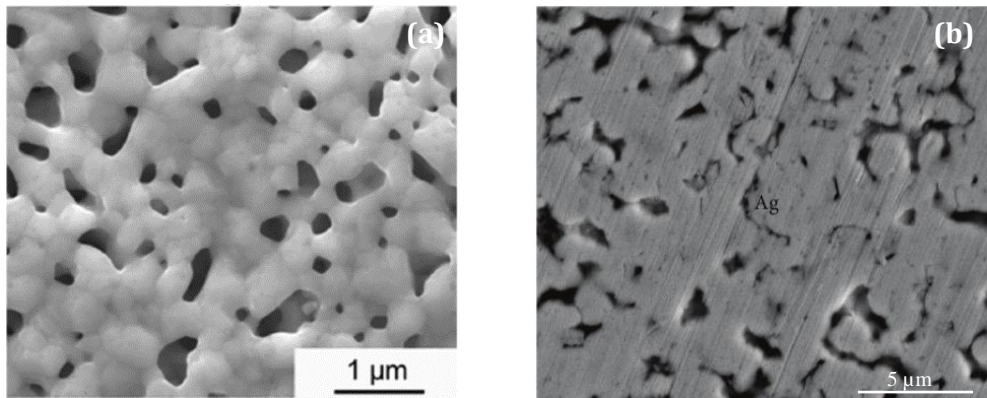

Figure 2.8: Scanning Electron Microscopic images of sintered silver nanoparticles. (a) Without a die on top (adopted from [49]), and (b) cross-section of sintered silver under a die (adopted from [23]).

The lattice diffusion of silver atoms inside the sintered silver nanoparticles' structure should remain similar to lattice diffusion in other silver materials. On the other hand, the grain boundary diffusions inside structures utilised in this research need to be calculated and investigated for the particular grain boundaries of the sintered material. This is due to the fact that grain boundary diffusion is sensitive to the chemical composition and structure of the grain boundaries [50], so that the values are different for each grain boundary structure. Similarly, surface diffusion on the sintered silver structures could potentially be affected by contamination from the silver paste, which contains many different organic compounds (see Table 2.1 as an example), which could reduce the speed of surface diffusion in comparison

with the diffusion on clean surfaces. As a result of the possible slowdown of surface diffusion, literature values cannot be relied on and it needs to be experimentally determined.

Understanding the mechanism of diffusion inside the sintered silver structure provides insight into the effects of possible interactions of sintered silver with the metallization of the die and substrate, as well as its interactions with its surrounding environment, especially at high operating temperatures. For example, by understanding the diffusivity of copper or gold inside sintered silver and their effects on its structure, more refined decisions on utilization of the gold or copper metallization can be made for sintered silver die attach. Therefore, a simple technique for investigating diffusion coefficients inside different materials will be briefly studied in this subsection, while further investigations on the particular sintered silver structures used in this research will be performed in the subsequent two chapters. Chapter 3 will include further discussions and analysis on the surface diffusion and its effect on grain growth of sintered silver, and Chapter 5 will include calculations of grain boundary diffusion and its consequence on potential unsuitability of the utilised gold metallization.

Due to limitation on the available techniques and equipment for investigating the diffusion coefficient of the materials inside the assemblies investigated in this work, there is a need to find a suitable and applicable method. One interesting technique for calculation of diffusion coefficient is utilisation of the Boltzmann–Matano equation [51, 52] shown below. In this technique the diffusion coefficient D can be calculated on a one-dimensional path from the concentration profile of the diffusing material inside the diffused structure for the diffusing period t.

$$D = -\frac{\int_{C_{max}}^{C(r^*)} r \, dC}{2t \left(\frac{dC}{dr}\right)_{r=r^*}}$$

2.9

where, r represents the point of equal concentration between the diffusing and diffused materials on the diffusion path, C_{max} is the concentration at the original interface of the two materials, and r^* is the distance at which evaluation of D would be performed. This equation is used in Chapter 5 to investigated the interaction between sintered silver die attach and the gold metallization of the substrate. The concentrations can be measured using Energy Dispersive X-ray (EDX) during TEM or Scanning Electron Microscopy (SEM). As this

technique can only be applied on diffusion of a material inside another material, it is not applicable to investigation of self-diffusion of silver atoms inside sintered silver.

2.3.2   Shape evolution of sintered silver grains

At high temperatures the self-diffusion of silver atoms inside a sintered silver structure can result in massive internal structural changes. For example, sintered silver die attach after high temperature storage at 300 °C has evolved into much coarser structures after just 24 h on silver substrate [53], see figure 2.9.
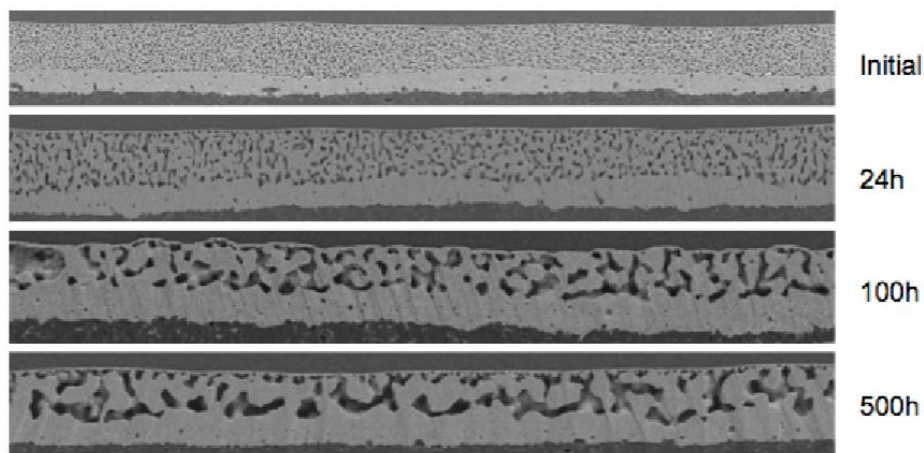

Figure 2.9: Microstructural evolution of sintered silver after storage at 300 °C. Adopted from [53].

In this subsection a simple theoretical method for modelling such shape evolution of sintered silver grains at high temperatures is presented.

The main technique utilised in this subsection is a modified version [54] of the Lagrangian-Eulerian (ALE) method [55]. In this technique surface diffusion is considered as the dominant factor in the shape evolution process, which is the condition applying to the sintered silver material as well. As mentioned before, this is due to the fact that the diffusion of sintered silver through the lattice or grain boundaries are about 14 [45] and 8 [46] orders of magnitude slower than surface diffusion [47] in order.

Therefore, only considering the surface diffusion as the main driving force for movement of atoms, the Nernst-Einstein relation [54, 56] and Boltzmann distribution [57] can be used to develop Equation 2.10 below for the drift velocity of atoms $\bar{v}$ in a two dimensional scenario [54, 56]:

$$\bar{\mathbf{v}} = - \frac{D_S \, \gamma \, \Omega}{k_B \, T} \left(\frac{\partial K}{\partial x} \mathbf{i} + \frac{\partial K}{\partial y} \mathbf{j} \right) \tag{2.10}$$

where D_S is the surface diffusion (m²/s), γ is the surface energy (J/m²), Ω is the atomic volume (m³/atom), k_B is the Boltzmann constant (J/K), T is the temperature of the particle (K), and K is the curvature at any point on the surface (1/m).

If the drift velocity of atoms is multiplied by the density of atoms on the surface X_S (atom/m²), the atomic current $\boldsymbol{j}$ can be found according to Equation 2.11 below:

$$\boldsymbol{j} = - \frac{D_S \, X_S \, \gamma \, \Omega}{k_B \, T} \left(\frac{\partial K}{\partial x} \boldsymbol{i} + \frac{\partial K}{\partial y} \boldsymbol{j} \right) \tag{2.11}$$

Furthermore, divergence of the current of atoms would be equivalent to the number of atoms moving out of a unit of area per second. On the other hand, the velocity of the surface perpendicular to any point on the grain, v_n, would be equal to the volume of atoms moving out of a unit of area per second. Therefore, by knowing that the volume of atoms divided by the atomic volume, Ω, would be the number of atoms, the relationship below can be produced for v_n.

$$v_n = \frac{D_S \, X_S \gamma \, \Omega^2}{k_B \, T} \left(\frac{\partial^2 K}{\partial x^2} + \frac{\partial^2 K}{\partial y^2} \right) \tag{2.12}$$

The equation above now models the movement of a grain surface towards a more stable shape, i.e. circular shape for this 2D instance.

References

[1] Morisada, Y., Nagaoka, T., Fukusumi, M., Kashiwagi, Y., Yamamoto, M., Nakamoto, M., Kakiuchi, H. and Yoshida, Y., 2011. A low-temperature pressureless bonding process using a trimodal mixture system of Ag nanoparticles. *Journal of electronic materials*, *40*(12), pp.2398-2402.

[2] Peng, P., Hu, A., Zhao, B., Gerlich, A.P. and Zhou, Y.N., 2012. Reinforcement of Ag nanoparticle paste with nanowires for low temperature pressureless bonding. *Journal of Materials Science*, *47*(19), pp.6801-6811.

[3] Alarifi, H., Hu, A., Yavuz, M. and Zhou, Y.N., 2011. Silver nanoparticle paste for low-temperature bonding of copper. *Journal of Electronic Materials*, *40*(6), pp.1394-1402.

[4] Bai, J.G. and Lu, G.Q., 2006. Thermomechanical reliability of low-temperature sintered silver die attached SiC power device assembly. *IEEE Transactions on device and materials reliability*, *6*(3), pp.436-441.

[5] Bai, J.G., Yin, J., Zhang, Z., Lu, G.Q. and van Wyk, J.D., 2007. High-temperature operation of SiC power devices by low-temperature sintered silver die-attachment. *IEEE transactions on advanced packaging*, *30*(3), pp.506-510.

[6] Bai, J.G., Lei, T.G., Calata, J.N. and Lu, G.Q., 2007. Control of nanosilver sintering attained through organic binder burnout. *Journal of Materials Research*, *22*(12), pp.3494-3500.

[7] Akada, Y., Tatsumi, H., Yamaguchi, T., Hirose, A., Morita, T. and Ide, E., 2008. Interfacial bonding mechanism using silver metallo-organic nanoparticles to bulk metals and observation of sintering behavior. *Materials transactions*, *49*(7), pp.1537-1545.

[8] Maruyama, M., Matsubayashi, R., Iwakuro, H., Isoda, S. and Komatsu, T., 2008. Silver nanosintering: a lead-free alternative to soldering. *Applied Physics A*, *93*(2), pp.467-470.

[9] Felba, J., Fałat, T. and Mościcki, A., 2013, August. Nano sized silver for electronic packaging. In *Nanotechnology (IEEE-NANO), 2013 13th IEEE Conference on* (pp. 30-33). IEEE.

[10] Mei, Y., Cao, Y., Chen, G., Li, X., Lu, G.Q. and Chen, X., 2013. Rapid sintering nanosilver joint by pulse current for power electronics packaging. *IEEE Transactions on Device and Materials Reliability*, *13*(1), pp.258-265.

[11] Lu, G.Q., Calata, J.N., Lei, G. and Chen, X., 2007, April. Low-temperature and pressureless sintering technology for high-performance and high-temperature interconnection of semiconductor devices. In *2007 International Conference on Thermal, Mechanical and Multi-Physics Simulation Experiments in Microelectronics and Micro-Systems. EuroSime 2007* (pp. 1-5). IEEE.

[12] Wang, T., Chen, X., Lu, G.Q. and Lei, G.Y., 2007. Low-temperature sintering with nano-silver paste in die-attached interconnection. *journal of electronic materials*, *36*(10), pp.1333-1340.

[13] Lei, T.G., Calata, J.N., Lu, G.Q., Chen, X. and Luo, S., 2010. Low-temperature sintering of nanoscale silver paste for attaching large-area chips. *IEEE Transactions on Components and Packaging Technologies*, *33*(1), pp.98-104.

[14] Lu, G.Q., Zhao, M., Lei, G., Calata, J.N., Chen, X. and Luo, S., 2009, August. Emerging lead-free, high-temperature die-attach technology enabled by low-temperature sintering of nanoscale silver pastes. In *Electronic Packaging Technology & High Density Packaging, 2009. ICEPT-HDP'09. International Conference on* (pp. 461-466). IEEE.

[15] Masson, A., Buttay, C., Morel, H., Raynaud, C., Hascoet, S. and Gremillard, L., 2011, August. High-temperature die-attaches for SiC power devices. In *EPE*.

[16] Yan, Y., Chen, X., Liu, X. and Lu, G.Q., 2011, August. Die bonding of single emitter semiconductor laser with nano-scale silver paste. In *Electronic Packaging Technology and High Density Packaging (ICEPT-HDP), 2011 12th International Conference on* (pp. 1-5). IEEE.

[17] Buttay, C., Masson, A., Li, J., Johnson, M., Lazar, M., Raynaud, C. and Morel, H., 2011. Die attach of power devices using silver sintering-Bonding process optimisation and characterization. *Additional Papers and Presentations*, *2011*(HITEN), pp. 84-90.

[18] Wang, T., Zhao, M., Chen, X., Lu, G.Q., Ngo, K. and Luo, S., 2012. Shrinkage and sintering behavior of a low-temperature sinterable nanosilver die-attach paste. *Journal of electronic materials*, *41*(9), pp.2543-2552.

[19] Lu, G.Q., Lei, G. and Calata, J.N., 2005. *Preparation of Stable High Concentration Coloidal Metal Particulate System*. U.S. Patent Application 11/573,303.

[20] Lu, G.Q., Bai, G., Calata, J. and Zhang, Z., 2005. *Nanoscale metal paste for interconnect and method of use*. U.S. Patent Application 10/589,399.

[21] Lu, K., 2012. *Nanoparticulate materials: synthesis, characterization, and processing*. John Wiley & Sons.

[22] Krutyakov, Y.A., Kudrinskiy, A.A., Olenin, A.Y. and Lisichkin, G.V., 2008. Synthesis and properties of silver nanoparticles: advances and prospects. *Russian Chemical Reviews*, *77*(3), pp.233-257.

[23] Xiliang, Q., Yang, C., Tiesong, L., Peng, H., Jun, W., Ping, L. and Xiaolong, G., 2014. Large-Scale synthesis of silver nanoparticles by aqueous reduction for low-temperature sintering bonding. *Journal of Nanomaterials*, *2014*, p.8.

[24] Durairaj, R., Ashayer, R., Kotadia, H.R., Haria, N., Lorenz, C., Mokhtari, O. and Mannan, S.H., 2012, August. Pressure free sintering of silver nanoparticles to silver substrate using weakly binding ligands. In *Nanotechnology (IEEE-NANO), 2012 12th IEEE Conference on* (pp. 1-4). IEEE.

[25] Guo, W., Zeng, Z., Zhang, X., Peng, P. and Tang, S., 2015. Low-Temperature sintering bonding using silver nanoparticle paste for electronics packaging. *Journal of Nanomaterials*, *2015*, p.10.

[26] Guzmán, M.G., Dille, J. and Godet, S., 2009. Synthesis of silver nanoparticles by chemical reduction method and their antibacterial activity. *Int J Chem Biomol Eng*, *2*(3), pp.104-111.

[27] Bai, G., 2005. Low-temperature sintering of nanoscale silver paste for semiconductor device interconnection (Doctoral dissertation, Virginia Polytechnic Institute and State University).

[28] Siow, K.S. and Lin, Y.T., 2016. Identifying the Development State of Sintered Silver (Ag) as a Bonding Material in the Microelectronic Packaging Via a Patent Landscape Study. *Journal of Electronic Packaging*, *138*(2), p.020804.

[29] Sun, Y., Gates, B., Mayers, B. and Xia, Y., 2002. Crystalline silver nanowires by soft solution processing. *Nano letters*, *2*(2), pp.165-168.

[30] Sun, Y. and Xia, Y., 2002. Shape-controlled synthesis of gold and silver nanoparticles. *Science*, *298*(5601), pp.2176-2179.

[31] Castro, R. and van Benthem, K. eds., 2012. *Sintering: mechanisms of convention nanodensification and field assisted processes* (Vol. 35). Springer Science & Business Media.

[32] Ide, E., Angata, S., Hirose, A. and Kobayashi, K.F., 2005. Metal–metal bonding process using Ag metallo-organic nanoparticles. *Acta Materialia*, *53*(8), pp.2385-2393.

[33] Thomson, W., 1872. 4. On the Equilibrium of Vapour at a Curved Surface of Liquid. *Proceedings of the Royal Society of Edinburgh*, *7*, pp.63-68.

[34] Chiang, Y. M., Birnie, D. P., and Kingery, W. D., 1997. *Physical ceramics*. NY: J. Wiley, pp. 343-345.

[35] Ch'ng, H.N. and Pan, J., 2007. Sintering of particles of different sizes. *Acta materialia*, *55*(3), pp.813-824.

[36] Ding, L., Davidchack, R.L. and Pan, J., 2009. A molecular dynamics study of sintering between nanoparticles. *Computational Materials Science*, *45*(2), pp.247-256.

[37] Fang, Z.Z. and Wang, H., 2008. Densification and grain growth during sintering of nanosized particles. *International Materials Reviews*, *53*(6), pp.326-352.

[38] Dannenberg, R., Stach, E., Groza, J.R. and Dresser, B.J., 2000. TEM annealing study of normal grain growth in silver thin films. *Thin Solid Films*, *379*(1), pp.133-138.

[39] Lin, Y.C. and Jean, J.H., 2004. Constrained sintering of silver circuit paste. *Journal of the American Ceramic Society*, *87*(2), pp.187-191.

[40] Choe, J., Calat, J.N. and Lu, G.Q., 1995. Constrained-film sintering of a gold circuit paste. *Journal of materials research*, *10*(04), pp.986-994.

[41] Albert, A.D., Becker, M.F., Keto, J.W. and Kovar, D., 2008. Low temperature, pressure-assisted sintering of nanoparticulate silver films. *Acta Materialia*, *56*(8), pp.1820-1829.

[42] Zheng, H., Calata, J., Ngo, K., Luo, S. and Lu, G.Q., 2012, March. Low-pressure (<5 MPa) Low-temperature Joining of Large-area Chips on Copper Using Nanosilver Paste. In *2012 7th International Conference on Integrated Power Electronics Systems (CIPS)* (pp. 1-6). IEEE.

[43] Bose, A. and German, R.M., 1988. Sintering atmosphere effects on tensile properties of heavy alloys. *Metallurgical Transactions A*, *19*(10), pp.2467-2476.

[44] Wang, S., Li, M., Ji, H. and Wang, C., 2013. Rapid pressureless low-temperature sintering of Ag nanoparticles for high-power density electronic packaging. *Scripta Materialia*, *69*(11), pp.789-792.

[45] Jaumot Jr, F.E. and Sawatzky, A., 1956. Diffusion of gold in single crystals of silver. *Journal of Applied Physics*, *27*(10), pp.1186-1188.

[46] Paknejad, S.A., Dumas, G., West, G., Lewis, G. and Mannan, S.H., 2014. Microstructure evolution during 300° C storage of sintered Ag nanoparticles on Ag and Au substrates. *Journal of Alloys and Compounds*, *617*, pp.994-1001.

[47] Antczak, G. and Ehrlich, G., 2010. *Surface diffusion: metals, metal atoms, and clusters*. Cambridge University Press, pp. 347.

[48] Mansfeld, F.B., 1986. *Corrosion mechanisms* (Vol. 28). CRC Press.

[49] Zheng, H., Berry, D., Ngo, K.D. and Lu, G.Q., 2014. Chip-bonding on copper by pressureless sintering of nanosilver paste under controlled atmosphere. *IEEE Transactions on Components, Packaging and Manufacturing Technology*, *4*(3), pp.377-384.

[50] Mishin, Y. and Herzig, C., 1999. Grain boundary diffusion: recent progress and future research. *Materials Science and Engineering: A*, *260*(1), pp.55-71.

[51] Matano, C., 1933. On the relation between the diffusion-coefficients and concentrations of solid metals (the nickel-copper system). *Jpn. J. Phys*, *8*(3), pp.109-113.

[52] Asai, M., Hirose, R., Kondo, A. and Koike, Y., 2007. High-bandwidth graded-index plastic optical fiber by the dopant diffusion coextrusion process. *Journal of Lightwave Technology*, *25*(10), pp.3062-3067.

[53] Yu, F., Johnson, R.W. and Hamilton, M., 2014. Pressureless, low temperature sintering of micro-scale silver paste for die attach for 300 C applications. *Additional Papers and Presentations*, *2014*(HITEC), pp.000165-000171.

[54] Turuelo, C.G., Bergmann, B. and Breitkopf, C., Void Shape Evolution of Silicon Simulation: Non-linear Three-dimensional Curvature Calculation by First Order Analysis.

[55] Stein, E., De Borst, R. and Hughes, T. J., 2004. *Encyclopedia of Computational Mechanics Volume 1: Fundamentals*. Wiley.

[56] Mullins, W.W., 1957. Theory of thermal grooving. *Journal of Applied Physics*, *28*(3), pp.333-339.

[57] Mehrer, H., 2007. *Diffusion in solids: fundamentals, methods, materials, diffusion-controlled processes* (Vol. 155). Springer Science & Business Media.

2.4 Review of silver nanoparticle based die attach materials for high power/temperature applications
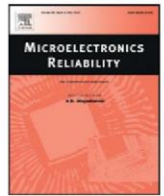
Review paper

Review of silver nanoparticle based die attach materials for high power/temperature applications

Seyed Amir Paknejad *, Samjid H. Mannan

King's College London, Physics Department, Strand, London WC2R 2LS, UK

ARTICLE INFO

ABSTRACT

There has been a significant rise in the number of research papers on silver nanoparticle based solutions for harsh environment die attach. However, sintering nanoparticles is a complex process, affected by many different factors, such as the sintering temperature profile, particle size, sintering pressure, sintering environment, and organic compounds inside the nanoparticle paste used for stabilisation of the particles and easier processing. Therefore, numerous routes exist for establishment of sintered structures, and each lab has selected their own techniques and criteria for sintering silver nanoparticles. This has resulted in formation of a significant amount of knowledge and data in this field, but without appropriate correlation between utilised parameters. In this review data has been collected from a wide range of researchers in the field and an attempt made to correlate the results. By finding connections between the datasets, we present a broad and general understanding of the sintering processes to help researchers produce desired sintered structures. The collected data and investigated parameters include sintering pressure, metallisation, effect of thermal aging and cycling, highest sintering temperature, and particle size distributions. Some particularly interesting innovations in the field to address the shortcomings of sintering silver joints are investigated and some insights on sintering process are also provided, such as the understanding that higher sintering pressure causing improved strength might potentially reduce the long term thermal resistance of the die attach.

© 2017 Elsevier Ltd. All rights reserved.

Contents

1. Introduction

The requirement for a high temperature die attach material is desirable for applications in areas such as high power electronics, aerospace, and hybrid vehicles. For example, utilisation of wide-band

---

* Corresponding author.
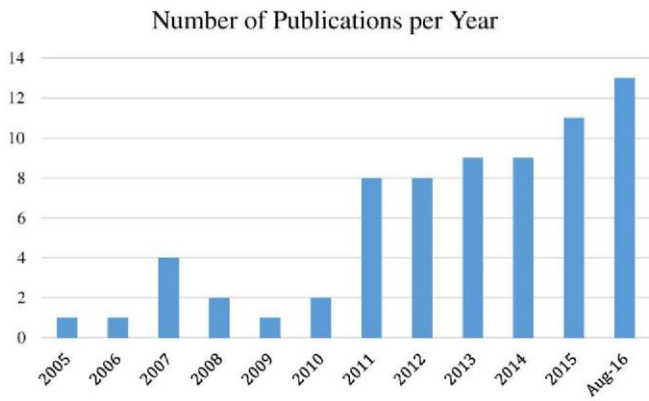*E-mail address:* sa.paknejad@kcl.ac.uk (S.A. Paknejad).

Fig. 1. Number of publications per year wherein silver nanoparticles constitute a significant proportion of the die attach paste. This graph is based on papers related to die attach materials utilising silver nanoparticles in this review.

gap semiconductors in power electronics compared to Si devices can increase the power density and switching speeds [1] when operated at high temperatures, and in the aerospace industry the trend of reducing aeroplane weight by reducing the cabling and getting the electronics closer to the jet engine has been a key driver for research into high temperature electronics. The operating temperature required for such applications can reach 300 °C or even 400 °C in some cases [2]. One promising class of die attach materials, which can be used for such high temperatures are based on the principle of solid-liquid interdiffusion bonding (SLID), but these systems can suffer from issues such as rapid rate of reduction of mechanical performance as temperatures increase [3].

Many researchers have been looking for alternative materials to withstand harsh conditions and silver nanoparticle sintering has attracted considerable interest [2,4–71]. The number of research papers and patents [7] in this field has increased considerably over the past few years, as shown in Fig. 1. One benefit of reducing particle size into the nanoscale range is reduced melting and sintering temperatures [4], which decouples the processing temperature from the operating temperature [5]. This is a key advantage over non-SLID solders, where operating temperatures should not exceed 80% of their processing temperature. This enables processing of sintered silver joints at much lower temperatures (100–300 °C) compared to the melting point of silver (961.8 °C). Moreover, sintered silver can operate even at 300 °C with homologous temperature of ~0.3, which is much lower than the homologous temperatures that solders are required to withstand at high temperature applications. The other main advantages of silver are its high thermal and electrical conductivities, with sintered silver having thermal and electrical conductivities in the range 3 to 5 times higher than
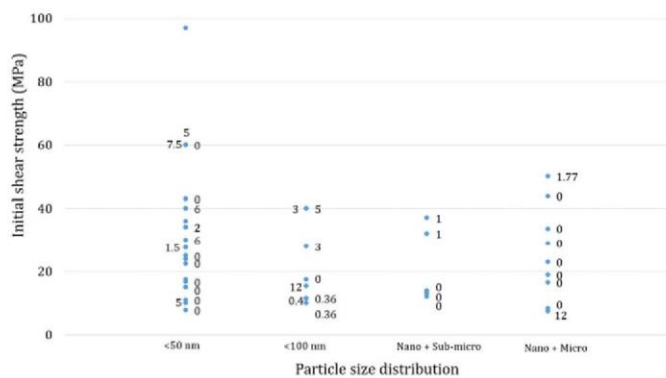

Fig. 2. Shear strength after sintering profile against the particle size distribution. The numbers next to each data point represents the sintering pressure in MPa.
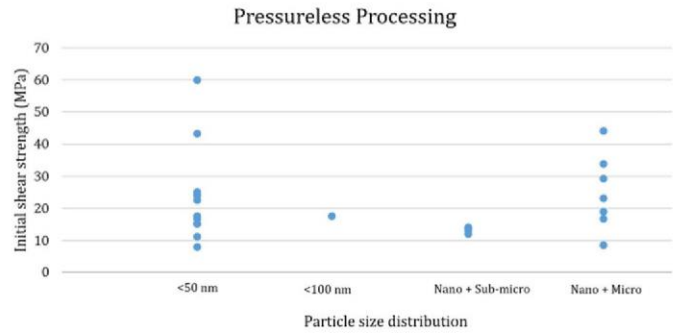

Fig. 3. Shear strength after sintering profile against the particle size distribution for pressureless processing.

lead based solders [46], and also reasonable mechanical performance for die attach applications [10].

While many publications address the use of silver nanoparticles in die attach materials [4,5,11–70], only a few reviews have been produced to investigate the results from the produced data in one place [2,6–10, 71]. Such reviews are however crucial for identifying the critical variables and their optimum values. Some of these variables are for example, the sintering pressure, sintering temperature profile, type of organic materials in the silver paste, size distribution of the particles, metallisation on the devices and substrates that are to be attached, and atmosphere in which the sintering takes place. This review aims to find trends and relationships amongst the variables to help faster identification of the most promising materials and processes. The review addresses only papers in which the sintering material of the die attach is made out of silver and has significant proportion of nanoparticles. Other approaches using Cu and Ni nanoparticles to form joints will not be included.

This review contains three main sections. Firstly, the shear strength of die attach materials, which is the main test for investigating the mechanical performance of the sintered joints, will be investigated. This section will summarise the information that the authors consider most critical, such as the performance of sintered silver on particular metallisations and the benefits and drawbacks of different porosity levels. The second section reviews innovations which could resolve current issues related to sintered silver die attach. In the third section, the authors will summarise their findings and suggest potential routes for future research.

2. Mechanical properties

The mechanical performance of sintered silver can be investigated using shear strength analysis, which is the most common technique for investigating mechanical performance in this field. Researchers generally perform shear strength tests after normal sintering, which is an important analysis of the mechanical performance and the results will be reviewed in the next subsection. Comprehensive data on shear
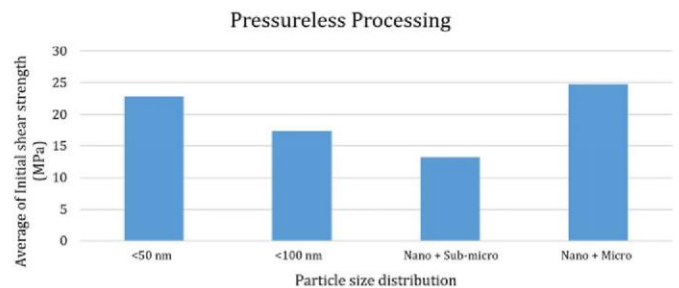

Fig. 4. Average of shear strengths after sintering profile against the particle size distribution for pressureless processing.
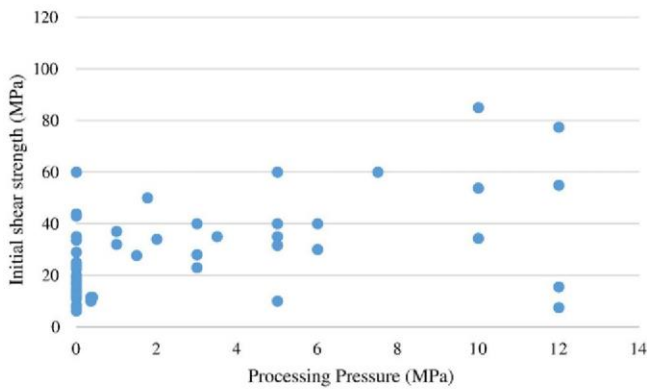
Fig. 5. Shear strengths after sintering against processing pressure. These values cover all the initial shear strength values presented in Table S1.

strength tests after or even during high temperature storage or thermal cycling would also be valuable, but the same depth of data is not currently available. Nevertheless, the existing test data after high temperature storage and after thermal cycling will be investigated in the second and third subsections.

It should also be noted that the shear strength measurement equipment and other materials, such as the die or substrate used for these shear strength measurements vary between publications and information on whether the failure was associated with the die attach or other materials is also not always present. Therefore, in order to make progress, it has been assumed that the shear strengths provided by the authors are associated with the die attach. In addition, in order to increase clarity, only the highest strength, or the optimised strength selected by their authors has been extracted. Furthermore, for some figures, where >15 references are present, they are not directly mentioned to improve the visualisation and to avoid long lists of references for each figure; please refer to Table S1 inside the Supplementary information for the values and references used for figures in this section.

2.1. Initial shear strength after sintering

The easily controlled parameters of the sintering process are particle size distribution, processing pressure, sintering profile, and the organic components of the silver paste. While most researchers do not provide the information regarding the organics inside the silver paste, the other parameters will be investigated below.

Firstly, to investigate the effect of particle size on mechanical performance of sintered silver, the sizes are divided into four main

distribution ranges to slim down the very broad possibilities. The four selected size distributions are nanoparticles with sizes mainly remain below 50 nm in diameter, below 100 nm, mixtures of nanoparticles with submicron particles, and mixtures of nano- and micro-sized particles.

Fig. 2, shows the shear strength of different sintered joints, using these four size distributions. As the sintering pressure remains a crucial contributor in the sintering process, the sintering pressure (where known) is shown next to each data point. As can be seen, no conclusions can be drawn from the data, only the fact that there appears to be a direct relation between the sintering pressure and shear strength. Therefore, only data for pressureless sintering have been included in Fig. 3 and averages for each size distribution in Fig. 4. There appears to be higher mechanical strength for two main size distributions; below 50 nm and nano + micro mix. The improved mechanical performance of smaller size distribution might be due to the fact that smaller particle sizes have higher driving force for sintering, and therefore, smaller particles should sinter more effectively in absence of applied pressure. This fact has also been pointed out by Ide (2005) [4], namely that by using 11 nm particles 4 times higher shear strength was achieved compared to 100 nm particles, but it should also be noted that Ide (2005) [4] used 5 MPa sintering pressure, and that the final sintered structure from 11 nm particles was less porous.

The reason for higher mechanical strength of the nano + micro mix be related to the denser final structures of these mixtures. For example, Zhao (2016) [28] utilised a mixture of nano, submicron, and microscale flakes and achieved about 12% porosity compared to 20% porosity typical of sintered silver. However, it should be also noted that for some applications the higher strength as a result of denser structures might not be unequivocally beneficial due to increased stresses transferred to the die as a result of Coefficient of Thermal Expansion (CTE) mismatches.

The next parameter to be investigated is the sintering pressure of the process, as shown in Fig. 5. As was expected, higher sintering pressure would normally result in higher shear strength of the sintered material. The averages are also plotted in Fig. 6 for improved comparison. The higher shear strength of zero sintering pressure compared to 0.36 and 0.4 MPa sintering pressures is related to intensive research and development of pressureless processes, which have enabled improvement over small sintering pressures. The slight decrease to shear strength for sintering pressures higher than 7.5 MPa have also been seen before by Li (2015) [40]. At 300 °C sintering temperature, increasing pressure resulted in increasing shear strength up to 11 MPa sintering pressure, but between 11 and 15 MPa a decrease in strength was reported. Different factors may have contributed in this effect. One possibility could be that high sintering pressures may prevent release of decomposed
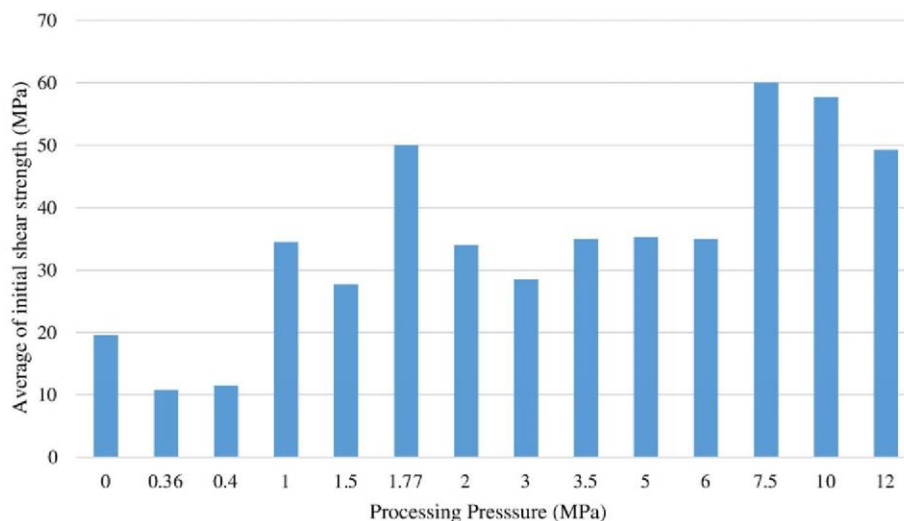

Fig. 6. Average of shear strengths after sintering against processing pressure.
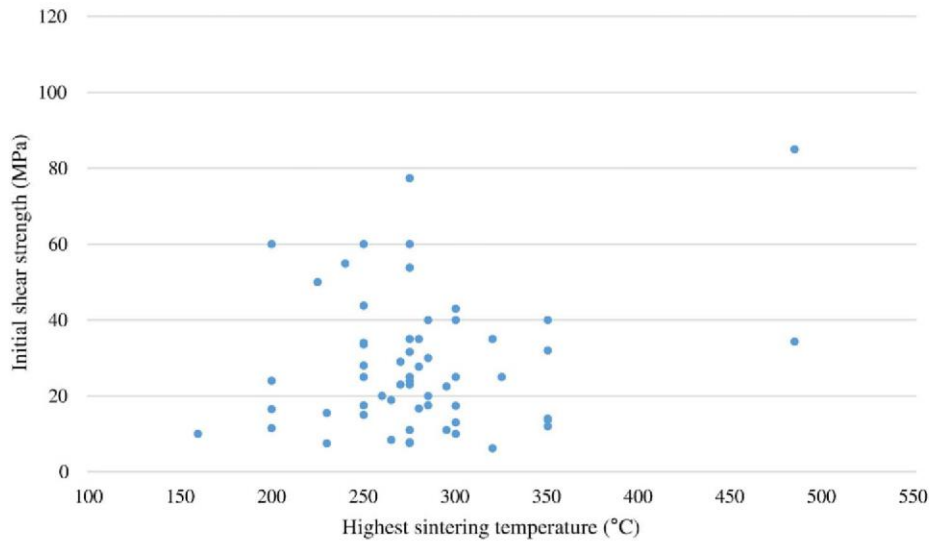
Fig. 7. Shear strength after sintering profile against the highest sintering temperature.

organics from the die attach. Another possibility is that higher densification due to sintering pressure may prevent easy penetration of oxygen inside the sintered structure during sintering, reducing effectiveness of sintering and compromising the overall mechanical connection.

To compare the effect of different sintering profiles the highest sintering temperatures is used as the defining characteristic of the profile, as sintering profiles have different dwell periods at different temperatures, which would make the comparison harder, and the lower dwelling temperatures are normally just for decomposition and removal of organics. However, no direct relationship between the sintering temperature and shear strength of the die attach materials have been observed, see Figs. 7 and 8. This has also been observed by Sakamoto (2011) [58], where shear strength of sintered silver nanoparticles was found to be similar for sintering temperatures of 160, 180 and 200 °C for 60 min under a load of 0.07 MPa.

The data for pressureless sintering only has been extracted and plotted in Fig. 9 with the sintering duration at the highest sintering temperature recorded in minutes next to each data point. Again no correlation between the data has been observed. The shear strength of pressureless processing at 275 °C has also been investigated for different sintering durations in Fig. 10, and again no correlations are observed. It should be noted that while for a given paste, the sintering duration should

make considerable differences, that for different pastes, which have each been optimised by their producers for their constituents, the sintering temperature should not necessarily have a consistent trend unlike the trends observed for processing pressure. For example, Wang (2015) [25] demonstrates an increase in the shear strength of the die attach from 10 MPa to 25 MPa by increasing the sintering temperature from 220 to 250 °C. However, Wang [25] have also pointed out that from 250 to 270 °C sintering temperature there was no further increase. This effect appears to indicate a temperature range within which no additional sintering or significant microstructural evolution is happening. However, at even higher temperatures considerable coarsening and evolution inside the sintered silver has been observed [66], very likely affecting its mechanical properties.

In addition to the parameters affecting the final sintered structure, the contact metallisations should also play a critical role on the mechanical performance of the die attach. Therefore, the average of shear strengths on different metallisations for general sintering processes and pressureless sintering have been presented in Figs. 11 and 12 against three kinds of substrate metallisations. As can be seen, there appears to be slight advantage on Ag metallisation especially for a pressureless processes. However, this higher shear strength on silver metallization is small and therefore should be treated with caution.
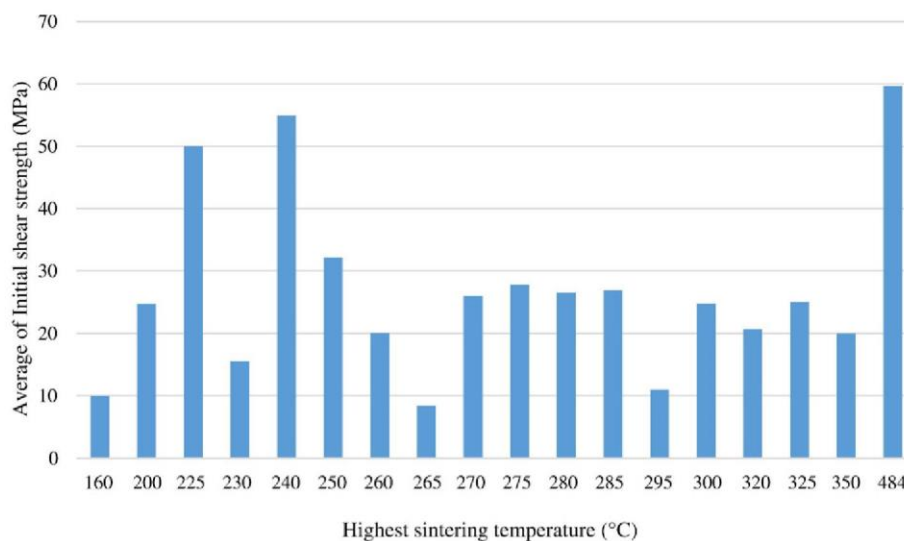

Fig. 8. Average of Shear strengths after sintering plotted against the highest sintering temperature.
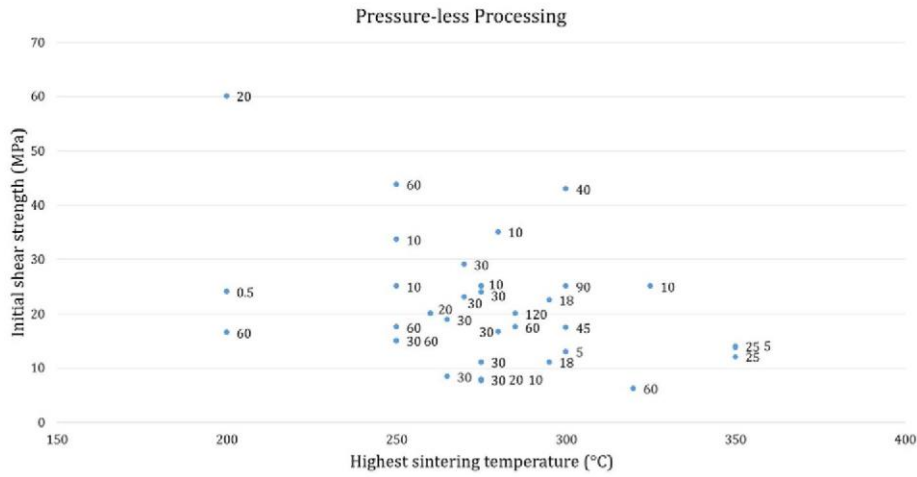
Fig. 9. Shear strength after sintering of pressureless processes plotted against the highest sintering temperature. The number next to each data point is the dwell time in minutes at the highest sintering temperature.

Furthermore, according to Zhao (2012) [46], shear strength of sintered silver die attach increased with increase of bond-line from 4.1 MPa at 9 μm to about 22 MPa at 20 μm bond-line. However, the shear strength remained almost constant afterwards. These results were obtained with the nano + submicron particles and silver flake mix. These results may indicate that a potential minimum edge area to die size ratio is required for penetration of oxygen into the system to facilitate decomposition of organics and effective sintering.

The relationship between the die size and shear strength is of interest. Therefore in Fig. 13 the average shear strength against the utilised die sizes have been plotted. Very interestingly, in contradiction to the generally accepted theory there appears to be no direct relationship between the die sizes and shear strength. Therefore,
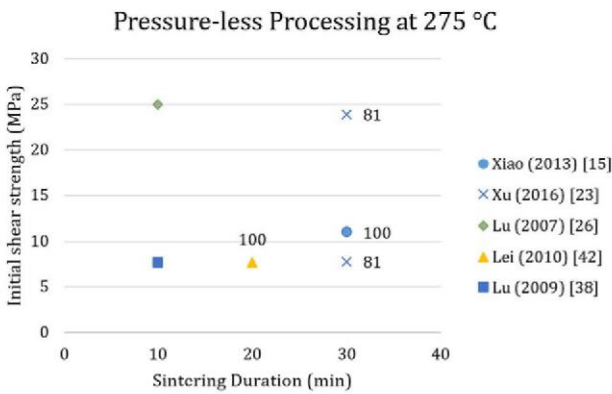
Fig. 10. Shear strengths after sintering plotted against the dwell time with peak sintering temperature 275 °C. The values next to each data point is the die size in mm squared.

Fig. 12. Shear strengths after sintering plotted against substrate metallisation for pressureless processing.

Fig. 11. Shear strengths after sintering plotted against substrate metallisation for both pressure assisted and pressureless sintering.

Fig. 13. Shear strengths after sintering plotted against die size.

Fig. 14. Shear strengths after sintering plotted against publication year.

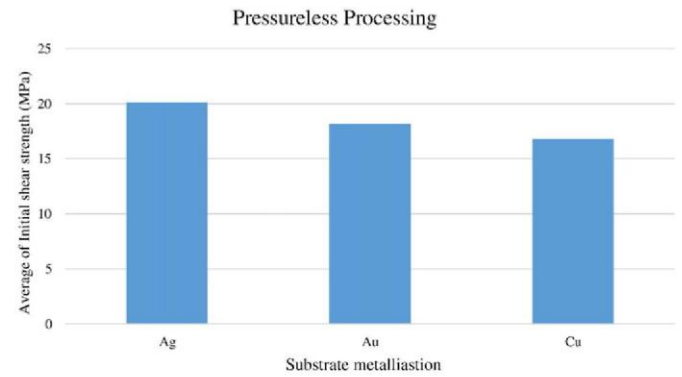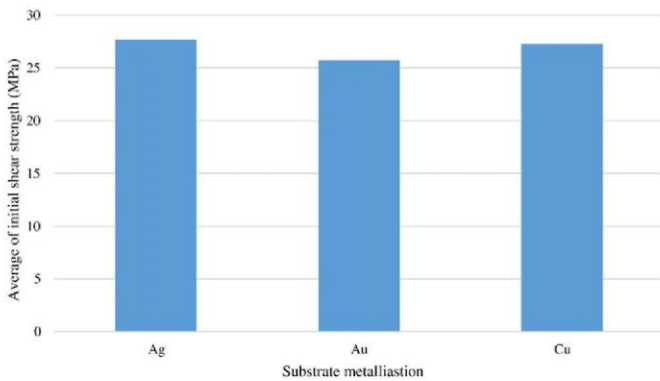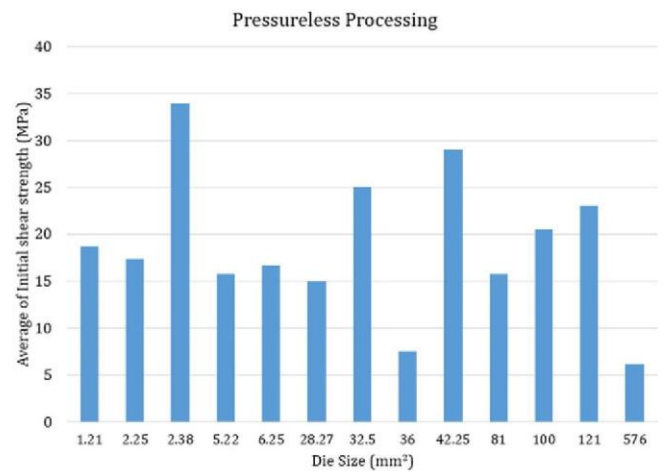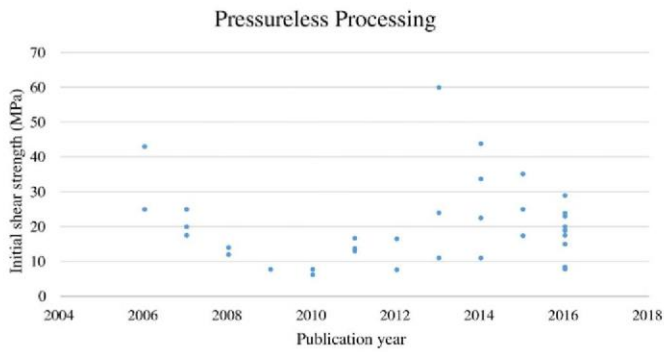sintered silver, if the sintering profile is selected correctly to remove the organics at the right time and enable strong sintering process, is independent of size.
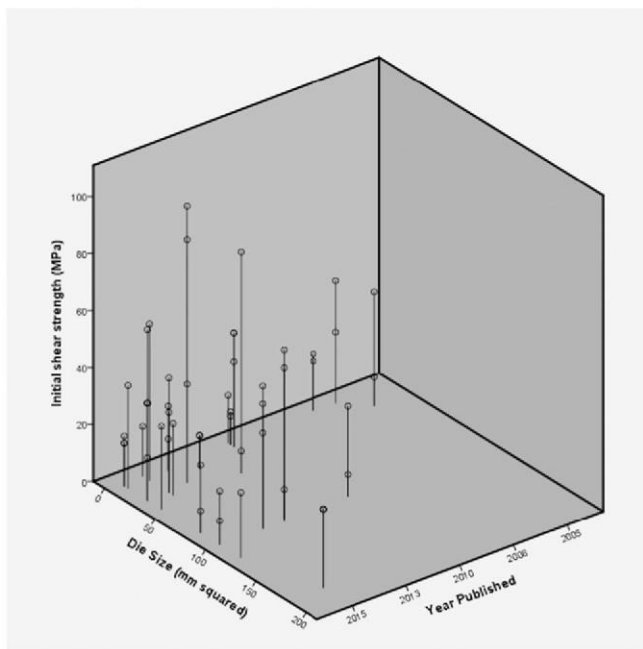

Fig. 15. Shear strengths after sintering plotted against publication year and die size.

The shear strength as a function of publication year has been plotted in Figs. 14, 15 and 16, showing the developments in the past decade. It is interesting to note that there does not appear to be any overall increase in strength shown in Fig. 14 over the past decade, indicating that the limit of shear strength may have been reached.

2.2. Shear strength after thermal aging

Fig. 17 is a summary of the shear strengths after high temperature storage with data divided into different series sorted by metallization. As can be seen from Fig. 17 different paste systems on silver metallisations have reacted differently to aging. *In-situ* observation of high temperature evolution of sintered silver indicated that the microstructure of sintered silver after a conventional sintering profile undergoes rapid microstructural changes at and above 250 °C [66]. Therefore, the observed fast changes to shear strength could be related to the fast changes of sintered silver microstructure at high temperatures. While in most cases the shear strength of die attach increases after high temperature storage at or below 300 °C, in some cases there appears to be slight reduction to shear strength, similar to the results of Lu (2007) [26].

On the other hand, shear strength of all die attach materials have reduced on Cu metallisation. Chua (2016) [48] observed that the Cu substrate would oxidise before 24 h storage at 300 °C because of oxygen penetration into the porous structure of sintered silver. According to Chua (2016) [48], even Ag metallisation on a Cu substrate cannot prevent oxidation of Cu substrate and there would be reduction of shear strength as a result. The growth of a Cu oxide layer on DBC, Cu metallisation, and Ag metallisation on Cu substrate, were all similar for the initial 50 h storage at 300 °C, each growing to a thickness of 3–5 μm. Pevsina (2014) [51] also reported that the shear strength on Cu metallisation reduces at high temperatures due to oxidation of the Cu and weakening of the die attach, which occurred at 350 °C. Therefore, the drop in shear strength of sintered silver in Lu (2007) [26] data might be related to Cu substrate oxidation as the metallisation was Ag/Ni/Cu DBC.

For Au metallisation shear strength reduces [5], as a result of fast diffusion of silver atoms towards the Au metallisation [5]. This phenomenon has been used in a modified silver sintering process using a gold mesh, to produce a thermally stable die attach material, which remained stable for at least 100 h at 600 °C and 1000 h at 450 °C [43]. While exhibiting excellent stability, shear strengths of only ~2 MPa were achieved, an order of magnitude lower than with conventional sintering, although it is expected that optimisation of mesh parameters
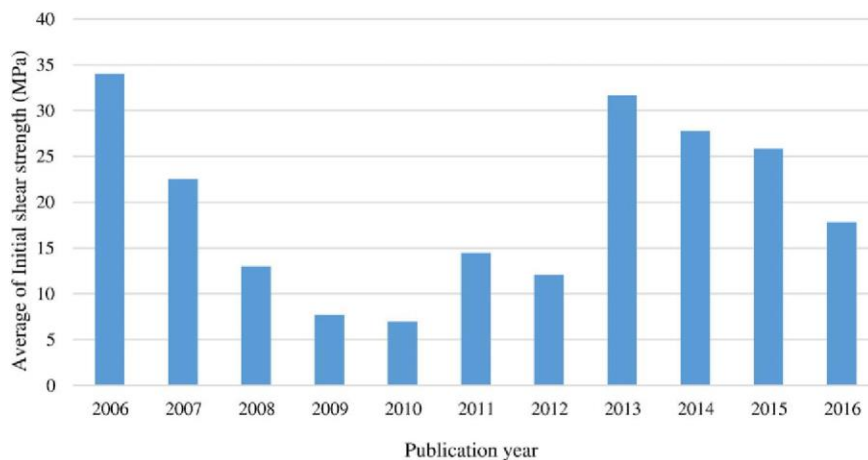

Fig. 16. Average of shear strength after sintering plotted against publication year.
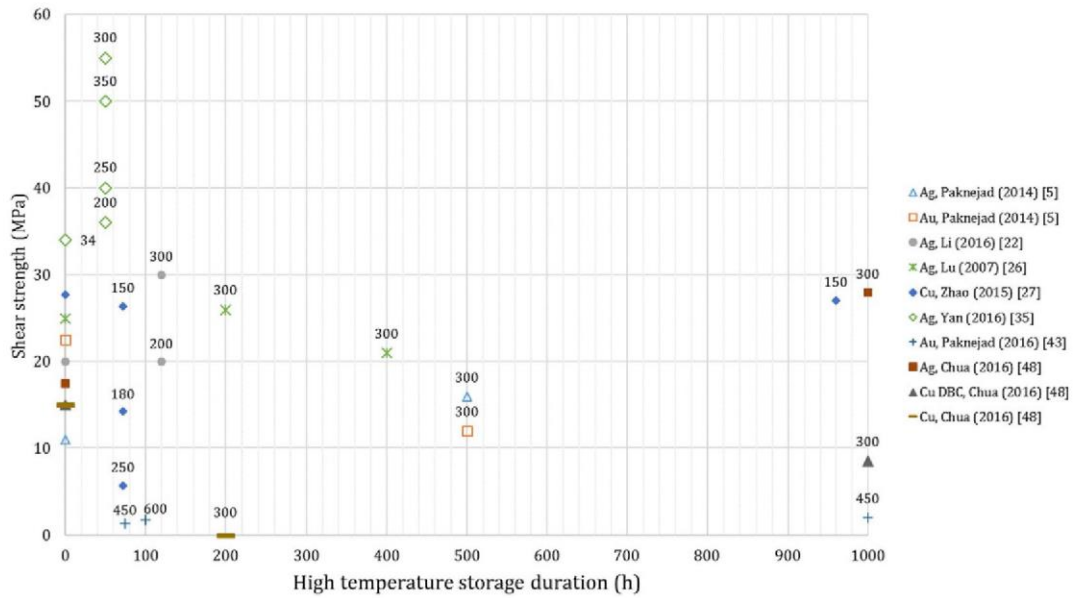
Fig. 17. Shear strengths against high temperature storage duration. The number next to each data point indicates the storage temperature for the specified duration.

should result in more comparable shear strength [43]. This technique is further discussed in Section 4.

2.3. Shear strength after thermal cycling

Comparing the thermal cycling data presents difficulties due to the different temperature ranges chosen by different groups. Nonetheless, the acquired data has been plotted against the number of thermal cycles in Fig. 18. There has been a lack of data on thermal cycling on a Cu metallisation, but according to the observations on thermal aging on Cu metallisation, it is unlikely that they can survive many cycles, and this could be the reason for lack of data on their performance. However, for the Ag and Au metallisation all the data indicates reduction of mechanical strength being in some cases minimal and in other cases significant, indicating the importance of other factors. Some sintering parameters have been investigated in attempt to understand the contribution of other parameters in thermal cycling lifetime, but due to lack of available data about sintering parameters, such comparisons are problematic. Nevertheless, the data corresponding to lower sintering pressure appeared to provide the best thermal cycling lifetime, with minimal reduction to shear strength after 500 cycles, Sakamoto (2012) [13]. For their sintering process they utilised 0.36 MPa of sintering pressure, while other studies have sintering pressure of

0 MPa or higher than 3 MPa. Therefore, it appears that a small sintering pressure might be necessary to establish good contact with metallisation and improved sintered structure before undergoing thermal stresses, while higher sintering pressure might have disadvantage, as this can densify the structure and exert higher thermal stresses as a result of lower flexibility and lower compensation of CTE mismatch. However, very surprisingly, unlike the mechanical performance after high temperature aging, the thermal cycling on Au metallisation appears to be better compared to Ag metallisation. Considering the data extracted from Bai (2006) [36] and Lu (2007) [26], the number of thermal cycles performed on the Au metallisation was both higher and resulted in smaller reduction of shear strength, indicating better reliability. The reduction of shear strength on Au metallisation has been associated with diffusion of Ag atoms towards the Ag/Au interface and formation of large voids inside the sintered structure [5] at 300 °C, but as the cycling data is acquired at a maximum of 250 °C, this effect might not have been triggered. Therefore, it might be possible to argue that the thermal reliability on Au would be better than Ag metallisation for operating temperatures at or below 250 °C, and Ag metallisation would be better for higher temperatures.

Another important point from Lu (2009) [38] data is that the sintered silver, produced by 5 MPa sintering pressure, could only survive 300 cycles from −40 to 125 °C to reach half of its initial shear
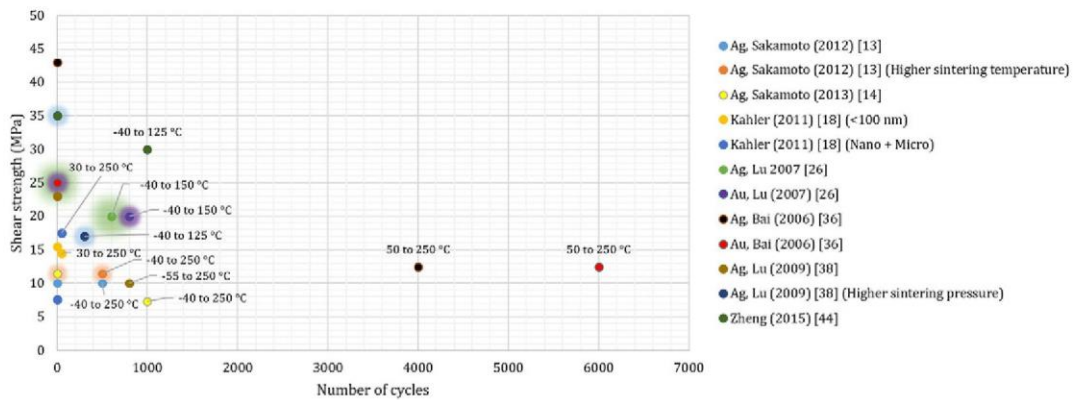

Fig. 18. Shear strength plotted against number of thermal cycles. The number next to each data point indicates thermal cycling temperature range. The glow of some data points are added to indicate presence of covered initial shear strength data of the same series with the same glow.

strength of 35 MPa. However, the sintered structure, produced with 3 MPa sintering pressure, could withstand 800 cycles of −55 to 250 °C and reaching 10 MPa from 25 MPa [38]. Therefore, higher sintering pressure can result in higher initial shear strength but less thermal cycling lifetime, most likely as a result of densification and loss of flexibility.

3. Innovative techniques:

There have been some interesting innovations by some researchers to improve properties of sintered silver joints. These techniques can be divided into two main categories; improving thermal stability or improving mechanical performance, as explored in the following subsections.

3.1. Improving thermal stability

3.1.1. Mesh interposer

Mesh structures, as shown in Fig. 19, have been introduced in a solid-solid inter-diffusion technique to establish a thermally stable die attach material [43]. In this technique, gold metallisation and a gold mesh interposer was used with the gaps in the mesh filled with silver nanoparticle paste. While the initial shear strength was lower than that of conventional techniques, the resulting die attach was found to suffer no reduction to shear strength during the extent of the trials; 1000 h at 450 °C and 100 h at 600 °C. By changing the wall design from the design in Fig. 19(c) to the ideal scenario in Fig. 19(a) it is claimed that the initial shear strength could be made comparable to conventional sintered silver strength.
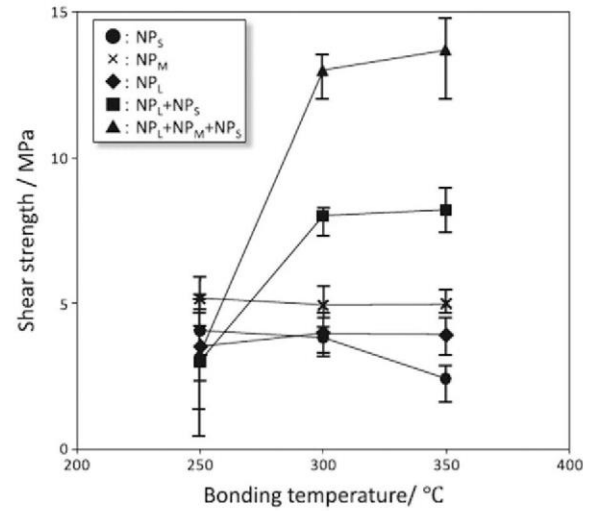
Fig. 20. Mechanical performance of three different size distribution and some of their mixtures. NP_S refers to nanoparticles with average 20 nm diameters, NP_M refers to 58.5 nm average of diameters, and NP_L has particles with average of 168 nm diameter [17].

3.2. Improving mechanical performance:

3.2.1. Mixture of three different sizes

Using a mixture of particles with average sizes of 20, 58.5, or 168 nm gained the highest shear strength compared with their separate performances [17], as seen in Fig. 20. However, this higher shear strength has been caused by higher densification of this mixture, which might not be
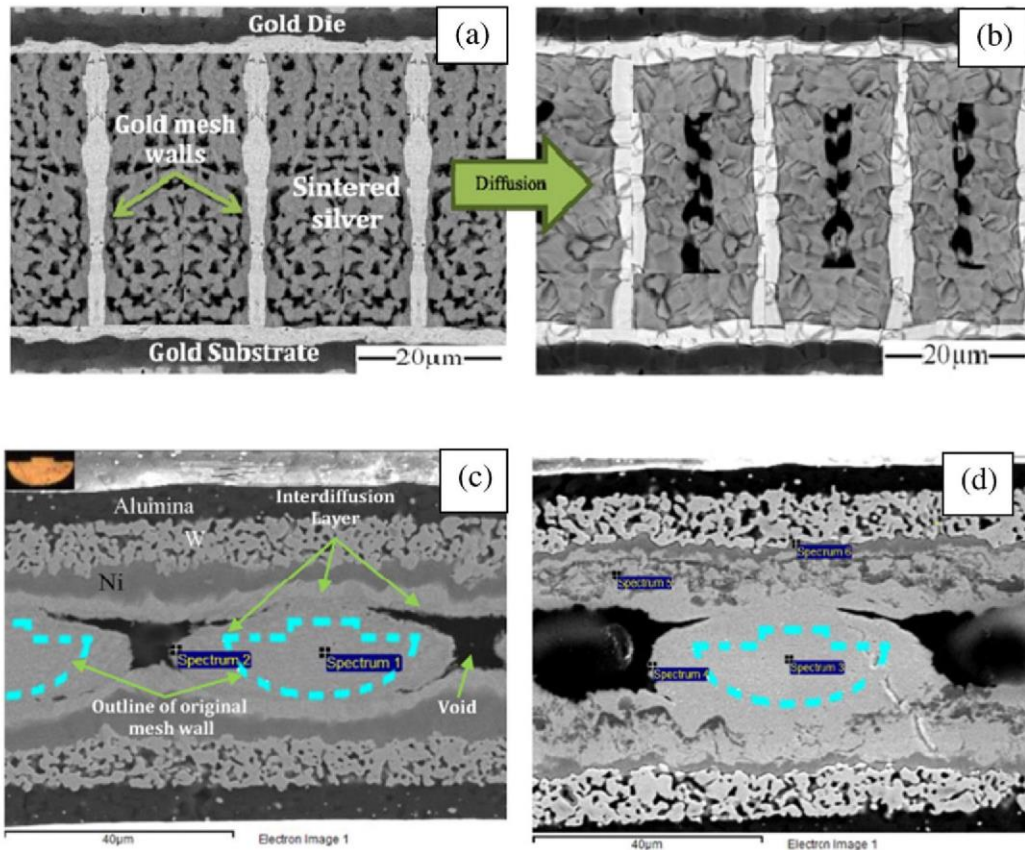
Fig. 19. Formation of a thermally stable die attach. (a) Concept after normal sintering profile. (b) Conceptual image after formation of inter-diffusion from die to substrate. (c) SEM image of a practical sample stored at 450 °C for 24 h. (d) After 1000 h at 450 °C with minor diffusion of Ni inside the die attach [43].
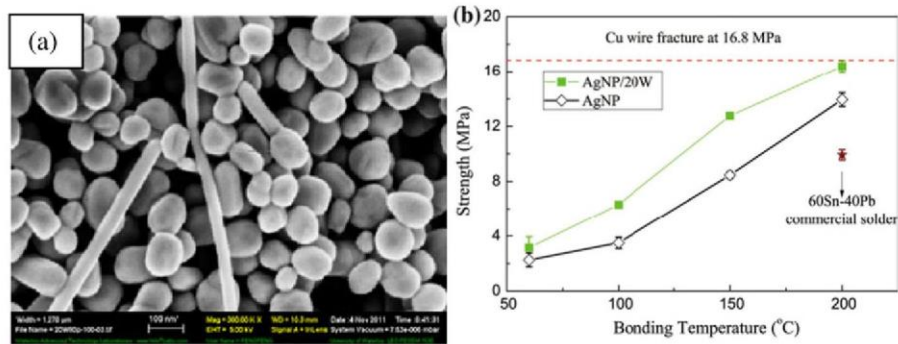
Fig. 21. Addition of silver nanowires for improved mechanical performance. (a) SEM image of mixture of nanoparticles and nanowires. (b) Higher mechanical strength as a result of addition of nanowires [19].

beneficial for applications requiring high flexibility and relaxation of CTE mismatch.

3.2.2. Utilisation of silver nanorods with nanoparticles

Addition of 10 wt% of nanowires to nanoparticles have resulted in higher shear strength of the die attach compared with the simply nanoparticles' system, as seen in Fig. 21 [19].

3.2.3. Start of sintering at high temperatures for higher densification

High current densities for fast heat up of silver nanoparticle paste have been utilised to quickly decompose the organics inside the paste and promote sintering at relatively high temperatures of >480 °C [30]. Sintering nanoparticles at high temperature would allow a densifying mechanism to act and enable higher densification and as a result higher shear strengths (Fig. 22). This technique produces many small voids, which can be beneficial in relaxing the CTE mismatch, but comparison with conventional techniques is required to demonstrate the potentially better performance. However, this technique might be hard to implement for practical die attachment, and the authors only recommend it for bus bar interconnects. However, if adopted for die attach applications it may bring many advantages. Mei (2014) [39] have also used this technique and produced strong attachment of two bare copper plates with sintered silver.

Sintering at densifying temperatures has also been achieved previously [62]. By using ligands (including 3% lignoceric acid and 10% polyvinyl butyral) with high evaporating temperatures, the nanoparticles during thermal treatment are preserved up to 350 °C, which results in start of sintering at densifying temperatures, driving grain boundary and lattice diffusions, which are more effective in densifying the structure. This enables formation of a denser sintered structure compared with nanoparticles protected by common ligands and highest sintering temperatures of about 200–300 °C. However, this produces denser structures with lower porosities of about only 5%.
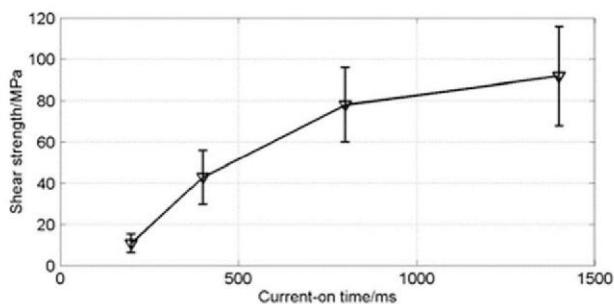

Fig. 22. Utilisation of high current densities for very short durations and establishment of good mechanical strength [30].

3.2.4. Ultrasonic mixing during sintering

Placement of the hot-plate inside an ultrasonic generator (ultrasonic cleaner) during sintering has resulted in a doubling of shear strength, from 8 MPa to 18 MPa [12]. The increased shear strength was a result of improved densification. In addition, this technique produced improved wetting at the interfaces, and therefore, improved adhesion to the die [12]. Some issues with this new technique remain, such as complication of the manufacturing process and poor sintering at the edges.

4. Conclusions

- Many papers have been published on the utilisation of silver nanoparticle paste for high temperature die attach, but they have utilised many different parameters and in this review, a large volume of data has been presented in one place in order to identify the most significant parameters.
- Higher shear strength achieved through higher densification may not lead to higher practical reliability and warrants further investigation. In particular, assemblies that survive the largest number of thermal cycles do not correlate with those exhibiting the highest initial shear strength.
- Ag metallisation appears to perform better than Cu and Au metallisation generally, but for application of thermal cycling below 250 °C, Au metallisation appears to last longer.
- No relation between the sintering temperature and shear strength could be observed, and therefore, the sintering profile should be optimised for any particular system individually rather than aiming for a particular target.
- There appears to be higher shear strength in pastes containing particles with two size distributions; either below 50 nm or nano + micron particle mix.
- Application of processing pressure on sintered silver has a direct effect on improving the initial shear strength by formation of denser structures.
- Presence of Cu inside the substrate can reduce the reliability of the system by Cu oxidation at high temperatures, mainly due to the porous nature of sintered silver allowing ingress of oxygen, and Ag metallisation over Cu cannot prevent the oxidation.
- There does not appear to be any overall increase in shear strength of die attach materials utilising silver nanoparticles over the past decade, indicating that the limit may have been reached, indicating potential requirement of different approaches to overcome the current shortcomings of pure silver nanoparticle.
- There exist some interesting techniques to improve the mechanical performance of sintered silver die attach, such as utilisation of 10 w% of nanowires inside the silver nanoparticles, ultrasonic being applied on the system during sintering, and finally utilisation of high current densities for initiating the sintering process at densifying temperature.

• Thermal stability of sintered silver was increased to 600 °C using a solid-solid inter-diffusion technique.

Supplementary data to this article can be found online at http://dx.doi.org/10.1016/j.microrel.2017.01.010.

References

[1] J. Hornberger, A. Lostetter, K. Olejniczak, T. McNutt, S.M. Lal, A. Mantooth, Silicon-carbide (SiC) semiconductor power electronics for extreme high-temperature environments, Aerospace Conference, 2004 Proceedings 2004 IEEE, vol. 4, 2004, pp. 2538–2555.

[2] C. Buttay, D. Planson, B. Allard, et al., State of the art of high temperature power electronics, Mater. Sci. Eng. B 176 (2011) 283–288.

[3] T.A. Tollefsen, O.M. Løvvik, K. Aasmundtveit, A. Larsson, Effect of temperature on the die shear strength of a Au-Sn SLID bond, Metall. Mater. Trans. A 44 (2013) 2914–2916.

[4] E. Ide, S. Angata, A. Hirose, K.F. Kobayashi, Metal-metal bonding process using Ag metallo-organic nanoparticles, Acta Mater. 53 (2005) 2385–2393.

[5] S. Paknejad, G. Dumas, G. West, G. Lewis, S. Mannan, Microstructure evolution during 300 °C storage of sintered Ag nanoparticles on Ag and Au substrates, J. Alloys Compd. 617 (2014) 994–1001.

[6] R. Khazaka, R. Hanna, et al., Survey of high-temperature reliability of power electronics packaging components, IEEE Trans. Power Electron. 30 (2015) 2456–2464.

[7] K.S. Siow, Y. Lin, Identifying the development state of sintered silver (Ag) as bonding material in microelectronic packaging via a patent landscape study, J. Electron. Packag. (2016).

[8] K.S. Siow, Are sintered silver joints ready for use as interconnect material in microelectronic packaging? J. Electron. Mater. 43 (2014) 947–961.

[9] K.S. Siow, Mechanical properties of nano-silver joints as die attach materials, J. Alloys Compd. 514 (2012) 6–19.

[10] V.R. Manikam, K.Y. Cheong, Die attach materials for high temperature applications: a review, IEEE Trans. Compon. Packag. Manuf. Technol. 1 (2011) 457–478.

[11] S. Fu, Y. Mei, G.-Q. Lu, X. Li, G. Chen, X. Chen, Pressureless sintering of nanosilver paste at low temperature to join large area (≥100 mm²) power chips for electronic packaging, Mater. Lett. 128 (2014) 42–45.

[12] Y. Li, H. Jing, Y. Han, L. Xu, G. Lu, Microstructure and joint properties of nano-silver paste by ultrasonic-assisted pressureless sintering, J. Electron. Mater. 45 (2016) 3003–3012.

[13] S. Sakamoto, K. Suganuma, Thermo mechanical reliability of low-temperature low-pressure die bonding using thin Ag flake pastes, Integrated Power Electronics Systems (CIPS), 2012 7th International Conference on 2012, pp. 1–2.

[14] S. Sakamoto, T. Sugahara, K. Suganuma, Microstructural stability of Ag sinter joining in thermal cycling, J. Mater. Sci. Mater. Electron. 24 (2013) 1332–1340.

[15] K. Xiao, J.N. Calata, H. Zheng, K.D. Ngo, G.-Q. Lu, Simplification of the nanosilver sintering process for large-area semiconductor chip bonding: reduction of hot-pressing temperature below 200/spl deg/C, IEEE Trans. Compon. Packag. Manuf. Technol. 3 (2013) 1271–1278.

[16] M. Maruyama, R. Matsubayashi, H. Iwakuro, S. Isoda, T. Komatsu, Silver nanosintering: a lead-free alternative to soldering, Appl. Phys. A 93 (2008) 467–470.

[17] Y. Morisada, T. Nagaoka, M. Fukusumi, Y. Kashiwagi, M. Yamamoto, M. Nakamoto, H. Kakiuchi, Y. Yoshida, A low-temperature pressureless bonding process using a trimodal mixture system of Ag nanoparticles, J. Electron. Mater. 40 (2011) 2398–2402.

[18] J. Kahler, N. Heuck, G. Palm, A. Stranz, A. Waag, E. Peiner, Low-pressure sintering of silver micro-and nanoparticles for a high temperature stable pick & place die attach, Microelectronics and Packaging Conference (EMPC), 2011 18th European 2011, pp. 1–7.

[19] P. Peng, A. Hu, B. Zhao, A.P. Gerlich, Y.N. Zhou, Reinforcement of Ag nanoparticle paste with nanowires for low temperature pressureless bonding, J. Mater. Sci. 47 (2012) 6801–6811.

[20] Y. Yan, X. Chen, X. Liu, G.-Q. Lu, Die bonding of single emitter semiconductor laser with nano-scale silver paste, Electronic Packaging Technology and High Density Packaging (ICEP-HDP), 2011 12th International Conference on 2011, pp. 1–5.

[21] T. Wang, X. Chen, G.-Q. Lu, G.-Y. Lei, Low-temperature sintering with nano-silver paste in die-attached interconnection, J. Electron. Mater. 36 (2007) 1333–1340.

[22] H. Li, H. Jing, Y. Han, G.-Q. Lu, L Xu, T. Liu, Interface evolution analysis of graded thermoelectric materials joined by low temperature sintering of nano-silver paste, J. Alloys Compd. 659 (2016) 95–100.

[23] Q. Xu, Y. Mei, X. Li, G.-Q. Lu, Correlation between interfacial microstructure and bonding strength of sintered nanosilver on ENIG and electroplated Ni/Au direct-bond-copper (DBC) substrates, J. Alloys Compd. 675 (2016) 317–324.

[24] . Wang, M. Li, H. Ji, C. Wang, Rapid pressureless low-temperature sintering of Ag nanoparticles for high-power density electronic packaging, Scr. Mater. 69 (2013) 789–792.

[25] M. Wang, Y. Mei, X. Li, G. Lu, Relationship between transient thermal impedance and shear strength of pressureless sintered silver as die attachment for power devices, Electronic Packaging and iMAPS All Asia Conference (ICEP-IACC), 2015 International Conference on 2015, pp. 559–564.

[26] G.-Q. Lu, J. Calata, G. Lei, X. Chen, Low-temperature and pressureless sintering technology for high-performance and high-temperature interconnection of semiconductor devices, Thermal, Mechanical and Multi-Physics Simulation Experiments in Microelectronics and Micro-Systems, 2007 EuroSime 2007 International Conference on 2007, pp. 1–5.

[27] S.-Y. Zhao, X. Li, Y.-H. Mei, G.-Q. Lu, Study on high temperature bonding reliability of sintered nano-silver joint on bare copper plate, Microelectron. Reliab. 55 (2015) 2524–2531.

[28] S.-Y. Zhao, X. Li, Y.-H. Mei, G.-Q. Lu, Novel interface material used in high power electronic die-attaching on bare Cu substrates, J. Mater. Sci. Mater. Electron. 27 (10) (2016) 10941–19050.

[29] C. Buttay, A. Masson, J. Li, M.C. Johnson, M. Lazar, C. Raynaud, H. Morel, et al., Die attach of power devices using silver sintering-bonding process optimization and characterization, Proceedings of the High Temperature Electronics Network Conference (HiTEN 2011) 2011, pp. 1–7.

[30] G. Lu, W. Li, Y. Mei, G. Chen, X. Li, X. Chen, Characterizations of Nanosilver Joints by Rapid Sintering at Low Temperature for Power Electronic Packaging, 2014.

[31] N. Heuck, G. Palm, T. Sauerberg, A. Stranz, A. Waag, A. Bakin, SiC-die-attachment for high temperature applications, Mater. Sci. Forum (2010).

[32] C.B. O'Neal, B. McGee, B. McPherson, J. Stabach, R. Lollar, R. Liederbach, B. Passmore, Advanced materials for high temperature, high performance, wide bandgap power modules, J. Electron. Mater. 45 (2016) 245–254.

[33] A. Masson, C. Buttay, H. Morel, C. Raynaud, S. Hascoet, L. Gremillard, High-temperature die-attaches for SiC power devices, Power Electronics and Applications (EPE 2011), Proceedings of the 2011-14th European Conference on 2011, pp. 1–10.

[34] Y. Mei, G. Chen, Y. Cao, X. Li, D. Han, X. Chen, Simplification of low-temperature sintering nanosilver for power electronics packaging, J. Electron. Mater. 42 (2013) 1209–1218.

[35] J. Yan, D. Zhang, G. Zou, L. Liu, H. Bai, A. Wu, Y.N. Zhou, Sintering bonding process with Ag nanoparticle paste and joint properties in high temperature environment, J. Nanomater. 2016 (2016) 32.

[36] J.G. Bai, G.-Q. Lu, Thermomechanical reliability of low-temperature sintered silver die attached SiC power device assembly, IEEE Trans. Device Mater. Reliab. 6 (2006) 436–441.

[37] H. Zheng, J. Calata, K. Ngo, S. Luo, G.-Q. Lu, Low-pressure (<5 MPa) low-temperature joining of large-area chips on copper using nanosilver paste, Integrated Power Electronics Systems (CIPS), 2012 7th International Conference on 2012, pp. 1–6.

[38] G.-Q. Lu, M. Zhao, G. Lei, J.N. Calata, X. Chen, S. Luo, Emerging lead-free, high-temperature die-attach technology enabled by low-temperature sintering of nano-scale silver pastes, Electronic Packaging Technology & High Density Packaging, 2009 ICEPT-HDP'09 International Conference on 2009, pp. 461–466.

[39] Y.-H. Mei, Y. Cao, G. Chen, X. Li, G.-Q. Lu, X. Chen, Characterization and reliability of sintered nanosilver joints by a rapid current-assisted method for power electronics packaging, IEEE Trans. Device Mater. Reliab. 14 (2014) 262–267.

[40] J. Li, C.M. Johnson, C. Buttay, W. Sabbah, S. Azzopardi, Bonding strength of multiple SiC die attachment prepared by sintering of Ag nanoparticles, J. Mater. Process. Technol. 215 (2015) 299–308.

[41] S. Seal, M.D. Glover, H.A. Mantooth, Nanosilver preform assisted die attach for high temperature applications, Applied Power Electronics Conference and Exposition (APEC), 2015 IEEE 2015, pp. 2925–2930.

[42] T.G. Lei, J.N. Calata, G.-Q. Lu, X. Chen, S. Luo, Low-temperature sintering of nanoscale silver paste for attaching large-Area < formula formulatype=, Components and Packaging Technologies, IEEE Trans. Compon. Packag. Technol. 33 (2010) 98–104.

[43] S.A. Paknejad, A. Mansourian, Y. Noh, K. Khtatba, S.H. Mannan, Thermally stable high temperature die attach solution, Mater. Des. 89 (2016) 1310–1314.

[44] H. Zheng, K. Ngo, G.-Q. Lu, Temperature Cycling Reliability Assessment of Die-Attachment on Bare Copper by Pressureless Nanosilver Sintering, 2015.

[45] F. Le Henaff, S. Azzopardi, E. Woirgard, T. Youssef, S. Bontemps, J. Joguet, Lifetime evaluation of nanoscale silver sintered power modules for automotive application based on experiments and finite-element modeling, IEEE Trans. Device Mater. Reliab. 15 (2015) 326–334.

[46] S.-Y. Zhao, X. Li, Y.-H. Mei, G.-Q. Lu, Effect of silver flakes in silver paste on the joining process and properties of sandwich power modules (IGBTs chip/silver paste/bare Cu), J. Electron. Mater. (2016) 1–11.

[47] W. Guo, Z. Zeng, X. Zhang, P. Peng, S. Tang, Low-temperature sintering bonding using silver nanoparticle paste for electronics packaging, J. Nanomater. 2015 (2015) 10.

[48] S. Chua, K.S. Siow, Microstructural studies and bonding strength of pressureless sintered nano-silver joints on silver, direct bond copper (DBC) and copper substrates aged at 300 °C, J. Alloys Compd. 687 (2016) 486–498.

[49] W. Rmili, N. Vivet, S. Chupin, T. Le Bihan, G. Le Quilliec, C. Richard, Quantitative analysis of porosity and transport properties by FIB-SEM 3D imaging of a solder based sintered silver for a new microelectronic component, J. Electron. Mater. 45 (4) (2016) 2242–2251.

[50] R. Wilcoxon, M. Dimke, C. Xie, Thermal performance and reliability assessment of nano-sintered silver die attach materials, Thermal Measurement, Modeling & Management Symposium (SEMI-THERM), 2015 31st 2015, pp. 240–247.

[51] Z. Pevsina, V. Vykoukal, M. Palcut, J. Sopoušek, Shear strength of copper joints prepared by low temperature sintering of silver nanoparticles, Electron. Mater. Lett. 10 (2014) 293–298.

[52] Q. Xiliang, C. Yang, L. Tiesong, H. Peng, W. Jun, L. Ping, G. Xiaolong, Large-scale synthesis of silver nanoparticles by aqueous reduction for low-temperature sintering bonding, J. Nanomater. 2014 (2014).

[53] G. Chen, L. Yu, Y.-H. Mei, X. Li, X. Chen, G.-Q. Lu, Reliability comparison between SAC305 joint and sintered nanosilver joint at high temperatures for power electronic packaging, J. Mater. Process. Technol. 214 (2014) 1900–1908.

[54] G. Chen, Z.-S. Zhang, Y.-H. Mei, X. Li, G.-Q. Lu, X. Chen, Ratcheting behavior of sandwiched assembly joined by sintered nanosilver for power electronics packaging, Microelectron. Reliab. 53 (4) (2013) 645–651.

[55] J. Felba, T. Falat, A. Mo'scicki, Nano sized silver for electronic packaging, Nanotechnology (IEEE-NANO), 2013 13th IEEE Conference on 2013, pp. 30–33.

[56] X. Li, G. Chen, L. Wang, Y.-H. Mei, X. Chen, G.-Q. Lu, Creep properties of low-temperature sintered nano-silver lap shear joints, Mater. Sci. Eng. A (2013).

[57] R. Durairaj, R. Ashayer, H.R. Kotadia, N. Haria, C. Lorenz, O. Mokhtari, S.H. Mannan, Pressure free sintering of silver nanoparticles to silver substrate using weakly binding ligands, Nanotechnology (IEEE-NANO), 2012 12th IEEE Conference on 2012, pp. 1–4.

[58] S. Sakamoto, K. Suganuma, Low temperature die-bonding with Ag flakes, Microelectronics and Packaging Conference (EMPC), 2011 18th European 2011, pp. 1–5.

[59] Y. Mei, G. Chen, L. Guo-Quan, X. Chen, Effect of joint sizes of low-temperature sintered nano-silver on thermal residual curvature of sandwiched assembly, Int. J. Adhes. Adhes. 35 (2012) 88–93.

[60] G. Chen, X.-H. Sun, P. Nie, Y.-H. Mei, G.-Q. Lu, X. Chen, High-temperature creep behavior of low-temperature-sintered nano-silver paste films, J. Electron. Mater. 41 (2012) 782–790.

[61] Y. Mei, G. Chen, X. Li, G.-Q. Lu, X. Chen, Evolution of curvature under thermal-cycling in sandwich assembly bonded by sintered nano-silver paste, Solder. Surf. Mount Technol. 25 (2013) 5.

[62] J.G. Bai, T.G. Lei, J.N. Calata, G.-Q. Lu, Control of nanosilver sintering attained through organic binder burnout, J. Mater. Res. 22 (2007) 3494.

[63] Y. Akada, H. Tatsumi, T. Yamaguchi, A. Hirose, T. Morita, E. Ide, Interfacial bonding mechanism using silver metallo-organic nanoparticles to bulk metals and observation of sintering behavior, Mater. Trans. 49 (2008) 1537–1545.

[64] J. Guofeng Bai, J. Yin, Z. Zhang, G.-Q. Lu, J.D. van Wyk, High-temperature operation of SiC power devices by low-temperature sintered silver die-attachment, IEEE Trans. Adv. Packag. 30 (2007) 506–510.

[65] T. Wang, M. Zhao, X. Chen, G.-Q. Lu, K. Ngo, S. Luo, Shrinkage and sintering behavior of a low-temperature sinterable nanosilver die-attach paste, J. Electron. Mater. 41 (2012) 2543–2552.

[66] S.A. Paknejad, A. Mansourian, J. Greenberg, K. Khtatba, L. Van Parijs, S.H. Mannan, Microstructural evolution of sintered silver at elevated temperatures, Microelectron. Reliab. 63 (2016) 125–133.

[67] S. Fu, Y. Xie, Y. Mei, Reliability of pressureless sintered nanosilver for attaching IGBT devices, International Conference on Electronics Packaging (ICEP), 2016, 2016, pp. 382–385.

[68] L. Jiang, T.G. Lei, K.D. Ngo, G.-Q. Lu, S. Luo, Evaluation of thermal cycling reliability of sintered nanosilver versus soldered joints by curvature measurement, IEEE Trans. Compon. Packag. Manuf. Technol. 4 (2014) 751–761.

[69] M. Edwards, K. Brinkfeldt, U. Rusche, T. Bukes, G. Gaiser, M. Da Silva, D. Andersson, The shear strength of nano-Ag sintered joints and the use of Ag interconnects in the design and manufacture of SiGe-based thermo-electric modules, Microelectron. Reliab. 55 (2015) 722–732.

[70] Y. Tan, X. Li, G. Chen, Y. Mei, X. Chen, Three-dimensional visualization of the crack-growth behavior of nano-silver joints during shear creep, J. Electron. Mater. 44 (2015) 761–769.

[71] P. Peng, A. Hu, A.P. Gerlich, G. Zou, L. Liu, Y.N. Zhou, Joining of silver nanomaterials at low temperatures: processes, properties, and applications, ACS Appl. Mater. Interfaces 7 (23) (2015) 12597–12618.

Addendum to Section 2.4

Different authors have concluded different optimum results for paste materials and processing conditions because of the large number of variables involved. Some of these variables may not be reported in detail, for example, application method of paste to the substrate and scrubbing motion when die is placed on paste, see Chapter 5. Indeed, the lack of standardization, causing the variations and scatter in the reported figures, such as the scatter in Figures 3 and 10, may itself be considered a major conclusion of this section. Another complicating factor may be the fact that some authors may have reported all their results and others only their best results, omitting combinations that did not work well. Some conclusions are unaffected by these factors because of very strong correlations observed, like the bullet point 6 inside the conclusions, or because they are based on direct evidences from the referenced papers, such as bullet points 2, 7, 9 and 10. However, bullet points 3, 4 and 5 may be affected by these factors and should therefore be treated with caution, pending further experimental trials.

Moreover, an important consideration for the conclusion recommending use of Au metallisation for operating temperatures below 250 °C is that it is based on thermal cycling data, and therefore, additional high temperature storage of sintered silver over gold metallisation at this temperature is recommended for development of a firmer conclusion.

Furthermore, please note that Table 1 of the supplementary data is provided below.

Table 1: Data obtained from references utilised for analysis in Section 2 of the review paper above.

First author	Year published	Reference	Particle size (distribution or average)	Die Size (mm²)	Die metallization	Substrate metallization	Highest sintering temperature (°C)	Sintering duration (min)	Sintering pressure (MPa)	Shear strength (MPa)	Aging temperature	Aging duration (h)	Aging shear strength (MPa)	Temperature range (°C)	Number of cycles	One cycle duration (h)	Shear strength (MPa)
S. Fu	2014	11	20 nm – 20 µm	100	Ag	Ag	225	10	1.77	50							
							250	10	0	33.6							
							250	60	0	43.8							
Y. Li	2016	12	nano to micro	100	Ag	Ag	265	30	0	8.4							
										18.9							
S. Sakamoto	2011	13	100 nm	4	Ag	Ag	160	60	0.36	10				250 to -40	500	1	Almost constant
							200	60	0.36	11.5							
S. Sakamoto	2013	14	100 nm	16	Ag	Ag	200	60	0.4	11.5				250 to -40	1000	1	11.5
														180 to -40	1000	1	7.3
														180 to -40	500	1	7.3
K. Xiao	2013	15		100	Ag	Ag	275	30	0	11							
								10	10	53.8							
S. A. Paknejad	2014	5	30 nm	6.25	Ag	Ag	295	18	0	11	300	500	16				
					Ag	Au				22.5	300	500	12				
M. Maruyama	2008	16	16 w% 5 nm + 84 w% 400 nm				350	25	0	12							
									1	32							
			40 w% 5 nm + 60 w% 400nm				350	25	0	14							
									1	37							
Y. Morisada	2011	17	Mixture 20, 59, and 168 nm		Cu	Cu	350	5	0	13.7							
					Cu	Cu	300	5	0	13							
J. Kahler	2011	18	<100 nm				230	2	12	15.5				30 to 250	50	0.033	14.5
			nano + micro							7.5							17.5
P. Peng	2012	19	50 to 100 nm + 20% nanowires 50 to 100 nm with 8 - 15 µm length		Cu	Cu	200	60	0	16.5							
Y. Yan	2011	20	<50 nm	1.6	Au	Au	280	30	0	16.7							
T. Wang	2007	21		1.21	Ag	Ag	285	60	0	17.52							
							285	120	0	19.97							

Author	Year	Ref	Particle size	Area	Metal 1	Metal 2	T1	t1	P1	O	B1	B2	B3	C1	C2	C3	C4
H. Li	2016	22			Ag	Ag	260	20	0	20	200	120	20				
											300	120	30				
Q. Xu	2016	23	40 nm	81	Ag	Au	275	30	0	23.9							
										7.8							
S. Wang	2013	24	13 nm				200	0.5	0	24							
							200	20		60							
M. Y. Wang	2015	25		32.5			250	10	0	25							
G. Q. Lu	2007	26			Ag	Ag	275	10	0	25	300	200	26				
					Ag	Ag	275	10	0		300	400	21	150 to -40	600	1	20
					Ag	Au	325	10	0	25				150 to -40	800	1	20
S. Y. Zhao	2015	27	<50 nm	182.25	Ag	Cu	280	10	1.5	27.7	150	72	26.4				
											150	960	27.1				
											180	72	14.2				
											250	72	5.7				
S. Y. Zhao	2016	28	nano and sub-micro particles (105nm av.) with flakes (4.8 μm av.)	42.25		Cu	270	30	0	29							
C. Buttay	2011	29	8 - 12 nm	7.29	Ag	Au	285	60	6	30							
					Ag	Cu				40							
G. Lu	2014	30		25	Ag	Ag	484	0.01	10	34.3							
					Ag	Ag	484	0.01	10	85							
N. Heuck	2010	31		576	Ag	Au	320	60	3.5	35							
					Ag	Au	320	60	0	6.2							
C. B. O'Neal	2016	32		9	Au	Au				36							
E. Ide	2005	4	11 nm	19.63	Cu	Cu	300	5	5	40							
			100 nm		Cu	Cu	300	5	5	10							
A. Masson	2011	33	8 - 12 nm	7.29		Cu	285	60	6	40							
Y. Mei	2013	34	30 nm	100	Ag	Ag	275	10	5	60							
J. Yan	2016	35	about 40 nm	28.27	Ag	Ag	250	30	7.5	60							
							250	30	0	15							
							250	30	2	34	200	50	36				
											250	50	40				

Author	Year	Ref	Particle size	Value	Mat1	Mat2	Temp	Time	Pressure	Value				Range	Cycles		Value
											300	50	55				
											350	50	50				
J. G. Bai	2006	36	30 – 50 nm	2.38	Ag	Ag	300	40	0	43				250 to 50	4000		21.5
					Ag	Au	300	90	0	25				250 to 50	6000		12.5
H. Zheng	2012	37		36	Ag	Cu	275		0	7.6							
					Ag	Cu	275		12	77.4							
G. Q. Lu	2009	38			Ag	Ag	275	10	3	23	300	200	26	250 to -55	800		10
							275	10	3	23	300	400	20				
							275	10	5	35				125 to -40	300		17
							275	10	0	7.7							
Y. H. Mei	2014	39	30 - 50 nm	25						97							
J. Li	2015	40		9	Au	Au	240		12	54.9							
S. Seal	2015	41	50 nm av.	2.25	Ag	Ag	300	45	0	17.4							
T. G. Lei	2010	42		100	Ag	Ag	275	20	0	7.7							
					Ag	Ag	275	20	5	31.6							
S. A. Paknejad	2016	43			Au	Au			0		450	75	1.35				
									0		450	1000	1.95				
									0		600	100	1.7				
H. Zheng	2015	44					280	10	0	35				125 to -40	1000	1	30
F. Le Henaff	2015	45		14.44		Ag	250	0.16	10					125 to -40	2800	1	Failed at
						Au, or Cu	250	0.16	10					125 to -40	>6000	1	Passed
S. Y. Zhao	2016	46	20 – 200 nm and 1 - 5 µm long flakes	121		Cu	270	30	0	23							
W. Guo	2015	47	20 - 80 nm (av. 40 nm)	28.27	Ag	Ag	250	5	3	28							
					Ag	Ag	350	5	3	40							
S. T. Chua	2016	48	10 - 20 nm	5.22	Ag	Ag	250	60	0	17.5	300	1000	28				
					Ag	Cu DBC				15	300	1000	8.5				
					Ag	Cu				15	300	200	0				

3 Microstructural evolution of sintered silver at elevated temperatures
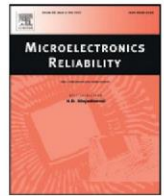
Microstructural evolution of sintered silver at elevated temperatures

Seyed Amir Paknejad *, Ali Mansourian, Julian Greenberg, Khalid Khtatba, Linde Van Parijs, Samjid H. Mannan

King's College London, Physics Department, Strand, London, WC2R 2LS, UK

ABSTRACT

Reduction in the sintering temperature of metal powders by lowering particle size into the nanoparticle range has resulted in a new class of porous sintered joining materials. Especially promising are sintered silver based materials which can be used to form bonds between wide-bandgap semiconductor die and circuit boards for use in high temperature applications. This work shows that for these materials the exterior sintered silver surface oxidizes preventing surface morphology changes, while the interior pore surfaces of the porous silver remain largely oxide-free. These pore surfaces facilitate fast atomic movement resulting in grain growth and changes in the internal microstructure. Morphology changes in the temperature range 200–400 °C are presented both as statistical averages of grain size and, uniquely in this type of study, by tracking individual pores and grains. It is shown that the internal structure will undergo changes during high temperature storage in contrast to the stable outer surface. A new technique, utilizing the electromigration effect to check the relative surface mobility of atoms in the interior pores and exterior surfaces was used to support the conclusions deduced from thermal ageing experiments. Finally, we speculate that the stability of the exterior surface could be reproduced in the interior if the chemistry of the paste was altered to allow formation of a passivating layer on the interior pores during the final stages of the sintering process, resulting in formation of a stable die attach material for applications of up to 400 °C, for which there is an urgent need.

© 2016 Elsevier Ltd. All rights reserved.

1. Introduction

The operating temperature of electronic materials in hybrid automotive, aerospace, space exploration, and deep oil and gas exploration can reach 300 °C and beyond [1]. Current high temperature die attach materials such as high temperature solders or Solid Liquid Inter-Diffusion (SLID) bonding materials suffer from high homologous temperatures and Pb content in case of high temperature solders or rapid reduction in mechanical strength by increase in temperature in case of SLID systems [2]. Therefore, there is a requirement for new joining materials that can be processed at low temperatures but that retains joint strength at high temperatures.

One of the potential solutions involves utilization of the unique properties of nanoparticles. By reduction in particle size, the ratio between surface area and volume increases, contributing to a rise in surface energy and a melting point that is considerably lower than that of the bulk material [3]. For example, in the case of silver the melting point of bulk silver is 961 °C, while melting point of 2.4 nm silver particles is 350 °C [4]. This feature of nanoparticles has been researched in the past decade in order to decouple the processing temperature from operating temperature of high-temperature electronic packaging materials, with silver receiving special interest because of its desirable

mechanical, electrical and thermal properties [4–9] as well as the noble metal nature of silver that prevents excessive oxide formation. In this case, the attachment or interconnects can be formed at considerably lower temperatures than the melting point of the bulk material which determines the ultimate operating temperature. The high surface energy available and noble metal surface of silver also allows sintering to take place without pressure being placed on the die; an added benefit for manufacturers, but one which leads to the final sintered structure containing 20–30% of pores.

Although many studies have been performed on the sintering behaviour of nanoparticles [10,11], and also the mechanical properties of their sintered structures [8,9,12,13], there exists few detailed studies on the high temperature behaviour and stability of sintered silver at temperatures above 300 °C as a high temperature die attach (excepting [14,15]), while previous studies below 300 °C concentrate on bulk mechanical properties and statistical averages of microstructural properties [8,9,16–20]. In the present work, we determine the nature and speed of microstructural changes in sintered silver throughout the 200–400 °C temperature range and investigate the atomic migration mechanisms that lead to these changes. Tracking of changes in individual grains and pores is found to be complicated by the fact that any exposure of the internal pore surfaces to air leads to rapid oxidation and freezing of the microstructure in its original state, similarly to the original exterior surface of the material. Therefore, we have utilised optical microscopy and a glass substrate to prevent the internal pore surfaces

---

70

from oxidizing while enabling in-situ observations to take place. These microstructural changes would in most cases lead to unreliability and weakening strength [9,17–19] so that these studies are an innovative technique for understanding long term mechanical reliability and strength preservation of sintered silver for applications in the range 200–400 °C.

2. Experimental

In these studies, two commercially available silver nanoparticle pastes produced by NBE Tech under the names of NanoTach® X and NanoTach® N have been utilised. NanoTach® N is recommended for small size die of 3×3 mm, while NanoTach® X is recommended for attachment of 10×10 mm die in a pressure-less sintering process. The composition of NanoTach® X is shown in Table 1 below. The assemblies, listed in Table 2, were all sintered using the recommended temperature profile from the paste manufacturer under zero applied pressure.

In a previous study [19], samples were cross sectioned after sintering, and aged at 300 °C for 24, 100 and 500 h to track properties such as porosity and average pore size. In that study the evolution of individual pores and grains could not be tracked continuously. In the current experiments, in order to track changes occurring inside the sintered silver microstructure and investigate them continuously, samples were assembled by manual deposition of the NanoTach® X paste onto glass slides followed by placement of approximately 150 μm thick, 10×10 mm Menzel–Gläser cover-slips on top of the paste. To investigate the grain growth mechanisms of the sintered silver, these samples have been placed on a cartridge heater at 250, 300, 350 and 400 °C and the grain evolution has been observed in-situ for up to 7 h using an optical microscope (See Fig. 1), while one sample has been placed inside a furnace at 200 °C for 5 h. This experiment is referred to as sample set 1.

Observation of high temperature behaviour of sintered silver structure through the cover-slip provides information on microstructural changes similar to those occurring inside non-sectioned samples which have not been exposed to air. The presence of the cover-slip planarizes the initial microstructure and may affect parameters such as local porosity. However, comparison with samples that have been aged at 300 °C and then cross-sectioned [19] show qualitatively similar results indicating that the same mechanisms are active. The optical images were then analysed using Image J 1.46r coupled with the image processing toolbox in Matlab with a methodology [21] that allowed the microstructural evolution of sintered silver at high temperatures to be studied statistically (e.g. average grain size). In this method the optical images of the sintered structures have been segmented using an Image J predesigned function to separate the grains and their sizes have been measured using Matlab to calculate the average grain sizes.

The second set of samples was prepared by deposition of the paste into wire shaped gaps with approximate dimensions of 1 mm by 1 mm cross-section and 3 mm length for the first sample and approximately 150 μm by 150 μm cross section and 4 mm length for the remaining samples of this set. The first sample was stored at 300 °C in air and the remainder were stored at 300 and 400 °C inside a vacuum of 5 mPa and at 450 and 500 °C in air to study microstructural evolution of the free surfaces.

Table 1
NanoTach® X composition.

Components	Weight percent
Silver	70–85
Silver oxide	0–10
Cellulose	1–8
Alpha terpineol	5–20
Menhaden fish oil	0–2
Isopropanol	<1
Ethanol	<1

Table 2
Sample sets.

Sample set no.	Purpose of experiment	Paste type and surface dimensions
1	Observation of microstructure evolution on a surface not exposed to air using optical microscope.	NanoTach® X 10×10 mm $\times$ 100 μm
2	Observation of exterior surface evolution under different atmospheres using SEM.	NanoTach® X 150×150 μm $\times$ 4 mm and $1 \times 1 \times 3$ mm
3	Observation of interior microstructure evolution after cross sectioning using SEM.	NanoTach® N 2.5×2.5 mm $\times$ 30 μm
4	Observation of exterior surface evolution after acid cleaning using SEM.	NanoTach® X $r = 2$ mm
5	Comparison of exterior and interior atomic migration patterns during electromigration using SEM.	NanoTach® X $175 \times 175 \times 812$ μm

The third sample set consisted of a single sample selected for thermal ageing after being first cross sectioned and polished in an attempt to observe evolution of the interior of sintered silver continuously. After the sintering step using NanoTach® N followed by cross sectioning, the sample was mounted using a hot mounting resin (LevoFast) from Struers, which consisted of melamine with minerals and glass filler. The sample was mechanically polished using successively finer grades of silicon carbide cloth before final polishing with water based suspensions of 3 and 0.25 μm monocrystalline diamonds. The hot mounting resin was selected to withstand high temperature storage. The assembly was stored at 300 °C in air in an oven for 1, 4, 5, and 20 h consecutively (30 h in total), and observed under a Scanning Electron Microscope (SEM) to track changes.

The fourth set of samples was prepared by sintering of the NanoTach® X paste inside glass sample holders, which were designed for surface cleaning of the samples by perchloric acid (effective for removing organic contamination on silver without causing damage from the utilised concentration [22,23]) before high temperature storage. After manual deposition of paste into the holder and sintering, the samples were stored for 30 min inside an aqueous solution containing 20% concentration of perchloric acid and then stored in deionised water before placement into the furnace for high temperature storage at 300 °C inside ~40 mPa vacuum for 5 h.

The fifth set of samples were prepared using the NanoTach® X paste with the same dimensions as the third set for electromigration studies [24]. These samples were subjected to high current densities of 2.4×10^8 A/m^2 for periods ranging from 20 to 25 days before cross sectioning in order to compare atomic migration patterns on the surface and interior of the porous material.

The free surfaces of the sintered silver were observed using a Hitachi S4000 SEM coupled with Electron Dispersive X-ray (EDX) for elemental analysis.

3. Results and discussion

3.1. Observation of microstructural evolution in the absence of air

Fig. 2 shows optical images from sample set 1 of three samples stored at constant temperatures of 250, 350 and 400 °C showing the continuous evolution of microstructure adjacent to the cover-slip. Fig. 3 is a more detailed examination of the 350 °C sample clearly showing coarsening of the microstructure. Using image processing software, the average grain sizes from the images were calculated and plotted in Fig. 4. For the 400 °C sample, the grain sizes go through three grain growth phases, each having a lower slope than the
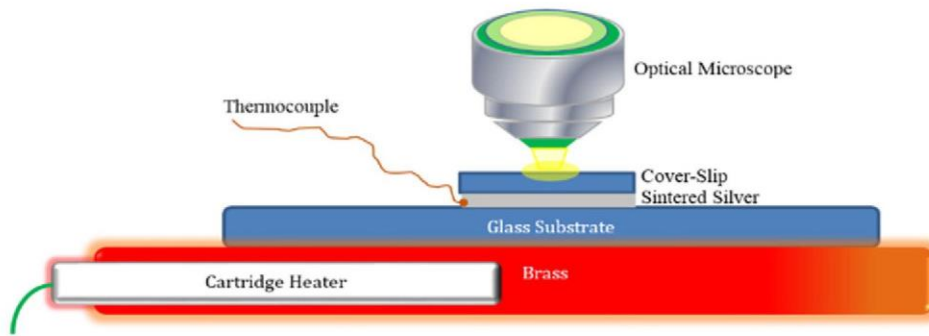
Fig. 1. Schematic representation of the experimental setup for in-situ observation of the changes to the grain structure of sintered silver at high temperature. (Cartridge heater was inserted inside the brass).

preceding grain growth phase as a result of increase in the initial grain sizes. The first phase of grain growth is defined as the period between start of heating to the point where the grain growth rate has decreased to a constant, low value. The second growth phase starts when the grain growth rate increases again and ends where the growth rate stabilizes again at a low value. For the 350 °C sample, after the first growth phase the average grain size remains almost constant for about 3.5 h before entering the second growth phase. This may be due to the fact that during this period reorientation of grains is required before further coalescence. The 250 and 300 °C samples showed that grain sizes reached a similar stable point after an initial grain growth phase. However, there may be further growth phases outside the timescale of the current experiments for those samples. In contrast, the faster diffusion mechanisms at 400 °C have caused the shortening of the grain growth phases such that a

larger number of phases are observable within the timescale of the experiment. At the lowest experimental temperature of 200 °C storage of sintered silver for 5 h did not indicate any grain growth implying greater stability of sintered silver material for such operating temperatures. Average grain size as a function of temperature is plotted in Fig. 5 for different storage times.

Errors for the average grain sizes have been calculated by performing five separate calculations of average grain size on random areas of the 350 °C sample after 90 min storage, which would provide a roughly middle point example. The standard deviation of those measurements has been used as the error for the average grain size of that particular temperature and time. The errors for the remaining average grain sizes has the same ratio to their corresponding average grain size values of the ratio of the measured error to its original average grain size.
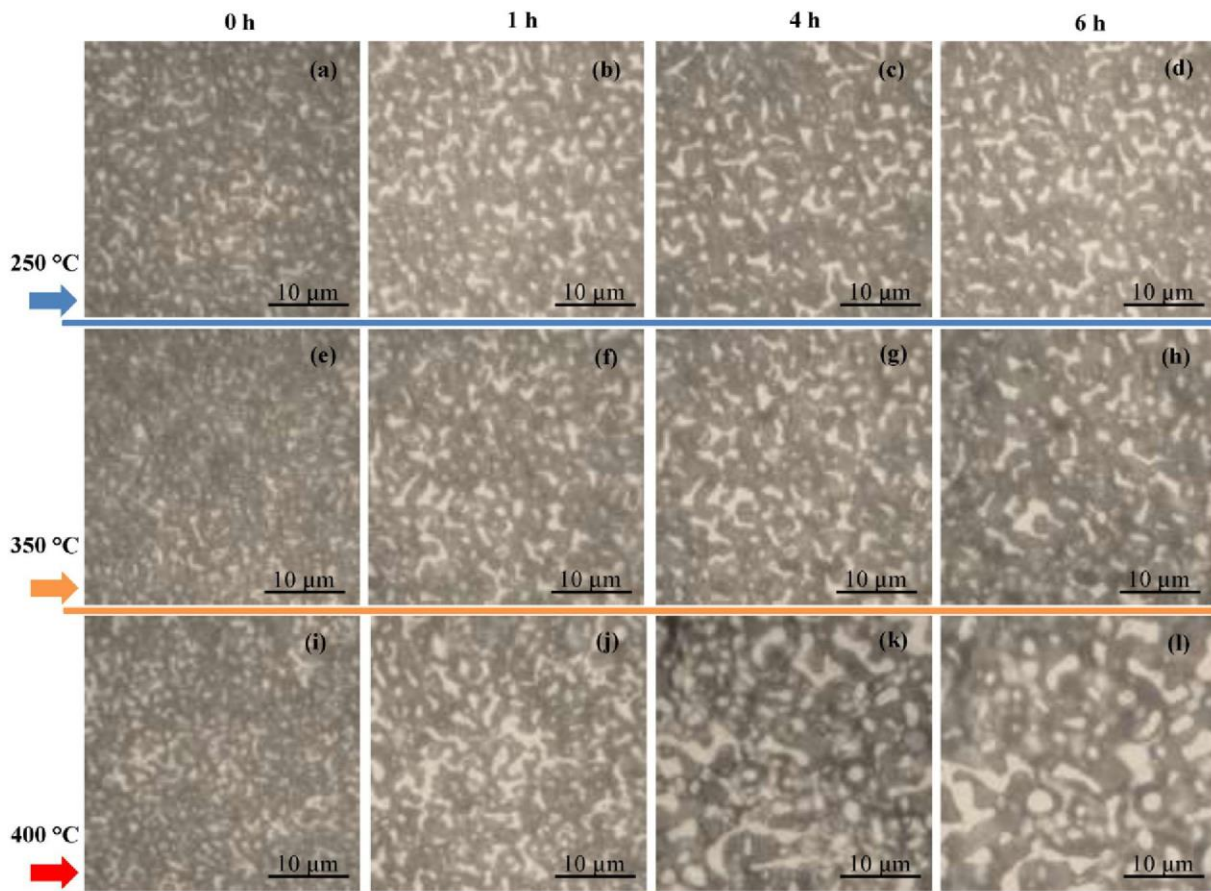
Fig. 2. Optical images of sintered silver under cover slip stored at high temperatures on top of a cartridge heater. (a–d) 250 °C storage. (e–h) 350 °C storage. (i–l) 400 °C storage.
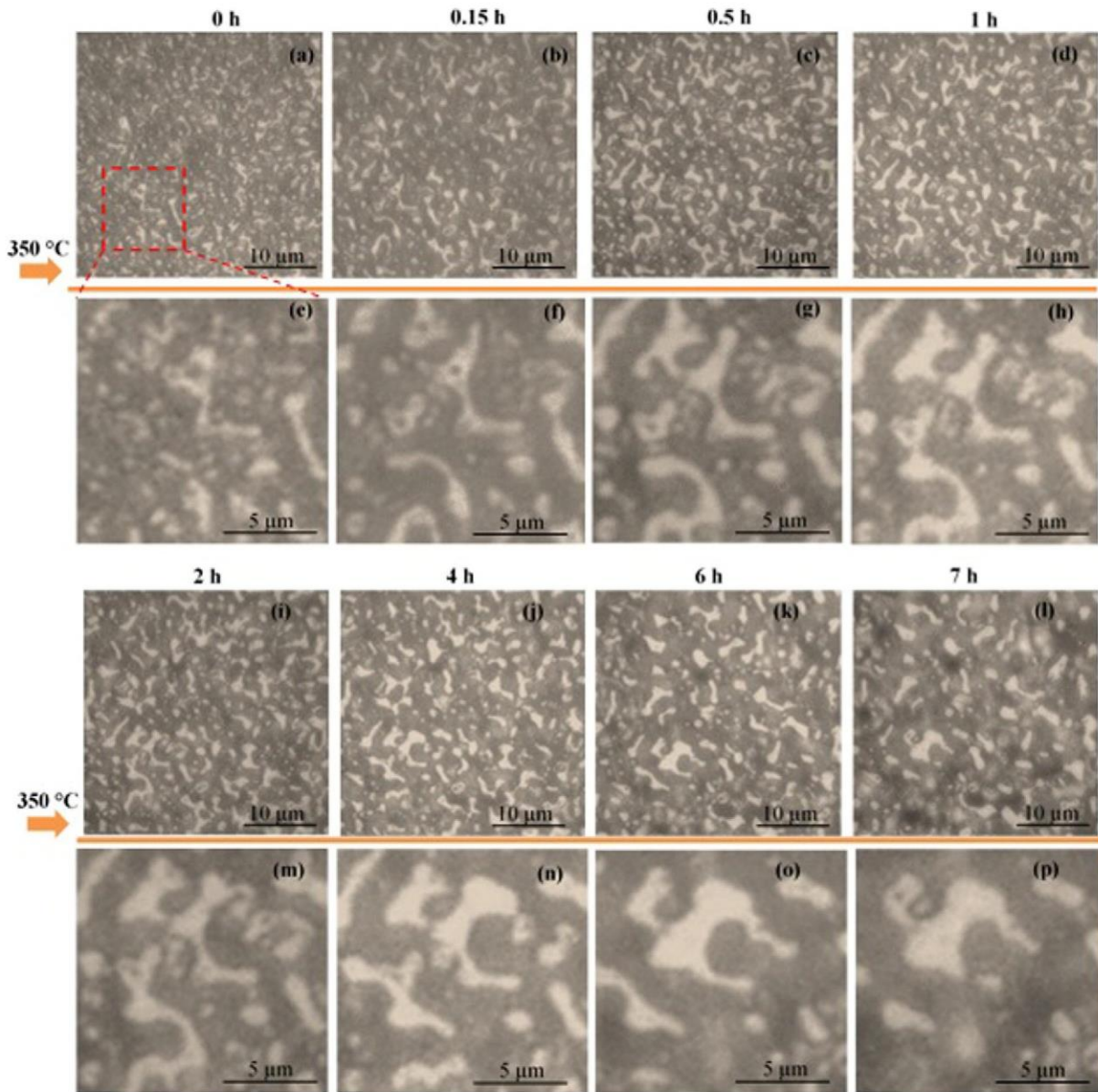
Fig. 3. Optical images showing continuous microstructural evolution of sintered silver under cover slip at 350 °C.
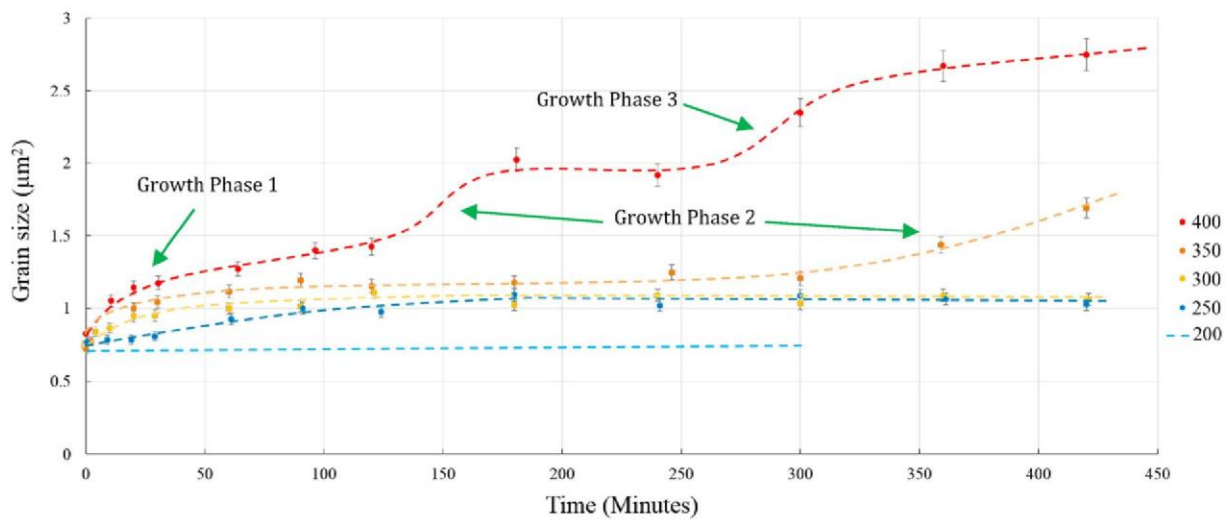

Fig. 4. Grain growth vs. time. (The curves are fitted manually for improved illustration).
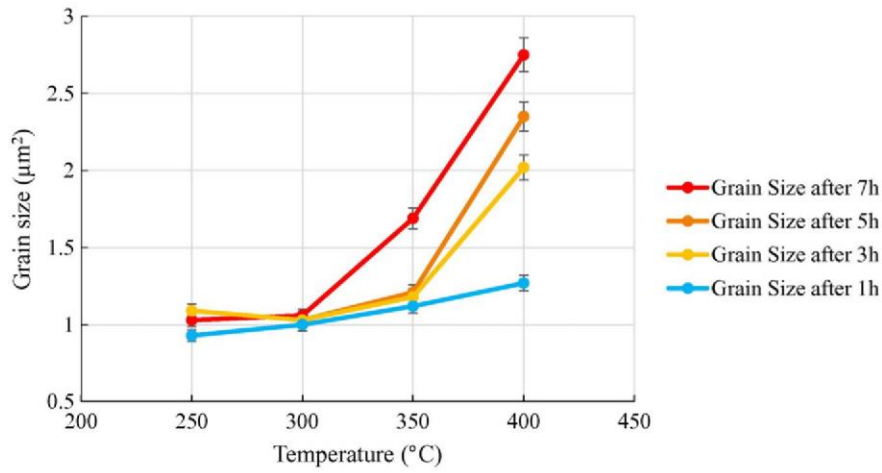
73

Fig. 5. Grain growth vs. temperature.

The general formula describing the rate of grain growth of the average grain size as a function of time can be written as [25]:

$$G^n - G_0^n = kt \qquad (1)$$

where G is a parameter meauring linear grain size at time t and G_0 is the grain size at time zero, n is the grain growth exponent, and k is a grain growth constant, and has the proportionality relationship below [26]:

$$k \propto e^{-Q/RT} \qquad (2)$$

where Q is the grain growth activation energy, R is the ideal gas constant and T is the temperature.

Dannenberg (2000) [26] estimated the value of n as 3 for grain growth of nanocrystaline silver and also for diffusion based grain growth, being applied here, it has been generally best fitted by $n = 3$ as well [25]. Therefore, for the intial grain growth phase of the samples

G^3 has been ploted against t to find the slope of the grain growth, shown in Fig. 6. For the second phases which have been found for the 350 and 400 °C sample, this relationship has been plotted in Fig. 7.

By plotting the ln$k$ against $1/T$, the activation energy of the grain growth can be calculated from the slopes for each of the grain growth phases from Eq. (2) (Fig. 8). As the second growth phase only occurred for the 350 °C and 400 °C samples, Fig. 8 (b) only contains two points. Therefore the activation energy calculated from the slope should be treated with caution.

The grain growth activation energies calculated for the first and second phases are 53 ± 2 kJ/mol and 52 ± 2 kJ/mol respectively. These values are in accordance with the literature value of 53 kJ/mol [26].

The cited literature value of the activation energy for grain growth was calculated for nano sized silver grains, and the initial size of the second grain growth phases were about twice the initial sizes for the first phase, but all provide the same activation energy. Therefore, these results indicate that the activation energies of grain growth are independent of the initial sizes up to ~2 µm². Moreover, the similarity of the
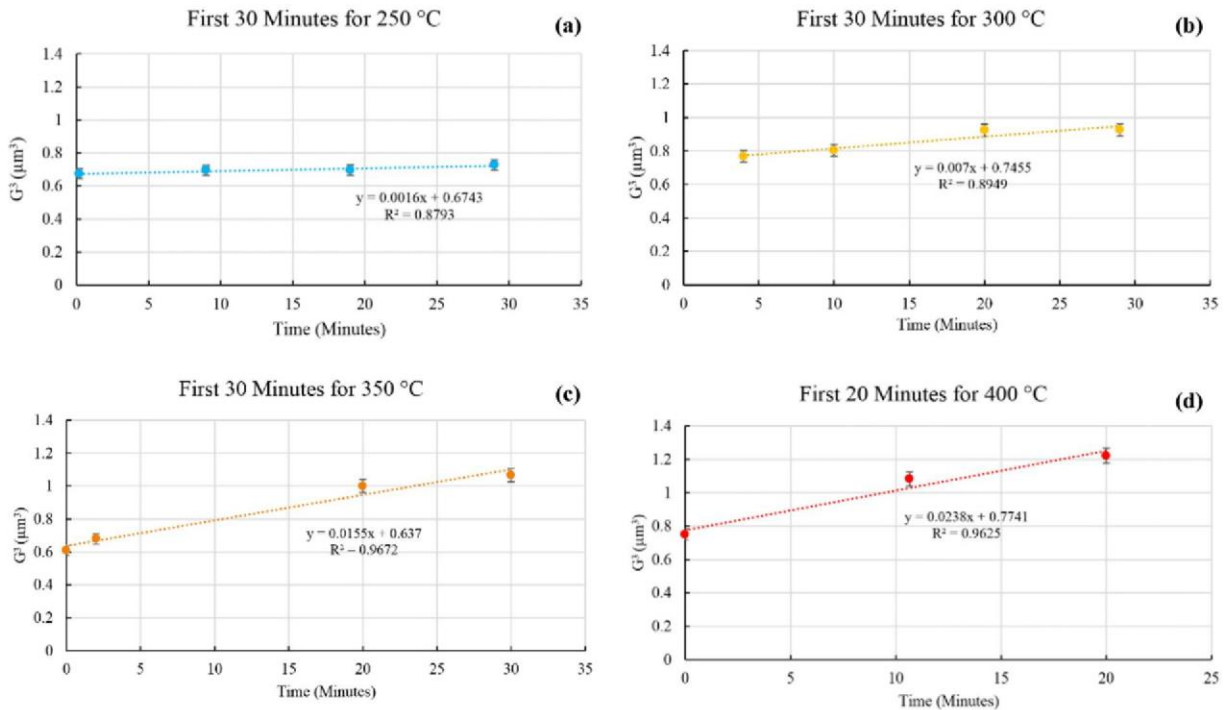
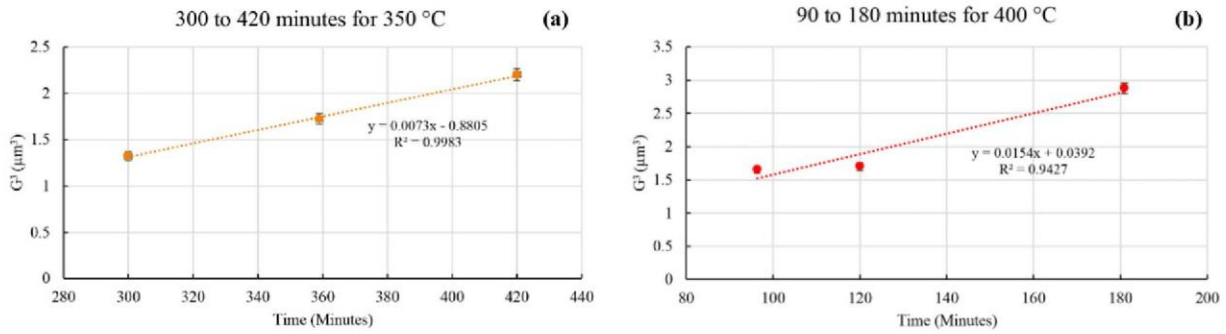**Fig. 6.** Initial grain growth vs. time.

74

Fig. 7. Grain growth vs. time of the second grain growth phase.

grain growth activation energy of the literature value, for which the grains were sputter-deposited, with the activation energy of the silver sintered under a cover-slip also confirms minimal contribution of the cover-slip to the diffusion mechanism of silver and its growth mechanisms.

While the rate of change of grain growth should be theoretically linearly dependent on surface diffusion and molar volume of the diffusing materials, on dimensional grounds we might expect the dependence of k on surface diffusivity to vary as:

$$k = C \frac{D_S \gamma V_m}{RT} \tag{3}$$

where D_S is the surface diffusion (measured values shown in Fig. 9), γ is the surface energy, (measured to be 1.14 J/m^2 [27]), V_m is the molar volume (1.03×10^{-5} m^3/mol), and C is a dimensionless constant (see e.g. [28] for a similar derivation). Fig. 9 shows the experimentally determined k value compared to the theoretical values computed from Eq. (3). The large discrepancy between the two shows that surface diffusion on a clean silver surface is not occuring and that a passivation layer on the interior pore surface also exists. The most likely explanation is that some organics from the silver paste remain on the interior pore surfaces after sintering or that partial oxidation of these surfaces has occurred. Future work is required to establish the exact composition of these surfaces.

3.2. Observation of microstructural evolution after exposure to air

One sample from sample set 2 exhibited no change in the exposed exterior surface microstructure after 20 h storage at 300 °C in air. Another sample from this sample set were stored in vacuum and also exhibited no change in exterior microstructure even at 400 °C for 66 h. When the sample stored at 400 °C, indicating no change, was stored for a further 24 h at 500 °C, massive grain coalescence occurred, as seen in

Fig. 10. Sample set 3 consisted of samples that were sintered, cross sectioned to expose the interior and then aged at 300 °C. These samples too showed no change in microstructure. Sample set 4 probed whether cleaning of the exterior surface by acid etching would enable microstructural evolution. However, since it was impossible to perform the acid etching in vacuum, the surface was exposed to water and air after etching and no microstructural evolution was observed after storage for 5 h at 300 °C. In summary, the common factor between sample sets 2–4 is that all have been exposed to air, while sample set 1 has not been exposed to air. Lack of microstructural evolution in the exterior is therefore caused by formation of a passivation layer after exposure to the atmosphere. By contrast, the surface under the cover slip underwent rapid evolution, and the changes in microstructure were similar to those observed previously [17–19] when the sintered silver is first aged at 300 °C and then cross sectioned to reveal changes compared to control samples.

The surface passivation layer blocks atomic surface diffusion, and therefore prevents the changes in grain structure seen in sample set 1 and in the interior of sintered silver in previous work [17–19]. The results indicate that after decomposition of the surface layer at 500 °C, the free movement of silver atoms on the surface of the sample resumed, leading to the morphological changes observed.

Given the change in microstructural behaviour between 400 °C and 500 °C, further investigation of microstructure evolution at 450 °C was carried out on a sample from sample set 2. As can be seen from Figs. 11, 1 h storage of the sample in air did not result in any changes to the morphology of the sample, but after an additional 1.5 h the changes were significant. During the initial 1 h at 450 °C the surface layer may have decomposed, allowing diffusion and grain evolution to take place during subsequent heating.

A further test of the presence of a passivating layer on free surfaces (as opposed to surfaces in the interior of the material or protected by glass) was carried out by passing a high current density through samples of sample set 5. Fig. 12 compares the free surface and internal
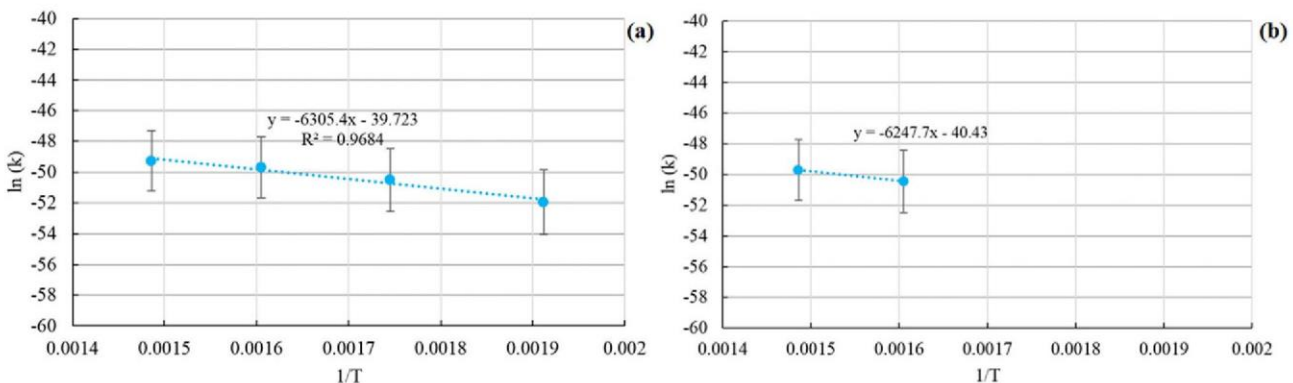

Fig. 8. ln(k) vs. reciprocal of temperature. (a) For the first grain growth phase. (b) For the second grain growth phase.
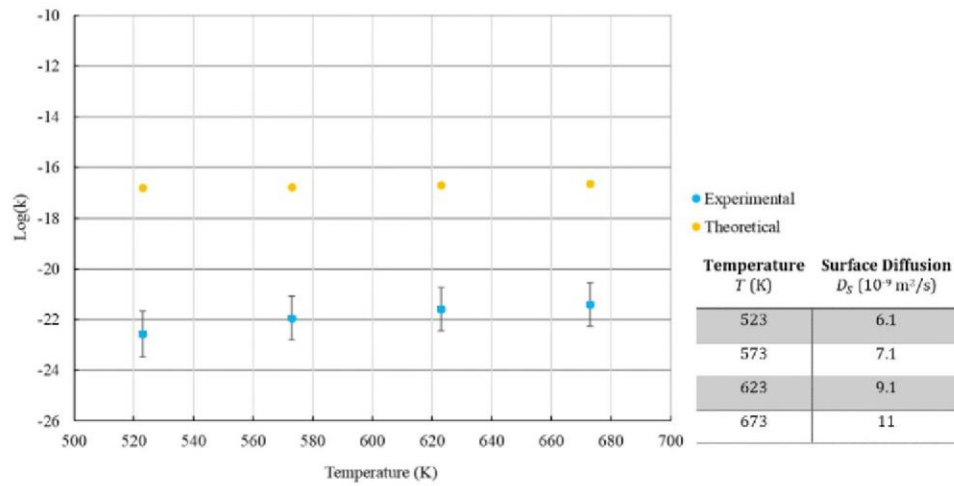
Fig. 9. The comparison between the theoretical and experimental values of *k*, with the values of surface diffusion [29] shown in the accompanying table .

structure of sintered silver before and after 25 days of application of 2.4×10^8 A/cm^2 current density through the material. Fig. 12 (a) and (b) show that on the free surface, electromigration results in the formation of nanorods due to atomic deposition in the interior of the grains causing stress build-up and eruption of material through the surface passivation layer. However, the overall shapes of the grains have not undergone any other transformation. Fig. 12 (c) and (d) were obtained by cross-sectioning samples before and after electromigration and indicate that in the interior of the material the morphology has radically changed. This shows the presence of a passivating layer on the exposed surfaces of sintered silver preventing the surface diffusion mechanisms, which are active in the interior of the sintered silver material. The temperature in the silver rose only to approximately 100 °C [24] and so

electromigration experiments have not proven that the same passivating layer exists in the thermal ageing experiments, since the layer may decompose at the higher temperatures. They do however show that a low temperature passivating layer exists with the same characteristics as those found in the thermal experiments, preventing atomic surface diffusion only at the exterior of the porous material.

Considering the results from sample sets 1–5 as a whole, the passivating layer cannot be due purely to organic compounds from the original paste, as these exist also in the interior of the material, and would have been removed from the exterior by the perchloric acid solution. The presence of oxygen on the free surface of sintered silver has been detected by EDX at room temperature in a similar study [24]. While some studies have shown that some silver oxides
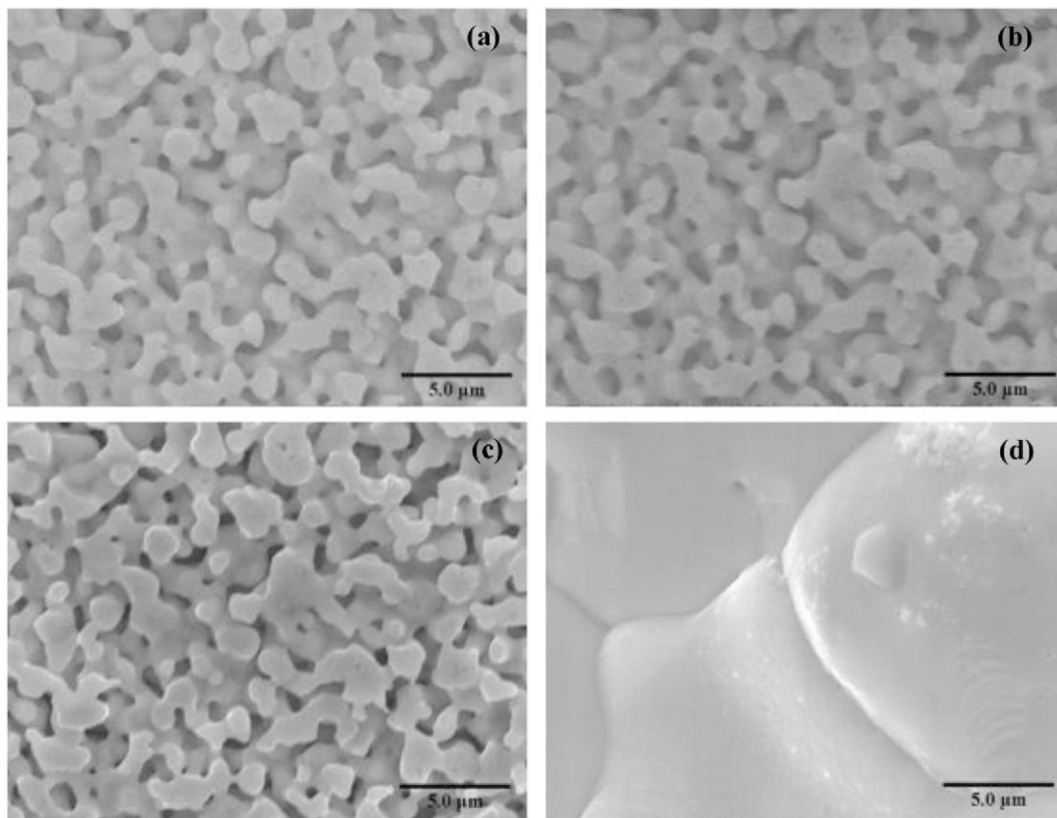
Fig. 10. SEM images of sintered silver from sample set 2. (a) Free surface of sintered silver at 0 h. (b) After storage for 24 h at 300 °C of (a). (c) Additional 16 h at 300 °C and 66 h at 400 °C of area (a) in vacuum. (d) Additional 24 h at 500 °C (not in vacuum, and area (a) could not be identified).
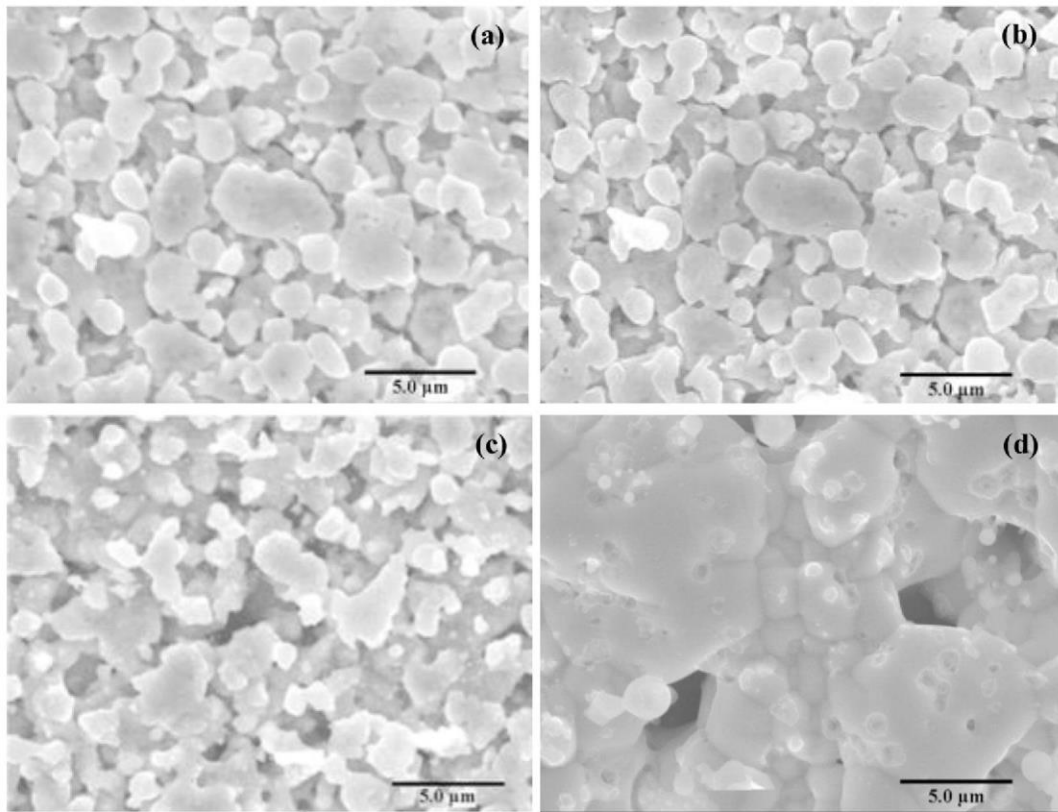
Fig. 11. SEM images of high temperature storage at 450 °C in air. (a) 0 h. (b) 1 h (c) Additional 1.5 h (d) Additional 2.5 h (same area was not identified).
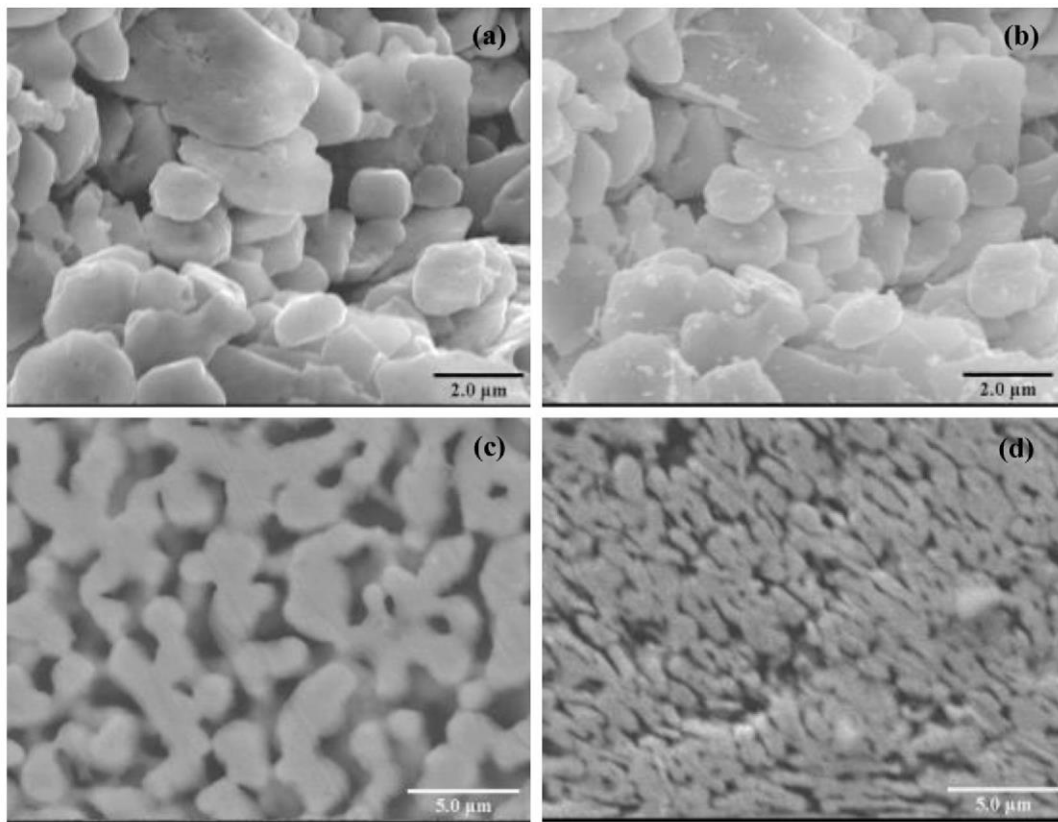

Fig. 12. SEM images for surface and interior evolution comparison. (a) Free surface before passing high current. (b) Free surface after passing high current. (c) Internal structure of a similar sample before passing high current. (d) Internal structure of a sample after passing high current.

start to decompose at 160 °C [30], the second most common type of silver oxide AgO will transform into the most common type Ag_2O at 300 °C [31], and Ag_2O completely decomposes only at 400 °C [32]. Therefore, silver oxide is the most likely composition of the passivating layer.

4. Conclusions

The microstructural behaviour of sintered silver at high temperatures has been investigated both in the absence of exposure to air and after exposure to air. In the absence of exposure to air, while 5 h exposure to 200 °C resulted in no evolution, rapid evolution was observed at temperatures of 250 °C and higher. Therefore, mechanical properties will remain stable, leading to higher reliability assurance for applications up to 200 °C. The grain structure evolution has been mapped out for different temperatures and it has been found that evolution consists of rapid growth stages interspersed with periods of relative stability. This evolution was studied in detail, tracking individual pores and grains. The activation energy of grain growth for the silver grains has been calculated as 52.5 (± 2.5) KJ/mol, which agrees with the literature value. However, exposure to atmosphere of the sintered silver surface stops the surface diffusion of silver atoms and preserves the initial microstructure. This phenomenon results in a stable structure on the free surface of sintered silver even at 400 °C. The stabilizing passivation layer is most likely to be silver oxide. The presence of the passivation layer was independently confirmed using a novel electromigration based technique which probed surface diffusivity of atoms in the interior of the sample. Moreover, the studies on the mechanical properties of sintered silver associate the coarsening of the grain structure with deterioration of mechanical properties [7,9,17–19,33,34], so that if the passivation layer could be grown in the interior of the material at the last stage of the sintering process, utilizing temperature triggered oxidation agents in the paste, then joint lifetimes could potentially be increased. The final conclusion is that until methods for stabilizing the microstructure above 200 °C are found, extensive long-term testing of mechanical properties during storage is required to ensure that joints formed from sintered silver retain adequate strength. Alternative solutions do also exist, but require the addition of interposers along with the sintered silver to produce a thermally stable die attach, increasing the high temperature reliability [35].

References

[1] V.R. Manikam, K.Y. Cheong, Die attach materials for high temperature applications: a review, IEEE Trans. Compon. Packag. Manuf. Technol. 4 (2011) 457–478.
[2] T.A. Tollefsen, O.M. Løvvik, K. Aasmundtveit, A. Larsson, Effect of temperature on the die shear strength of a Au–Sn SLID bond, Metall. Mater. Trans. A 44 (7) (2013) 2914–2916.
[3] H. Li, P.D. Han, X.B. Zhang, M. Li, Size-dependent melting point of nanoparticles based on bond number calculation, Mater. Chem. Phys. 137 (2013) 1007–1011.
[4] M. Maruyama, R. Matsubayashi, H. Iwakuro, S. Isoda, T. Komatsu, Silver nanosintering: a lead-free alternative to soldering, Appl. Phys. A Mater. Sci. Process. 93 (2008) 467–470.
[5] Y. Akada, H. Tatsumi, T. Yamaguchi, A. Hirose, T. Morita, E. Ide, Interfacial bonding mechanism using silver metallo-organic nanoparticles to bulk metals and observation of sintering behavior, Mater. Trans. 49 (2008) 1537–1545.
[6] J.G. Bai, G.Q. Lu, Thermomechanical reliability of low-temperature sintered silver die attached SiC power device assembly, IEEE Trans. Device Mater. Reliab. 6 (2006) 436–441.
[7] V. Caccuri, X. Milhet, P. Gadaud, D. Bertheau, M. Gerland, Mechanical properties of sintered Ag as a new material for die bonding: Influence of the density, J. Electron. Mater. 43 (2014) 4510–4514.
[8] K.S. Siow, Mechanical properties of nano-silver joints as die attach materials, J. Alloys Compd. 514 (2012) 6–19.
[9] K.S. Siow, Are sintered silver joints ready for use as interconnect material in microelectronic packaging? J. Electron. Mater. 1 (2014) 947–961.
[10] K. Nakaso, M. Shimada, K. Okuyama, K. Deppert, Evaluation of the change in the morphology of gold nanoparticles during sintering, J. Aerosol Sci. 33 (2002) 1061–1074.
[11] A. Moitra, S. Kim, S.-G. Kim, S.J. Park, R.M. German, M.F. Horstemeyer, Investigation on sintering mechanism of nanoscale tungsten powder based on atomistic simulation, Acta Mater. 58 (2010) 3939–3951.
[12] E. Ide, S. Angata, A. Hirose, K.F. Kobayashi, Metal–metal bonding process using Ag metallo-organic nanoparticles, Acta Mater. 53 (2005) 2385–2393.
[13] P. Peng, A. Hu, B. Zhao, A.P. Gerlich, Y.N. Zhou, Reinforcement of Ag nanoparticle paste with nanowires for low temperature pressureless bonding, J. Mater. Sci. 47 (2012) 6801–6811.
[14] M. Puchalski, P.J. Kowalczyk, I. Zasada, P. Krukowski, W. Olejniczak, Alloying process at the interface of silver nanoparticles deposited on Au (111) substrate due to the high-temperature treatments, J. Alloys Compd. 481 (1) (2009) 486–491.
[15] M. Edwards, K. Brinkfeldt, U. Rusche, T. Bukes, G. Gaiser, M. Da Silva, D. Andersson, The shear strength of nano-Ag sintered joints and the use of Ag interconnects in the design and manufacture of SiGe-based thermo-electric modules, Microelectron. Reliab. 55 (5) (2015) 722–732.
[16] L.C. Wai, W.W. Seit, E.P.J. Rong, M.Z. Ding, V.S. Rao, D.R. MinWoo, Study on Silver Sintered Die Attach Material with Different Metal Surfaces for High Temperature and High Pressure (300 °c/30kpsi) Applications, Electronics Packaging Technology Conference 2013 (EPTC 2013), IEEE Singapore 2013, pp. 335–340.
[17] G. Dumas, G. Lewis, S.H. Mannan, Evaluation of Pressure Free Nanoparticle Sintered Silver Die Attach on Silver and Gold Surfaces, HiTEN 2013, IMAPS Oxford, 2013 237–245.
[18] F. Yu, R.W. Johnson, M. Hamilton, Low Temperature, Fast Sintering of Micro-Scale Silver Paste for Die Attach for 300 °C Applications, HiTEC 2014, IMAPS, Albuquerque, 2014 654–660.
[19] S. Paknejad, G. Dumas, G. West, G. Lewis, S. Mannan, Microstructure evolution during 300 °C storage of sintered Ag nanoparticles on Ag and Au substrates, J. Alloys Compd. 617 (2014) 994–1001.
[20] S.A. Paknejad, A. Mansourian, Y. Noh, K. Khtatba, L. Van Parijs, S.H. Mannan, Factors Influencing Microstructural Evolution in Nanoparticle Sintered Ag Die Attach, HiTEN 2015, IMAPS Cambridge, 2015 50–58.
[21] B. Shoelson, ThresholdLocallyAccessed on 13/04/2015 from http://www.mathworks.com/matlabcentral/fileexchange/29764-thresholdlocally (last update 08/02/2011).
[22] D.L. Van Hyning, C.F. Zukoski, Formation mechanisms and aggregation behavior of borohydride reduced silver particles, Langmuir 14 (24) (1998) 7034–7046.
[23] D.N. Craig, C.A. Law, W.J. Hamer, Stability of silver and Pyrex in perchloric acid-silver perchlorate solutions and in conductivity water, J. Res. Natl. Bur. Stand. 127-34 (1960).
[24] A. Mansourian, S.A. Paknejad, Q. Wen, G. Vizcay-Barrena, R.A. Fleck, A.V. Zayats, S.H. Mannan, Tunable ultra-high aspect ratio Nanorod architectures grown on porous substrate via electromigration, Sci. Rep. 6 (2016) 22272.
[25] Z. Fang, H. Wang, Densification and grain growth during sintering of nanosized particles, Int. Mater. Rev. 53 (2008) 326–352.
[26] R. Dannenberg, E. Stach, J.R. Groza, B.J. Dresser, TEM annealing study of normal grain growth in silver thin films, Thin Solid Films 379 (2000) 133–138.
[27] Y. Nishida, Introduction to Metal Matrix Composites: Fabrication and Recycling, Springer Sci. & Bus. Media, 2013.
[28] R. Castro, K. van Benthem (Eds.), Sintering: Mechanisms of Convention Nanodensification and Field Assisted Processes, vol. 35, Springer Sci. & Bus. Media 2012, pp. 11–12 (35).
[29] G. Antczak, G. Ehrlich, Surface Diffusion: Metals, Metal Atoms, and Clusters, Cambridge Univ. Press, 2010.
[30] J. Tominaga, The application of silver oxide thin films to plasmon photonic devices, J. Phys. Condens. Matter 15 (25) (2003) R1101.
[31] G.B. Hoflund, Z.F. Hazos, G.N. Salaita, Surface characterization study of Ag, AgO, and Ag 2 O using X-ray photoelectron spectroscopy and electron energy-loss spectroscopy, Phys. Rev. B 62 (16) (2000) 11126–11133.
[32] T. Morita, Y. Yasuda, E. Ide, Y. Akada, A. Hirose, Bonding technique using microscaled silver-oxide particles for in-situ formation of silver nanoparticles, Mater. Trans. 49 (2008) 2875–2880.
[33] X. Milhet, P. Gadaud, V. Caccuri, D. Bertheau, D. Mellier, M. Gerland, Influence of the porous microstructure on the elastic properties of sintered Ag paste as replacement material for die attachment, J. Electron. Mater. 44 (10) (2015) 3948–3956.
[34] J. Carr, X. Milhet, P. Gadaud, S.A. Boyer, G.E. Thompson, P. Lee, Quantitative characterization of porosity and determination of elastic modulus for sintered micro-silver joints, J. Mater. Process. Technol. 225 (2015) 19–23.
[35] S.A. Paknejad, A. Mansourian, Y. Noh, K. Khtatba, S.H. Mannan, Thermally stable high temperature die attach solution, Mater. Des. 89 (2015) 1310–1314.

Addendum to Chapter 3

As it might cause confusion for some readers, it would be worth emphasising the principal idea behind utilisation of cover-slip on sintered silver to investigate the microstructural evolution again here.

There exists minimal contribution of cover-slip to the sintered silver's grain growth mechanics, which has also been confirmed here from the grain growth activation value of sintered silver grains adjacent to cover-slip versus free silver grains. Therefore, it would be reasonable to assume that cover-slip would only act as if the sintered silver is cross-sectioned and the grains are being investigated as such.

Furthermore, as it has been seen in this paper, Equations 1 and 2 could only be used to explain the grain growth phases and not the whole time-frame observed. This derivation from the classical models can be explained by the requirement of the grains to rearrange into more convenient positions to follow another observed phase of grain growth according to the classical models, where the need for repositioning of the grains inside a porous structure has not been considered.

In addition, as it has been cited in the paper, the readers are invited to read Appendix A1 for more information regarding the techniques used for calculating the average grain sizes from the optical images.

4 Ultra-Stable Sintered Silver Die Attach for Demanding High Power/Temperature Applications

Letters

Ultra-Stable Sintered Silver Die Attach for Demanding High-Power/Temperature Applications

Seyed Amir Paknejad, Khalid Khtatba, Ali Mansourian,
and Samjid H. Mannan

Abstract—A novel and simple processing step has been demonstrated to produce thermally stable sintered silver nanoparticles structures. Sintered silver has been investigated as a die attach to resolve the long-standing demand for a reliable material to enable high-power/temperature electronics operating above 300 °C. However, it is now a well-known fact that such materials undergo massive microstructural evolution at 250 °C and above, creating doubts about their long-term reliability. Here, an additional processing step utilizing oxidizing treatment is demonstrated to immobilize the silver atoms through formation of Ag_2O. This technique stabilizes sintered silver up to 400 °C, taking advantage of the open-pore network to facilitate treatment deep in the material interior.

Index Terms—Reliability, aging, semiconductor device packaging, silver, nanotechnology.

I. INTRODUCTION

One of the most important reliability concerns for high power/temperature electronics is lack of a thermally stable die attach to withstand the new temperature requirement of 300 °C and above [1]. Many different sectors can benefit from such a die attach material such as power electronics, deep-well oil and gas exploration, and implementation of wide-bandgap semiconductors into industry, where even 400 °C operating temperature is a target for near future applications [2]. Two important categories of die attach materials intended for high power/temperature applications are high temperature solders, mainly high gold content solders [3], [4], and Transient Liquid Phase Diffusion Bonding (TLPDB) materials [5]. However, the impetus for research on developing more reliable die attach materials arises from problems with these current materials, which are residual stresses in case of solders [6], and reduction of mechanical strength at elevated temperature in case of TLPDB materials, even if the temperature is well below the melting point of the system intermetallics [7].

A relatively new technique to overcome the issues related to the current die attach materials is sintering of silver nanoparticles to form a porous silver joint between the die and substrate. While this technique has attracted much attention and many research papers have been dedicated to studying this material [8], it has been recently found that this material is strongly susceptible to microstructural variations above 200 °C. As these microstructural changes are normally linked to reduction in mechanical reliability [10], [11], sintered silver materials remain unsuitable for applications above 200 °C unless the internal microstructure can be stabilised as one of the important concerns for its utilisation [8]. No known technique currently exists to stabilise the porous microstructure of pure pressure-less sintered

silver above 200 °C. Allowing a second material to be added to help stabilize the silver gives rise to two techniques found in the literature. In one technique, insertion of a gold mesh into the silver nanoparticle paste has resulted in stability during thermal aging at 600 °C for a minimum of 100 h [12]. In the other technique, addition of SiC to silver paste has been able to increase the thermal stability of the material to at least 250 °C although processing pressure was required [13]. Both techniques complicate the processing steps, and potentially lengthy optimisation of the materials and processing, will need to be followed by extensive testing that pure sintered silver has already undergone, such as shear strength, aging, thermal cycling and flexibility tests [8]. However, in this letter a novel and simple technique for freezing and stabilizing the microstructure of pure sintered silver after the normal processing steps is presented. This technique has shown an increase in microstructural stability to 400 °C.

II. MATERIAL AND METHODS

Silver nanoparticle based pastes from NBE Tech, LLC, known as NanoTach X-Paste and N-Paste, have been utilised in 4 sets of experiments, as shown in Table I. All the samples were prepared with the pressure-less sintering profile recommended by the paste manufacturer, which involves heating at 7.5 °C/min from room temperature to 260 °C followed by about 30 – 60 minutes at this temperature for X-Paste (for Sample sets 1, 2, 4 and Sample 3.3), and involves a slightly different temperature profile for Samples 3.1 and 3.2 requiring 10 min storage at 275 °C for the final sintering stage. The first two sample sets were sintered on a glass slide and under a cover-slip in order to allow continuous optical observations of microstructure evolution without exposure to air during high temperature ageing. It has been shown previously that the cover-slip does not affect the microstructural evolution of sintered silver [9], making this technique ideal for exploring continuous evolution inside sintered silver at high temperatures. Ageing was carried out by placement on a cartridge heater or inside an oven at high temperature to monitor the changes to the microstructure. Sample set 1 was stored at high temperature after sintering without further processing steps, while sample set 2 underwent oxidizing treatment after the sintering profile by storage inside an oven at 150 °C for 24 h along with beakers containing overall 500 mL of water in a sealed system. This process step allows steam to penetrate through the porous structure of the sintered silver, causing a reaction between the steam and sintered silver surfaces. Optical images for sample set 1 were produced before and after high temperature aging at 250 to 400 °C for up to 7 h, while the optical images for sample set 2 were produced before and after storage at 300 °C up to 603 h and aging up to 24 h at 350 to 450 °C. The optical images from these samples were then analysed using ImageJ 1.46 and the MATLAB image processing toolbox to investigate the microstructural changes of sintered silver grains. Refer to [9] and [14] for further information on the image processing techniques utilised and algorithms for extracting grain size, which references also include further information regarding the benefits and implications of observations of sintered silver microstructure through a cover-slip.

The third sample set was produced for cross-sectional analysis, and was again sintered using the recommended sintering profile.

TABLE I
SAMPLE SETS AND THEIR TREATMENTS

Sample Set	Sample Number	Treatment	High Temperature Aging
1	1.1	Untreated	250 °C up to 7 h
	1.2		300 °C up to 7 h
	1.3		350 °C up to 7 h
	1.4		400 °C up to 7 h
2	2.1	Treated with Steam	300 °C up to 603 h
	2.2		350, 400, 450 °C for 24 h each
3	3.1	Untreated	No Aging (Control)
	3.2		300 °C for 24 h
	3.3	Treated with Steam	300 °C for 124 h
4	4.1	Treated with Water	300 °C for 24 h

Processing Steps
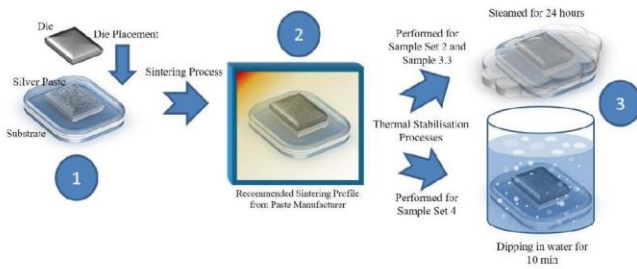
Fig. 1. Schematic representation of sample preparation process. Steps 1 and 2 were performed for all samples and step 3 shows the additional treatment for thermal stabilization.
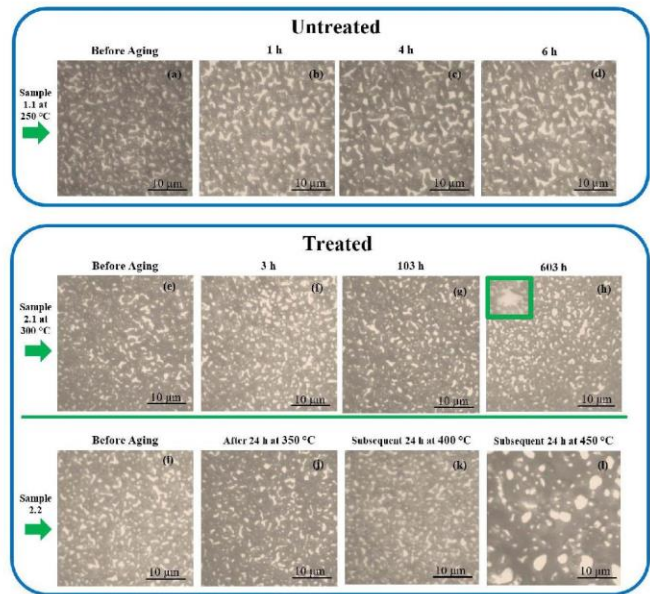

Fig. 2. Optical images of sintered silver under cover-slip. The bright areas correspond to silver grains in contact with the cover-slip. (a-d) Untreated Sample 1.2. (e-h) Treated Sample 2.1 (image (h) contains image of a bigger grain in the top left corner from another area with the same magnification). (i-l) Treated Sample 2.2.

Samples 3.1 and 3.2 did not undergo oxidizing treatment, while sample 3.3 went through the same steaming process as of sample set 2. Sample 3.1 was kept as a control sample and samples 3.2 and 3.3, were then stored at 300 °C for 24 h and 124 h respectively. All samples from set 3 were mounted using a cold mounting resin and polished mechanically with silicon carbide cloths and water based diamond solutions. These samples were then observed by SEM and compared to understand whether the effects of steaming observed in sample set 2 occurred throughout the interior of the sintered silver joint. The thickness of other sample sets can be estimated from the SEM images of Sample set 3 to be around 23 µm.

While 24 h steaming has been selected as the oxidizing treatment to ensure that steam has penetrated throughout the whole sample, other oxidizing treatments may achieve the same effect. For example, Sample 4.1 was stored under water for 10 min and then was partially dried at room temperature for 24 h before being stored at 300 °C for 24 h to observe the microstructural stabilization of this technique. Residual water would have converted to steam and contributed to oxidation via the open pore network during the storage phase. See Figure 1 for schematic representation of the processing steps for all the samples.

III. RESULTS AND DISCUSSION

Optical images from the first and second sample sets are compared in Figure 2. Untreated samples from set 1 were only stored at their designated high temperatures for up to 7 hours since changes in microstructure were clearly visible in that timescale. Figure 2 (a-d) shows the fast microstructural evolution of sample 1.1 at 250 °C. However, the treated sample number 2.1 shown in Figure 2 (e-h) has been stored for 603 h at 300 °C and only at 603 h did a few isolated grains begin to grow. One example of such grains is inserted in top left corner of Figure 2 (h); note that this image was specifically selected to capture one of these rare grains (observed 1 in 7000 grains), while all other images in Figure 2 are from random areas. These growing grains could correspond to the small number of closed spaces expected inside sintered silver, while 96-99.9% of the pores will be part of an open network [15], [16]. Inside the closed spaces steam cannot penetrate and therefore grain growth can occur. Grain size measurements indicate that the average size of the grains at 300 °C remained constant up to 603 h; the effect of isolated grain growth being negligible. By contrast the untreated samples went through significant grain growth even at 250 °C in less than 2 h. A summary of the grain size evolution for sample set 1 and 2 are presented in Figure 3. It can be seen in this figure that 24 h storage of Sample 2.2 at 350 °C and subsequently at 400 °C results in no changes to microstructure, as seen in Figure 2 (i-k), while storage at 450 °C does result in significant grain growth, showing that the protection provided by oxidation wears off between 400 °C and 450 °C, see Figure 2 (l).

Given that the decomposition temperature of the most stable silver oxide (Ag_2O) is 400 °C from Differential Thermal Analysis of silver oxide (Ag_2O) [17], and exposure of silver to air results in oxidation and halt to surface diffusion and grain growth [18], the stability after treatment can be attributed to formation of a silver oxide passivating layer. The exterior of the air exposed sample is seen to be immediately stabilized but not the interior microstructure [9], which remains stable only after the oxidizing treatment. This is shown in Figure 4 where the microstructural stability seen in sample set 2 is seen to occur throughout the sample cross-section only in the treated case and significant grain growth can be observed for the untreated sample. As can be seen from Figure 4 (c and e) as schematic representations of the likely
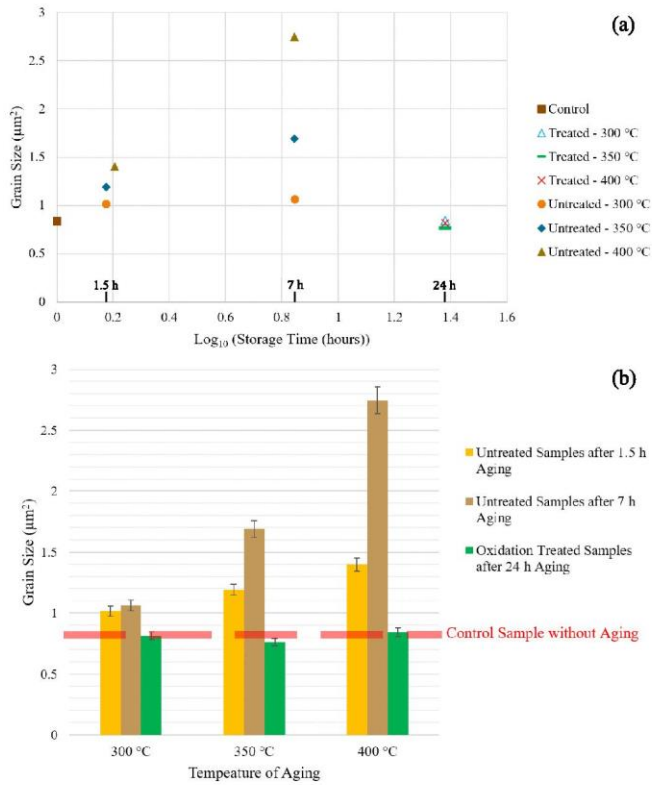
Fig. 3. Comparison of grains sizes of treated and untreated samples. (a) Grain size versus storage time. (b) Grain size versus temperature. Untreated results are obtained from Sample set 1 and treated results from sample set 2.
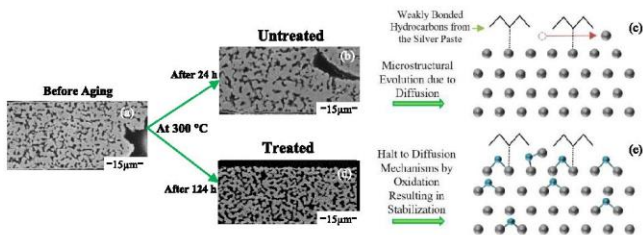

Fig. 4. SEM images of cross-sections of sample set 3 and their microstructural evolution's underlying mechanisms. (a) Before aging, sample 3.1. (b) Untreated sample 3.1 after 24 h at 300 °C. (c) Schematic representation of easy surface diffusion mechanism of silver atoms on sintered silver. (d) Treated sample 3.3 after 124 h at 300 °C. (e) Schematic illustration of halt to diffusion as a result of oxygen atoms pinning silver atoms. The dotted lines in (c) and (d) represent weak Van der Waals type bonds and solid lines represent strong ionic bonds preventing surface diffusion.

processes, this effect can be explained by the fact that while silver atoms inside pure silver can migrate and diffuse easily via surface diffusion, the oxidation has the effect of immobilising and pinning the silver atoms and stabilizing the structure up to the decomposition temperature of Ag_2O, which has also been observed and confirmed previously through direct exposure to atmosphere [18]. Although calculations of morphology changes driven by surface self-diffusion on pure silver are orders of magnitude faster than those observed experimentally [9], reduction of surface diffusion coefficients in the presence of organic residues from the original paste and partial oxidation can explain the discrepancy. Oxygen and humidity from air can penetrate the pore network in limited quantities without treatment, but an external oxidizing treatment with high intensity has been shown to be necessary in order to achieve thermal stability at 400 °C.

Another simpler oxidation treatment has indicated the same stabilization effect. Sample 4.1 exhibits the same stabilization after dipping the sample in water for 10 min, in which ageing at 300 °C for 24 h results in no visible changes to microstructure.

IV. CONCLUSION

In summary, oxidizing treatment of sintered silver has resulted in increased stability and arrest of high temperature microstructural evolution up to 400 °C. While normal sintered silver undergoes significant grain growth even at 250 °C in less than 1 h, the treated samples have been stable for at least 24 h at 400 °C. At 300 °C almost the entire sample is seen to be stable up to at least 600 h, while only a few isolated grains coalesce, confirming the existence of closed pores inside sintered silver at these locations. The increased stability has been explained as a result of oxidation of sintered silver, which enables the possibility of a broad range of possible techniques for boosting the stability temperature range of sintered silver from the existing 200 °C up to 400 °C. These patent pending techniques [19] can be applied conveniently after sintering by introducing oxidizing mechanisms such as dipping in water. The existence of simple stabilizing treatments also opens up the possibility of using higher porosity silver for large die applications where the stress exerted on the die is a limiting factor. While the stabilisation technique utilised here has been demonstrated only for the NBE Tech pastes, the mechanism should hold generally but further work is needed to establish this.

REFERENCES

[1] V. R. Manikam and K. Y. Cheong, "Die attach materials for high temperature applications: A review," *IEEE Trans. Compon. Packag. Manuf. Technol.*, vol. 1, no. 4, pp. 457–478, Apr. 2011.

[2] K. S. Tan and K. Y. Cheong, "Mechanical properties of sintered Ag–Cu die-attach nanopaste for application on SiC device," *Mater. Design*, vol. 64, pp. 166–176, Dec. 2014.

[3] V. Chidambaram, J. Hattel, and J. Hald, "Design of lead-free candidate alloys for high-temperature soldering based on the Au–Sn system," *Mater. Design*, vol. 31, no. 10, pp. 4638–4645, 2010.

[4] Y. Du, C. Li, B. Huang, M. Tang, and C. Du, "Research and prospect of binary high-temperature Pb-free solders," *Soldering Surface Mount Technol.*, vol. 27, no. 1, pp. 7–12, 2015.

[5] R. I. Rodriguez, D. Ibitayo, and P. O. Quintero, "Kinetics of dissolution and isothermal solidification for gold-enriched solid–liquid interdiffusion (SLID) bonding," *J. Elect. Mater.*, vol. 42, no. 8, pp. 2677–2685, 2013.

[6] A. Masson *et al.*, "High-temperature die-attaches for SiC power devices," in *Power Electron. Appl. (EPE)*, Birmingham, U.K., 2011, pp. 1–10.

[7] T. A. Tollefsen, O. M. Løvvik, K. Aasmundtveit, and A. Larsson, "Effect of temperature on the die shear strength of a Au-Sn SLID bond," *Metallurgical Mater. Trans. A*, vol. 44, no. 7, pp. 2914–2916, 2013.

[8] S. A. Paknejad and S. H. Mannan, "Review of silver nanoparticle based die attach materials for high power/temperature applications," *Microelectron. Rel.*, vol. 70, pp. 1–11, Mar. 2017.

[9] S. A. Paknejad *et al.*, "Microstructural evolution of sintered silver at elevated temperatures," *Microelectron. Rel.*, vol. 63, pp. 125–133, Aug. 2016.

[10] F. Yu, R. W. Johnson, and M. Hamilton, "Pressureless, low temperature sintering of micro-scale silver paste for die attach for 300 °C applications," presented at the Additional Papers (HITEC), vol. 2014. 2014, pp. 000165–000171. [Online]. Available: https://doi.org/10.4071/HITEC-WA21

[11] V. Caccuri, X. Milhet, P. Gadaud, D. Bertheau, and M. Gerland, "Mechanical properties of sintered Ag as a new material for die bonding: Influence of the density," *J. Electron. Mater.*, vol. 43, no. 12, pp. 4510–4514, 2014.

[12] S. A. Paknejad, A. Mansourian, Y. Noh, K. Khtatba, and S. H. Mannan, "Thermally stable high temperature die attach solution," *Mater. Design*, vol. 89, pp. 1310–1314, Jan. 2016.

[13] H. Zhang, S. Nagao, and K. Suganuma, "Addition of SiC particles to Ag die-attach paste to improve high-temperature stability; grain growth kinetics of sintered porous Ag," *J. Electron. Mater.*, vol. 44, no. 10, pp. 3896–3903, 2015.

[14] S. A. Paknejad *et al.*, "Factors influencing microstructural evolution in nanoparticle sintered Ag die attach," presented at the Int. Conf. Exhibit. High Temperature Electron. Netw., 2015, pp. 50–58.

[15] J. Carr *et al.*, "Quantitative characterization of porosity and determination of elastic modulus for sintered micro-silver joints," *J. Mater. Process. Technol.*, vol. 225, pp. 19–23, Nov. 2015.

[16] W. Rmili *et al.*, "Quantitative analysis of porosity and transport properties by FIB-SEM 3D imaging of a solder based sintered silver for a new microelectronic component," *J. Electron. Mater.*, vol. 45, no. 4, pp. 2242–2251, 2016.

[17] T. Morita, Y. Yasuda, E. Ide, Y. Akada, and A. Hirose, "Bonding technique using micro-scaled silver-oxide particles for in-situ formation of silver nanoparticles," *Mater. Trans.*, vol. 49, no. 12, pp. 2875–2880, 2008.

[18] R. Dannenberg, E. A. Stach, J. R. Groza, and B. J. Dresser, "In-situ TEM observations of abnormal grain growth, coarsening, and substrate de-wetting in nanocrystalline Ag thin films," *Thin Solid Films*, vol. 370, nos. 1–2, pp. 54–62, 2000.

[19] S. A. Paknejad, "Increasing stability of porous silver to at least 400 °C," U.S. Patent 62 448 240, 2017.

Addendum to Chapter 4

5 Microstructure evolution during 300 °C storage of sintered Ag nanoparticles on Ag and Au substrates

Microstructure evolution during 300 °C storage of sintered Ag nanoparticles on Ag and Au substrates

S.A. Paknejad [a], G. Dumas [b], G. West [c], G. Lewis [b], S.H. Mannan [a,*]

[a] King's College London, Physics Department, Strand, London WC2R 2LS, UK
[b] Eltek Semiconductors Ltd, Nelson Road Industrial Estate, Dartmouth, Devon TQ6 9LA, UK
[c] Loughborough University, Materials Department, Loughborough LE11 3TU, UK

ABSTRACT

A silver nanoparticle based die attach material was used in a pressure free process to bond 2.5 mm square Ag plated Si die to Ag and Au plated substrates. The assemblies were stored at 300 °C for up to 500 h and the morphology of the sintered Ag and the shear strength were monitored as a function of time. On Ag substrate it was found that die shear strength increased and that the Ag grains grew in size and porosity decreased over time. There was also a clear difference in morphology between sintered Ag at the die edge and centre. On Au substrate, it was observed that the initially high die shear strength decreased with storage time and that voids migrated away from the Ag/Au interface and into the Ag joint. This has led to the formation of a void free layer at the interface followed by a high porosity region, which weakened the joint. The microstructure reveals a high density of grain and twin boundaries which facilitate the Ag and Au atomic diffusion responsible. The grain structure of the plated Au led to diffusion of Au into the Ag via high-angle tilt grain boundaries, and grain boundary migration further dispersed the Au into the Ag layer.

© 2014 Elsevier B.V. All rights reserved.

1. Introduction

Electronics for applications in aircraft, automotive, space exploration, deep oil and gas drilling, can require operating temperatures of 300 °C or higher. For example, requirements for deep oil and gas exploration have been reported as 300 °C [1]. Semiconductor die are attached to substrates in these applications using die attach materials such as high melting point solders e.g. AuIn or AuGe. One problem with solders in high temperature applications is that they must melt during processing, leading to operating temperature as a fraction of melting point (homologous temperature) of 0.75 or higher since use of even higher melting point solders requires processing which can damage the semiconductor and lead to high residual stresses after joining. Alternative approaches include liquid interconnects [2], Transient Liquid Phase Bonding (also referred to as solid liquid interdiffusion bonding) [3] and nanoparticle (NP) sintering [4–8]; the basic idea behind these is to decouple the processing temperature from the operating temperature. For NP sintering, detailed analysis of the initial sintering mechanisms including ripening and twinning can be found in [9].

In the case of silver NP sintered materials, joints can be formed at significantly lower temperatures and pressures as compared to

micron-sized particles. This stems from the increased proportion of atoms at the surface of the nanoparticles, leading to increased free energy in the system and surface premelting [10]. For example, the melting point of bulk silver is 961 °C, whereas the melting temperature of silver particles with a diameter of 2.4 nm reduces to around 350 °C [11]. After sintering, the joint can operate at 350 °C with a corresponding homologous temperature of only 0.5. Nanoparticle sintering for high power and high temperature die attach applications have been previously reported using Ag NPs [6,8,12–15] while sintering using Cu NPs have also been reported [16–19] although these typically require applied pressure, UV light or a reducing atmosphere for successful sintering. The present work reports on changes in shear strength and the corresponding evolution of voids and grain boundaries when a commercially available Ag NP paste is used to bond Si test die to a ceramic package with Ni/Au surface metallization, followed by storage at 300 °C.

2. Experimental

The die-attach material selected for studies was the NanoTach® N silver paste produced by NBE Tech. This paste is recommended for small size dies of less than 3 × 3 mm in a pressure free sintering process. The paste consists of ~30 nm diameter Ag particles together with ligands to prevent agglomeration and organic components to improve paste rheology; further details are reported elsewhere, together with details of bondline thickness measurements after sintering and ageing, and images of fracture surfaces after shear testing [20]. In the present work 2.5 × 2.5 mm Si die

with Ni/Ag plating were employed, with the final vacuum deposited Ag layer 0.6 μm thick. The Ag substrates are identical to the die (Si with Ni/Ag plating layers) with dimensions 5 × 5 mm. The Au substrates consist of a W/Ni/Au metallized co-fired alumina package with the final electroplated Au layer 2 μm thick.

During assembly no pressure was applied to the die after placement onto the substrate using a scrubbing motion to initiate contact between paste and substrate/die metallizations [20]. The manufacturers' recommended temperature profile consists of ramping from room temperature to 150 °C with an average ramp rate of 1.6 °C/min, followed by a 20 °C/min ramp to 290 °C and a hold of 10 min at 290 °C. This schedule was followed except for the final stage where temperatures varied between 290–300 °C for 18 min rather than the recommended 10 min hold at 290 °C. After bonding, the assemblies were stored at 300 °C for 24 h, 100 h, and 500 h. For each condition cross sections were produced for observation of the effects of the high temperature storage and also compared to a "control" sample, which experienced the same sintering profile (and heating overshoot) as the other samples but was not aged at 300 °C. At each stage, the die shear strength was tested using a Dage 4000 system in accordance with MIL STD 883, method 2019. The shear tests were performed at 75 μm height from the base of the component and using a shear speed of 200 μm/s.

The samples were observed by Scanning Electron Microscopy (SEM) using a Field Emission Gun SEM (FEI QuantaFEG) with Energy Dispersive X-ray (EDX) analysis to determine elemental maps and compositions, Electron Backscatter Diffraction (EBSD) was employed on the 24 h sample on the Au substrate to identify the lattice orientations of the grains at the interface of the sintered silver and the gold layer on the substrate. For SEM, the cross sections were first produced by cutting through the dies vertically with a circular diamond saw. Next, the samples were potted in a cold mounting resin and polished with silicon carbide cloths, followed by polishing with three- micron and quarter- micron mono-crystalline diamond in water base suspensions.

Two of the samples (the control and 24 h on Au substrates) were also prepared using an argon ion Cross-Section Polisher (CSP) (JEOL SM-09010) to first polish and then etch the samples to bring out grain boundaries in the method described in [21]. These two samples were also prepared for TEM by using an in situ lift out technique in a Nova 600 Nano Lab dual beam. This system consists of a Field Emission Gun Scanning Electron Microscope (FEG-SEM) and a Focusses Ion Beam (FIB). The samples were analysed in a JEOL JEM 2000FX Transmission Electron Microscope (TEM) operating at 200 kV in bright field mode and images were recorded using a Erlangshen (Gatan) CCD camera.

3. Results and discussions

3.1. Shear test results

Fig. 1 shows the shear strength of the assemblies under thermal ageing at 300 °C. Each point on the graphs corresponds to an individual test. Four samples were tested at each condition but samples which fractured leaving more than 5% of the die in contact with the substrate are not shown; the average and standard deviation of shear force for all four tests irrespective of fracture are plotted on the inset graphs. It can be seen that there is considerable scatter in the measurements. On Ag substrate the initial shear strength of ~11 MPa is in agreement with the typical values of 11–12 MPa reported [4] but lower than the ~20 MPa found [22] using a modified paste with reduced organics. However after ageing the shear strength shows an increasing trend, rising to ~15 MPa at some time between 24 and 100 h ageing. On the Au substrate, the initial shear strength is 22.5 MPa in one instance, but only 7.5 MPa in the two other cases. Previous results also using Au substrate and Ag metallized die [15] recorded 6 MPa initial bond strength, suggesting that the initial sintering time of 10 min may not be enough to guarantee good contact between the nanoparticles and the metallizations. However, as the samples were aged, it is seen that the shear strength trend is decreasing, reducing to ~12 MPa after 500 h. In order to investigate the cause of the changes in shear strength, the assemblies, which had been aged but not shear tested, were cross sectioned.

3.2. Au substrate microstructure

Fig. 2 shows SEM images of cross sections of the control and aged samples after ion beam etching. In the control sample, the original sintered Ag microstructure shows porosity of ~20%, typical of
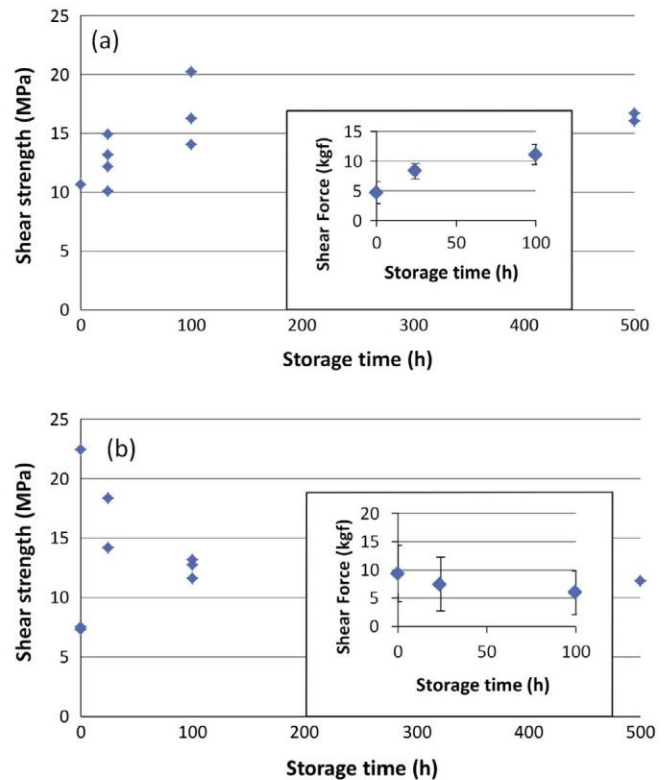

Fig. 1. (a) Shear strength on Ag substrate. (b) Shear strength on Au substrate. Main body shows individual shear test results and insets show shear strength of all samples including those which fractured during the test.

a pressure-free Ag sintering process [23,13] and a high degree of contact between the Ag and Au phases at the interface. Subsequently, a layer grows Fig. 2(b)–(d) which is almost free of voids and this is henceforth designated as the Void Free Layer (VFL). Average thickness of the VFL increases as a function of time as shown in Fig. 3, rising from 8 μm after 24 h to 16 μm after 500 h. Above the VFL, a high porosity zone (~44% porosity after 24 h rising to ~65% porosity for 100 h and 500 h aged samples) forms which leads to the progressive weakening of the assembly seen in Fig. 1b. For the 100 h and 500 h samples, the Au layer is seen to dissolve locally into the Ag, see Fig. 2c and d and Fig. 3 (inset). A previous study investigating reliability of sintered Ag nanoparticles on Au substrates at 300 °C did not report these phenomena as storage time was limited to 90 min [24].

The increase in the thickness of the VFL during the studied storage periods indicates fast migration of the Ag atoms towards the Au layer and migration of Au in the opposite direction. This observation was quantitatively estimated by evaluation of diffusion coefficient (D) of Au into the sintered silver by two different techniques. First, the diffusion length x of Au into the Ag is used in the standard parabolic 1-d diffusion solution

$$D = \frac{x^2}{4t} \tag{1}$$

where t is the diffusion time. Fig. 4a shows Au diffusion on the 100 h sample from which x is calculated as $(5 \pm 1)\,μm$ based on an average value of nine linear Au diffusion lengths chosen randomly, but above the regions where the Au layer has dissolved into the sintered Ag. Calculation of the uncertainty in diffusion length was affected by three different factors, which were (i) slight drift of the sample during elemental composition analysis, (ii) variability of diffusion lengths, and (iii) EDX analysis errors leading to noise which has been filtered out of the Au distributions by removing
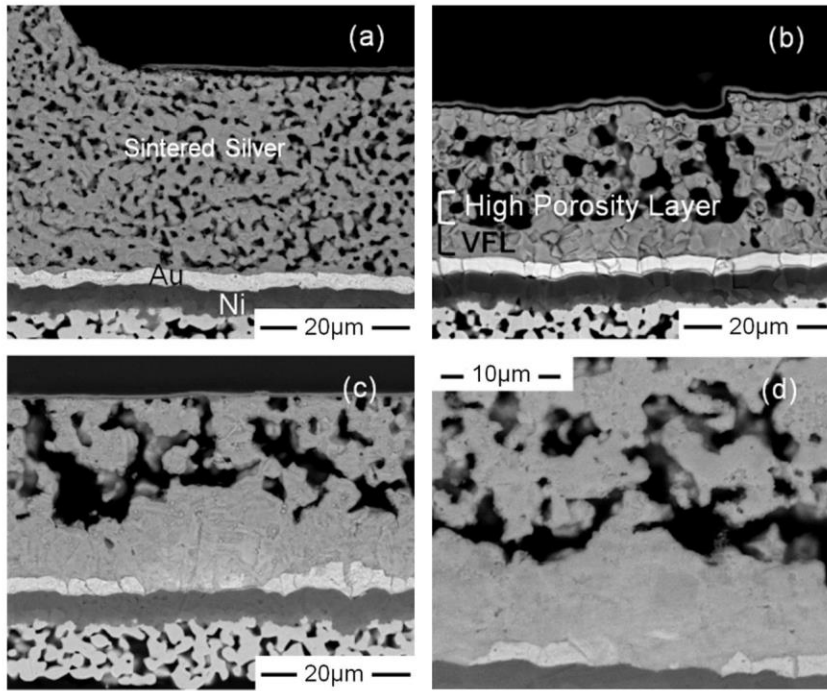
Fig. 2. Backscatter SEM images of (a) control. (b) 24 h (prepared using CSP). (c) 100 h. (d) 500 h sample (higher magnification).
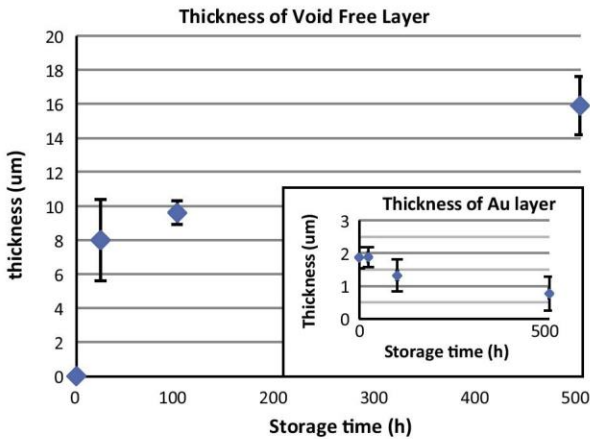

Fig. 3. Thickness of Void Free Layer (VFL) as a function of storage time. Inset shows thickness of the residual Au plating (error bars represent one standard deviation).

low intensity and isolated pixels. D is now estimated from Eq. (1) as $(1.7 \pm 0.7) \times 10^{-17}$ m^2/s.

The second technique for calculation of D utilizes elemental composition information on a line vertical to the interface between the sintered silver and Au layer measured by EDX for the 500 h sample. The concentration of Au C as a function of distance from the Matano interface (where the number of atoms of Au on one side of the interface equals the number of atoms of Ag on the other), r, is used to solve the Boltzmann–Matano equation [25]

$$D = -\frac{\int_{C_{max}}^{C(r^*)} r \, dC}{2t\left(\frac{dC}{dr}\right)_{r=r^*}} \tag{2}$$

where C_{max} is the concentration at the original Au/Ag interface , and r^* is the distance at which D is evaluated. This gives an estimate of $\bar{D} = 1.1 \times 10^{-18}$ m^2/s where the average is calculated over the diffusion path.

Denoting D_{GB} and D_l as the grain boundary and lattice diffusion coefficients of Au in Ag and μ as the volume fraction of grain boundaries inside the sintered silver, the effective D measured can be written as [26]

$$D = \mu D_{GB} + (1 - \mu)D_l \tag{3}$$

According to the literature $D_l \cong 1.9 \times 10^{-22}$ m^2/s [27] at 300 °C leading to the conclusion that diffusion in the sintered Ag is dominated by grain boundaries. D_{GB} is reported to vary widely as it depends on the exact nature of the grain boundaries. Therefore, the 24 h sample has been used to estimate D_{GB} as in this case, etching has clearly brought out the grain boundaries and it is possible to map Au diffusion along these as shown in Fig. 4c and d. Using Eq. (1) where x now represents distance along the grain boundary, we find D_{GB} estimated as 1.9×10^{-17} m^2/s. An explanation of the difference between the values of D calculated from the two different techniques can now be suggested. The closeness of the first value to D_{GB} appears to be caused by calculation of the maximum diffusion length from Fig. 4a, which corresponds to grain boundary diffusion rather than effective diffusion. This is because the calculation considers only the furthest extent of diffusion, which occurs along the grain boundaries. By contrast, the Boltzmann–Matano technique utilizes a random straight line during calculation of D taking into account information from both grain boundaries and lattice diffusion. The value of μ is found to be 0.06 from Eq. (3) and using the average value of D calculated from Eq. (2). This calculation indicates a very high fraction of grain boundaries inside sintered silver nanoparticles. To evaluate the reliability of this calculation TEM analysis of the control and 24 h samples is shown in Fig. 5.

These confirm firstly that there is a high density of twin boundaries present in the sintered Ag. The occurrence of twin boundaries in pressure-free sintering of Ag nanoparticles was recently predicted from molecular dynamics simulations [28] although the high density of twins observed in the present work suggests that simulations with small numbers of particles still do not fully capture the relevant stress relaxation mechanisms. Experimental
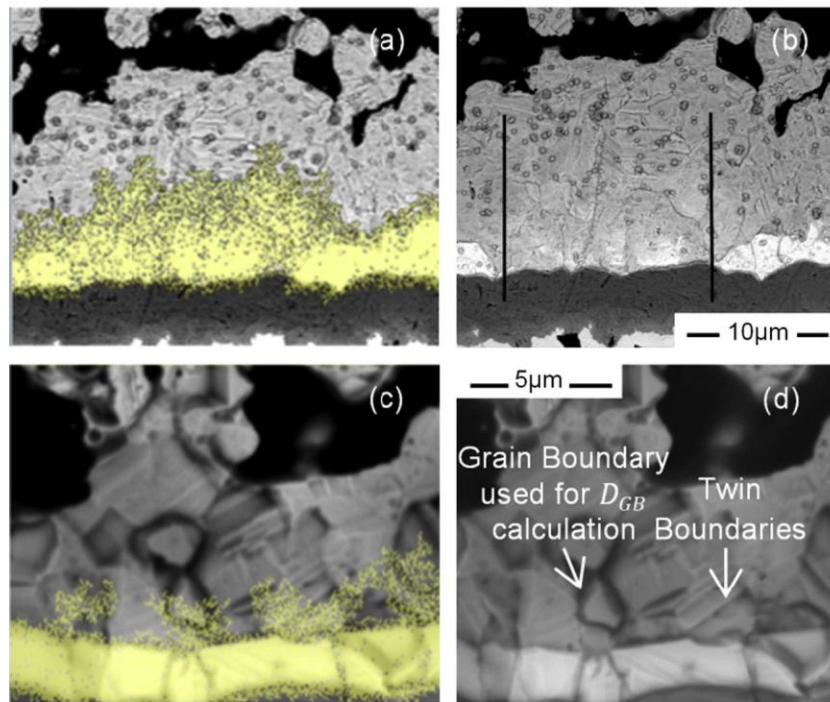
Fig. 4. EDX generated maps of Au distributions. (a) Au distribution superimposed on SEM image of 100 h sample. (b) Original SEM image with vertical lines showing region used for calculation of x. (c) Au distribution superimposed on SEM image of 24 h sample (enhanced by a video accessible online). (d) Original SEM image with indicated grain boundary used for calculation of D_{GB}.
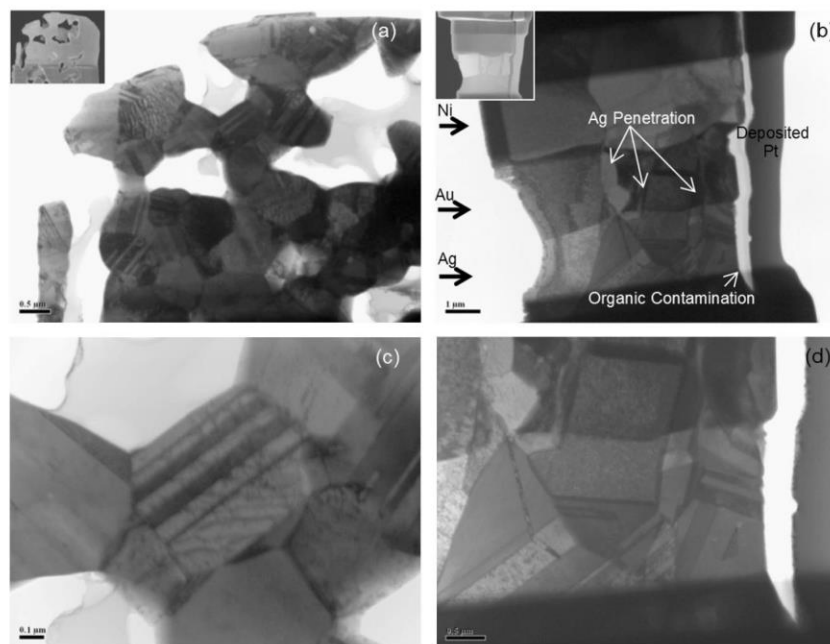

Fig. 5. TEM images of control and 24 h sample. (a) and (c) are TEM images of the control sample inside the sintered silver. (b) and (d) are TEM images of 24 h sample at the Ag/Au interface. The corresponding SEM images of the TEM samples are shown in the top right corners of (a) and (b) images. The SEM image embedded in (b) shows areas of Ag penetration into the Au layer as dark zones and these are then indicated by the arrows in the TEM image.

observation of a high density of twin boundaries after pressure free Ag NP sintering at 200 °C appears to show an even higher density of grain boundaries than observed in the present paper [29]. The TEM images also confirm absence of nano-scale pores in the material and that grain boundaries in the Ni layer lead to grain boundaries inside the Au layer and then into the sintered Ag. This strongly suggests that epitaxial growth of Ag on the Au surface

occurs as expected from molecular dynamics simulation studies [30], and previously observed experimentally [31]. It can also be seen that Ag has penetrated into the Au grain boundaries (see Fig. 5b and d) causing rapid dissolution of the Au at some grain boundary interfaces, while epitaxial interfaces show minimal dissolution of Au. EBSD analysis in Fig. 6 further confirms the presence of high-angle tilt grain boundaries spanning Ni, Au and Ag

layers while the interface between Ag and Au consists of low angle boundaries (epitaxial growth).

The free energy of a miscible mixture of silver and gold is lowest at 50% concentration of each [32]. This produces a driving force for Au to migrate into the Ag and for Ag to migrate into the Au. The presence of voids in the Ag allows fast diffusion of Ag on the void surface towards the Au rich areas beneath the voids. This flux of Ag towards the Au is not equalled exactly by Au flux towards the top surface of the void because the source of Au atoms is limited, resulting in void migration away from the Ag/Au interface. The Au shows negligible dissolution into the Ag at epitaxial interfaces and hence the only source of Au is initially from the grain boundaries within the plated Au layer. fig. 7 shows maps of Au distribution in the sintered Ag layer, showing that Au diffusion into the sintered Ag occurs only at these grain boundaries. Movement of the sintered Ag grain boundaries then deposits the Au deep inside sintered Ag grains [33,34]; typically in fig. 7, one edge of the Au containing regions is seen to match a current grain boundary while other edges do not match current grain boundaries, but must instead have been the original grain boundary location before grain boundary migration. Even inside the plated Au grain boundaries, Fig. 5 indicates that there are some Au/Ag interfaces that exhibit rapid Au dissolution while at others the original Au boundary seems intact. This suggests that dissolution is strongly dependent on the exact orientation between Ag and Au grains. Au diffusion is concentrated along the major grain boundaries in the sintered Ag, but grain boundary migration and possibly diffusion along twin boundaries [35] also contributes to diffusion to match the high μ values necessary to explain the high value of the effective diffusion coefficient which is some 4 orders of magnitude above the value expected from lattice diffusion alone. In summary, the main effect of the Au and Ag migrations, is a flux of Ag atoms across the inner surface of the voids, towards the Au layer, displacing the void in the opposite direction, and leading to growth of the void free layer and corresponding high porosity layer.

3.3. Ag substrate microstructure results

Images of progressively aged samples on Ag substrates are shown in Figs. 8–10. As in the Au substrate case, there is coarsening of the Ag grains as the samples are aged. Also, in the 500 h sample there is separation of the Ag layer though now this occurs within the plated Ag layer. The images show that after ageing there is greater contact area between the sintered Ag and the plated Ag layers on die and substrate, leading to the increasing shear strength trend observed in Fig. 1a. As expected, given the geometry of Ag
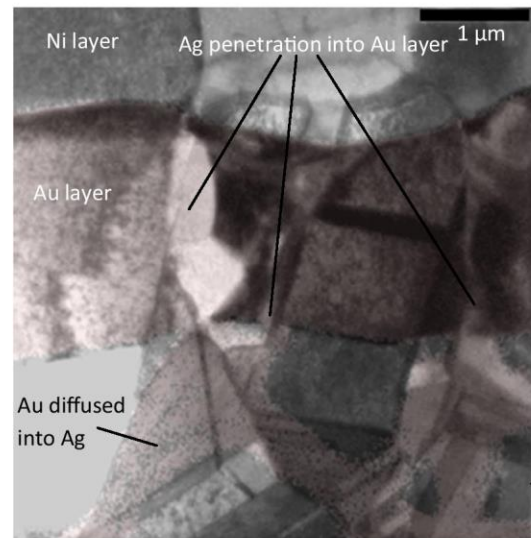

Fig. 7. Map of Au distribution in the region of Fig. 5(d) (presence of Au indicated by pink colouring). (For interpretation of the references to colour in this figure legend, the reader is referred to the web version of this article.)

to Ag interfaces, the joint is relatively homogenous and no highly porous layer forms analogous to that in the Au substrate system. In the absence of the complications caused by Au diffusion, trends in void and porosity evolution as functions of time and spatial position across the substrate can be analysed.

The image processing toolbox in Matlab was used to define pores and quantify porosity, average pore size and numbers of pores, as shown in Fig. 11 which confirms that the porosity in the central areas is much lower than at the edge. Moreover, the porosity decreases rapidly after only 24 h ageing, driven by a dramatic collapse of the void density. The void size by contrast remains relatively stable with the exception of the 500 h central sample where a few extremely large voids develop. Further detail is given in Fig. 12 where the pore size distribution evolution is shown. The pore size distributions after 24 h and 100 h are very similar to the 500 h case with a strong peak in pore sizes between 10 and 100 μm^2 at the edge and lower numbers of pores of all sizes in the centre.

The reason for the difference in porosity between the central portions and outer areas of the chip may be linked to the original placement process. When a highly loaded paste is compressed (squeeze film flow), there is a tendency for the particulates to flow
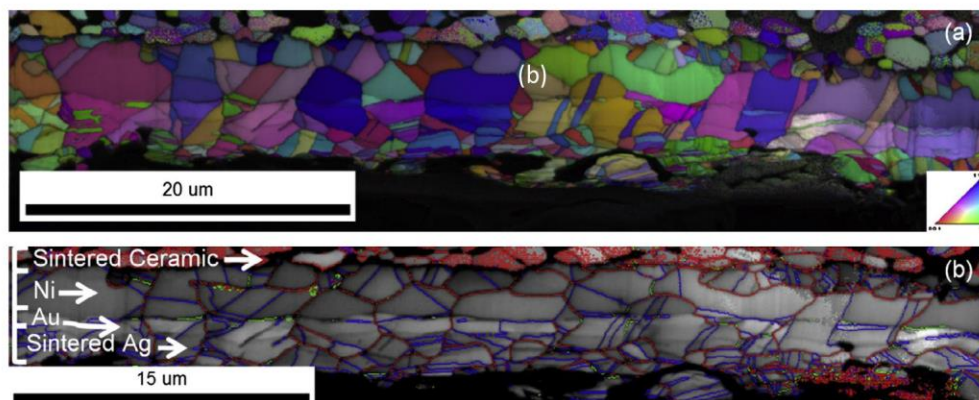

Fig. 6. EBSD images of 24 h sample showing (a) lattice orientation of grains. (b) SEM image of (a) showing grain and twin boundaries, where in the online version red lines indicate high angle grain boundaries (>15°) and blue lines potential coherent twin boundaries. The scale bar does not apply to vertical dimensions as the sample was subjected to a tilt during the measurements. (For interpretation of the references to colour in this figure legend, the reader is referred to the web version of this article.)
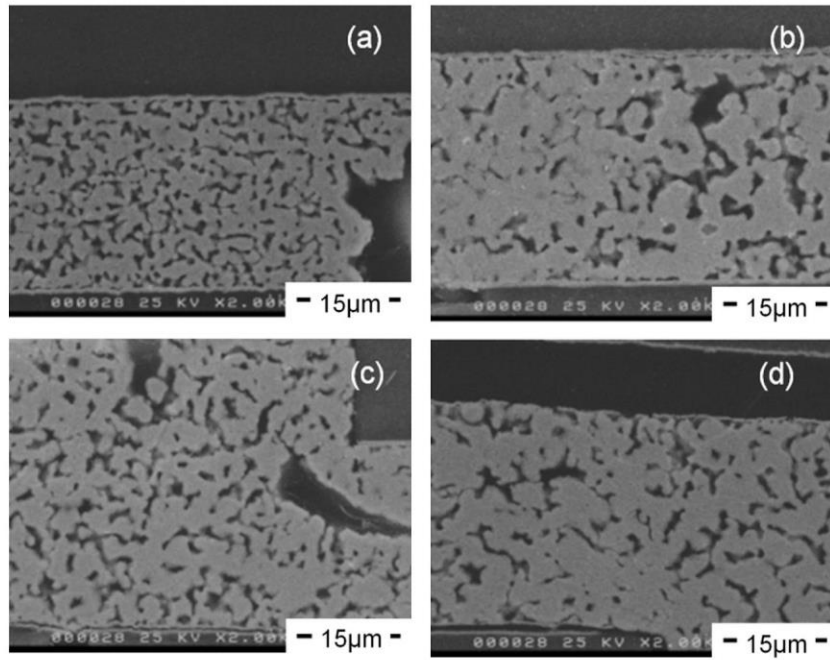
92

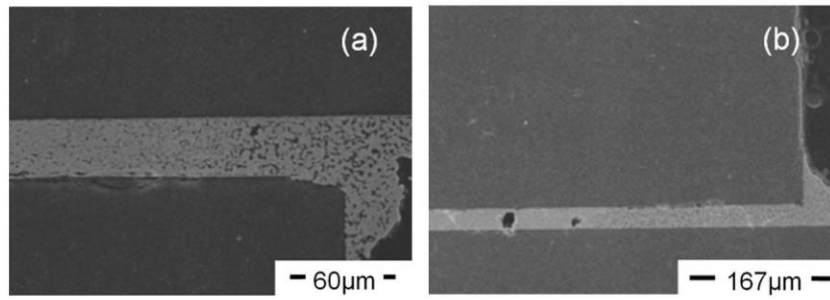**Fig. 8.** Ag substrate at edge of die: (a) control. (b) 24 h. (c) 100 h. (d) 500 h.

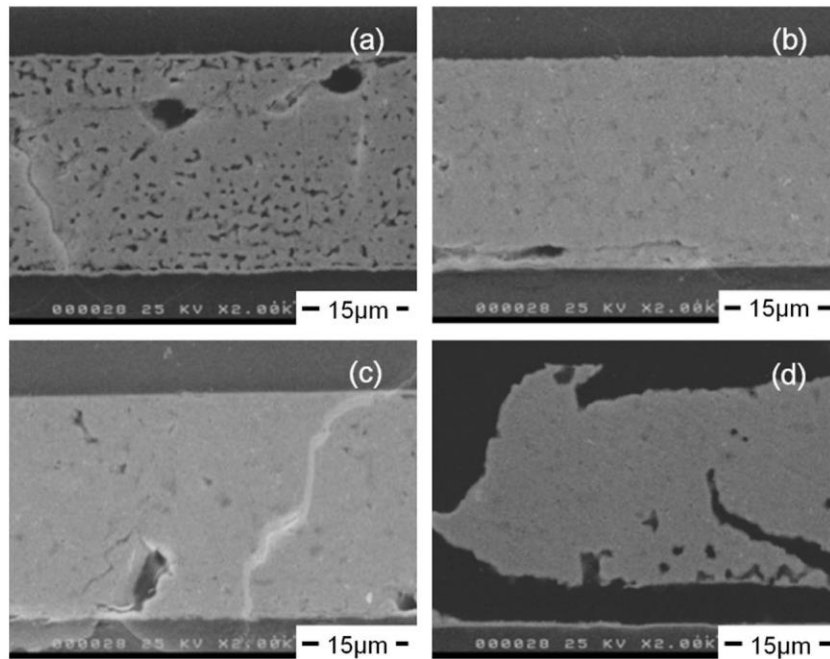**Fig. 9.** Variation of porosity across die for (a) 24 h. (b) 100 h.

Fig. 10. Ag substrate at die centre: (a) control. (b) 24 h. (c) 100 h. (d) 500 h distributions (chip detached from substrate during sectioning).
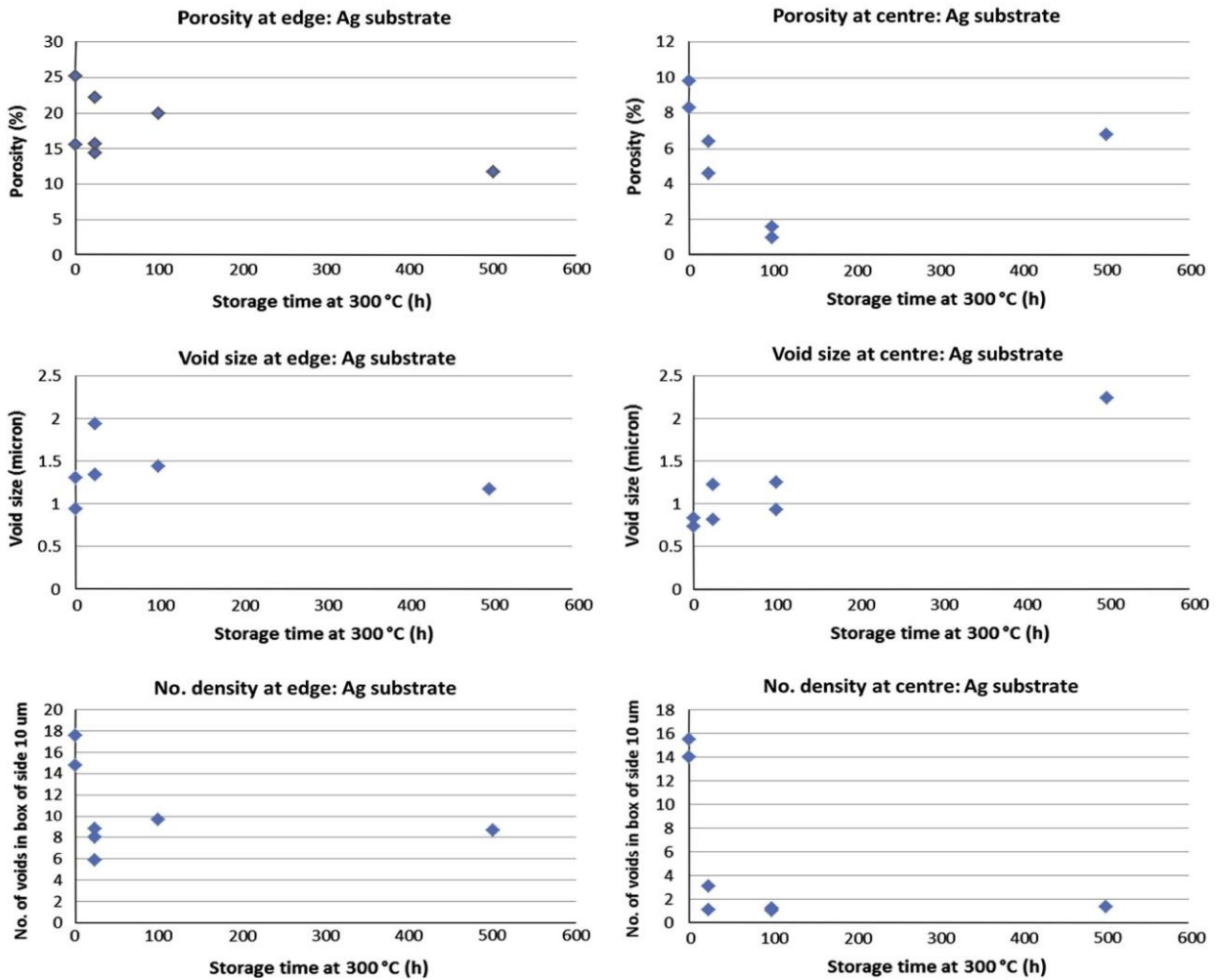
Fig. 11. Porosity statistics as a function of ageing time (multiple points correspond to slightly varying locations of same sample).
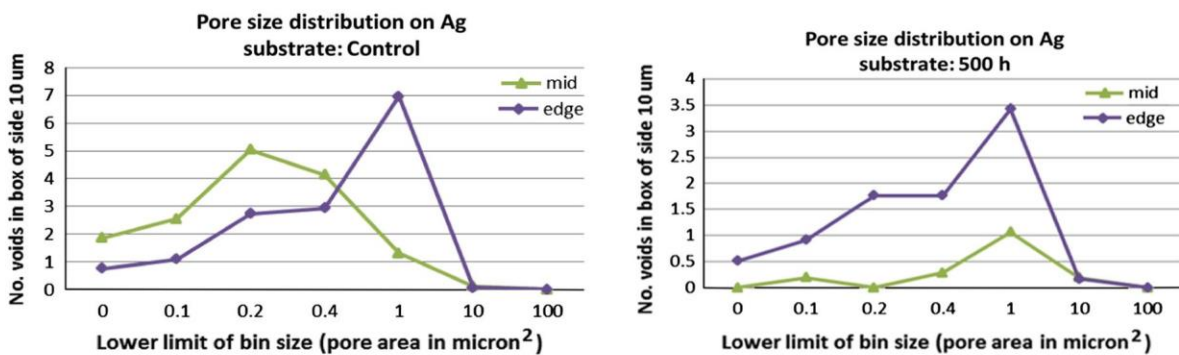

Fig. 12. Pore size distribution after 0 h and 500 h in central and edge (fillet) areas.

out of the gap at a slightly reduced velocity compared to the liquid component of the paste [36]. This will cause the effective volume fraction of particles to increase at the centre of the joint and to decrease at the edges. This is observable in the placement process as a distinct increase in paste viscosity. When sintering occurs the inner regions, being denser and possibly with some particle–particle contact already having occurred, have a lower porosity than the edges. The minimum extent of the porous zone penetration under the chip measured from the cross sections was 54 μm while the maximum was 319 μm. The average was 174 microns.

4. Conclusions

Enhanced atomic mobility at the storage temperature of 300 °C has led to changes in microstructure of the sintered Ag on both Ag and Au substrates. In the case of the Ag substrate, increase in contact area between the plated Ag and the sintered Ag has led to an increase in shear strength. Immediately after sintering a fine porous structure develops, but after 24 h ageing, the small pores have decreased in number, and the overall porosity also decreases slightly. Larger pores remain and grow under the centre of the

93

die. The porosity levels are well below 30%, and the porosity is consistently higher at the edges of the die compared to the central region.

In the case of the Au substrate, Au diffusion from cracks within the Au layer has led to void movement away from the Ag/Au interface to form a high porosity layer that weakens the joint. The exact role of the twin boundaries in facilitating void migration is a topic of further research, but Au is seen to diffuse along grain boundaries in the Ag with a high lattice orientation mismatch. Subsequent grain boundary migration leads to the presence of Au deep inside the sintered Ag grains. From a practical perspective, unmodified industry standard plated thick Au is not a suitable substrate for pressure-free sintered Ag for applications at temperatures of 300 °C or higher; a result also confirmed recently by Yu et al. [37].

Acknowledgements

Appendix A. Supplementary data

Supplementary data associated with this article can be found, in the online version, at http://dx.doi.org/10.1016/j.jallcom.2014.08.062.

References

[1] G. Fusiek, P. Niewczas, J.R. McDonald, presented at the Instrumentation and Measurement Technology Conference, 2009. I2MTC'09. IEEE, 2009.
[2] S.H. Mannan, M.P. Clode, Advanced packaging, IEEE Transactions on 27 (3) (2004) 508–514.
[3] A. Hu, J. Guo, H. Alarifi, G. Patane, Y. Zhou, G. Compagnini, C. Xu, Applied Physics Letters 97 (15) (2010) 153113–153117.
[4] K.S. Siow, J. Alloys Comp. 514 (2012) 6–19.
[5] E. Ide, S. Angata, A. Hirose, K.F. Kobayashi, Acta Mater. 53 (8) (2005) 2385–2393.
[6] T. Wang, M. Zhao, X. Chen, G.-Q. Lu, K. Ngo, S. Luo, J. Electron. Mater. 41 (9) (2012) 2543–2552.
[7] H. Alarifi, A. Hu, M. Yavuz, Y.N. Zhou, J. Electron. Mater. 40 (6) (2011) 1394–1402.
[8] S. Sakamoto, T. Sugahara, K. Suganuma, J. Mater. Sci.: Mater. Electron. 1–9 (2013).
[9] S.K. Volkman, S. Yin, T. Bakhishev, K. Puntambekar, V. Subramanian, M.F. Toney, Chem. Mater. 23 (20) (2011) 4634–4640.
[10] P.R. Couchman, W.A. Jesser, Nature 269 (1977) 481–483.
[11] M. Maruyama, R. Matsubayashi, H. Iwakuro, S. Isoda, T. Komatsu, Appl. Phys. A 93 (2) (2008) 467–470.
[12] Y. Mei, Y. Cao, G. Chen, X. Li, G.-Q. Lu, X. Chen, Device and materials reliability, IEEE Transactions on 13 (1) (2013) 258–265.
[13] T.G. Lei, J.N. Calata, G.-Q. Lu, X. Chen, S. Luo, Components and packaging technologies, IEEE Transactions on 33 (1) (2010) 98–104.
[14] G. Chen, Z.-S. Zhang, Y.-H. Mei, X. Li, G.-Q. Lu, X. Chen, Microelectron. Reliab. 53 (4) (2013) 645–651.
[15] A. Drevin-Bazin, F. Lacroix, J.-F. Barbot, J. Electron. Mater. 43 (2014) 695–701.
[16] T. Kim Seah, C. Kuan Yew, Components, Packaging and Manufacturing Technology, IEEE Transactions on 4 (1) (2014) 8–15.
[17] T. Yamakawa, T. Takemoto, M. Shimoda, H. Nishikawa, K. Shiokawa, N. Terada, J. Electron. Mater. 42 (6) (2013) 1260–1267.
[18] J. Ryu, H.-S. Kim, H.T. Hahn, J. Electron. Mater. 40 (1) (2011) 42–50.
[19] S.J. Kim, E.A. Stach, C.A. Handwerker, Appl. Phys. Lett. 96 (14) (2010) 144101.
[20] G. Lewis, G. Dumas, S.H. Mannan, in: IMAPS Conference & Exhibition on High Temperature Electronics Network (HiTEN 2013), IMAPS, 2013, pp. 237–245.
[21] O.M. Amirmajdi, R. Ashyer-Soltani, M.P. Clode, S.H. Mannan, Y. Wang, E. Cabruja, G. Pellegrini, Electronics packaging manufacturing, IEEE Transactions on 32 (4) (2009) 265–271.
[22] J. Yan, G. Zou, A.-P. Wu, J. Ren, J. Yan, A. Hu, Y. Zhou, Scripta Mater. 66 (8) (2012) 582–585.
[23] J.G. Bai, Z.Z. Zhang, J.N. Calata, G.-Q. Lu, Components and packaging technologies, IEEE Transactions on 29 (3) (2006) 589–593.
[24] J.G. Bai, G.-Q. Lu, Device and materials reliability, IEEE Transactions on 6 (3) (2006) 436–441.
[25] C. Matano, Jpn. J. Phys 8 (3) (1933) 109–113.
[26] J. Bernardini, D.L Beke, in: Nanocrystalline Metals and Oxides, Springer, 2002. pp. 41–79.
[27] F. Jaumot, A. Sawatzky, J. Appl. Phys. 27 (10) (1956) 1186–1188.
[28] H. Alarifi, M. Atis, C. Özdoğan, A. Hu, M. Yavuz, Y. Zhou, Mater. Trans. 54 (06) (2013) 884–889.
[29] S. Wang, M. Li, H. Ji, C. Wang, Scripta Mater. 69 (11) (2013) 789–792.
[30] H. Dong, K.-S. Moon, C. Wong, in: Proceedings 9th International Symposium on Advanced Packaging Materials: Processes, Properties and Interfaces, 2004.
[31] Y. Akada, H. Tatsumi, T. Yamaguchi, A. Hirose, T. Morita, E. Ide, Mater. Trans. 49 (7) (2008) 1537–1545.
[32] Z. Lu, B. Klein, A. Zunger, J. Phase Equilib. 16 (1) (1995) 36–45.
[33] R. Kirsch, J. Poate, M. Eibschutz, Appl. Phys. Lett. 29 (12) (2008) 772–775.
[34] A. Bukaluk, M. Rozwadowski, R. Siuda, Appl. Phys. A 34 (3) (1984) 193–194.
[35] V. Rothová, J. Buršík, J. Phys. Chem. Solids 68 (5) (2007) 785–790.
[36] M. Nikkhoo, K. Khodabandehlou, L. Brozovsky, F. Gadala-Maria, Rheol. Acta 52 (2) (2013) 155–163.
[37] F. Yu, R.W. Johnson, M. Hamilton, presented at IMAPS HiTEC, Albuquerque, NM, May 13–15, 2014.

Addendum to Chapter 5

For the benefit of readers on the type of compositional analysis technique used for Fig. 7 it is added here that Energy-Dispersive X-ray spectroscopy (EDX) has been utilised.

The video mentioned for Figure 4 can be accesses at:

https://doi.org/10.1016/j.jallcom.2014.08.062

6 Thermally stable high temperature die attach solution

Thermally stable high temperature die attach solution

Seyed Amir Paknejad [a,*], Ali Mansourian [a], Yohan Noh [b], Khalid Khtatba [a], Samjid H. Mannan [a]

[a] King's College London, Physics Department, Strand, London WC2R 2LS, UK
[b] King's College London, Department of Informatics, Strand, London WC2R 2LS, UK

A R T I C L E   I N F O

A B S T R A C T

A new design for semiconductor die attach results in a thermodynamically stable microstructure for high temperature electronics applications. The design takes advantage of solid–solid interdiffusion bonding utilizing silver nanoparticles and gold mesh interposer. This results in a die attach assembly with a continuous, non-porous gold-silver interdiffusion layer running all the way from the die to the substrate. The processing of these assemblies is simple and does not require any applied pressure on the die. These assemblies resisted degradation to shear strength for at least 1000 h storage at 450 °C and at least 100 h storage at 600 °C. The random porosity of standard pressure-free sintered silver die attach is converted into single voids at the center of each mesh cell and can be controlled by the mesh geometry.

© 2015 Elsevier Ltd. All rights reserved.

1. Introduction

There is growing interest in solutions for attaching wide-bandgap semiconductor die to substrates in order to manufacture functional electronics for applications where the temperature at the die exceeds 300 °C. Two examples of applications for such high temperature electronics are deep oil and gas exploration, and power semiconductors devices, in which operating temperatures of more than 400 °C may be required [1]. Current research is focused on three main areas; sintering nanoparticles [1–4], high gold content solders [5–6], and solid–liquid interdiffusion (SLID) bonding [7–9]. However, these techniques suffer from various disadvantages. For example, solders have a higher processing temperature than their operating temperature, which results in formation of residual stresses inside the joint [10]. SLID systems suffer from reduction in their mechanical strength at high temperatures [11], while sintered nanoparticle techniques are in their infancy and questions remain over their long term reliability [3].

In this study, the interaction at the interface between sintered silver and gold has been utilized to design a die attach for high temperature applications that is thermally stable i.e. does not degrade at high temperatures. The fundamental interaction is shown in Fig. 1. Fig. 1 (a) shows cross-section of sintered silver on top of a gold substrate. After storage of such assemblies at 300 °C, fast migration of silver and gold occurred resulting a dense and mostly void free interdiffusion layer at the interface (Fig. 1(b)) [12]. This effect can be explained by the preference of gold and silver to mix to minimize the free energy in

the system, since the mixing energy of silver and gold is minimized at 50% concentration of each element [13]. In addition, due to presence of a high concentration of grain and twin boundaries inside sintered silver [10], silver and gold atoms can easily migrate inside the sintered structure extending the interdiffusion layer. In particular, movement of silver across the pore surfaces towards the gold rich interdiffusion zone results in movement of pores in the opposite direction away from the interface. This effect has been further investigated elsewhere [10].

The interdiffusion layer appears to retain its mechanical strength and remains stable at high temperatures [12]. On account of this interesting property, an attempt was made to form a continuous vertical solid–solid interdiffusion layer extending from the die to the substrate producing a thermally resistant attachment for the die. The concept shown in Fig. 2(a), involving a gold mesh structure with vertical walls and silver nanoparticle paste, was developed in order to test the idea. Storage of the assembly at elevated temperature was used to activate the interdiffusion between the gold and silver. Fig. 2(b) shows the conceptual implementation of this technique. After high temperature storage the assembly should theoretically develop into the structure shown in the conceptual Fig. 2(c). The structure should then only further evolve into a more stable mixture of gold and silver during further exposure to high temperatures.

2. Experimental

For a practical demonstration of the interdiffusion layer extending from the die to the substrate commercially available gold meshes from Gilder Grids were utilized. These meshes were not the ideal geometry

* Corresponding author.
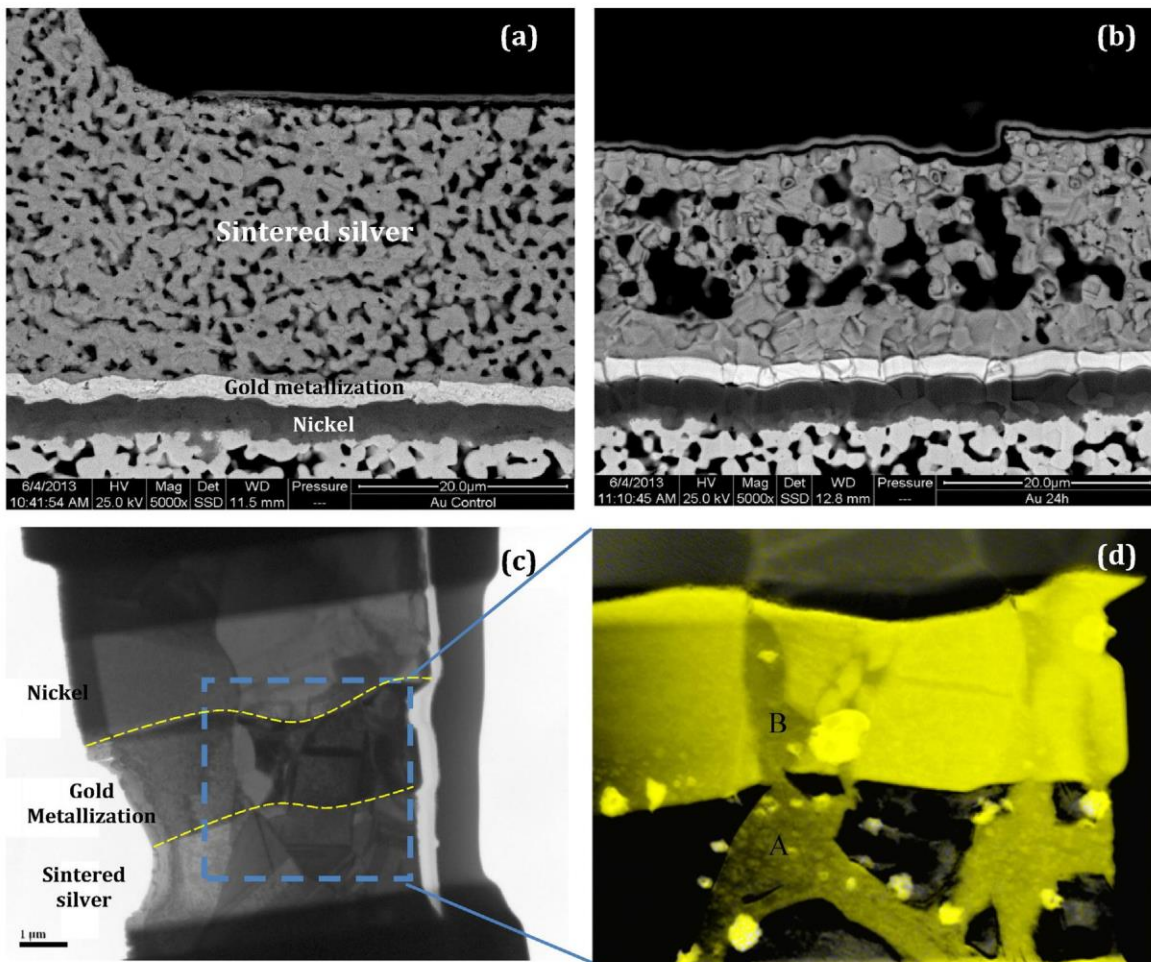 E-mail address: sa.paknejad@kcl.ac.uk (S.A. Paknejad).

Fig. 1. Cross-sections showing formation of a dense interdiffusion layer at the interface of sintered silver and gold mating surface. (a) SEM image of cross-section before storage at high temperature. (b) SEM image of cross-section after storage at 300 °C for 24 h. (c) TEM image of interface between gold substrate and sintered silver die attach of sample shown in (b). (d) Elemental map of (c) with yellow representing gold such that the area marked "A" shows Au penetrating into the silver and the darker area marked "B" represents penetration of silver into the gold metallization.

for this task, but even so have produced very promising results. The substrates and die were both cut from W/Ni/Au metalized cofired alumina. For shear strength tests, some die were cut into rectangles measuring 2 mm by 1 mm (450 °C tests) and the remainder into 3 mm by 1 mm rectangles (600 °C tests). Silver paste was manually dispensed onto both the die and substrate surfaces. The silver paste used was a commercially available nanoparticle silver paste designed for use in pressure-free die attach produced by NBE Tech; NanoTach® X. After deposition of the paste, the mesh is placed on top of the substrate and the die placed on top of the mesh. Light manual pressure was applied to the die to squeeze the mesh into the paste layers. To perform the sintering the samples were ramped slowly from room temperature to storage temperature (450 or 600 °C) at a ramp rate of ~0.5 °C/min. Two different mesh structures with a square cellular geometry or with parallel walls have been utilized, with the dimensions of the parallel walled mesh chosen for shear strength trials shown in Fig. 3.

The assemblies were stored inside a furnace for a range of temperatures and times in air after the initial sintering step. Some samples were then cross sectioned and others used for shear test trials. The cross sectioning was performed by potting in a low temperature cure resin, grinding with silicon carbide papers followed by 3 μm and 1/4 micron mono-crystalline diamond suspension polishing. The cross sections have been observed optically and also using a Scanning Electron Microscope (SEM) (Hitachi S4000) coupled with Electron Dispersive X-ray (EDX) for elemental analysis. Eight samples were prepared for investigation of shear strength after high temperature storage. The first four

samples were prepared for storage at 450 °C for 75 h; two with the mesh and two without. Two samples with mesh were stored at 450 °C for 1000 h and the final two samples with mesh were stored at 600 °C for 100 h. The shear strength tests were carried out using a NANO 17 ip65 force sensor produced by ATI Industrial Automation.

3. Results and discussion

Fig. 4(a) shows a top view of a square mesh before filling with paste, and Fig. 4(b) shows the top view after filling with silver paste and storage by ramping from room temperature to 400 °C 0.1 °C/min and then cooling down back to room temperature in order to enable the interdiffusion effect anticipated in Fig. 2(c). Shear testing was carried out on the parallel mesh samples and Fig. 4(c) shows a cross section of such a mesh after storage at 450 °C for approximately 24 h, indicating that the continuous interdiffusion layer extending from substrate to die has formed. Previous work [10] details the diffusion mechanism for silver and gold interdiffusion. It was found that there is simultaneous diffusion of gold into the silver and silver into the gold. In particular, it was found that the silver initially penetrates the gold at gold grain boundaries, and that these grain boundaries extend into the sintered silver, leading to rapid diffusion pathways for gold to penetrate into the silver (see Fig. 1).

An SEM image of Fig. 4(c) is shown in Fig. 5(a), while the SEM image of the corresponding sample after storage at 450 °C for 1000 h is shown in Fig. 5(b) and elemental composition of the various layers shown in Fig. 5(c). The results show that the mesh has alloyed with the sintered
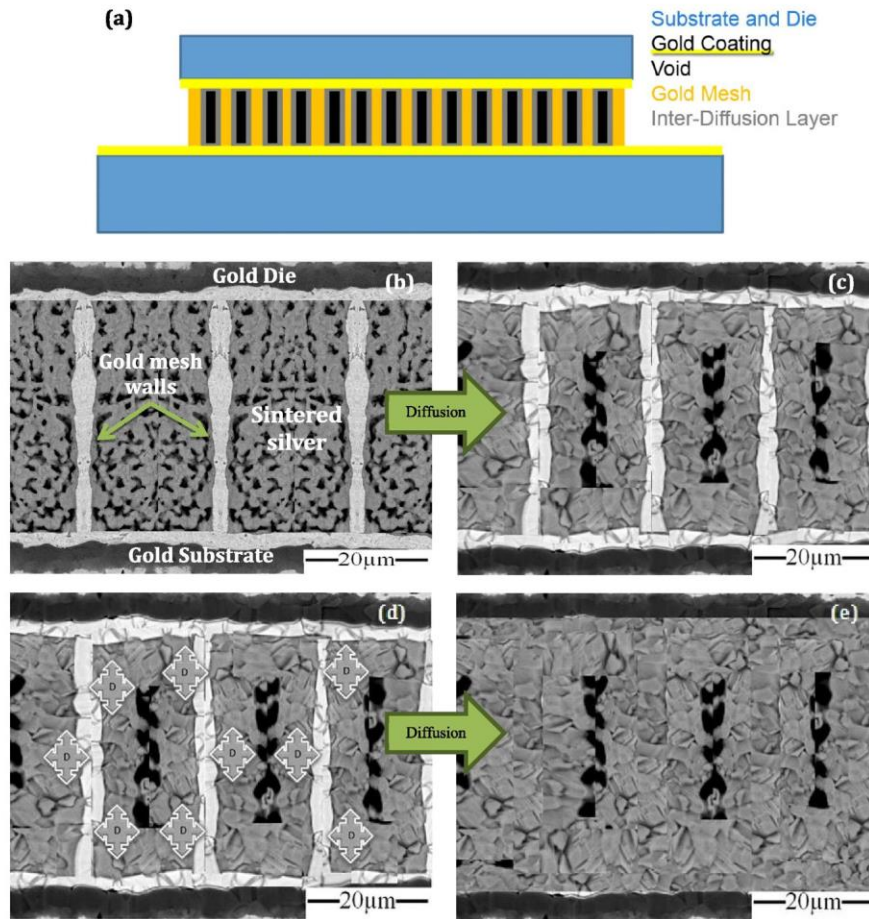
Fig. 2. Conceptual images of the die attach assembly. (a) Schematic cross-section of a die attach assembly, where inserts (mesh) are used for formation of a continuous interdiffusion layer from die to substrate as the main part of the die attach. (b) Conceptual cross-section of a die attach assembly showing the pre-formation of the continuous interdiffusion connection. (c) Conceptual cross-section of the die attach assembly after storage of the assembly in (b) at high temperatures and forming the continuous interdiffusion layer. (d) Arrows labeled "D" showing schematic diffusion pathways of gold and silver. (e) Showing the formation of the thermally stable structure after complete diffusion of silver and gold. (Images (b) to (e) are edited versions of the SEM images of samples shown in Fig. 1.)

Ag and formed a single interdiffusion layer with composition predominantly Ag at the edge of the wall and predominantly Au at the center, but that with the increasing storage time the composition becomes more homogenous. In particular, while points 1 and 2 show 30% change in atomic Au content between the wall center and edge after 24 h, points 3 and 4 show this difference in composition reduced to 16% after 1000 h. Further storage is expected to reduce the difference to zero due to continued diffusion, with the effective diffusion coefficient found to be 1.1×10^{-18} m^2/s in the gold/sintered silver system [10]. It can be seen from Fig. 5(a–b) that the die attach system has withstood 450 °C extremely well and the Au mesh/sintered Ag behaves as

predicted. At this temperature however the Ni metallization has diffused into the Au/Ag layer and oxidized so that reduction or elimination of the Ni layer may be desirable.

For the two samples without mesh stored for 75 h at 450 °C the die fell off during handling of the samples, resulting in an effective shear strength of zero at these extreme temperatures. The shear strength results of the parallel mesh samples are shown in Fig. 6.

Due to the poor properties of the mesh such as variation in the mesh wall heights, these results are not uniform. However, by comparing with the shear strength results of the two 450 °C storage samples stored for 75 h, it may be inferred that the die attach assemblies are at least not
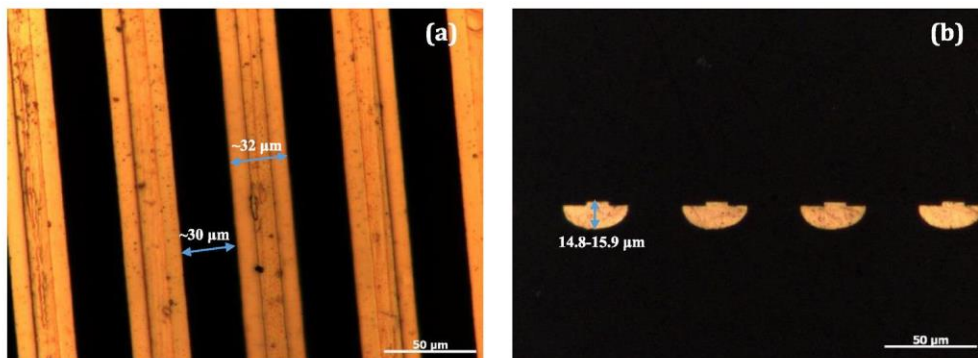

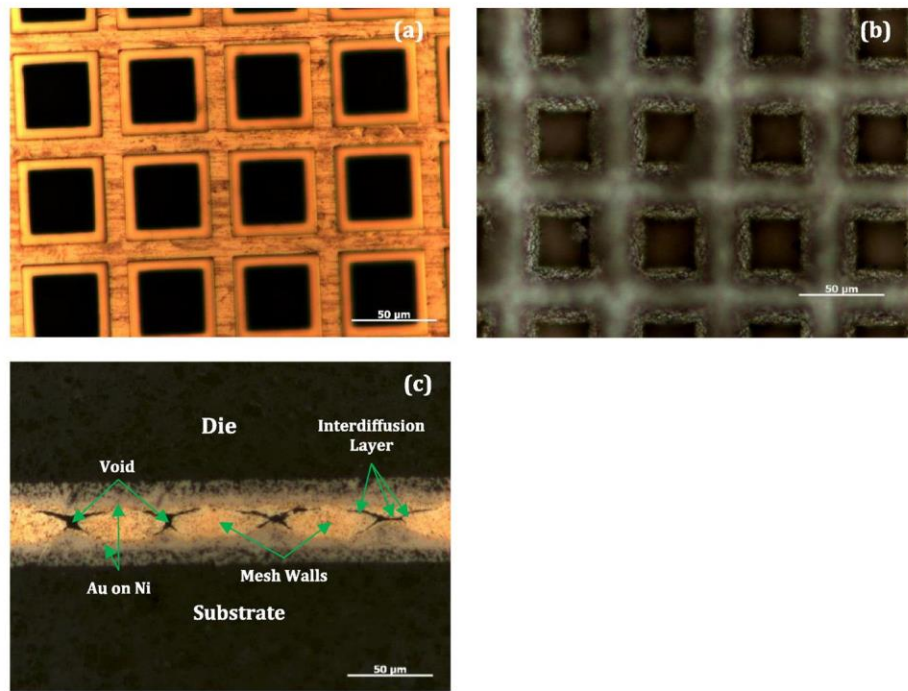**Fig. 3.** Optical images of the parallel walled mesh. (a) Top view of mesh. (b) Cross-section of the mesh.

Fig. 4. Formation of continuous interdiffusion layer around the mesh walls. (a) Top view of a square mesh. (b) Top view of (a) showing the interdiffusion layer around the mesh walls (c) Cross-section of parallel mesh sample similar to Fig. 3(c) showing a continuous interdiffusion layer formed from the die to substrate.

deteriorating during high temperature storage and that the shear strength may even be improving. Theoretically, these assemblies would only evolve towards a more stable structure due to further interdiffusion between gold and silver. Longer storage of the samples at 600 °C was not possible as the die and substrate formed cracks inside their structures after the initial 100 h.

In the present work there is no CTE mismatch between the die and the substrate as both are made from the same material. Future work is therefore needed to examine the effect of high temperature storage and temperature cycling on shear strength in the presence of a CTE mismatch. The presence of porosity in sintered silver is normally considered

a positive aspect in this regard [14] as the porosity makes the material more compliant. The present design replaces random pores with single voids located at the center of each mesh cell, and with void volume determined by mesh wall thickness and spacing, and hence this aspect of the die-attach system can be used to further mitigate against CTE mismatch. For example a higher density of mesh walls at the center could enhance mechanical strength there while a lower density of walls further away from the center could lead to a more compliant structure to compensate for CTE mismatch between the die and substrate. The bond line thickness is determined by the thickness of the mesh and hence mesh design can also be used to deliver the optimized bond
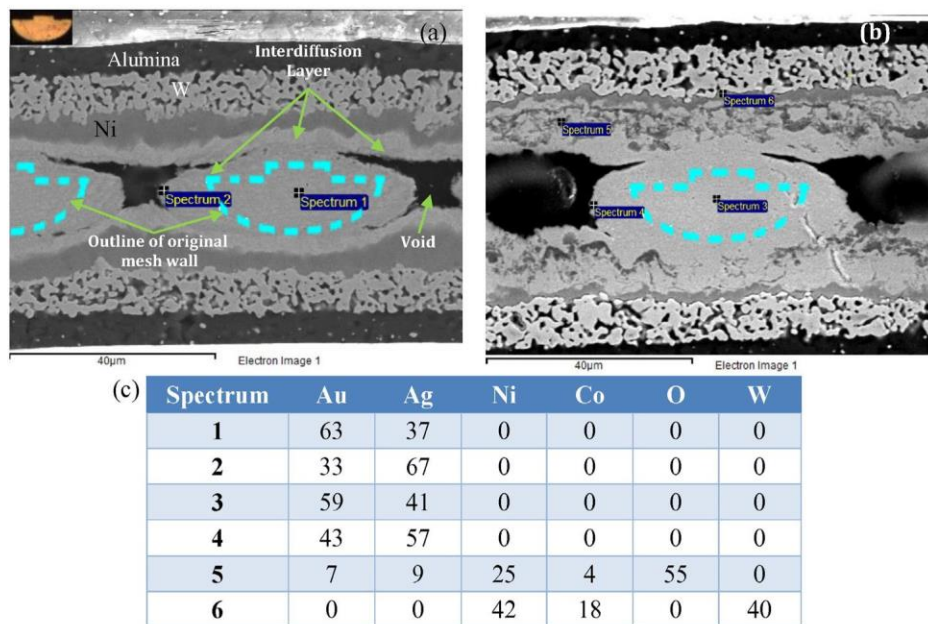

Spectrum	Au	Ag	Ni	Co	O	W
1	63	37	0	0	0	0
2	33	67	0	0	0	0
3	59	41	0	0	0	0
4	43	57	0	0	0	0
5	7	9	25	4	55	0
6	0	0	42	18	0	40

Fig. 5. SEM images of the assembly cross sections (a) Sample stored at 450 °C for 24 h, (top left corner showing optical image of original mesh wall). (b) Sample stored at 450 °C for 1000 h. (c) Elemental composition (atomic %) of the points shown in (a) and (b).
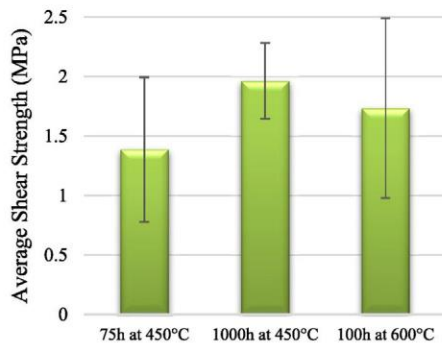
Fig. 6. Average shear strength results of assemblies made using gold meshes.

line thickness which is found to mitigate against CTE mismatch. As described, the current assembly method is suitable for low throughput applications, such as those in the downhole oil and gas, and aerospace industries. Extension to higher throughput applications such as automotive would require further development of automated mesh placement and stencil printing of silver paste into the mesh which is outside the scope of the current work.

4. Conclusions

In summary, by addition of a gold mesh inserted between die and substrate in the presence of silver nanoparticle paste, a continuous interdiffusion layer has been formed that extends from the die to the substrate after sintering. The samples survive harsh high temperature treatments in contrast to samples without the mesh insert and the continuous interdiffusion layer establishes a thermally resistant connection, which can withstand long operating times at high temperatures without degradation of shear strength. Such die attach may provide lower initial shear strength compared to conventional sintered silver die attach as the mesh would reduce the volume percentage of sintered silver. However, after high temperature aging of conventional sintered silver the structure goes through unpredictable changes usually leading to loss of mechanical strength as reported in this work using Au metallization without a mesh and also reported by Yu et al. [15] for a variety of metallizations. In contrast the die attach concept presented in this work evolves towards a predictable thermally stable structure, with gradual incorporation of the mesh into the bonding structure, leading to retention and enhancement of mechanical performance at high

temperatures. In addition, by control of the mesh size and density mechanical properties may be altered as desired.

References

[1] V.R. Manikam, K.Y. Cheong, Die Attach Materials for High Temperature Applications: A Review, 1Components, Packaging and Manufacturing Technology, IEEE Transactions on, 2011 457–478.
[2] K.S. Tan, K.Y. Cheong, Mechanical properties of sintered Ag–Cu die-attach nanopaste for application on SiC device, Mater. Des. 64 (2014) 166–176.
[3] K.S. Siow, Are sintered silver joints ready for use as interconnect material in microelectronic packaging? J. Electron. Mater. 43 (4) (2014) 947–961.
[4] E. Ide, S. Angata, A. Hirose, K.F. Kobayashi, Metal–metal bonding process using Ag metallo-organic nanoparticles, Acta Mater. 53 (8) (2005) 2385–2393.
[5] V. Chidambaram, J. Hattel, J. Hald, Design of lead-free candidate alloys for high-temperature soldering based on the Au–Sn system, Mater. Des. 31 (10) (2010) 4638–4645.
[6] Y. Du, C. Li, B. Huang, M. Tang, C. Du, Research and prospect of binary high-temperature Pb-free solders, Soldering & Surface Mount Technology 27 (1) (2015) 7–12.
[7] R.I. Rodriguez, D. Ibitayo, P.O. Quintero, Kinetics of dissolution and isothermal solidification for gold-enriched solid–liquid interdiffusion (SLID) bonding, J. Electron. Mater. 42 (8) (2013) 2677–2685.
[8] M.M. Hou, T.W. Eagar, Low temperature transient liquid phase (LTTLP) bonding for Au/Cu and Cu/Cu interconnections, J. Electron. Packag. 114 (4) (1992) 443–447.
[9] F.S. Shieu, Z.C. Chang, J.G. Sheen, C.F. Chen, Microstructure and shear strength of a Au–in microjoint, Intermetallics 8 (5) (2000) 623–627.
[10] S.A. Paknejad, G. Dumas, G. West, G. Lewis, S.H. Mannan, Microstructure evolution during 300 °C storage of sintered Ag nanoparticles on Ag and Au substrates, J. Alloys Compd. 617 (2014) 994–1001.
[11] T.A. Tollefsen, O.M. Løvvik, K. Aasmundtveit, A. Larsson, Effect of temperature on the die shear strength of a Au–Sn SLID bond, Metall. Mater. Trans. A 44 (7) (2013) 2914–2916.
[12] G. Lewis, G. Dumas, S.H. Mannan, Evaluation of pressure free nanoparticle sintered silver die attach on silver and gold surface, Oxford: IMAPS Conference & Exhibition on High Temperature Electonics Network (HiTEN 2013) 2013, pp. 237–245.
[13] Z.W. Lu, B.M. Klein, A. Zunger, Ordering tendencies in Pd–Pt, Rh–Pt, and Ag–Au alloys, Journal of Phase Equilibria 16 (1) (1995) 36–45.
[14] V. Caccuri, X. Milhet, P. Gadaud, D. Bertheau, M. Gerland, Mechanical properties of sintered Ag as a new material for die bonding: influence of the density, J. Electron. Mater. 43 (12) (2014) 4510–4514.
[15] F. Yu, R.W. Johnson, M. Hamilton, Pressureless, low temperature sintering of micro-scale silver paste for die attach for 300oC applications, International Conference on High Temperature Electronics (HiTEC), 2014.

7 Conclusions and recommendations for further work

The requirement for a high temperature die attach material for wide-bandgap semiconductors has been strongly felt in recent years. The future requirements for die attach include withstanding high temperatures of at least 300 °C while surviving thermal and mechanical stresses and vibration.

There are some potential materials available currently, but they mostly suffer from inherent limitations, excluding sintered silver nanoparticles, which so far have not exhibited any fundamental issues preventing it from becoming a suitable high temperature die attach. The main issue related to sintered silver die attach is the limited knowledge about its complicated behaviour at high temperatures and the physical mechanisms in operation during interactions with its surroundings. By understanding these behaviours or halting them at the operating temperatures, silver nanoparticle based material might become a suitable die attach for harsh environment applications.

In this project, suitability of sintered silver as a high temperature die attach has been investigated. Initially the physical mechanisms of evolution of sintered silver at high temperatures have been studied, indicating very unpredictable high temperature behaviour in the time period investigated. However, a new technique for production of sintered silver structures, withstanding temperatures up to 400 °C, has been proposed and approved. Then, the high temperature interactions of sintered silver with two common metallizations of electronic devices have been explored. The main point of that observation was that storage of these die assemblies on silver metallization did not indicate any reduction to shear strength even after 500 h storage at 300 °C, while the internal structure of sintered silver evolved considerably. On the other hand, the high temperature behaviour on gold metallization has shown very fast diffusion of silver atoms towards the gold metallization, resulting in considerable reduction in shear strength after just 24 h storage of the assembly at 300 °C. Finally, this fast migration of silver atoms towards the gold metallization considered a disadvantage, has been utilised positively to establish a thermally stable die attach for high temperatures. This new die attach has produced the same shear strength after storage at 450 °C for 75 h or 1000 h, or even 600 °C for 100 h, indicating a thermally stable die attach.

The following sections will summarize the main findings in this project and its second section will recommend some potential routes for furthering the research. In addition, there will be a brief verdict of this project in the final section of this chapter.

7.1 Summary

The main finding of this project will be presented in the following subsections. These subsections are organised by order of main body Chapters 3 - 6.

7.1.1 Microstructural evolution of sintered silver at elevated temperatures

The high temperature behaviour of sintered silver has been continuously investigated *in situ* in a newly designed experimental setup at temperatures from 250 - 400 °C. These observations showed rapid grain growth intervals combined with periods of steady average grain sizes before another rise of average grain sizes. By detailed study of the physical mechanisms of grain growth, the activation energy for grain growth has been calculated as 52.5 ± 2.5 KJ/mol. By comparing this result with the observations on free surface of sintered silver and with published work on this topic, it has been postulated that there exists a passivation layer of silver oxide on the free surface of sintered silver resulting in a stable structure up to about 400 °C, which has been further confirmed in the next chapter. Therefore, a proposal has been made to investigate possibility of growing silver oxide on the internal structure of sintered silver to establish a die attach with potential of staying stable for temperatures up to 400 °C.

- In-situ observations of thermal grain growth
- Fast grain growth intervals are followed by relative stability of average grain sizes before another grain growth phase
- This complex behaviour limits the ability to assure long-term reliability from standard tests
- The passivation layer resulting in thermal stability up to 400 °C appears to be silver oxide.

7.1.2 Ultra-stable sintered silver die attach for demanding high power/temperature applications

The sintered structure of silver has been stabilised using a novel oxidising technique. By placing water inside the oven next to the die attach assembly at 150 °C for 24 h, the produced steam has been able to oxidise the internal structure of sintered silver and stopped the microstructural evolution, which also applies to samples that were dipped inside water for 10 min. In addition to the main evidences for nature of the passivation layer presented inside

this chapter, such as references [6] and [7], which indicated stability of silver oxide up to 400 °C [6, 7] and its effect on stability of silver microstructure up to this temperature [7], further evidence can be mentioned as Energy Dispersive X-ray (EDX) results presented in Appendix A2 and observations of presence of Ag-O bonds in X-ray Photoelectron Spectroscopy (XPS) performed by Mr Khalid Khtatba on surface of sintered silver exposed to atmosphere, which is being prepared for publication. The oxidation treated samples were stable even at 400 °C, which have previously showed massive microstructural changes without this treatment.

- The internal structure of sintered silver has been successfully oxidised with water or steam
- This technique produced the same effect as the atmosphere, which stabilises the surface of sintered silver, but this treatment can stabilise the material even inside the structure
- The steamed structures withstood the whole course of aging for 24 h at 400 °C
- On the other hand, sintered silver without this treatment would start microstructural changes at 250 °C in less than an hour.

7.1.3 Microstructure evolution during 300 °C storage of sintered Ag nanoparticles on Ag and Au substrates

The high temperature interactions of sintered silver with silver and gold metallization have been investigated. The interactions with silver substrate have resulted in increased contact points of sintered silver with the metallization slightly increasing the shear strength during storage at 300 °C for 500 h. On the other hand, the storage of sintered silver on gold metallization at 300 °C has led to formation of horizontal voids along the die attach reducing the shear strength of the joint over time. This behaviour is severe for sintered silver structures, because of existence of many twin and grain boundaries inside such structures, which have been observed by TEM.

- Presence of gold metallization results in fast mass migration of silver atoms towards the interface at 300 °C
- The fast migration leaves horizontal voids along the die attach
- Consequently, the shear strength of the die attach reduces over time

- The shear strength of sintered silver on silver metallization increased slightly over time at 300 °C.

7.1.4 Thermally stable high temperature die attach solution

In Chapter 6, a new technique to establish a thermally stable die attach has been investigated. The die attach here is produced using an interposer inside the die attach assembly forming a solid-solid interfusion layer continuous from the die to the substrate. This technique enables the die attach to move towards a stable structure at high temperatures, which can be designed by the structure of the interposer.

- Thermally stable die attach as a result of continuous inter-diffusion layer
- The shear strength after high temperature aging has not reduced
- The final structure of die attach can be specially designed allowing for optimization of mechanical properties, including possibly stress relief on the die
- The inter-diffusion and void evolution is controlled, resulting in high reliability.

The main points of the conference paper are also summarised below.

7.1.5 Factors influencing microstructural evolution in nanoparticle sintered Ag die attach

In this study it has been discovered that high temperature behaviour of sintered silver differs significantly when exposed to atmosphere or when not exposed. It has also been observed that the rate of grain growth over time for unexposed sintered silver differs greatly for temperatures in the range 200 - 350 °C compared to the 400 - 500 °C range. In addition, 200 °C storage of sintered silver for 5 h has not indicated any changes to microstructure showing potential for applications up to 200 °C.

- Significant high temperature behaviour difference between surfaces exposed and not exposed to atmosphere
- Presence of a passivation layer on exposed surface to the atmosphere resulting in thermal stability up to 400 °C
- Much faster grain growth rate after 400 °C of unexposed sintered grains

- Thermal stability up to 200 °C.

7.2 Recommendations on future work

The following subsections will present recommendations for further work for each of the three main areas investigated in this thesis.

7.2.1 Microstructural evolution inside sintered silver at high temperatures

The most interesting finding of this study was the understanding of the difference between the exposed and non-exposed surfaces of sintered silver. The exposed surface had a higher thermal stability than the internal structure of sintered silver. Therefore, development of a new silver nanoparticle paste to oxidise the internal surface of sintered silver during the sintering process might produce a thermally stable die attach for applications up to 400 °C.

7.2.2 Ultra-stable sintered silver die attach for demanding high power/temperature applications

The stabilisation of the microstructure observed in this work should be investigated against mechanical strength tests to confirm that retaining the microstructure would also preserve the mechanical properties of the die attach. In addition, as the stabilisation is through oxidation of silver atoms on the surface of sintered silver structure, it would be recommended to also confirm the benefits of the stabilisation on prevention of electromigration and silver tarnish from the presence of sulphur.

7.2.3 Microstructure evolution during 300 °C storage of sintered Ag nanoparticles on Ag and Au substrates

The main question remaining in this study for the author was determination of the different mechanisms of diffusion of gold or silver atoms inside the sintered silver structure. Understanding the surface composition of sintered silver inside the pores can make a significant contribution to understanding the diffusion mechanism. Consequently, performing X-ray Photoelectron Spectroscopy (XPS) on the internal pore structure of sintered silver could yield further insight.

7.2.4 Thermally stable high temperature die attach solution

For the die attach system using interposers, investigations with a specially designed mesh structure for increased shear strength are recommended. Practical tests of the idea involve designing and producing meshes with different designs and running reliability trials,

such as shear strength and thermal cycling tests. Computer simulations could also be useful in determining the optimized mesh design. Investigating cheaper materials, such as nickel and bismuth which would undergo similar interactions as silver and gold, could help in reducing overall cost of the die attach.

7.3   Final Verdict

According to the authors opinion, silver sintering appears to be a suitable technique for production of die attach materials for harsh and dynamic environments up to 200 °C if used without further modifications. Sintered silver appears to provide a high mechanical strength with good flexibility to reduce stresses on the die and to withstand high number of thermal cycles. For applications above 200 °C, an easy oxidation treatment step can be implemented into the processing procedure to stabilise its structure against thermal evolutions, which would, in authors opinion, retain its mechanical capabilities as well. Nevertheless, the additional oxidising step found should also be used for applications below 200 °C, as it would bring further assurances on stability of the sintered material, and it could be easily applied by only dipping the material inside water for 10 min. Therefore, the advantages of sintered silver nanoparticles, such as its high mechanical strength, high flexibility and pressure-less sintering, can be used up to 400 °C with this additional fast and easy processioning step. However, for applications requiring higher operating temperatures, utilisation of a continuous interdiffusion layer from die to substrate, which can be easily formed with addition of an interposer would be recommended. This technique has been shown to retain mechanical strength even at 600 °C storage, at which ceramic substrate would decompose into ash. This technique is also a pressure-less sintering process, and it has high potential for many different applications as mixture of other materials to reduce cost or to increase the high temperature capabilities even above 600 °C are not far from applicable.

Appendices

A1 **Factors influencing microstructural evolution in nanoparticle sintered Ag die attach**

Factors influencing microstructural evolution in nanoparticle sintered Ag die attach

S.A. Paknejad[1], A. Mansourian[1], Y. Noh[2], K. Khtatba[1], L. Van Parijs[1], S.H. Mannan[1]

[1]King's College London

Physics Department, Strand, London, WC2R 2LS, UK

Tel: 44 (0) 207 8481780 Fax: 44 (0) 207 8482420 Email: samjid.mannan@kcl.ac.uk

[2]King's College London

Department of Informatics, Strand, London, WC2R 2LS, UK

Abstract

The behaviour of sintered silver die attach at high temperature has been investigated. Assemblies were made by sintering a commercially available paste composed of Ag nanoparticles with zero applied pressure on the die. The morphology of the cross sectioned surface of assemblies remains stable even at temperatures of up to 400 °C. This behaviour remained consistent even inside vacuum or after acid cleaning of the free surface. In contrast, the same sintered Ag material in the interior of a joint or sintered under a glass cover slip showed rapid microstructural changes even at 300 °C. These samples were investigated using an optical microscope to analyse the changes in the microstructure after storage at 200 to 500 °C. The observations showed a 20% increase in silver grain size after only 5 h storage at 300 °C. However, in the case of a free surface, no changes were observed after 60h storage at 400 °C. These observations were combined with DSC experiments in order to suggest the cause of the difference in behaviour. The results suggest ways of stabilizing sintered silver materials so that they can be used in applications up to 400 °C without significant structural changes occurring in the material.

1. Introduction

The intended operating temperature for near future electronics in many applications such as oil and gas exploration, aerospace, and automotive can be as high as 300 °C. The current available die attach materials for such applications have disadvantages such as high homologous temperature or high lead content in case of high temperature solders or sharp reduction in mechanical strength in case of Solid Liquid Inter-Diffusion (SLID) bonding materials [1].

To overcome these issues, many researchers have been trying to develop a technique using sintering of nanoparticles [2-5]. In this case the small size of nanoparticles contribute to a high surface energy and therefore lower melting and sintering temperatures. For instance, 2.4 nm silver particles have a melting point of about only 350 °C [2], which can be compared with the 961°C melting point of bulk silver. In this case as the processing temperature can be lower than the operating temperature, the issues with the homologous temperature can be avoided.

While many studies have been performed on sintering of nanoparticles [6, 7], or the general mechanical features of sintered structures [8, 9], only a small number of these studies are focused on high temperature behaviour of sintered silver at or above 300 °C [10-13]. In the present study in-situ observations of morphological changes on sintered silver have been performed. The conclusions suggest possible routes to enable sintered silver to perform in extreme high temperature applications.

1

2. Experimental

Two silver nanoparticle pastes intended for pressure-less sintering processes, NanoTach® N and NanoTach® X from NBE Tech have been used for these studies. NanoTach® N is only recommended for die sizes of up to 3×3 mm, whereas NanoTach® X is recommended for die sizes up to 10×10 mm. All the samples have been produced under zero applied pressure and by following the recommended sintering profiles.

Sample set 1, was prepared by assembling Ag backed Si die onto Ag backed Si substrates, using NanoTach® N paste. The samples were mounted using a hot mounting resin, LevoFast from Struers after the sintering, this resin being chosen because it was capable of withstanding high temperature storage. The samples were cross sectioned and mechanical polished using silicon carbide cloths followed by diamond suspensions of 3 and 0.25 µm diameter. They were then put into high temperature storage in order to track the shape evolution of individual pores and grains at the cross sectioned surface. The samples were stored at 300 °C for periods of 1, 3, 4, and 20 h. Previous studies using identical pastes and die, but with the cross-sectioning carried out only after high temperature storage indicated that significant changes in pore and grain shape should be expected [11,13].

Three other sample sets were produced using NanoTach® X paste. Sample set 2 was produced by manual paste deposition onto glass slides followed by cover-slip placement on top of the paste (substituting for die placement). The cover-slips were produced by Menzel-Gläser with 150 µm thicknesses, and they were cut into 10×10 mm squares. These samples were then observed pre and post high temperature storage at 200, 300, 350, 400, 450, and 500 °C in air to analyse and compare the microstructural changes of constrained sintered silver under the cover-slip. Sample set 3 was prepared by stencil printing of NanoTach® X into wire shaped gaps with 150 µm thickness and width and with ~4 mm length. These samples were prepared in order to observe the changes of the microstructure on a planar free surface of sintered silver, without exposure to the cross sectioning process of sample set 1. These samples were kept at 300 and 400 °C inside 5 mPa vacuum and at 450 and 500 °C in air. The final set of samples were prepared by deposition of the paste inside custom-made glass sample holders, see Fig. 1 below. These sample holders were designed for surface cleaning of the sintered silver samples in 20% concentration perchloric acid. The newly cleaned surface was kept under deionised water for protection against atmosphere until transfer to a vacuum oven. This set was stored at 300 °C inside about 40mPa of pressure for 5 h. Table 1 lists the materials used in each sample set together with the intended experiment.
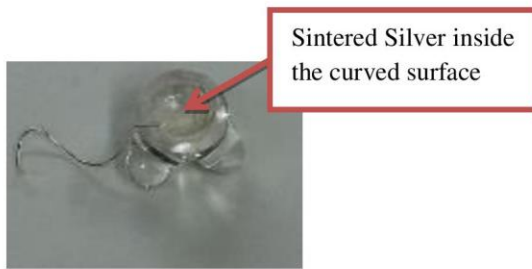
2

Sintered Silver inside the curved surface

Fig. 1. Customized glass sample holder for surface contamination removal process and protection of the sample against atmosphere by merging under deionized water. The silver wire coming out of the sample holder has been intended for charge removal

A Hitachi S4000 Scanning Electron Microscope (SEM) was used for investigating the free surfaces of sintered silver samples. For the samples sintered under cover-slips a Zeiss Axio Lab.A1 optical microscope has been utilized. The produced images were then further analysed using the Image processing toolbox in Matlab and ImageJ 1.46r. The Samples of NanoTach® X paste both pre and post sintering were analysed using a Differential Scanning Calorimetry (DSC) (Mettler Toledo DSC822e).

Sample set No.	Purpose of experiment	Paste type and surface dimensions	Preparation Method
Table 1. Sample sets.			
1	Free surface observation after high temperature storage once cross sectioned	NanoTach® N 2.5×2.5 mm	Recommended sintering profile after manual paste deposition and die placement
2	Constrained surface observation after high temperature storage	NanoTach® X 10×10 mm	Recommended sintering profile after manual paste deposition and cover slip placement
3	Free surface observation without cross sectioning after high temperature storage	NanoTach® X 150 µm ×4 mm	Recommended sintering profile after stencil printing of the paste
4	Free surface observation after acid cleaning and high temperature storage	NanoTach® X $r = 2$ mm	Recommended sintering profile after paste deposition

3. Results and Discussions

The cross-sectioned sample, sample set 1, did not indicate any changes in the morphology of sintered silver even after overall storage of 30 h at 300 °C, vividly contrasting with previously reported observations [11-13]. The difference here was the order of procedures, in that cross sectioning was performed before aging at high temperatures. Therefore, sample sets 2-4 have been produced to investigate whether contamination from cross-sectioning or exposure to air was the primary cause of the difference in microstructural behaviour.

Sample set 2 was produced in order to eliminate the various environmental factors that sample set 1 had been exposed to, while still

allowing in-situ observation of individual pore and grain evolution. Fig. 2 demonstrates considerable differences between pre and post high temperature storage, observed through the glass cover slip. While Fig. 2 (a) and (b) indicate no apparent change in the grain structure after 5 h storage at 200 °C, Fig 2 (c) and (d) shows considerable changes in the microstructure of sintered silver after only 5 h at 300 °C. Fig 2 (e) and (f) indicate a sharp rise in grain growth at higher temperature.
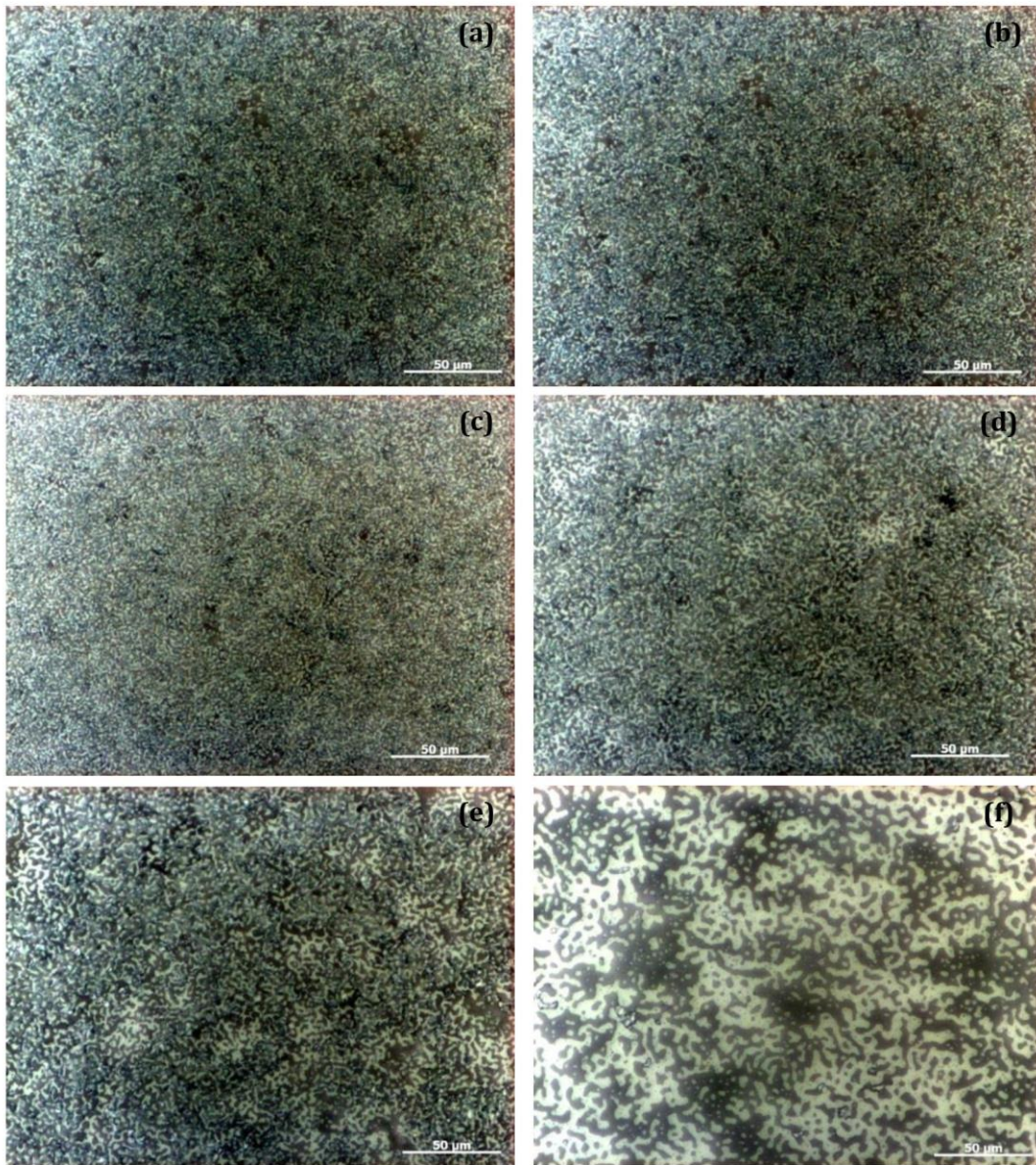

Fig. 2. Optical images of sintered silver under cover slip stored in air. (a) before storage at 200°C. (b) Image of same area as (a) after 200°C for 5h. (c) Image before storage at 300°C. (d) Image of same area as (c) after 300°C for 5h. (e) 400°C for 5h. (f) 500°C for 5h.

4

To quantitatively analyse the grain growth of sintered silver during the 5 h storage, the Matlab image processing toolbox and ImageJ software were used. Fig. 3 shows the steps taken to perform the grain size measurements on the optical images of sample set 2. The data obtained from these measurements have been plotted against temperature to compare the grain sizes after storage to their initial sizes, shown in Fig. 4. It is interesting to note that the grain growth rate increases sharply after 350 °C, and

presence of two linear sections with very different gradients suggests presence of two different grain growth mechanism at those temperature regimes. In addition, the average grain size has increased by about 20% after 5 h storage at 300 °C, which is unlike sample set 1 where no grain change was been observed even after 30 h at this temperature. Furthermore, negligible changes to the grain sizes at 200 h indicate a relatively stable structure of sintered silver up to such temperatures.
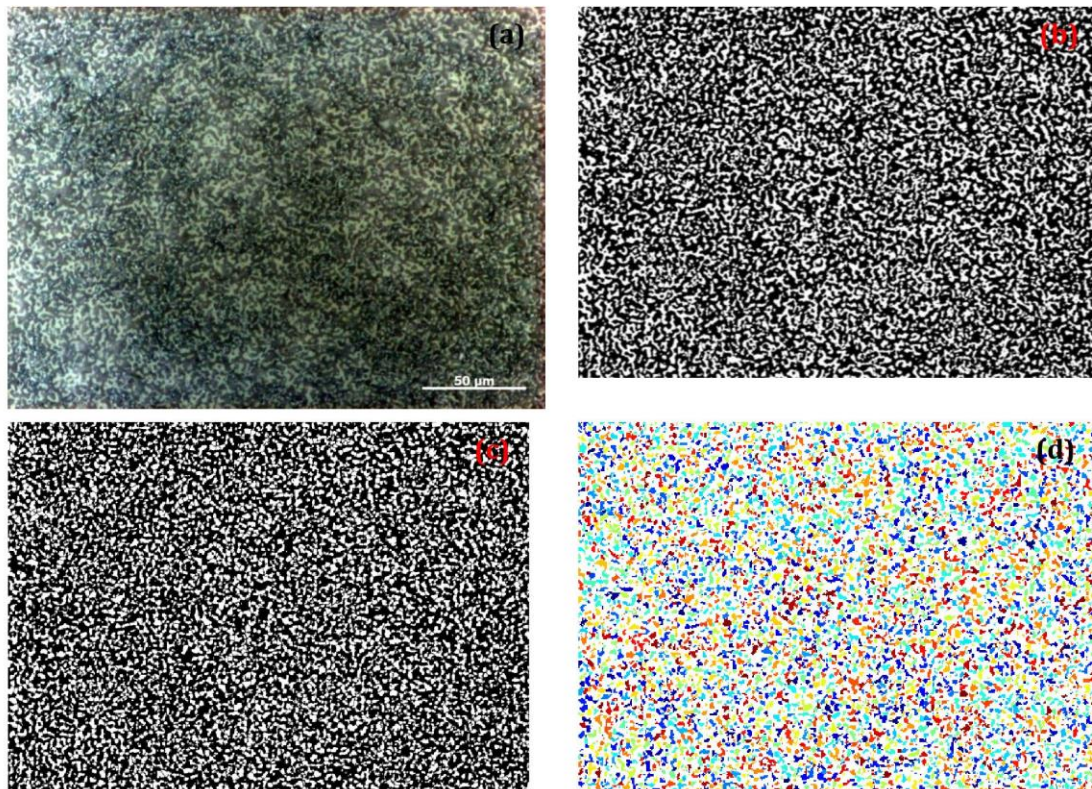
Fig. 3. Processing of optical images for grain size measurements. (a) Typical area on sintered silver stored at 350 °C for 5h to illustrate the technique. (b) Binary image of (a) produced in Matlab by a local thresholding technique [14] to overcome the uneven background. (c) Watershed segmentation of (b) using ImageJ. (d) Grain area and quantity calculated for estimating the average grain size using MatLab (coloured for illustration proposes).
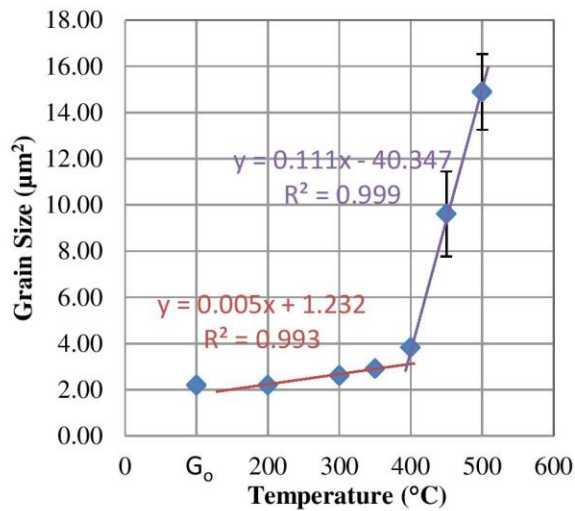
Fig. 4. The average grain sizes vs. storage temperature for 5h. G_o is the initial grain size after sintering.

The third set of samples eliminated the cross sectioning process by stencil printing of the silver paste. Therefore, the only contributing factor to any microstructural behaviour difference to sample set 2 and the previously performed experiments [11-13] is exposure to atmosphere prior to aging. Fig. 5 (a) shows the free surface of the sintered silver before aging, showing that it is identical to Fig 5 (b) and (c), where the samples experienced overall aging of 40h at 300 °C and 66 h at 400 °C both in vacuum. However, additional storage at 500 °C in air for 24 h has greatly changed the structure of the sintered silver; Fig. 5 (d). Performing 300 °C aging of another sample from set 3 for 24 h in air also did not result in any changes. While 66 h at 400 °C did not produce any changes to the morphology, only half hour storage at 500 °C resulted in considerable changes; Fig. 6.
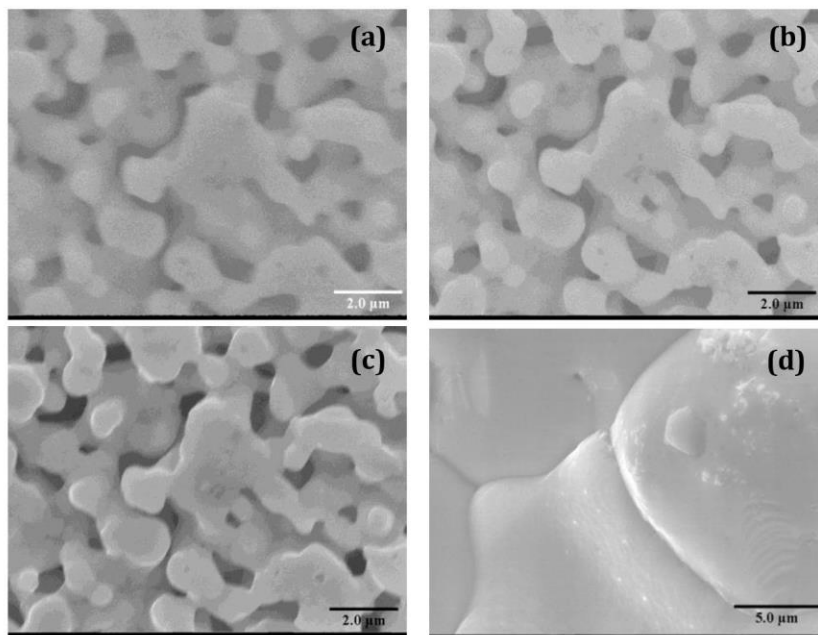
Fig. 5. SEM images from sample set 3 after high temperature storage in vacuum each looking at the same area of the sintered silver. (a) 0h. (b) 24h at 300°C. (c) Additional 16h at 300°C and 66h at 400°C. (d) Additional 24h at 500°C (not in vacuum, and the original area was not identified).

6
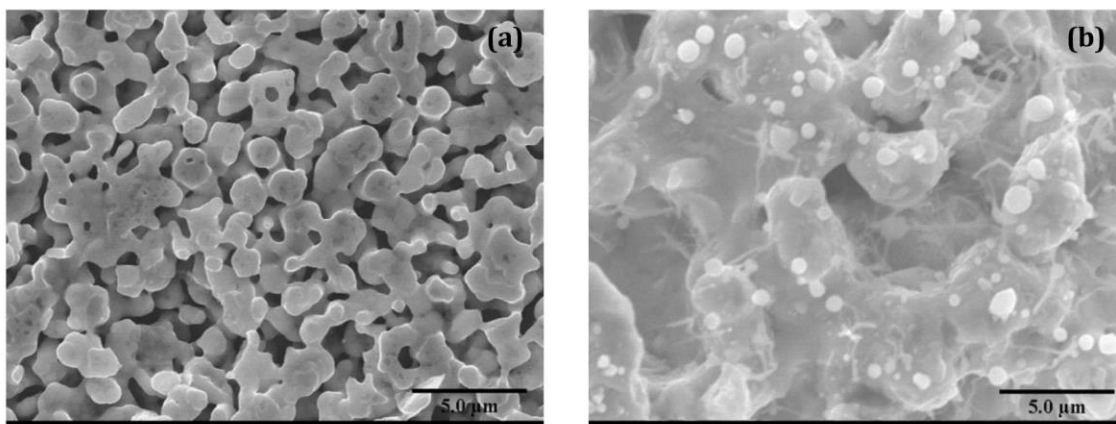
Fig. 6. SEM image of high temperature storage at 500°C in air. (a) 0h. (b) 0.5h (original area was not identified).

These observations point out to the presence of a passivating material on the surface of the sintered silver, which appears to prevent the surface diffusion of atoms on their free surfaces. As a result of the arrest of surface diffusion, the expected changes to the microstructure are also halted. DSC experiments on NanoTach® X show the presence of an exothermic and irreversible peak at around 450 °C, (see Fig. 7), which appears to confirm the decomposition of the surface passivating material. Further observations on the high temperature behaviour of sintered silver from sample set 3 have shown interesting results. As shown in Fig. 8, storage at 450 °C for 1 h in air did not result in any observable changes to the structure, while an additional 1.5 h completely changed the structure. This again seems to be resulted by the passivating layer, which requires the initial 1 h period to decompose and enable surface diffusion and consequently grain evolution. To further investigate the passivating layer, sample set

4 has been stored inside perchloric solution for 30 min and after cleaning, stored under deionised water for further protection. However, after placement of the sample inside 300 °C for 5 h no change has been observed indicating the possibility of nonorganic background of the passivating layer.
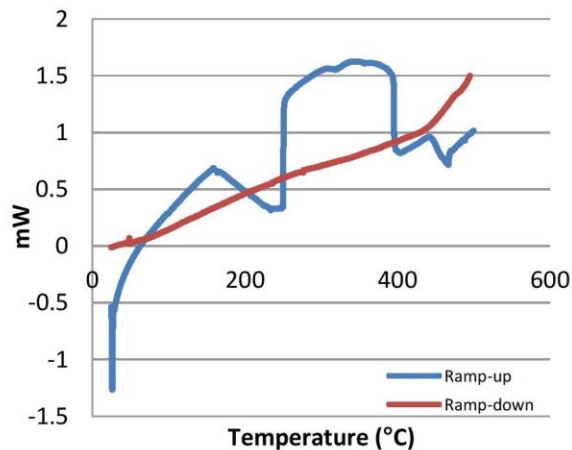
Fig. 7. DSC of sintered silver. Ramp rate 10 °C/min and sample weight 10.5 mg.
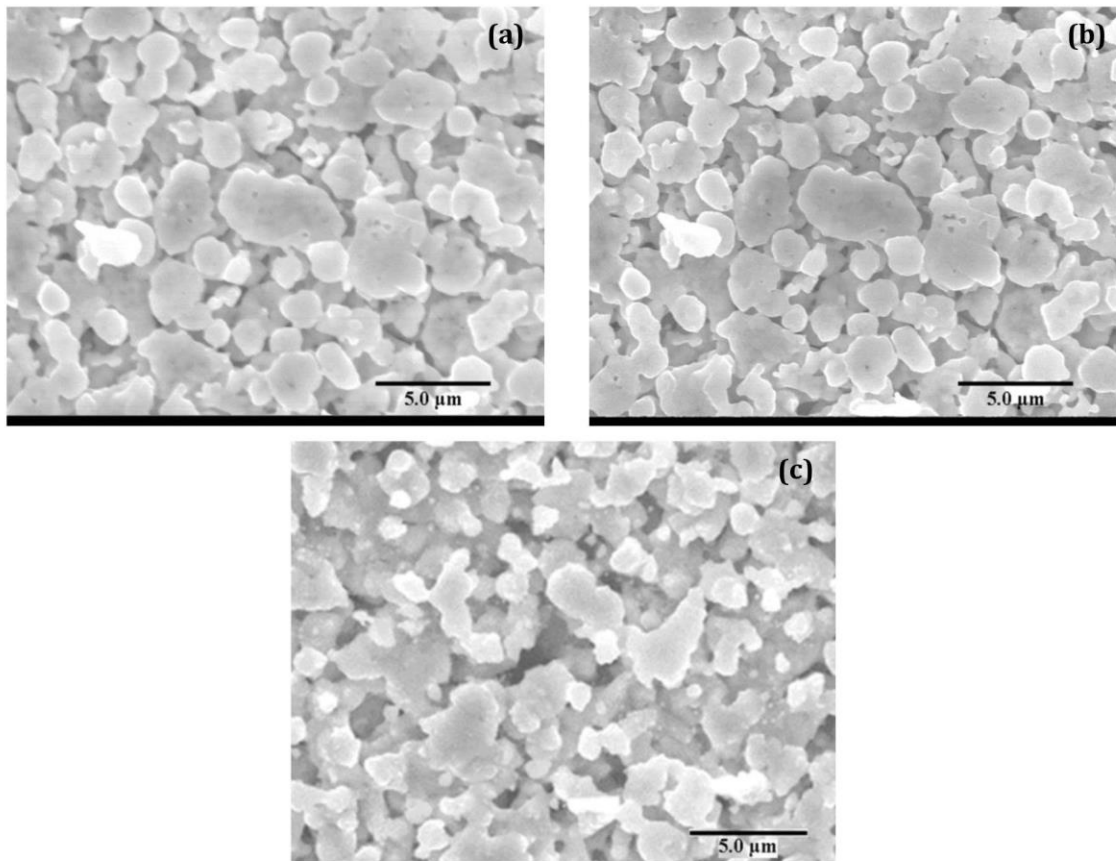
Fig. 8. SEM images of high temperature storage at 450°C in air. (a) 0h. (b) 1h (c) Additional 1.5h.

4. Conclusions

It has been observed that exposure to atmosphere of sintered silver can stop the surface diffusion of atoms and result in preservation of the initial structure even at 400 °C. However, the surface of sintered silver protected by cover-slip has greatly changed during storage at 300 °C. Therefore, if the passivation layer could be formed on the interior sintered silver pore surfaces, e.g. by altering the chemical composition of the paste, it may stabilize the microstructure and result in die attach materials with longer lifetimes at high temperatures than current systems.

It has also been noted that the microstructural evolution of sintered silver without the passivation layer increases gradually from 200 °C to 350 °C, but from 400 °C to 500 °C the changes happen much more rapidly. In addition, the microstructure on the free surface of sintered silver evolves after a delay of more than 1 h at 450 °C, which can be attributed to the time required for removal of the passivation layer. Furthermore, the acid cleaning procedure indicates that the passivation layer is unlikely to be composed of organic compounds, and is more likely to be one of the silver oxides which can form.

For future work, it is recommended to perform XPS on the free surface of sintered silver to fully determine the composition of the passivating layer.

8

References

[1] T. Tollefsen, O. Løvvik, K. Aasmundtveit, A. Larsson, Metallurgical and Materials Transactions A, 44 (2013) 2914-2916.

[2] M. Maruyama, R. Matsubayashi, H. Iwakuro, S. Isoda, T. Komatsu, Applied Physics A, 93 (2008) 467-470.

[3] Y. Akada, H. Tatsumi, T. Yamaguchi, A. Hirose, T. Morita, E. Ide, Materials transactions, 49 (2008) 1537-1545.

[4] J.G. Bai, G.-Q. Lu, Device and Materials Reliability, IEEE Transactions on, 6 (2006) 436-441.

[5] K.S. Siow, Journal of alloys and compounds, 514 (2012) 6-19.

[6] K. Nakaso, M. Shimada, K. Okuyama, K. Deppert, Journal of Aerosol Science, 33 (2002) 1061-1074.

[7] A. Moitra, S. Kim, S.-G. Kim, S.J. Park, R.M. German, M.F. Horstemeyer, Acta Materialia, 58 (2010) 3939-3951.

[8] E. Ide, S. Angata, A. Hirose, K.F. Kobayashi, Acta Materialia, 53 (2005) 2385-2393.

[9] P. Peng, A. Hu, B. Zhao, A.P. Gerlich, Y.N. Zhou, Journal of Materials Science, 47 (2012) 6801-6811.

[10] W. Leong Ching, S. Wen Wei, E.P.J. Rong, D. Mian Zhi, V.S. Rao, D.R. MinWoo, Electronics Packaging Technology Conference (EPTC 2013), 2013 IEEE 15th, 2013, pp. 335-340.

[11] G.D. G. Lewis, and S. H. Mannan, HiTEN 2013, IMAPS Oxford, 2013, pp. 237 – 245.

[12] F. Yu, R.W. Johnson, M. Hamilton, HiTEC 2014, IMAPS, Albuquerque, 2014.

[13] S. Paknejad, G. Dumas, G. West, G. Lewis, S. Mannan, Journal of Alloys and Compounds, 617 (2014) 994-1001.

[14] B. Shoelson, ThresholdLocally. Accessed on 13/04/2015 from http://www.mathworks.com/matlabcentral/fileexchange/29764-thresholdlocally, last update 08/02/2011.

9

A2 **Tunable ultra-high aspect ratio nanorod architectures grown on porous substrate via electromigration**

SCIENTIFIC REP✺RTS

Tunable Ultra-high Aspect Ratio Nanorod Architectures grown on Porous Substrate via Electromigration

Ali Mansourian[1], Seyed Amir Paknejad[1], Qiannan Wen[2], Gema Vizcay-Barrena[3], Roland A. Fleck[3], Anatoly V. Zayats[1] & Samjid H. Mannan[1]

The interplay between porosity and electromigration can be used to manipulate atoms resulting in mass fabrication of nanoscale structures. Electromigration usually results in the accumulation of atoms accompanied by protrusions at the anode and atomic depletion causing voids at the cathode. Here we show that in porous media the pattern of atomic deposition and depletion is altered such that atomic accumulation occurs over the whole surface and not just at the anode. The effect is explained by the interaction between atomic drift due to electric current and local temperature gradients resulting from intense Joule heating at constrictions between grains. Utilizing this effect, a porous silver substrate is used to mass produce free-standing silver nanorods with very high aspect ratios of more than 200 using current densities of the order of 10^8 A/m^2. This simple method results in reproducible formation of shaped nanorods, with independent control over their density and length. Consequently, complex patterns of high quality single crystal nanorods can be formed *in-situ* with significant advantages over competing methods of nanorod formation for plasmonics, energy storage and sensing applications.

Electromigration (EM) is defined as the transport of atoms driven by momentum transfer from electron flow inside a current carrying material. This can lead to structural changes such as whisker growth and stress induced voids[1,2]. Electromigration is normally depicted in a negative light, as a serious problem for Very-Large-Scale Integration (VLSI) and Ultra-Large-Scale Integration (ULSI) electronic circuits due to the increasing current densities that accompany miniaturization[3]. Therefore much effort has been directed at developing new electronic materials, wiring designs and fabrication methods so as to minimize the effects of electromigration[4]. However, electromigration has recently been used constructively as a tool for fabrication of zero and one dimensional nanocrystals[5] nanostructures for local electric field enhancement in plasmonics[6,7], molecular-scale biochemistry measurements[8–11] and to control the kinetic faceting of surface orientations that belong to the equilibrium shape of the crystals[12]. In general electromigration is affected by a large number of parameters such as current density, temperature, film thickness, grain size and timescale[1–4,13]. Previous attempts to create whiskers using electromigration either resulted in whiskers growing only at the anode[14,15] or required precise local conditioning of the substrate to generate localised whiskers[15,16]. An industrial method with control over mass production of whiskers over an entire substrate would have applications in plasmonics[17], energy storage[18] and sensing applications[3,4,6,7] due to the high aspect ratio and large surface area structures that could be produced.

In this work, we demonstrate that electromigration can be applied to grow a dense structure of nanorods on a porous Ag substrate rather than the sparse nanorod formation previously observed. Electromigration in a porous medium is also shown to result in nanorods being formed along the length of the conductor rather than being confined to the anode as in a typical non-porous media. In addition to the high density of nanorod formation, it is found that the density and nanorod length can be independently controlled. The ability of the process to produce single crystal nanorods with aspect ratios exceeding 200 is also highly noteworthy, as is the production

[1]Department of Physics, King's College London, Strand, London WC2R 2LS, UK. [2]Department of Physics and Materials Science and Centre for Functional Photonics (CFP), City University of Hong Kong, Tat Chee Avenue, Kowloon, Hong Kong. [3]Centre for Ultrastructural Imaging (CUI), King's College London, New Hunt's House, Guy's Campus, London, SE1 1UL, UK. Correspondence and requests for materials should be addressed to S.H.M. (email: Samjid.mannan@kcl.ac.uk)

of high aspect ratio platelets in addition to nanorods. Furthermore, electromigration in a porous medium results in transformation of the internal pore and grain structure, an effect which has not previously been reported but which may have interesting technological applications in its own right. The growth mechanism of nanorods along the length of the conductor can be explained by the interaction of the normal electron wind force[19] driving atoms from cathode to anode with thermal gradients generated by the presence of the pores causing current constrictions. The simplicity of nanorod formation by electromigration, utilizing voltages ~7 mV across the ~500 μm length of the conducting stripe to generate high current density, may have significant advantages over other methods of nanorod growth[20] and in particular may allow complex patterns of nanorods being grown simply by controlling the local current densities.

Results

A schematic of the EM experimental setup is shown in Fig. 1a. The nanorod density, location, size and diameter are controlled by EM duration, current density and interruptions. EM was carried out on five samples (see Methods and Supplementary information) in air, at two temperatures (ambient and 200 °C) with current densities ranging from 2.2×10^8 to 2.45×10^8 A/m^2 (Table S1). The duration of the electromigration processes was from 6–480 h. Electron microscopy (SEM and TEM) analysis reveals high quality single crystal nanorods with diameter down to 20 nm (Fig. 1b,e). Straight nanorods occur in short duration EM experiments of up to 240 h (Fig. 1b). Figure 1c shows constant diameter curly nanorods formed after long duration uninterrupted EM. Platelets with hexagonal tips (Fig. 1d) can also be formed as a result of the initial protrusions expanding followed by growth. The hexagonal shape indicates that the rod emerges from a [1, 1, 1] plane of the fcc Ag lattice[21,22]. The EM experiments running for 480 h (Fig. 1c,g) show that the nanorods continue to grow until the density of the generated nanorods is high enough for them to meet neighbouring nanorods which may be responsible for limiting nanorod growth to a maximum length of ~20 μm (Fig. S1b–d). Figure 1g shows a high density of nanorods with possible instances of welding between them. Previous studies have reported welding of individual silver nanorods under high current density at the point of contact[23]. Increasing current density to 1.70×10^9 A m^{-2} results in amalgamation of grains and pores at the cathode where reduction in the number of conduction paths leads to high localised heating and circuit failure after a short time of 18 h (Fig. S2). Increasing temperature up to 200 °C in samples (for 120 and 240 h) does not result in nanorod formation after EM.

Figure 2 shows a comparison of the top surface of the Ag stripe S3 before and after EM for 240 h, at the anode, centre and cathode. The number density of nanorods decreases steadily between anode and cathode, with the density of nanorods at the cathode approximately one third that of the anode. This suggests that a uniform coverage of nanorods might be achieved by simply reversing the flow of current so that both ends of the stripe spend equal times as anode and cathode. Figure 2a–f shows the change in nanorod size distribution and number density across the stripe. Figure 2g–i summarizes the changes in number density and average nanorod length (not adjusted for orientation) across sample S3 for time periods of 120, 240 and 480 h. The average length of the nanorods ranges from 400 to 550 nm and longer nanorods do still appear across the sample, with the largest rods reaching an apparent length of 20 μm (Fig. 1f). Nanorod diameter is relatively constant at 25–40 nm, with some larger diameter rods (up to 100 nm) produced in one sample S2 (Table S1) which experienced multiple connection and disconnection events.

Characterisation of the fabricated nanorods shows the formation of good quality single crystal nanorods at the top surface of the samples. The TEM image of the 20 nm diameter nanorod is shown in Fig. 3a,b and the Selected Area Electron Diffraction (SAED) patterns[22,24] are interpreted as the overlapping of [111] and [110] zone axes which indicate a six fold symmetry previously associated with silver nanorod growth. The orientation of nanorods with respect to the electron beam is shown in the inset of (Fig. 3b). Previous studies have suggested that weak points in a metal oxide layer act as nucleation sites for nanorod growth[25]. Figure 3c shows Energy Dispersive X-Ray (EDX) analysis on a nanorod and on a grain at the surface of the stripe. The bar chart shows that at the surface of the sintered silver grains after electromigration the composition contains 8% oxygen whereas the composition is 0% oxygen in the spectrum taken from the nanorod. These results suggest the existence of a thin oxide layer on the surface of the silver stripe during the EM process. In order to test this hypothesis further, EM on sample S3 (Fig. 3d,e) was interrupted after 120 h for a period of 240 h and then restarted with the same current density as before for an additional 120 h. The original rods (indicated by the red arrows) did not continue growing after the interruption, but new rods emerged, as shown by Fig. 3f. This behaviour was repeated at other locations and in other samples, suggesting that new weak spots in the thin oxide layer form when the samples cool down and contract during the interruption. The spectrum of nanorods after multiple interruption (Table S1) shows evidence of an oxide layer forming on the original nanorods which could account for the lack of growth in these nanorods (Fig. S4).

While there is no change in surface grain morphology during EM evident from either Fig. 2 or Fig. 3 apart from nanorod growth, massive change in internal grain structure is seen in Fig. 3g,i. This is not purely a result of thermal effects as shown by the control (Fig. 3h) which was stored at 200 °C for 480 h while the sample of Fig. 3i was subjected to EM. It should be noted that the structure seen in Fig. 3i after EM was found throughout the stripe at anode, centre and cathode and that the orientation of the elliptical grains changes throughout the stripe and does not appear to be simply correlated with the cathode-anode axis (arrow, Fig. 3i). The contrasting surface and interior behaviour indicates that while the oxide layer at the stripe surface prevents atomic migration along grain surfaces, in the stripe interior, grain surfaces do not support an oxide layer that prevents surface diffusion. Voids have not been directly detected at the surface of the porous sample, but formation of nanorods is accompanied by an increase in resistance (1–5%), followed by rapid resistance fluctuations and finally open circuit, accompanied by a crack. This can be explained with reference to Fig. 3g,i where it is seen that significant internal transformation of structure is occurring. Calata et al.[26] also observed formation of cracks at locations where the current density increases abruptly and attributed this to high atomic flux density in those regions.
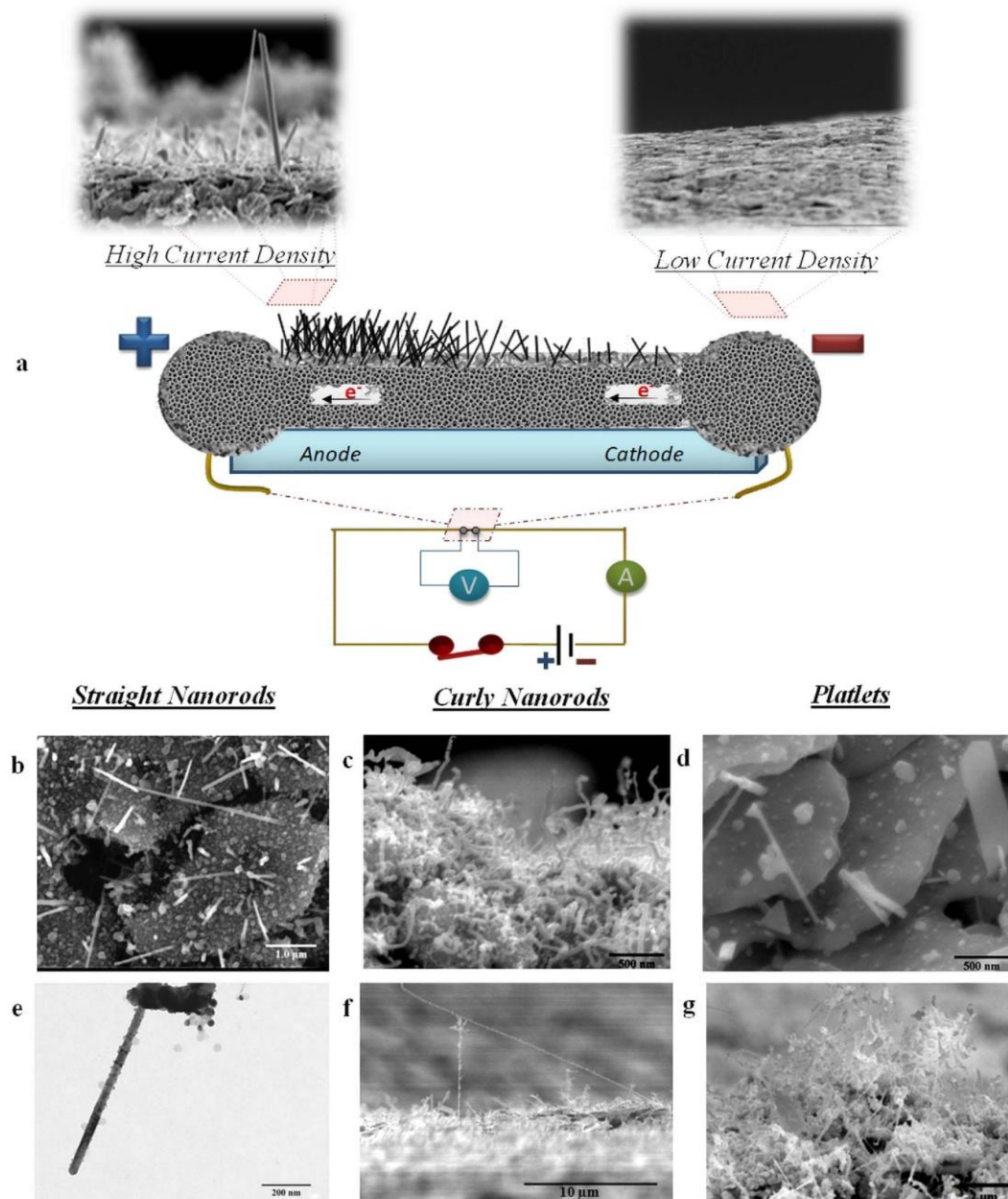
Figure 1. Schematic of experimental setup and different types of nanorod fabricated via the EM process.
(**a**) Schematic diagram of porous sintered silver stripe and the EM experimental setup. SEM image top left shows side view of nanorods at high current density regions (2.34×10^8 A/m^2), and SEM image top right shows a low current density region after 240 hours. (**b**) SEM micrograph of straight silver nanorods under current density of 2.45×10^8 A/m^2 after 240 hours (uninterrupted). (**c**) SEM micrograph of curly nanorods under current density of 2.24×10^8 A/m^2 (uninterrupted) for 480 hours. (**d**) SEM image showing mix of nodules, nanorods and platelets at current density of 2.34×10^8 A/m^2 after 240 hours (interrupted). (**e**) TEM image of a typical 20 nm diameter nanorod. (**f**) SEM image of nanorod with high aspect ratio ~200 generated on the substrate after 240 hours continuous EM. (**g**) SEM image of the nanorods growing until their density is high enough to meet neighbouring nanorods.

Thermal gradients are known to affect the divergence of the atomic flux and hence void and hillock (or nano-wire) formation in EM experiments due to the dependence of electrical resistivity with temperature[13,27]. In order to calculate the magnitude of thermal gradients, electrical resistivity measurements of the stripe were performed using the four point probe method as the current was varied and the temperature in the stripe calculated using the coefficient of electrical resistivity variation with temperature. As an example, it was found that a current density of 2.4×10^8 A/m^2 resulted in a temperature rise of 83 °C.

The experimental determination and modeling of temperature distributions at the scale of the stripe and the scale of individual grains are shown in Fig. 4a,b. The temperature calculations for all samples from experimental

	Anode Region	**Centre Region**	**Cathode Region**

Control SEM Image Before EM

After Applying Current

Nanorod size distribution and number density graphs
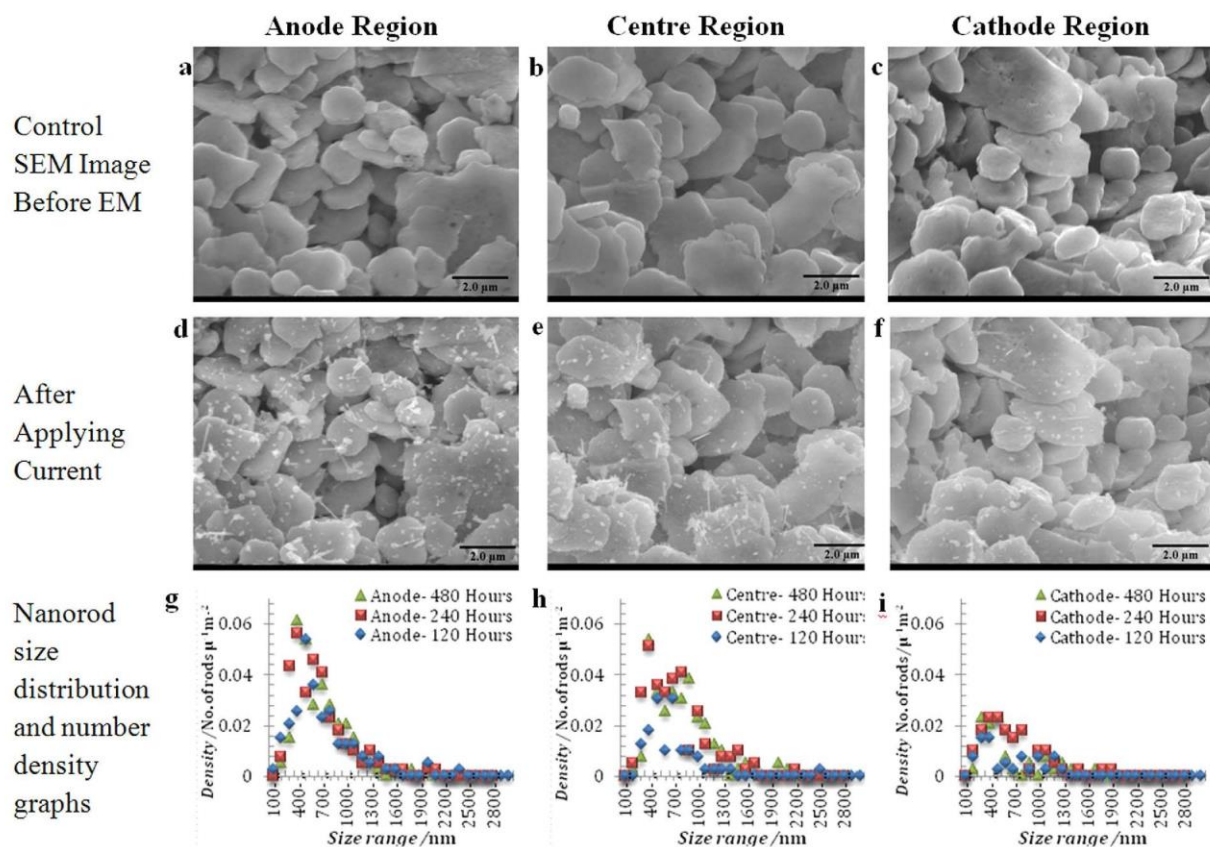
Figure 2. Comparison of nanorod formation in anode, centre and cathode regions. Comparison of size distribution and number density of nanorods on the sintered silver stripe taken (**a–c**) before and (**d–f**) after applying current at (**a,d**) anode, (**b,e**) centre of stripe and (**c,f**) cathode under current density of $2.45 \times 10^{+8}$ A/m^2 after 240 hours. The graphs (**g–i**) represent the number density of nanorods versus their length at the anode (**g**), centre (**h**), and cathode (**i**) regions of the corresponding images after 120, 240, and 480 hours, respectively.

results are in good agreement with temperature calculations using the Finite Element (FEM) model (details in Methods). SEM images of porous silver (Fig. 4c) have been used to construct a simple numerical model of current flowing between grains via a constriction and the resulting temperature gradients are shown in Fig. 4d. The results indicate high values of temperature gradients at the outer edges of the grains and especially near the constrictions. The atomic flux divergence (accumulation rate of atoms) is proportional to the dot product of atomic flux density and the temperature gradient[13,27,28], $\vec{J}_a \cdot \nabla T$ and hence the numerical simulations (Table S2) can be used to estimate the rate of atomic accumulation due to the local temperature variations at grain level in order to test the hypothesis that these variations, together with the stripe level variations (Fig. 4a) are responsible for the observed pattern of nanorod growth across the stripe.

The number of atoms deposited on a grain surface is estimated from the volume of nanorods in SEM images taken from two similar sized grains after two consecutive EM time periods of 120 h. The experimental results are then compared with the atomic flux divergence model. We have taken the temperature gradient value from FEM simulations to calculate the Atomic Flux Divergence (AFD) using the portion of atomic flux from Eq. 3 due to electromigration, $\vec{J}_{Em}$[1,25,28]:

$$Div(\vec{J}_{Em}) = \left(\frac{E_a}{kT^2} - \frac{1}{T}\right)\frac{C_a Z^* e\rho}{kT}D_0 \exp\left(-\frac{E_a}{kT}\right)\vec{J}_e \cdot \nabla T$$

(1)

The value of the AFD ($Div(\vec{J}_{Em})$), representing the number of atoms deposited per unit volume and in unit time, has been calculated as $3.46 \times 10^{+19}$ atom/m^3/s using the values in Table S2 as an input. Multiplying the AFD by the volume of the grain and timescale of EM (120 h and 240 h) results in an estimate of the number of atoms deposited in a grain and is compared to values measured from SEM images in Fig. 5 experimentally in Table 1.

Discussion

The anomalous Ag nanorod formation at anode and central locations can be explained by the presence of complex thermal gradients generated by Joule heating in the constrictions between grains. An analysis based on Fick's laws of diffusion shows that atoms should accumulate in high current density regions where thermal gradients exist (See Methods). This calculation has considered only lattice diffusion in order to give a lower bound, explaining
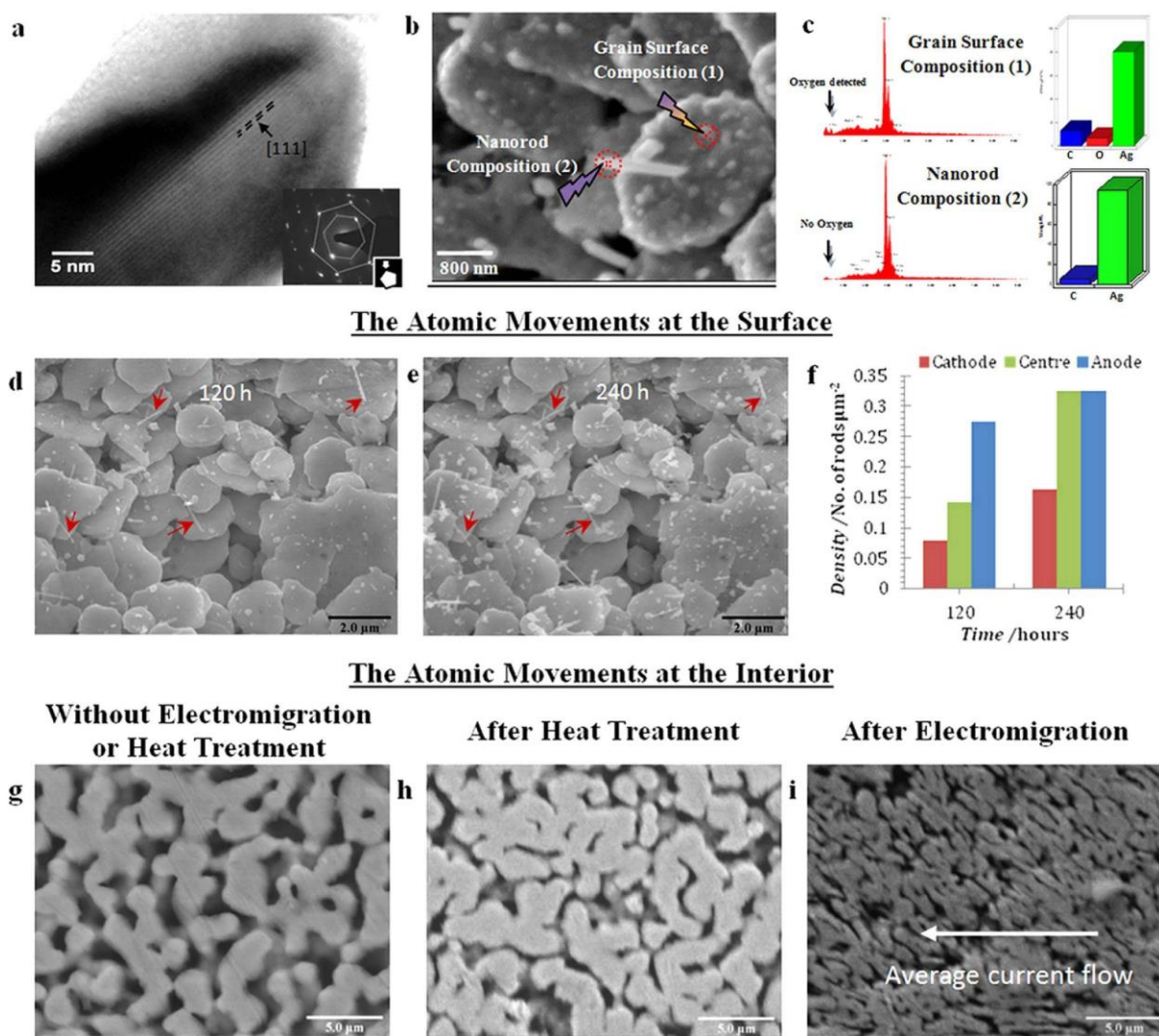
126

Figure 3. Characterisation of generated nanorods and the effect of the oxide layer. (**a**) TEM image of a single 40 nm diameter nanorod. The selected area electron diffraction (SAED) pattern indicates a standard FCC structure interpreted as the overlapping of the [111] and [110] zone axes[21]. The orientation of nanorods with respect to the electron beam is shown in the inset of image. (**b,c**) EDX spectral analysis at the positions marked with crosses on the SEM micrograph (**b**) from sample with current density of 2.45×10^8 A/m². Spectrum (1) shows oxygen on the substrate indicating an oxide layer whereas the nanorod spectrum (2) shows no oxygen. (**d**) Formation of nanorods after EM for 120 hours. (**e**) Disconnection and reconnection followed by another 120 hours EM; red arrows indicate the nanorods formed after the first 120 hours which all showed zero growth after reconnection. (**f**) Total nanorod number density before and after disconnection/reconnection event. (**g–i**) SEM micrographs of the internal structure of sintered silver (**g**) before EM, (**h**) under 200 °C heat treatment for 480 hours showing no structural change and (**i**) after EM for 480 hours with a current density of 2.34×10^8 A/m² showing massive EM driven grain restructuring.

the discrepancy in Table 1. A detailed calculation including grain boundary diffusion should result in closer agreement between the measured and calculated values and will be the subject of further work. However, the present work shows that the proposed mechanism of thermal gradients operating over the length scale of individual grains in combination with electromigration being responsible for nanorod growth is reasonable.

Within the interior of the sample, fast diffusion along the grain surfaces facilitates the internal grain refinement observed in (Fig. 3i) while at the surface the oxide layer prevents rapid surface diffusion and allows compressive stresses to build up locally, eventually leading to the observed nodule (nanodot) and nanorod formation at weak spots in the oxide layer. We note that in a porous material therefore, electromigration can be used to probe the chemical composition at the surface of the internal pores and in particular the absence or presence of an oxide layer inhibiting diffusion. The Ag oxide layer is key to formation of the nanorods and explains why the elevated temperature experiments failed to produce nanorods. Previously reported experimental data[29] shows there are three phases of AgO_x film commonly found on a Ag surface. These are a silver rich phase (phase I), mostly
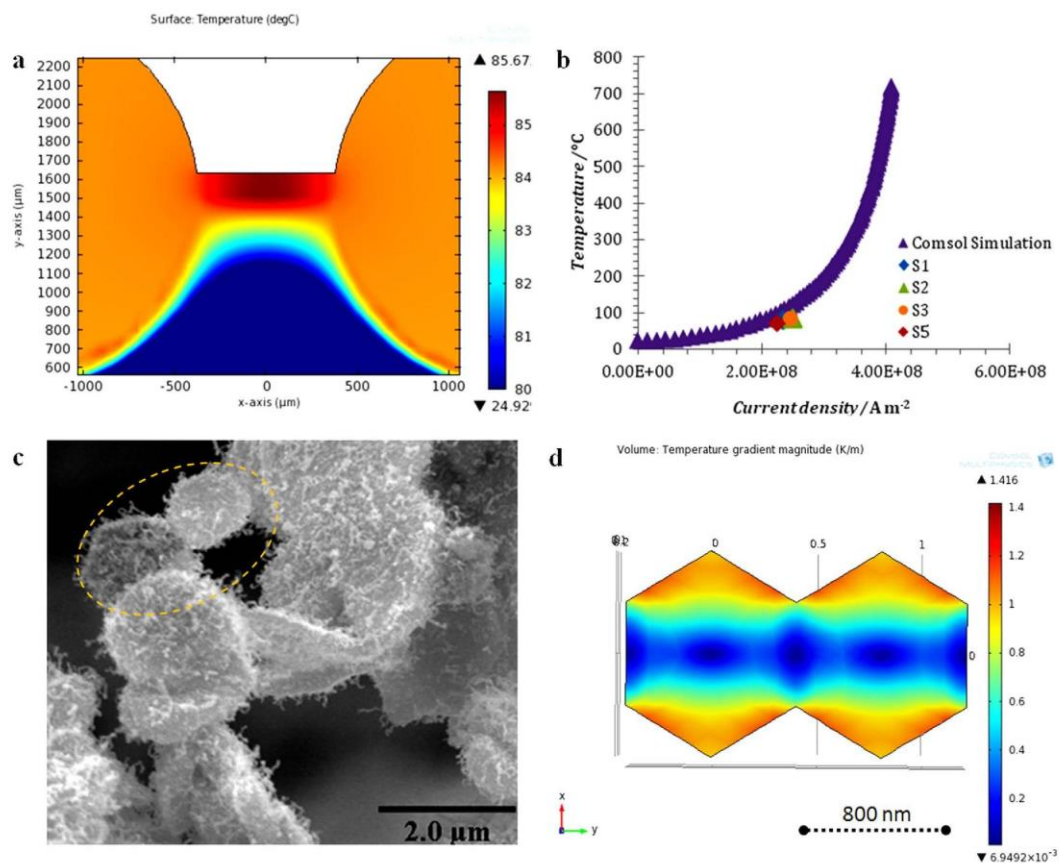
Figure 4. Temperature distribution at stripe and grains. (**a**) Temperature distribution within the stripe found using FEM simulations, (**b**) Experimental and simulated temperature at the centre of the stripe. (**c**) SEM image of silver grains for sample S3. (**d**) FEM simulations of the temperature gradient magnitude in two neighbouring grains similar to those highlighted by the dotted line in (**c**).

Ag_2O (phase II) and finally a mixed phase of Ag_2O and AgO (phase III). The Phase III is the least stable and can easily decompose to Ag_2O and O_2 even at temperatures below 160 °C. The elevated temperature tests and the high current density experiment presumably lead to decomposition of the Phase III layer and prevention of the compressive stress build up that is a prerequisite for nanorod formation. Similarly, the interrupted EM experiments which lead to growth of new nanorods can be explained by the interruption allowing oxide to form on fresh nanorod surfaces and the thermo-mechanical stresses as a result of temperature changes leading to formation of new weak spots on the grain surfaces. The ability to modify nanorod characteristics after initial fabrication can be used to construct sensors with nanorods grown *in situ* or modified *in situ* to optimize their sensitivity.

Conclusion

EM has been used as a constructive process leading to mass fabrication of nanorods simply by passing current through a stripe of porous material under controlled current density. Additionally, the internal grain refinement observed in the porous structure has no analogy in non-porous materials, and is facilitated by the large oxide free surface area present in these porous materials. Absence of grain refinement at the surface of the substrate, EDX measurements on the nanorods, heated samples and interrupted EM experiments all indicate that an oxide layer on the exterior Ag surface restricts atomic diffusion here and hence allows compressive stress build up leading to nanodot and then nanorod formation at weak points of the oxide layer. The mechanism of nanorod growth away from the anode in a porous substrate was investigated by atomic flux divergence calculations taking into account thermal gradients on the scale of a single grain and assuming only lattice diffusion. The calculations show that the number of deposited atoms in a grain due to thermal gradient fluctuations is an order of magnitude lower than observed experimentally but supports the hypothesis that grain-scale thermal gradients are responsible for the observed nanorods once the higher atomic flux from grain boundary diffusion is taken into account. In contrast to the exterior surface with its oxide layer constraining surface diffusion, the internal pore surfaces in sintered silver offer fast surface diffusion pathways. This results in refining of the pore structure during EM. Electromigration can hence be used as an *in-situ* probe of the surface condition of the interior pores in conducting porous media as well as a mechanism by which these pores can be transformed. Finally the experimental approach reported here suggests that high density, high aspect ratio nanorods can be fabricated using EM with precise control of nucleation density and size achievable by modulating the current density.
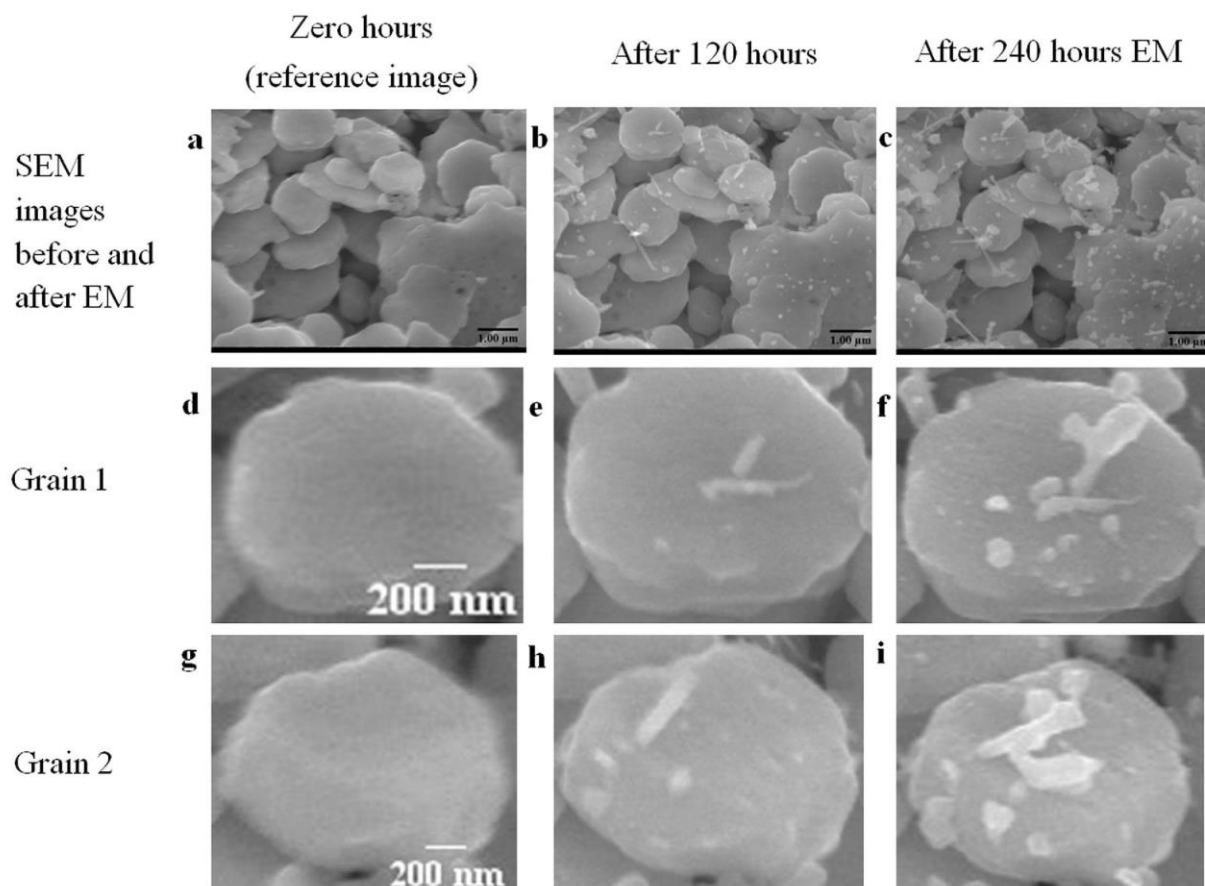
128

Figure 5. Source images for Atomic Flux Divergence (AFD) calculation in Table 1 of number of atoms deposited in two similar sized grains. SEM images of the anode region of sample S3 (**a**) before EM, (**b**) after 120 hours and (**c**) after 240 hours at the same location. Two similar sized grains (Grain 1 (**d**) and 2 (**g**)) were selected to compare the calculation of atomic deposition numbers after 120 hours (**e,h**) and after 240 hours (**f,i**).

	Number of atoms (Grain 1)		Number of atoms (Grain 2)	
Time (h)	Atomic Flux Divergence Model (AFD)	Experimental Measurement	Atomic Flux Divergence Model (AFD)	Experimental Measurement
120	2.37×10^6	5.92×10^7	2.53×10^6	5.85×10^7
240	4.74×10^6	1.32×10^8	5.06×10^6	1.49×10^8

Table 1. Comparison of the deposited number of atoms calculated both from the Atomic Flux Divergence model and experimental measurements on two similar size grains on sample S3 for two different time periods of 120 and 240 h.

Methods

Experimental. The porous Ag samples were fabricated using NanoTach® X silver paste produced by NBE Tech, a paste used for attaching semiconductor die to ceramic substrates typically for power electronics applications. The paste consists of ~30 nm diameter Ag particles together with ligands to prevent agglomeration and organic components to improve paste rheology. The paste is printed onto the edge of a glass cover slip to create a simple sample geometry with a high degree of control over parameters such as length, width and thickness. The same paste is then applied at both ends to connect gold wires at anode and cathode ends after a further sintering step. A feature of this EM setup is that the anode and cathode is not defined by junctions with a refractory metal as in a typical Blech setup[30], but by the existence of sharp variations of cross sectional area resulting in high current density inside the stripe and low current densities beyond the anode and cathode to form a 3D analogue of the bow-tie structure[31]. Figure 1a shows a schematic of the experimental setup. Figure S1a shows a TEM image of a cross section through the sintered material revealing that the original nanoparticles have merged to form grains ~1 μm diameter with a high density of twin boundaries and a porosity of ~25% (see[32] for further details of the structure).

129

Diffusion model of atomic accumulation and Finite Element Modeling (FEM) simulations.

Voids form during electromigration by depletion of atoms while nanorods grow in regions where atoms accumulate. Based on Fick's laws of diffusion, the governing diffusion-convection equation for atomic evolution can be written as[13,27,28]

$$\frac{\partial C_a}{\partial t} + \nabla \cdot \vec{J}_a = r \tag{2}$$

where C_a is the atomic concentration, $\vec{J}_a$ is the total atomic flux, r is the source/sink term which in the simplest models is given by $-\Delta C_a / \tau$ where ΔC_a represents the excess of atoms from its equilibrium value and τ represents a relaxation time. The atomic flux vector contains contributions from self-diffusion, electric current ('wind force'), temperature gradient and hydrostatic stress gradient shown respectively as the terms in Eq. (2) [1,25,28]

$$\vec{J}_a = -D_a \left[\nabla C_a + \frac{|Z^*| \rho e}{k_b T} C_a \vec{J}_e + \frac{Q^*}{k_b T^2} C_a \nabla T - \frac{f\Omega}{k_b T} C_a \nabla \sigma \right] \tag{3}$$

where D_a is the diffusivity of atoms, Z^* is the effective charge, e is the elementary charge, k_b is Boltzmann's constant, T is the absolute temperature, $\vec{J}_e$ is the current density, Q^* is the heat of transport, f is the atomic relaxation factor, Ω is the atomic volume, and σ is the hydrostatic stress. D_a can further be expressed by Arrhenius law as

$$D_a = D_0 \exp\left(-\frac{E_a}{k_b T}\right) \tag{4}$$

where D_0 is the pre-exponential factor and E_a is the activation energy. Equations (1–3) form the standard base for discussion of electromigration, and have been investigated extensively for Cu and Al on-chip interconnects[13,28]. Numerical estimates of the temperature gradient term in Eq. (2) show that the direct effect of the temperature gradient on $\vec{J}_a$ is negligible. However, the $\nabla \cdot \vec{J}_a$ term in Eq. (1) leads to significant atomic accumulation or depletion arising from temperature gradients via the spatial variation in D_a given by Eq. (3) in the presence of a thermal gradient. Hence knowledge of the local current density and temperature distribution is required to calculate $\nabla \cdot \vec{J}_a$ and nanorod growth.

To calculate the current and temperature distribution within the stripe we have used commercial FEM software COMSOL (Joule heating module). The electrical current has been simulated within the silver stripe from the source electrode to the drain electrode taking into account Joule heating, conduction through the glass at a current density of 2.4×10^8 A/m². The temperature of the bottom surface of 3000 μm thick SiO_2 substrate on which the stripe is located was set to the room temperature of 298.15 K. The thermal Conductivity of SiO_2 was given the textbook value of 0.8 W/mK[33] and the thermal conductivity and electrical resistivity of material were similarly set at 250 W/mK and 7.33×10^{-8} Ω m respectively[34].

References

1. Tu, K.-N. In Solder Joint Technology Vol. 117 *Springer Series in Materials Science* Ch. 8, 211–243, doi: http://dx.doi.org/10.1007/978-0-387-38892-2 (Springer New York, 2007).
2. Saka, M. & Sasagawa, K. In *Metallic Micro and Nano Materials Engineering Materials* (ed. Masumi, Saka) Ch. 3, 53–92, doi: http://dx.doi.org/10.1007/978-3-642-15411-9 (Springer Berlin Heidelberg, 2011).
3. Tan, C. M. & Roy, A. Electromigration in ULSI interconnects. *Materials Science and Engineering: R: Reports* **58**, 1–75, doi: http://dx.doi.org/10.1016/j.mser.2007.04.002 (2007).
4. Tu, K. N. Recent advances on electromigration in very-large-scale-integration of interconnects. *J. Appl. Phys.* **94**, 5451–5473, doi: http://dx.doi.org/10.1063/1.1611263 (2003).
5. Yuk, J. M. *et al.* Direct Fabrication of Zero- and One-Dimensional Metal Nanocrystals by Thermally Assisted Electromigration. *Acs. Nano* **4**, 2999–3004, doi: http://dx.doi.org/10.1021/nn901674p (2010).
6. Ward, D. R., Corley, D. A., Tour, J. M. & Natelson, D. Vibrational and electronic heating in nanoscale junctions. *Nat. Nanotechnol.* **6**, 33–38, doi: http://dx.doi.org/10.1038/Nnano.2010.240 (2011).
7. Coppens, Z. J., Li, W., Walker, D. G. & Valentine, J. G. Probing and Controlling Photothermal Heat Generation in Plasmonic Nanostructures. *Nano Lett* **13**, 1023–1028, doi: http://dx.doi.org/10.1021/Nl304208s (2013).
8. Tsutsui, M. *et al.* Single-molecule sensing electrode embedded in-plane nanopore. *Sci Rep-Uk* **1**, 46, doi: http://dx.doi.org/10.1038/Srep00046 (2011).
9. Kim, Y., Jeong, W., Kim, K., Lee, W. & Reddy, P. Electrostatic control of thermoelectricity in molecular junctions. *Nat.Nanotechnol.* **9**, 881–885, doi: http://dx.doi.org/10.1038/Nnano.2014.209 (2014).
10. Tsutsui, M., Shoji, K., Taniguchi, M. & Kawai, T. Formation and self-breaking mechanism of stable atom-sized junctions. *Nano Lett* **8**, 345–349, doi: http://dx.doi.org/10.1021/nl073003j (2008).
11. Tomizuka, C. T. & Sonder, E. Self-Diffusion in Silver. *Physical Review* **103**, 1182–1184, doi: http://dx.doi.org/10.1103/PhysRev.103.1182 (1956).
12. Metois, J. J., Saul, A. & Muller, P. Measuring the surface stress polar dependence. *Nat. Mater.* **4**, 238–242, doi: http://dx.doi.org/10.1038/nmat1328 (2005).
13. Sasagawa, K., Hasegawa, M., Saka, M. & Abé, H. Governing parameter for electromigration damage in the polycrystalline line covered with a passivation layer. *J. Appl. Phys.* **91**, 1882–1890, doi: http://dx.doi.org/10.1063/1.1432120 (2002).
14. Lu, Y. & Saka, M. Fabrication of Al micro-belts by utilizing electromigration. *Mater Lett* **63**, 2227–2229, doi: http://dx.doi.org/10.1016/j.matlet.2009.07.031 (2009).
15. Lu, Y. & Saka, M. Effect of purity on the fabrication of Al micro/thin-materials by utilizing electromigration. *Mater Lett.* **63**, 2294–2296, doi: http://dx.doi.org/10.1016/j.matlet.2009.07.055 (2009).
16. Saka, M., Kato, K., Tohmyoh, H. & Sun, Y. Controlling electromigration to selectively form thin metal wires and metal microspheres. *J. Mater. Res.* **23**, 3122–3128, doi: http://dx.doi.org/10.1557/JMR.2008.0374 (2008).
17. Guo, X., Ma, Y., Wang, Y. & Tong, L. Nanowire plasmonic waveguides, circuits and devices. *Laser & Photonics Reviews* **7**, 855–881, doi: http://dx.doi.org/10.1002/lpor.201200067 (2013).

130

18. Anh Dinh, D. *et al.* Silver Nanowires: A Promising Transparent Conducting Electrode Material for Optoelectronic and Electronic Applications. *Reviews in Advanced Sciences and Engineering* **2,** 324–345, doi: http://dx.doi.org/10.1166/rase.2013.1048 (2013).
19. Huntington, H. B. & Grone, A. R. Current-Induced Marker Motion in Gold Wires. *J. Phys. Chem. Solids* **20,** 76–87, doi: http://dx.doi.org/10.1016/0022-3697(61)90138-X (1961).
20. Shankar, K. S. & Raychaudhuri, A. K. Fabrication of nanowires of multicomponent oxides: Review of recent advances. *Mat. Sci. Eng. C* **25,** 738–751, doi: http://dx.doi.org/10.1016/j.msec.2005.06.054 (2005).
21. Hofmeister, H. Shape variations and anisotropic growth of multiply twinned nanoparticles. *Z. Kristallogr.* **224,** 528–538, doi: http://dx.doi.org/10.1524/zkri.2009.1034 (2009).
22. Garnett, E. C. *et al.* Self-limited plasmonic welding of silver nanowire junctions. *Nat. Mater.* **11,** 241–249, doi: http://dx.doi.org/10.1038/Nmat3238 (2012).
23. Tokuno, T. *et al.* Fabrication of silver nanowire transparent electrodes at room temperature. *Nano Res.* **4,** 1215–1222, doi: http://dx.doi.org/10.1007/s12274-011-0172-3 (2011).
24. Elechiguerra, J. L., Reyes-Gasga, J. & Yacaman, M. J. The role of twinning in shape evolution of anisotropic noble metal nanostructures. *J. Mater. Chem.* **16,** 3906–3919, doi: http://dx.doi.org/10.1039/B607128g (2006).
25. Saka, M. & Ueda, R. Formation of metallic nanowires by utilizing electromigration. *J. Mater. Res.* **20,** 2712–2718, doi: http://dx.doi.org/10.1557/Jmr.2005.0340 (2005).
26. Calata, J. N., Lu, G. Q., Ngo, K. & Nguyen, L. Electromigration in Sintered Nanoscale Silver Films at Elevated Temperature. *J. Electron. Mater.* **43,** 109–116, doi: http://dx.doi.org/10.1007/s11664-013-2783-9 (2014).
27. Sasagawa, K., Hasegawa, M., Saka, M. & Abé, H. Prediction of electromigration failure in passivated polycrystalline line. *J. Appl. Phys.* **91,** 9005–9014, doi: http://dx.doi.org/10.1063/1.1475354 (2002).
28. Zhu, X. *et al.* Electromigration in Sn–Ag solder thin films under high current density. *Thin Solid Films* **565,** 193–201, doi: http://dx.doi.org/10.1016/j.tsf.2014.06.030 (2014).
29. Tominaga, J. The application of silver oxide thin films to plasmon photonic devices. *J. Phys-Condens. Mat.* **15,** R1101–R1122, doi: http://dx.doi.org/10.1088/0953-8984/15/25/201 (2003).
30. Blech, I. A. & Herring, C. Stress Generation by Electromigration. *Appl. Phys. Lett.* **29,** 131–133, doi: http://dx.doi.org/10.1063/1.89024 (1976).
31. Jeong, W., Kim, K., Kim, Y., Lee, W. & Reddy, P. Characterization of nanoscale temperature fields during electromigration of nanowires (vol 4, 4975, 2014). *Sci Rep-Uk* **4,** 5690, doi: http://dx.doi.org/10.1038/srep04975 (2014).
32. Paknejad, S. A., Dumas, G., West, G., Lewis, G. & Mannan, S. H. Microstructure evolution during 300 degrees C storage of sintered Ag nanoparticles on Ag and Au substrates. *J. Alloy. Compd.* **617,** 994–1001, doi: http://dx.doi.org/10.1016/j.jallcom.2014.08.062 (2014).
33. Hust, J. G. In *Thermal Conductivity 14* (eds P. G. Klemens & T. K. Chu) 221–231, doi: http://dx.doi.org/10.1007/978-1-4899-3751-3_35 (Springer US, 1976).
34. Panaccione, P., Wang, T., Chen, X., Luo, S. & Lu, G.-Q. Improved Heat Dissipation and Optical Performance of High-Power LED Packaging with Sintered Nanosilver Die-Attach Material. *Journal of Microelectronics and Electronic Packaging* **7,** 164–168, doi: http://dx.doi.org/10.4071/imaps.264 (2010).

Acknowledgements

Author Contributions

A.M. and Q.W. prepared the samples. A.M., S.A.P. and Q.W. performed the electrical measurements. A.M., G.V.-B., S.H.M. and R.F. carried out the electron microscopy. A.M., S.A.P. and S.H.M. carried out the calculations and simulations, A.M., S.H.M. and A.V.Z. wrote the manuscript. S.H.M. and A.V.Z. directed the research.

## Additional Information

131

A3 **Stereoscopic nanoscale-precision growth of free-standing silver nanorods by electron beam irradiation**

Stereoscopic Nanoscale-Precision Growth of Free-Standing Silver Nanorods by Electron Beam Irradiation

Ali Mansourian, Seyed Amir Paknejad, Anatoly V. Zayats, and Samjid H. Mannan*

Department of Physics, King's College London, Strand, London WC2R 2LS, U.K.

ABSTRACT: Nanoscale manipulation of atoms is desirable in modern technologies. Atoms in a material are typically manipulated by mechanical contact or thermal and electric effects. The electron beam of a scanning electron microscope is usually used for two-dimensional patterning of a substrate with nanoscale precision. Here we report stereoscopic growth of nanoparticles and nanorods on silver surfaces with nanometric precision under exposure to the electron beam with precise control over their position, size, and orientation. Nanorod length (50−1000 nm) and diameter (30−100 nm) can be independently controlled by adjusting the electron beam characteristics of a scanning electron microscope. Silver nanorods with diameters as small as 30 nm with location accuracy limited only by the resolution of the scanning electron microscope have been fabricated with repeatable orientation and size. Cascaded nanorod structures can be grown directly on other nanorods. The results open up a number of exciting possibilities for three-dimensional, nanoscale-controlled direct fabrication of nanoparticles and nanowires by an electron beam *in situ* using conventional SEM facilities.
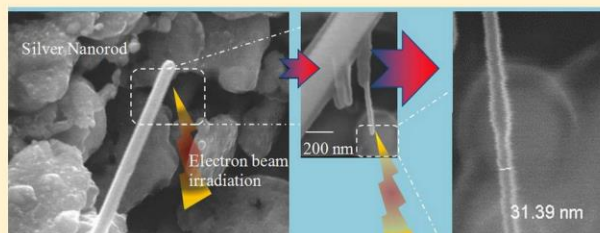
■ INTRODUCTION

Controllable fabrication of nanostructures is a cornerstone of modern nanoelectronic, optoelectronic, and nanophotonic technologies. Both top-down as well as bottom-up approaches for the fabrication of nanostructured devices have been developed.[1] Electron beam lithography (EBL)[2] and focused-ion-beam (FIB) milling[3] are two sophisticated fabrication techniques that require specialized equipment and are primarily limited to two-dimensional objects, while full control over three-dimensional positioning and orientation of individual nanostructures on planar and, especially, curved surfaces is still in its infancy.

Here we demonstrate a stereoscopic growth of Ag nanorods on a surface of Ag nanorods, resulting in a 3D nanostructure, in vacuum conditions with dimensions, orientation, and position controlled by the electron beam parameters of a scanning electron microscope (SEM). We present results of nanorod on nanorod formation with precise control over diameter (30—70 nm) and length (50—1000 nm) achieved by adjusting the exposure time and nanorod positioning better than 5 nm limited by the electron-beam spot size. Previous studies reported that silver ions migrate in silver-containing materials under the influence of electron beam irradiation.[4–11] We have confirmed that the conventional SEM imaging mode (scanning mode) results in randomly located growth of nodules and wires and showed that continuous exposure to the electron beam in the EDX mode results in formation of high-aspect-ratio nanorods with controlled dimensions and orientations at the chosen location. Nanoscale manipulation of atoms is desirable for many modern technologies, and the results open up a number of exciting possibilities for nanoscale-controlled in situ fabrication of nanoparticles and nanowires.

Previous attempts have successfully demonstrated the growth of nanowires at random locations within the area irradiated by electron beams.[5–7,9,10,12,13] Mesoporous zeolites show high sensitivity to electron beam irradiation under high vacuum, and the formation of silver nanorods with high aspect ratios of up to 3000 have been reported in studies on silver-containing zeolites.[6,7,10,14] Copper-containing materials can also form high aspect ratio nanorods.[13] In addition to solid-phase transitions, the effect has also been reported in the liquid phase, using transmission electron microscopy (TEM), scanning transmission electron microscopy (STEM), and scanning electron microscopy (SEM) techniques.[8,15–17] For example, silver nanocrystals have been grown from dilute solutions of silver nitrate by STEM irradiation.[18] Fine experimental control over the initiation and the growth process is required for practical applications of the technique for fabrication of designer nanostructures for nanoelectronic and nanophotonic applications.

We have demonstrated electron-beam-assisted growth of stereoscopic structures with control over nanorod diameter, length, and orientation and nanoscale precision in their position on the example of a nanorod-on-nanopillar geometry using as "a substrate" prefabricated silver nanopillars with typical dimensions of 100−250 nm diameter and 1−4 μm length. Hereafter, we refer to structures formed by the electron beam as nanorods and the prefabricated base as nanopillars. The nanopillars were formed via electromigration in a thin strip of porous silver. Initially, the porous silver was created by sintering
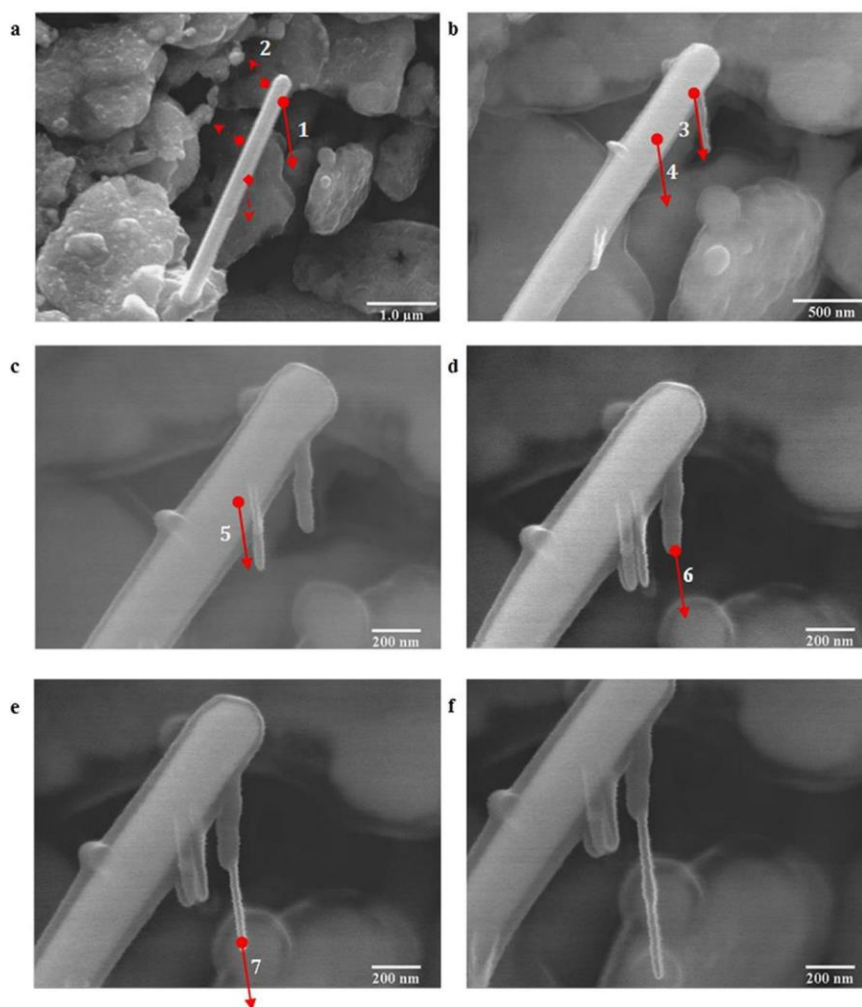
Figure 1. Nanorod growth with precise control over base location, growth direction, and size. (a) SEM image of the nanopillar (280 nm diameter and 3.4 μm length) used as a substrate for electron-beam-induced growth. Positions of the electron beam and its drift direction are shown for the 4 initial experiments. (b) SEM images of the resulting nanorods and nodules. Positions 3 and 4 of the beam for growing additional nanorods are also shown. (c) SEM image of nanorods after the previous growth cycles. Position 5 of the beam is shown for growing an additional nanorod at a distance of 10 nm parallel to nanorod 4. (d) SEM image of the resulting nanorod and the location and displacement of a further beam spot. (e) SEM image of resulting 31 nm diameter nanorod on nanorod structure and location 7 for further nanorod growth. (f) SEM image of the final structure. The growth is performed with the FEG-1 electron beam parameters.

a paste (NanoTach X Silver paste from NBE Tech) containing silver nanoparticles with an average diameter of 30 nm at 300 °C in air. After sintering, nanorods were formed in the silver stripe by connecting the ends of the stripe to a voltage source (~7 mV across the stripe) to generate a current density of ~2.4 × 10^8 A/m^2 for a time period of 240 h. The electromigration process leads to substrate nanopillars forming all over the surface of the silver stripe as described in detail elsewhere.[19]

■ METHODS

The electron beam irradiation experiments were carried out with two different field emission guns (FEGs) in a Hitachi S4000 SEM (FEG-1) and FEI Quanta SEM (FEG-2), both equipped with energy-dispersive X-ray (EDX) analysis instruments. FEG-1 was used in the spot mode (EDX regime) to generate nanorods at specific sites and provides an electron beam diameter of 30 nm, accelerating voltage of 25 kV, spot

diameter of 14 nm, beam drift of 5 nm/s, and surface exposure times of 10−100 s. The EDX spot mode, focusing the beam on a point on the surface of a substrate nanopillar, was found to result in the formation of individual nanorods at the targeted point of the surface. FEG-2 provides an electron beam diameter of 50 nm, accelerating voltage of 25 kV, and spot diameter of 20 nm and was used in the scanning mode, with beam drift of 10 nm/s and surface exposure times of 30−70 s. The normal SEM scanning mode shows that after 2 min of uninterrupted electron beam scanning nanoparticles were generated at random locations, covering approximately 5% of the nanopillars. All samples were connected to the SEM stage, but the charging was still observed across the sample and in the targeted nanopillar samples in high-magnification SEM images. Charging of samples provides a drift velocity of 10 nm/s with FEG-2 and 5 nm/s with FEG-1, which results in the directional formation of nanorods along the drift direction. By changing the

Table 1. Length and Diameter of Different Nanorods Formed via Electron Beam Irradiation (EBI) in Figure 1a−f

nanorod in Figure 1a−f	arrow number 1 (Figure 1a,b)	arrow number 3 (Figure 1b,c)	arrow number 4 (Figure 1b,c)	arrow number 5 (Figure 1c,d)	arrow number 6 (Figure 1d,e)	arrow number 7 (Figure 1e,f)
length (nm)	379	375	372	378	375	376
diameter (nm)	37	70	34	55	34	32
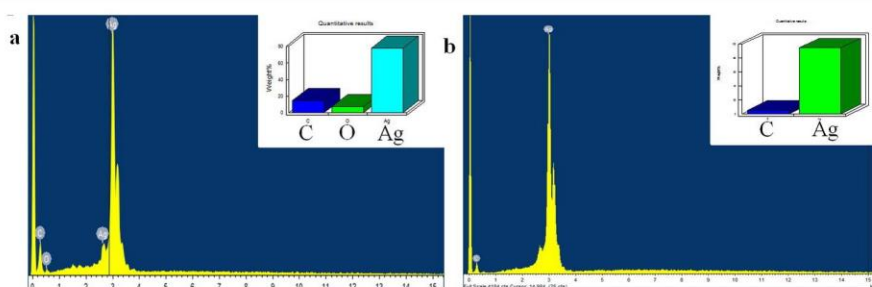
Figure 2. EDX spectra and composition of (a) nanopillar (b) electron-beam-grown nanorod after 70 s EDX irradiation of the nanopillar.
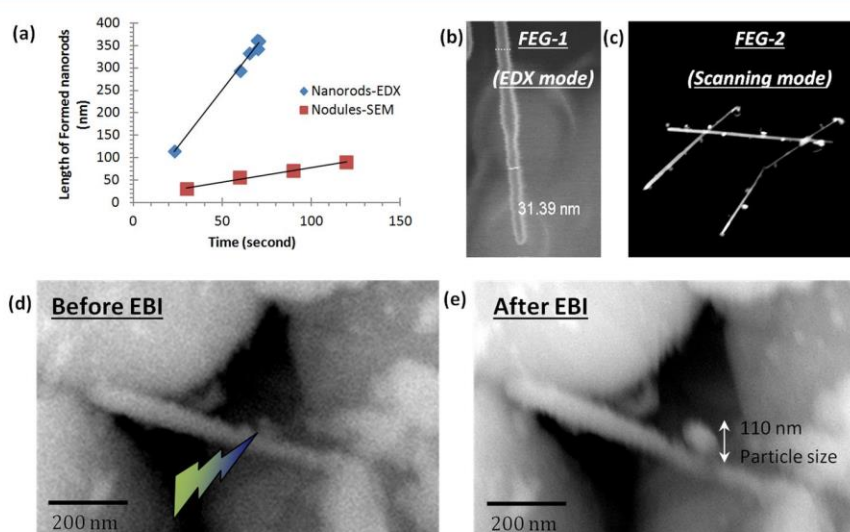
Figure 3. (a) Comparison of the growth rate between nanorods and nodules formed using EDX and SEM, respectively. (b) Nanorods for the size measurements for the growth rate curve. (c) Nodules for the size measurements for the growth rate curve. (d) SEM image with arrow showing EDX spot location before irradiation on a single nanorod. (e) SEM image after EDX spot irradiation showing growth of a single 110 nm nodule.

orientation of the surface, it is possible to change the direction of drift and, thus, the direction of nanorod formation.

The electron beam of the field-emission gun (FEG-1) was positioned sequentially at multiple points on the Ag surface with a resolution of approximately 5 nm, provided by the SEM. One can initially observe the formation of the nanoparticles at the position of the electron beam (25 kV for 70 s) which, with the increase of the exposure time, develop into distinct nanorods with increasing aspect ratio. The experiments show that the nanorod diameter can be increased by rescanning the base of an existing nanorod. Since the generated nanorods follow the electron beam drift, the length of nanorods can simply be controlled by changing the exposure time.

■ RESULTS

Figure 1a−f shows the electron-beam spot location and the displacement vector for a number of growth cycles resulting in the formation of nanorods leading to the controllable stereoscopic decoration of the supporting nanopillar. The solid arrows indicate exact displacement vectors calculated from images taken before and after the electron beam irradiation, with the base of the arrow representing the initial location of the e-beam spot. In all cases, except the irradiation event labeled "2", the exposure time was 70 s, but for "2" the time was halved (35 s). The drift direction was altered (Figure 1a) by changing the orientation of the sample (leaving the tilt unchanged), while the drift velocity was kept at 5 nm/s. Figure 1b shows the location of two more beam spots and drift directions. The event labeled "3" resulted in a doubling of the thickness of the nanorod grown during the exposure "3", while the event labeled "4" resulted in a new nanorod (Figure 1c). A further irradiation event labeled "5" results in a new nanorod parallel to the neighboring nanorod and with the same length at a separation distance of 10 nm (Figure 1d). The lengths of the nanorods are the same at 340 ± 5 nm. The images in Figures 1(c) and (d) confirm that at 5 nm/s beam speed, the nanorod growth direction, and length can be controlled by the drift during irradiation. Figure 1d demonstrates that nanorods can be generated parallel to each other with high precision (position control better than 5 nm). They can be grown either

135

parallel to each other on the substrate (Figure 1b and c) or indeed on the tips of existing nanorods (Figure 1d−f). The 34 nm diameter and 375 nm long nanorod in Figure 1e formed in similar fashion, and again a 376 nm long nanorod formed on the previously formed nanorods in Figure 1f. The formed nanorods in Figure 1e and f consist of both 70 and 32 nm diameter segments, controlled by single and double exposures.

Table 1 lists the nanorods in Figure 1 and their lengths and widths. While the length of nanorods is controlled by the exposure time, the width exhibits more variability. Although the majority of the widths is 35 ± 5 nm except nanorod 3 which had a double exposure, we see that nanorod 5 has an anomalously large width of 55 nm possibly caused by close proximity to nanorod 4.

The SEM images from nanopillars at high magnification (80 000×, Figure 1c−f) seem to indicate that the nanopillar is covered with a thin 20 nm shell. The core/shell appearance of nanopillars and nanorods at high magnification could indicate the presence of an oxide layer or carbon contamination. The results for energy-dispersed X-ray (EDX) spectra are shown in Figure 2a and b for a particular nanopillar with similar composition observed for all nanopillars and nanorods studied. Figure 2a shows that the nanopillar composition is silver (77.8%), carbon (14.6%), and oxygen (7.6%), while the composition of the generated nanorod (Figure 2b) is Ag (97%) and carbon (3%). The presence of both carbon and a thin oxide layer is normal on silver surfaces, but there is also a possibility that the halo effect is caused by SEM optics at high magnification which is known to result in differing contrast and blurring at the edges of 1D and 2D structures.

Figure 3a shows that the growth rate as a function of exposure time for nanorods (Figure 3b) and nodules (Figure 3c) is higher in spot mode (FEG-1) compared to scanning mode (FEG-2) as expected given the different effective exposure times of the surface to the electron beam. In scanning mode (FEG-2, 25 kV accelerating voltage, Figure 3c), with the electron beam constantly scanning the surface, low aspect ratio particles are formed after irradiation for 120 s. The size of the nodules approximately doubles from 80 to 170 nm, when the electron beam exposure time was doubled from 60 to 120 s. For FEG-2 in EDX spot mode, the drift velocity was double that of the FEG-1 mode and equal to 10 nm/s, resulting in formation of 100 nm nanoparticles at the spot location (Figure 3d and e). The energy-dispersive X-ray (EDX) analysis of the nanoparticles shows similar composition as the nanorods with 97% Ag and 3% carbon. For both FEG-1 and FEG-2 spot-mode experiments, the monotonic drift was caused by sample charging. It is proposed that in the future this constant drift can be eliminated and a dynamically controlled drift implemented by using a motorized sample stage. In the current implementation, the drift speed and direction were both constant. The drift at 5 nm/s resulted in growth of high aspect ratio nanorods, while the drift at 10 nm/s resulted in growth of nodules. This suggests that the ion drift speed responsible for growth lies between these two values.

■ DISCUSSION

To the best of our knowledge and as also stated in other studies,[4−6] there is no general and comprehensive model explaining the growth mechanism of whiskers and nanostructures due to electron beam irradiation.[5] In general, the electron beam used in scanning electron microscopy can cause a temporary or permanent change in the surface or bulk structure of a specimen, arising from elastic and inelastic electron scattering and related heating, electrostatic charging, ionization damage (radiolysis), displacement damage, and sputtering. Studies which explicitly observed growth of silver nanostructures under electron beam irradiation include refs 4−11 and 14. Ref 5 proposes the most relevant growth mechanisms: (i) migration of silver ions from a silver nanowire substrate in the presence of an electric field, (ii) the presence of an oxide layer (in that publication TiO_2, in the present work, silver oxide), and (iii) stresses caused by thermal gradients caused by electron beam heating are present also in the current work. In general terms, initial heating of the substrate during the interaction with the beam provides energy for atomic migration.[5,6] This can be also coupled to softening of the internal material structure under the electron irradiation. Charging of the silver under the irradiation simultaneously results in attraction of silver ions to the regions exposed to the electron beam. Additional driving forces are also present due to temperature gradients over the silver surface, which, combined with the electric fields,[6,16] continuously drive ions toward the region exposed to the electron beam as it drifts. Longer exposure to the electron beam tends to result in longer, curved whiskers[5−7] as opposed to the straight nanorods observed in this work with short exposures.

■ CONCLUSIONS

Electron-beam irradiation has been used to fabricate stereoscopic nanorods on curved surfaces over existing nanoscale structures. Both high control over nanorod dimensions and high placement accuracy have been demonstrated. The conventional SEM imaging mode results in growth of nodules, while continuous exposure to higher energy electron beams, typical of the EDX mode, results in the formation of high aspect ratio nanorods. The nanorod growth rate and direction can be controlled by movement of the electron beam spot over the surface of the substrate at low drift velocities (5 nm/s), caused by charging, and could in the future be reproduced by manipulation of the SEM stage. The location of the growing nanorods can be controlled by the position of the electron beam spot and can be used to induce growth of nanorods on selected pre-existing nanorods. The method opens up a number of exciting possibilities involving controlled, direct fabrication and manipulation of nanowires in an electron beam using conventional SEM facilities. Examples could be the creation of closely spaced parallel structures as has been demonstrated or fabrication of complex three-dimensional plasmonic structures and their networks for applications in sensing, surface-enhanced Raman scattering, and photochemistry applications. Given the sequential nature of fabrication the first applications would necessarily be small-scale lab-based applications to produce bespoke 3-d structures made of linear segments branching off at desired angles. Further applications are expected to follow once the properties and unique benefits of these structures are explored.

■ AUTHOR INFORMATION

Corresponding Author
*E-mail: samjid.mannan@kcl.ac.uk. Tel.: +44 (0)20 7848 1780.
Author Contributions
AM performed experiments. All authors were involved with planning the experiments, analyzing the results, and writing the manuscript.

136

Notes

■ ACKNOWLEDGMENTS

■ ABBREVIATIONS

TEM, transmission electron microscopy; STEM, scanning transmission electron microscopy; FIB, focused-ion-beam milling; EBL, electron-beam lithography; FEG-2, field emission gun 2 on FEI quanta microscope; FEG-1, field emission gun 1 on Hitachi S4000 microscope; EBI, electron beam irradiation; SEM, scanning electron microscopy; EDX, energy-dispersive X-ray

■ REFERENCES

(1) Biswas, A.; Bayer, I. S.; Biris, A. S.; Wang, T.; Dervishi, E.; Faupel, F. Advances in Top-Down and Bottom-Up Surface Nanofabrication: Techniques, Applications & Future Prospects. *Adv. Colloid Interface Sci.* **2012**, *170*, 2−27.

(2) Altissimo, M. E-Beam Lithography for Micro-/Nanofabrication. *Biomicrofluidics* **2010**, *4*, 026503.

(3) Bassim, N.; Scott, K.; Giannuzzi, L. A. Recent Advances in Focused Ion Beam Technology and Applications. *MRS Bull.* **2014**, *39*, 317−325.

(4) Shi, G. H.; Bao, S. X.; Lai, W. M.; Rao, Z. Z.; Zhang, X. W.; Wang, Z. W. Electron Beam Induced Growth of Silver Nanoparticles. *Scanning* **2013**, *35*, 69−74.

(5) Umalas, M.; Vlassov, S.; Polyakov, B.; Dorogin, L. M.; Saar, R.; Kink, I.; Lohmus, R.; Lohmus, A.; Romanov, A. E. Electron Beam Induced Growth of Silver Nanowhiskers. *J. Cryst. Growth* **2015**, *410*, 63−68.

(6) Makita, Y.; Ikai, O.; Hosokawa, J.; Ooi, K.; Okuyama, S.; Sumida, N. Synthesis of Long Silver Nanowires by Electron Beam Irradiation on Ag-Exchanged Material. *J. Ion Exch.* **2003**, *14*, 409−412.

(7) Edmondson, M. J.; Zhou, W. Z.; Sieber, S. A.; Jones, I. P.; Gameson, I.; Anderson, P. A.; Edwards, P. P. Electron-Beam Induced Growth of Bare Silver Nanowires from Zeolite Crystallites. *Adv. Mater.* **2001**, *13*, 1608−1611.

(8) Pattabi, M.; Pattabi, R. M.; Sanjeev, G. Studies on the Growth and Stability of Silver Nanoparticles Synthesized by Electron Beam Irradiation. *J. Mater. Sci.: Mater. Electron.* **2009**, *20*, 1233−1238.

(9) Roca, R. A.; Lemos, P. S.; Andres, J.; Longo, E. Formation of Ag Nanoparticles on Metastable Beta-Ag2WO4Microcrystals Induced by Electron Irradiation. *Chem. Phys. Lett.* **2016**, *644*, 68−72.

(10) Yuan, Z. Y.; Zhou, W. Z.; Parvulescu, V.; Su, B. L. Electron Beam Irradiation Effect on Nanostructured Molecular Sieve Catalysts. *J. Electron Spectrosc. Relat. Phenom.* **2003**, *129*, 189−194.

(11) Li, K.; Zhang, F. S. A Novel Approach for Preparing Silver Nanoparticles Under Electron Beam Irradiation. *J. Nanopart. Res.* **2010**, *12*, 1423−1428.

(12) Makita, Y.; Ikai, O.; Ookubo, A.; Ooi, K. Preparation of Long Silver Nanowires from Silver Matrix by Electron Beam Irradiation. *Chem. Lett.* **2002**, *31*, 928−929.

(13) Anderson, P. A.; Edmondson, M. J.; Edwards, P. P.; Gameson, I.; Meadows, P. J.; Johnson, S. R.; Zhou, W. Z. Production of Ultrafine Single-Crystal Copper Wires Through Electron Beam Irradiation of Cu-Containing Zeolite X. *Z. Anorg. Allg. Chem.* **2005**, *631*, 443−447.

(14) Hofmeister, H.; Thiel, S.; Dubiel, M.; Schurig, E. Synthesis of Nanosized Silver Particles in Ion-Exchanged Glass by Electron Beam Irradiation. *Appl. Phys. Lett.* **1997**, *70*, 1694−1696.

(15) Belloni, J. Nucleation, Growth and Properties of Nanoclusters Studied by Radiation Chemistry - Application to Catalysis. *Catal. Today* **2006**, *113*, 141−156.

(16) Sutter, E.; Jungjohann, K.; Bliznakov, S.; Courty, A.; Maisonhaute, E.; Tenney, S.; Sutter, P. In Situ Liquid-Cell Electron Microscopy of Silver-Palladium Galvanic Replacement Reactions on Silver Nanoparticles. *Nat. Commun.* **2014**, *5*, 4946.

(17) Donev, E. U.; Schardein, G.; Wright, J. C.; Hastings, J. T. Substrate Effects on the Electron-Beam-Induced Deposition of Platinum from a Liquid Precursor. *Nanoscale* **2011**, *3*, 2709−2717.

(18) Woehl, T. J.; Evans, J. E.; Arslan, L.; Ristenpart, W. D.; Browning, N. D. Direct in Situ Determination of the Mechanisms Controlling Nanoparticle Nucleation and Growth. *ACS Nano* **2012**, *6*, 8599−8610.

(19) Mansourian, A.; Paknejad, S. A.; Wen, Q. N.; Vizcay-Barrena, G.; Fleck, R. A.; Zayats, A. V.; Mannan, S. H. Tunable Ultra-High Aspect Ratio Nanorod Architectures Grown on Porous Substrate via Electromigration. *Sci. Rep.* **2016**, *6*, 22272.

Addendum to Appendix A3

A4   Electromigration Phenomena in Sintered Nanoparticle Ag Systems under High Current Density

Electromigration Phenomena in Sintered Nanoparticle Ag Systems Under High Current Density

Ali Mansourian[1], Seyed Amir Paknejad[1], Qiannan Wen[2], Khalid Khtatba[1], Anatoly Zayats[1], Samjid H. Mannan[1*]

[1]Department of Physics, King's College London, Strand, London WC2R 2LS, U.K
[2]Department of Physics and Materials Science and Centre for Functional Photonics (CFP), City University of Hong Kong, Tat Chee Avenue, Kowloon, Hong Kong

Abstract

Electromigration (EM) refers to the movement of atoms inside a conductor due to momentum exchange with the conduction electrons. In this work the EM effect in samples of porous Ag fabricated from nanoparticles of Ag in a pressure free sintering process is studied. Current densities of $2.5 \times 10^4 - 1.7 \times 10^5$ A/cm^2 were applied to the samples for periods ranging up to 500 h. In a typical EM setup with a non-porous conductor, void formation occurs at the cathode and hillock formation at the anode. In this study, voids were not directly observed, but cracks were formed after prolonged electromigration, presumably as a result of void accumulation and coalescence. When the samples were placed in 150 ℃ ambient no hillocks were observed, but at room temperature nanorods were formed with sizes ranging up to 20 μm in length, typically 25 nm in diameter and with aspect ratios ranging from 20 to 1000. It was found that interrupting and restarting the current resulted in growth of new nanorods rather than growth of existing ones, and that growth was limited by welding of individual nanorods when a critical number density was reached. While similar nanorods have been formed from Ag thin films using thermal stress , the location of nanorods was unusual in that while the number density was highest at the anode, significant numbers also appeared at central and cathode locations. Another unusual feature of the observed EM was that the initial porous structure became refined with coarse pores and grains transforming into a fine grained and fine pored structure with elongated and locally orientated pores and grains. Elemental composition studies provide tentative understanding of the nanorod number density, size distribution and growth mechanism. In the geometry utilized for this study, temperature gradients are known to strongly influence the divergence of the EM induced atomic flux and hence resistivity measurements and COMSOL Finite Element modelling was used to determine the temperature in the sample taking into account joule heating, convection and conduction processes.

Ali Mansourian
Email:ali.mansourian@kcl.ac.uk

HiTEN 2015
Page 1

000059

140

1. Introduction

Electromigration has traditionally been associated with failures in on-chip interconnections in VLSI circuits. With increasing miniaturisation it has also become an issue for solder ball interconnections as decreases in dimensions lead to increased current densities[1]. In this paper we study electromigration in sintered Ag systems where the Ag is used as a die attach or component attach material, replacing traditional materials such as solder[2,3]. The Ag is deposited on the substrate in the form of a paste with high concentration of Ag nanoparticles. After component placement, the assembly is heated to ~300 °C and sintering occurs at temperatures well below the melting point of bulk Ag (961 °C). These systems are of interest because of their potential applications in high temperature environments. One worry for such systems is the potential for silver migration caused by high electric fields, resulting in dendritic growth and short circuits. In the present work the nanorods also have a potential for causing short circuits but these are fabricated by high current densities inside the conductor rather than high electric field strengths between electrodes. The high current densities also cause massive atomic displacement inside the conductor which results in elongation of grains and pores and eventual crack formation in the material [4] Specifically, we find that a period of 500 h with a current density of 2.5×10^4 A/cm^2 leads to nanorods up to 20 microns in length and cracks forming at the cathode side of the conducting strip.

1. Experimental

A nanoparticle paste intended for pressure-less sintering, NanoTach® X from NBE Tech was used for these studies. The paste contained silver nanoparticles with 30 nm diameter and after sintering a porosity of 20-30% was obtained after sintering at 260 ° C for one hour [5]. Figure 1 shows the schematic sample preparation. The silver strip is prepared at the edge of a glass cover slip to facilitate control over the width and thickness. Typically the dimensions of the strip are width 150 μm, thickness 150 μm and length 1 μm. Finally the sintered wire is checked optically for flaws and geometrical uniformity and connected to gold wire at both ends using the 500 mg (+5ms) of the same paste and further sintering process. Figure 1 show the schematic of experimental setup. The resistivity of specimen has been measured using four point probe measurements experiments and the resistivity used to estimate the temperature in the strip due to Joule heating. Subsequently the sample was linked to a voltage generator and electromigration was allowed to occur for the duration of the experiment. After the completion of the electromigration period samples were checked under a Scanning Electron Microscope (SEM) to monitor nanorod growth and cross sectioned to examine internal structural changes.
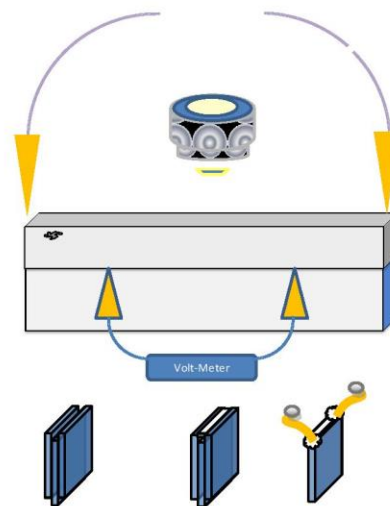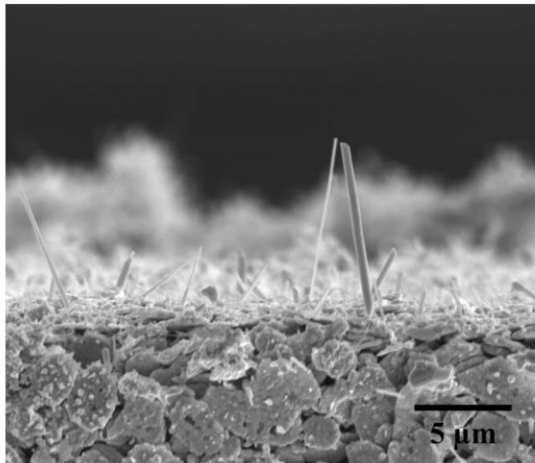

Figure 1: Schematic diagram of experimental setup and the steps used to fabricate sintered silver using three cover slips.

Ali Mansourian
Email:ali.mansourian@kcl.ac.uk

2. Results and discussion

Mass growth of nanorods has been obtained at a current density 2.4×10^8 A/m^2 for 120 hours. Figure 2 shows the formation of nanorods after applying this standard condition.


(a)

Figure 2: Formation of nanorods with diameter between 20 to 100 nm on surface of sintered silver after applying current of 2.4×10^4 A/cm^2 for 5 days.

Figure 3 shows that the nanorods can form in different shapes and lengths. In our standard fabrication condition the side view SEM images at longer period of time ranging between 120 to 480 hours shows that very high aspect ratio nanorods up to 1000 or above reaching the length of 20 μm, and potentially causing short circuits. The Nanorods grow in random directions and typically meet each other after growing between 1 to 4 μm, resulting in welding or

The internal structure cross sections, Fig. 4 a-c) show that the changes in internal structure cannot purely be the results of thermal effects. Fig. 4 a) shows typical internal morphology of the sintered silver strip before any thermal or EM process. Fig. 4b) shows a sample placed at 200 °C for 480 h. Fig. 4c) shows a sample after EM. It should be noted that the structure seen in Fig. 4c was found throughout the stripe at anode, centre and cathode and that the

nanorods [6]. However, performing EM on samples placed on a hotplate with the measured temperature of 200 °C resulted in no nanorods being formed, which strongly suggests that the presence of an oxide layer on the sintered Ag surface which is required to limit surface atomic diffusion and allow stress build-up and formation of the nanorods[7].
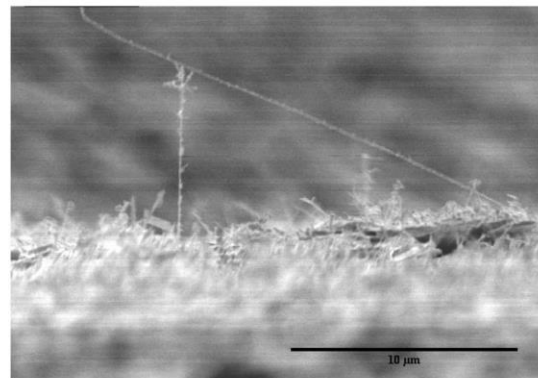
(a)
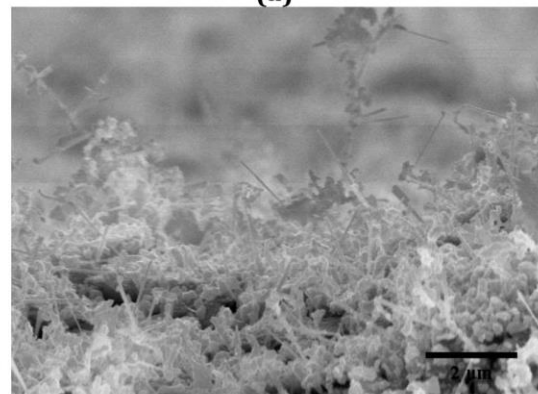
(b)

Figure 3: a) shows merger of high aspect ratio nanorods formed at the anode after 480 hours EM with diameter of 25 nm and length over 20 μm. b) shows nanorods at high density merging together.

orientation of the elliptical grains changes throughout the stripe and does not appear to be simply correlated with the cathode-anode axis (indicated by the arrow in Fig. 4c).

Ali Mansourian
Email:ali.mansourian@kcl.ac.uk

000061

142

Cross section SEM images Without Electromigration or Heat Treatment

Cross section SEM images After Heat Treatment only

Cross section SEM images After Electromigration
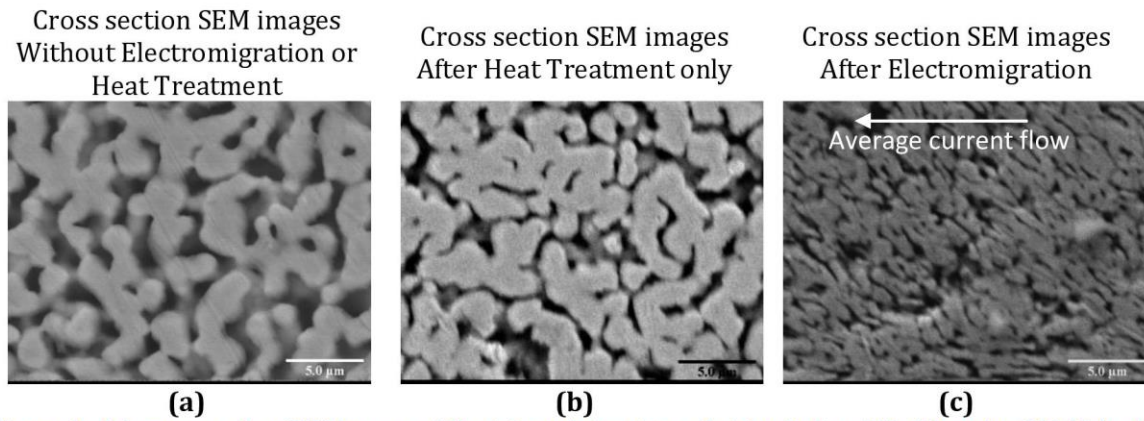

Average current flow

(a) **(b)** **(c)**

Figure 4: (a) cross section SEM images of the internal structure of stripe before EM. (b) under 200 °C heat treatment for 480 h (c) after EM for 480 h at current density of 2.34×10⁴ A/cm².

Similarly, under conditions of higher current density ($1.17×10^5$ A/cm² for 6 hours), we observe partial melting of the silver (Fig.5).

Anode region **Centre of strip** **Cathode region**

SEM reference images before SEM

(a) **(b)** **(c)**

SEM images after EM

(d) **(e)** **(f)**
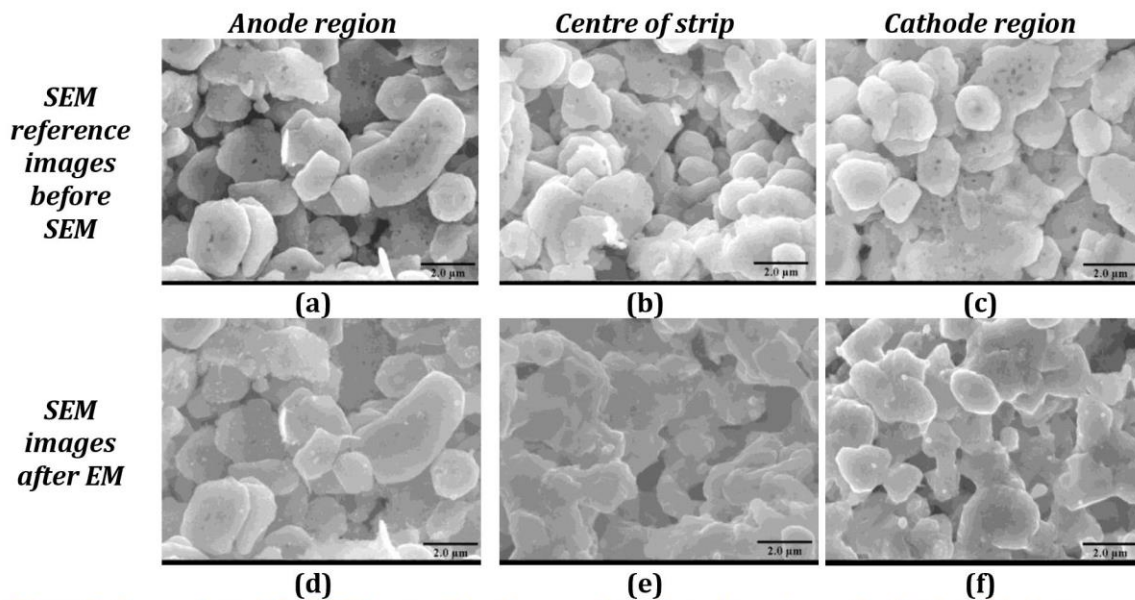
Figure 5: Comparison of the SEM images taken from surface of anode, centre and cathode a-c) before electromigration as a reference images and d-f) after electromigration under the high current density of $1.17×10^5$ A/cm².

Both the resistivity calculations and Finite Element Modelling using COMSOL taking into account convection in air and thermal conduction through glass show temperatures in the strip of around 80 °C under the standard condition(figure 6.a). The melting phenomena at higher current density is expected to be as a result of the internal re-arrangement leading to increased porosity in the cathode and reduction in the number of conduction pathways through the material leading to increasing current confinement to smaller volumes.

Ali Mansourian
Email:ali.mansourian@kcl.ac.uk

(a)

(b)
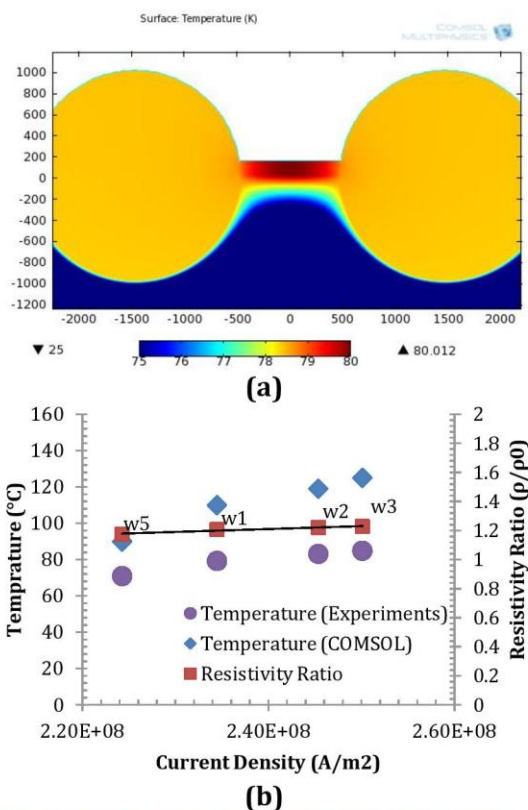
Figure 6: a)Temperature profile within the strip simulated using Finite Element Method (FEM) software COMSOL (Joule heating module), b) the EM operating temperature and resistivity ratio of the 4 different wires in their corresponding current density.

3. Conclusion

In conclusion. we have studied the effect of EM at different current densities on porous sintered silver. Applying a current density of 2.4×10^8 for a time 120 hours results in formation of nanorods with 5 μm length. Extended EM results in a self limiting mechanism for nanorod growth, limiting typical nanorod length to 4 μm though atypical 20 μm rods were also observed. At the same time, surface diffusion along the internal pores result in elongation of the grains and eventual open circuit condition. Growth of the nanorods can be prevented if the external ambient is higher than 200 °C, but the internal rearrangement still occurs.

References

1 Tu, K. N. Recent advances on electromigration in very-large-scale-integration of interconnects. *J Appl Phys* **94**, 5451-5473, doi:Doi 10.1063/1.1611263 (2003).

2 Zhu, X. *et al.* Electromigration in Sn–Ag solder thin films under high current density. *Thin Solid Films* **565**, 193-201, doi:http://dx.doi.org/10.1016/j.tsf.2014.06.030 (2014).

3 Durairaj, R. *et al.* in *Nanotechnology (IEEE-NANO), 2012 12th IEEE Conference on.* 1-4.

4 Calata, J., Lu, G.-Q., Ngo, K. & Nguyen, L. Electromigration in Sintered Nanoscale Silver Films at Elevated Temperature. *J Electron Mater* **43**, 109-116, doi:10.1007/s11664-013-2783-9 (2014).

5 Paknejad, S. A., Dumas, G., West, G., Lewis, G. & Mannan, S. H. Microstructure evolution during 300 °C storage of sintered Ag nanoparticles on Ag and Au substrates. *J Alloy Compd* **617**, 994-1001, doi:http://dx.doi.org/10.1016/j.jallcom.2014.08.062 (2014).

6 Garnett, E. C. *et al.* Self-limited plasmonic welding of silver nanowire junctions. *Nat Mater* **11**, 241-249, doi:http://www.nature.com/nmat/journal/v11/n3/abs/nmat3238.html#supplementary-information (2012).

7 Saka, M. & Sasagawa, K. in *Metallic Micro and Nano Materials Engineering Materials* (ed Masumi Saka) Ch. 3, 53-92 (Springer Berlin Heidelberg, 2011).

Ali Mansourian
Email:ali.mansourian@kcl.ac.uk

A5   Internal Structure Refinement of Porous Sintered Silver via Electromigration

Internal Structure Refinement of Porous Sintered Silver via Electromigration

Ali Mansourian[1*], Seyed Amir Paknejad[1], Qiannan Wen[2], Khalid Khtatba[1], Anatoly V. Zayats[1], Samjid H. Mannan[1]

[1]Department of Physics, King's College London, Strand, London WC2R 2LS, U.K.

[2]Department of Physics and Materials Science, City University of Hong Kong, Tat Chee Avenue, Kowloon, Hong Kong

[*]ali.mansourian@kcl.ac.uk

Atoms can move under high stress conditions such as temperature, mechanical pressure or electric current. Electromigration provides a driving force to move the atoms in metals conducting current usually resulting in the accumulation of atoms and void formation in anode and cathode respectively. The electromigration effect is normally considered a serious problem for electronic circuits but the recent works[1-7] show that it can be used constructively for controlled fabrication of nanostructures[2-4].We demonstrate that electromigration can be utilized to refine the porous structure of a sintered silver stripe leading to transformation of the internal pore and grain structure. The results show that pore shape, size and distribution are significantly changed after electromigration. Similarly, we have used the electromigration effect to mass produce nanorods under current densities of the order of $2.4 \times 10^{+8}$ A/m^2. Nanorods were formed across the whole stripe contrasting with studies on non-porous substrates which show nanorod production at the anode only. The results show the internal pore structure can be transformed and refined by electromigration. The results also suggest that by controlling current densities in a porous substrate, complex patterns of porous structures and high-quality single crystal nanorods can be formed in-situ with significant advantages over competing methods of nanorod formation for sensor applications.

Key words: Electromigration, Internal Structure Refinement, Porous sintered silver, Nanorod.

Introduction

The interaction between nanoscale porosity and electromigration can be used to manipulate surface and internal structure of materials resulting in structure refinement in nanoscale objects. Electromigration continues to be one of the most important reliability issues for nanostructured new devices in microelectronic circuits. Since 1967 most industrial research has been focused on increasing the lifetime under electromigration operating conditions[1,2]. Electromigration occurs at high current density where the atomic flux caused by electron wind force (electromigration) is normally accompanied by a Joule heating effect.

Previous attempts to modify materials via electromigration either resulted in whisker/nanorod growth at the anode only, cracks and disconnection[3,4] or required precise local conditioning of the substrate to change the morphology of substrate[4,5]. The interaction between ions, electrons and atoms results in the movement of grain boundaries (grain growth), recrystallization of grain structure and finally the evolution of the microstructure and chemical compositions[6]. However the microstructure effect on electromigration is found to be a complex function of the porosity, defect, impurity, grain boundaries and grain size distribution, chemical composition, atomic diffusivity and is the origin of non-steady-state mass transport such that the concentration of atoms changes locally[7-11]. In general, electromigration is affected by a large number of parameters such as current density,

temperature, film thickness, grain size and timescale[12-16]. As a result, an uneven material with different grain size morphology can have different responses to atomic diffusion (for example a single crystal, bamboo type crystals or porous structures)[11, 17]. Although many studies have been published on electromigration on bulk materials and thin films, none save Calata[18] have ever experimentally studied the EM effect in porous substrates, and even Calata's study lacked detail, concentrating only on the eventual breakdown of conductance in the material. The electromigration effect of microstructures has been studied in the literature[6-11].

We present the electromigration effect on porous silver stripe, showing phenomena that are not encountered in electromigration studies of solid conductors, such as nanorod formation both at anode and cathode of samples. We demonstrate microstructural changes inside the stripe that have not been observed in non-porous materials. We show the mass growth of nanorods utilizing this effect with very high aspect ratios up to 200 and above. The results show that the internal pore structure can be transformed and refined by electromigration, and that hence electromigration can be used as a non-destructive probe of the surface composition of the pores. These unique observations suggest a method of opening up an interesting research field on an effective method for modifying the internal morphology of conductive porous materials in particular sintered silver which is a promising high temperature electronics joining material.

Experimental details

A nanoparticle paste NanoTach® X from NBE Tech was used for these studies. The paste contained silver nanoparticles with 30 nm diameter and after sintering a porosity of 20-30% was obtained after sintering at 260 °C for one hour[19]. The silver stripe is prepared with typical dimensions of width 150 µm, thickness 150 µm and length 1 µm. The details of experimental procedures are explained in our previous work [19].

Finally, the sintered stripe is checked optically for flaws and geometrical uniformity and connected to gold wire at both ends using 500 mg of the same paste and a further sintering process. The resistivity of the specimen has been measured using four-point probe measurements experiments and the resistivity used to estimate the temperature in the strip due to Joule heating. Subsequently, the sample was linked to a voltage generator and electromigration was allowed to occur for the duration of the experiment. After the completion of the electromigration period samples were checked under a Scanning Electron Microscope (SEM) to monitor nanorod growth and cross-sectioned to examine internal structural changes. Both Matlab and Image J software used for measuring the grains and pore density.

Results

The phenomenon of microstructure refinement after electromigration that occurs in the interior of the porous substrate was investigated in a series of experiments in which samples were cross-sectioned under conditions of varying electromigration duration and current density. Recently we reported the mass fabrication of nanorods using electromigration[19]. In this work the electromigration effects on the internal structure changes are investigated in more detail in the three different regions of anode, centre and cathode. Figure 1d-f demonstrates changes at the surface resulting in formation of nanorods both at the anode and cathode surface while the interior of the substrate Figure 1g-i experiences mass atomic transport and morphology change. The micrograph SEM images of Figure 2a-d shows the cross-sectioned samples. The morphology change after electromigration shows that the interior grains morphology has changed from coarse to fine and also the interpore-spacing between each grain has significantly decreased. The electromigration effect on porous structure refinement is opposite to the thermodynamic grain growth response expected from the sample stored at 200 °C and higher tempratures[20].
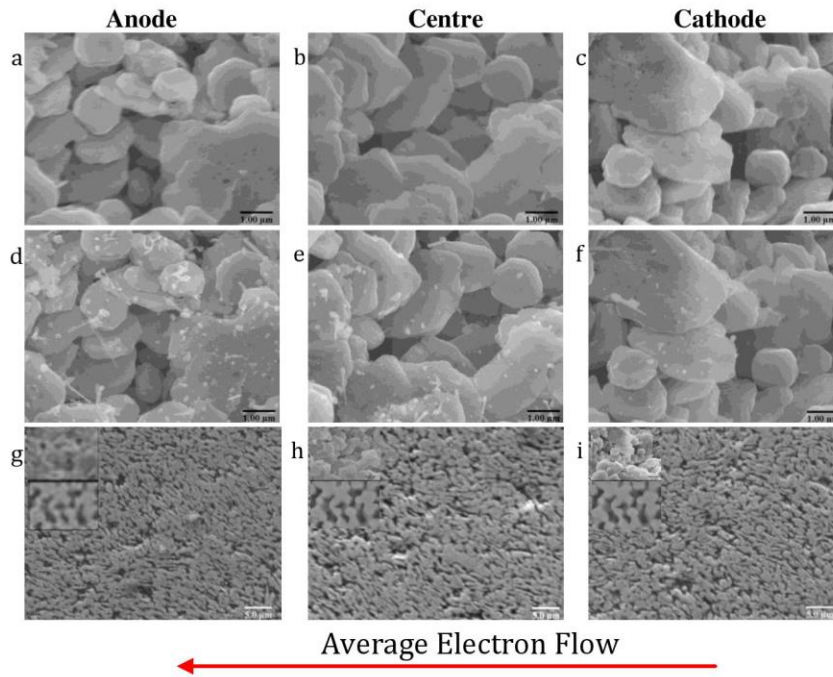
Average Electron Flow

Figure 1 (a-i) Comparison of surface and interior evolution; (a-c) before EM, (d-f) Surface after EM, (g-i) interior after EM with insets showing pre-EM surface and cross sections to the same scale.

Figure 2a-d shows the comparison of measured grain and pore size cross section SEM images of the sintered silver before and after electromigration. The SEM images show that the average grain size of porous sintered silver decreased from 2500 to 800 nm after electromigration. The porosity changes after electromigration are calculated using the Matlab software and image recognition techniques. The results show the similar porosity of 0.29, 0.28, and 0.30 for the regions near the anode, cathode and centre respectively. The pores are stretched out almost in the same direction of the average current flow (Figure 2b, d the elongation direction denoted by white arrows), but that locally there may be significant deviations to the expected current flow due to porosity related effects.
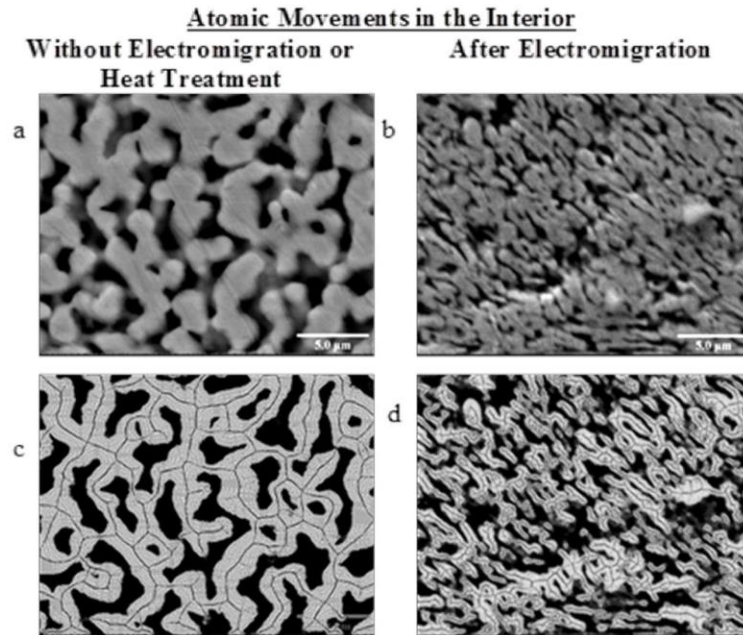
Figure 2 (a) shows the SEM image of cross sectioned Sintered silver wire (b) shows the cross sectioned SEM image of the sintered silver wire after electromigration (c and d) shows the comparison of changes in grain size before and after electromigration for the same SEM images from the sample produced in the same way.

000192

148

Electromigration is not the only method for pore engineering. Recently we proposed a novel method to control the formation of of a pore free structure for sintered silver [20]. We have found by addition of a gold mesh inserted between die and substrate in the presence of silver nanoparticle paste, a continuous interdiffusion layer can be formed that extends from the die to the substrate after sintering. This results in an alternative method of pore engineering wherein the pores coalesce into a single void which is located at the centre of each mesh cell. The samples survive harsh high-temperature treatments up to 600 °C in contrast to samples without the mesh insert, and the continuous interdiffusion layer establishes a connection which can in principle withstand long operating times at high temperatures without degradation of shear strength. Such die attach provides lower initial shear strength (~2MPa) compared to conventional sintered silver die attach (~16 MPa) as the mesh reduces the volume percentage of sintered silver. However, the gradual incorporation of the mesh into the bonding structure leads to retention and enhancement of mechanical performance at high temperatures. In addition, by control of the mesh size and density, mechanical properties may be altered as desired, for example resulting in lower Young's modulus at the edge of the die and higher Young's Modulus in the centre. Electromigration suggest new possibilities of structure refinement with even more flexibility[21].

In contrast to the significant changes of morphology in the interior of the sample, the oxide layer on the surface prevents transformation of grains except for nanorod growth. Upon exposure to atmosphere after sectioning, high temperature storage experiments also show that surface diffusion is strongly suppressed. Nanorods grow through weak points in the surface oxide as seen for example in straight line shaped nanorods of Figure 3a showing formation of both the nanorods and nodules after 240 hour electromigration at a high current density of $2.4 \times 10^{+8}$ A/m^2.
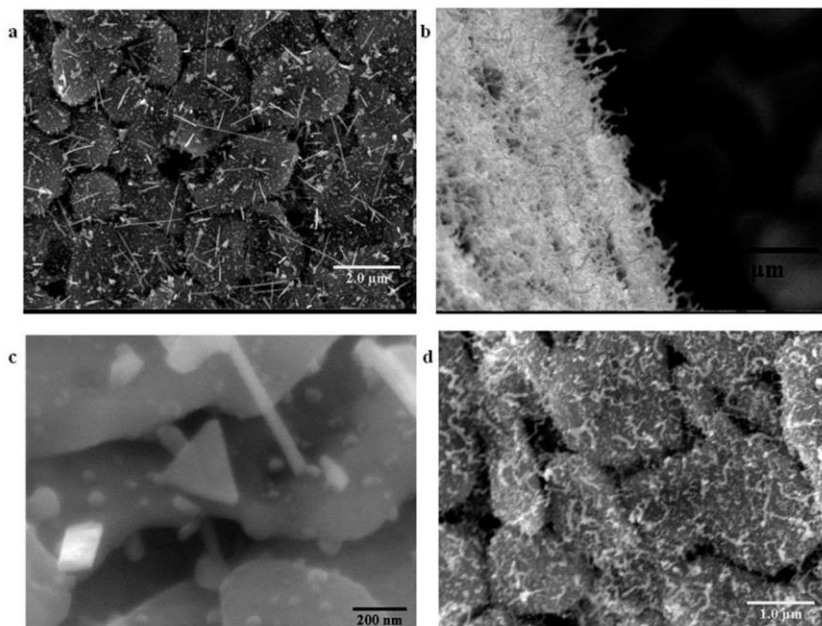
Figure 3. Different shapes of nanorods from straight line to curly shape. (a) The nanorods after 120 hours are (b) long enough to meet each other and (c) they either weld or disconnected in longer period of electromigration time eventually because of high density of nanorods and short cut event their growth above certain length it limited and the shape of nanorods change to curly structure over time. (d) Shows the formation of curly nanorods for uninterrupted electromigration experiment after 480 hours.

The SEM images provided from the samples that experience interruption during the experiment at longer periods above 240 hours, show control of shape and number density and length of nanorods by using interruptions[19]. This eventually leads to a nanorod forest (Figure 3b). Figure 3b shows that the short cut events between generated nanorods could lead to welding or disconnection events. As a result it seems that the growth of the nanorods is limited by the electromigration time of welding and disconnection events at high nanorod density (around 480 hours). The prism and platelet structures were observed for samples experience multiple interruptions (Figure 3c). The curly shape nanorods was produced without any interruption for longer electromigration period of 480 hours (Figure 3d). It should be noted that nanorod growth was completely suppressed when the electromigration took place at elevated temperatures (200 °C).

Potential Applications

The disordered porous silver structure has a potentially wide range of application in electronics, plasmonics, biosensing, energy storage and catalysis. We now outline some of these applications below. Silver has unique optical properties, crystal structure and mechanical properties. Silver is an interesting electrocatalyst owing to its capability of converting carbon dioxide to carbon monoxide selectively at room temperature; however, the traditional polycrystalline silver electrocatalyst requires a large overpotential. A recent report on novel silver catalyst from porous silver suggests it could be used to turn greenhouse gases into useful chemicals[22] with 3,000 times more activity than polycrystalline silver, a catalyst commonly used in converting carbon dioxide to carbon monoxide for green fuel energy. Another potential application makes use of silver's optical properties. Disordered silver nanowire membranes have been used for extraction and surface-enhanced Raman spectroscopy detection[23]. Gold and silver nanowires have also been used for Fluorescence Enhancement [24]. Silver nanorod networks and films are widely used in stretchable transparent electrodes [25] The electromigration synthesis route reported in this chapter widens the range of possible applications. There are numerous advantages that pave the way for electromigration nanorod fabrication to be used industrially. These include simplicity of process and mass production capability of high quality single crystal nanorods with high aspect ratios up to ~200. Control over the shape (straight, curly, etc.) and also control over number density, and the ability to modify these characteristics by control of current density

We have demonstrated that electromigration can be utilized to refine the porous structure of sintered silver leading to transformation of the internal pore and grain structure. The results show that pore shape, size and distribution are significantly changed after electromigration. Similarly, we have used the electromigration effect to mass produce nanorods both at anode and cathode under current densities of the order of $2.4 \times 10^{+8}$ A/m^2. The results from the calculated porosity at anode, centre and cathode show that both grains and pore sizes decreased but the difference in porosity and grain size at the anode, centre and cathode is negligible. The electromigration structure refinement provides

distribution across a surface is unique. Similar to our experimental setup for generating the nanorods, here we suggest a design for nanorods fabrication in an integrated complex pre-pattern structure. A Wheatstone bridge sensing device is a simple illustration of the concept. Figure 4 shows the concept of using electromigration fabricated nanorods in a well known Wheatstone bridge assembly as a sensor device. The advantage of the method is that the nanorods can be grown in situ, simply by passing current through the structure, and the whole sensor miniaturised, limited only by the printing resolution of the nanoparticle paste.
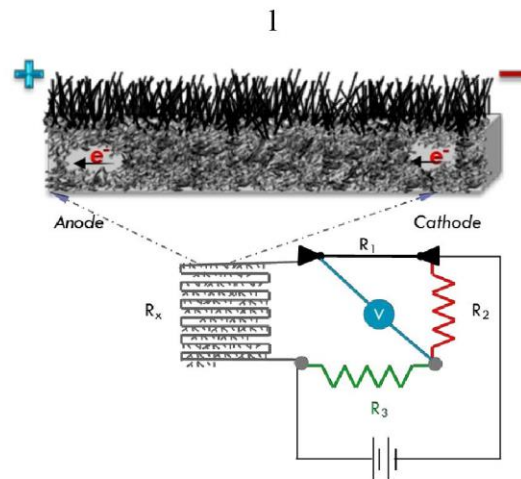

Figure 4. The schematic concept of a printed sensor device based on a Wheatstone bridge circuit with sensing element formed in-situ and miniaturised.

Conclusions

additional flexibility compared to other pore engineering methods. The results show the changes are reproducible, and the internal pore structure can be transformed and refined by electromigration, and that hence electromigration can be used as a probe of the surface composition of the pores. The results suggest that by controlling current densities in a porous substrate, complex patterns of porous structures can be engineered via electromigration effect. Potential applications include Sensors constructed using changes in the resistivity of silver structures which is advantageous for high temperature sensors.

References

[1]   Blech, I. A. & Meieran, E. S. Direct transmission electron microscope observation of electrotransport in aluminum thin films. *Appl Phys Lett* **11**, 263-266, doi:doi:http://dx.doi.org/10.1063/1.1755127 (1967).

[2]   Ho, P. S. & Kwok, T. Electromigration in metals. *Reports on Progress in Physics* **52**, 301 (1989).

[3]   Lu, Y. & Saka, M. Fabrication of Al micro-belts by utilizing electromigration. *Mater Lett* **63**, 2227-2229, doi:http://dx.doi.org/10.1016/j.matlet.2009.07.031 (2009).

[4]   Lu, Y. & Saka, M. Effect of purity on the fabrication of Al micro/thin-materials by utilizing electromigration. *Mater Lett* **63**, 2294-2296, doi:http://dx.doi.org/10.1016/j.matlet.2009.07.055 (2009).

[5]   Saka, M., Kato, K., Tohmyoh, H. & Sun, Y. Controlling electromigration to selectively form thin metal wires and metal microspheres. *J Mater Res* **23**, 3122-3128, doi:doi:10.1557/JMR.2008.0374 (2008).

[6]   Choi, Z. S., Monig, R. & Thompson, C. V. Effects of microstructure on the formation, shape, and motion of voids during electromigration in passivated copper interconnects. *J Mater Res* **23**, 383-391, doi:10.1557/Jmr.2008.0054 (2008).

[7]   Hu, C. K. *et al.* Microstructure, impurity and metal cap effects on Cu electromigration. *Stress Induced Phenomena and Reliability in 3d Microelectronics* **1601**, 67-78, doi:10.1063/1.4881341 (2014).

[8]   Tu, K. Recent advances on electromigration in very-large-scale-integration of interconnects. *J Appl Phys* **94**, 5451-5473 (2003).

[9]   Agarwala, B. N., Schnitze.R & Patnaik, B. Effect of Microstructure on Electromigration Life of Thin-Film Al-Cu Conductors. *J Vac Sci Technol* **9**, 283-&, doi:Doi 10.1116/1.1316581 (1972).

[10]   Patrinos, A. J. & Schwarz, J. A. The Effect of Microstructure on the Resistance to Electromigration of Al-Cu Thin-Film Conductors. *Thin Solid Films* **196**, 47-63, doi:Doi 10.1016/0040-6090(91)90173-U (1991).

[11]   Knorr, D. B. & Rodbell, K. P. Effects of Texture, Microstructure, and Alloy Content on Electromigration of Aluminum-Based Metallization. *Submicrometer Metallization : The Challenges, Opportunities, and Limitations* **1805**, 210-221, doi:Doi 10.1117/12.145483 (1993).

[12]   Tan, C. M. & Roy, A. Electromigration in ULSI interconnects. *Materials Science and Engineering: R: Reports* **58**, 1-75, doi:http://dx.doi.org/10.1016/j.mser.2007.04.002 (2007).

[13]   Tu, K.-N. in *Solder Joint Technology* Vol. 117 *Springer Series in Materials Science* Ch. 8, 211-243 (Springer New York, 2007).

[14]   Saka, M. & Sasagawa, K. in *Metallic Micro and Nano Materials Engineering Materials* (ed Masumi Saka) Ch. 3, 53-92 (Springer Berlin Heidelberg, 2011).

[15]   Tu, K. N. Recent advances on electromigration in very-large-scale-integration of interconnects. *J Appl Phys* **94**, 5451-5473, doi:doi:http://dx.doi.org/10.1063/1.1611263 (2003).

[16]   Sasagawa, K., Hasegawa, M., Saka, M. & Abé, H. Governing parameter for electromigration damage in the polycrystalline line covered with a passivation layer. *J Appl Phys* **91**, 1882-1890, doi:doi:http://dx.doi.org/10.1063/1.1432120 (2002).

[17]   Bauguess, S. *et al.* The effects of test condition, microstructure and linewidth on electromigration void morphology. *Materials Reliability in Microelectronics V* **391**, 379-384 (1995).

[18]   Calata, J., Lu, G.-Q., Ngo, K. & Nguyen, L. Electromigration in Sintered Nanoscale Silver Films at Elevated Temperature. *J Electron Mater* **43**, 109-116, doi:10.1007/s11664-013-2783-9 (2014).

[19]   Mansourian, A. *et al.* Tunable Ultra-high Aspect Ratio Nanorod Architectures grown on Porous Substrate via Electromigration. *Sci Rep-Uk* **6**, doi:10.1038/Srep22272 (2016).

[20]   Paknejad, S. A., Mansourian, A., Noh, Y., Khtatba, K. & Mannan, S. H. Thermally stable high temperature die attach solution. *Mater Design* **89**, 1310-1314, doi:10.1016/j.matdes.2015.10.074 (2016).

[21]   Siow, K. S. Are Sintered Silver Joints Ready for Use as Interconnect Material in Microelectronic Packaging? *J Electron Mater* **43**, 947-961, doi:10.1007/s11664-013-2967-3 (2014).

[22]   Lu, Q. *et al.* A selective and efficient electrocatalyst for carbon dioxide reduction. *Nat Commun* **5**, doi:10.1038/ncomms4242 (2014).

[23]   Shi, Y.-e. *et al.* A disordered silver nanowires membrane for extraction and surface-enhanced Raman spectroscopy detection. *Analyst* **139**, 2525-2530, doi:10.1039/c4an00163j (2014).

[24]   Goldys & Drozdowicz-Tomsi, K. Gold and Silver Nanowires for Fluorescence Enhancement. doi:10.5772/16330 (2011).

[25]   Liang, J. *et al.* Intrinsically stretchable and transparent thin-film transistors based on printable silver nanowires, carbon nanotubes and an elastomeric dielectric. *Nat Commun* **6**, doi:10.1038/ncomms8647 (2015).

A6   Summary of the Project in a Confined Format

Microstructural Evolution and Arrest in a Silver Nanoparticle Based Die Attach Material for Extreme Environments

Outline of the Summary

- Introduction

- Author's Contributions

- Conclusions and Future Work

Introduction

The need for a suitable die attach is on the rise for harsh environments above 300 °C, applications:

Jet Engines

Typical Electronics Location
Intended High Temp Electronics Area

*Steve Riches, HiTEN 2015 Cambridge

Space Exploration

*http://www.wallcoo.com/cartoon/space_image_space_and_satellite_02_widescreen/images/Space%20Satellite%20CG%20art%20images%20EF08_SI030 0.jpg

WBG Semiconductors

*http://www.siliconsemiconductor.net/article/80143-GlobalFoundries-develops-55nm-advanced-automotive-platform.php

Current Materials:
- High Melting Point Solders
  - Residual stress

- Solid Liquid Inter-Diffusion Bonding (SLID)
  - Kirkendall voiding
  - Brittle intermetallic layer

Alternative Solution:
- **Silver Nanoparticles**

- ✓ Excellent Properties
- ✓ Relatively Low Cost

Organic Ligands

Metallic Core
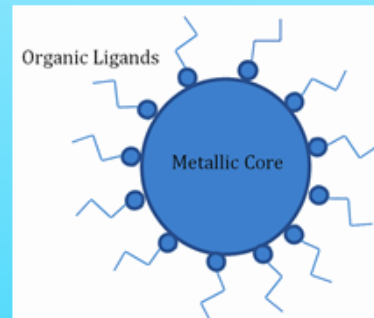
- ✓ Lower Processing Temperature
- ✓ Melting point of 2.4 nm 350°C
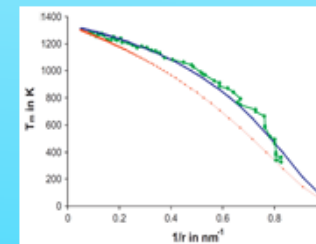
* Omar, M. S. (2012). Models for mean bonding length, melting point and lattice thermal expansion of nanoparticle materials. Materials Research Bulletin,47(11), 3518-3522.

155

Introduction

Background:

• Our review, which included data from 60 + papers on silver nanoparticle based high temperature die attach, concluded that:

> ➢ Increased initial shear strength as a result of processing pressure reduces thermal cycling lifetime

> ➢ Average shear strength has not significantly increased over the past decade

> ➢ The intrinsic limits of shear strength for pure nanosilver appear to have been reached

> ➢ Addition of interposers or nanowires can overcome pure nanosilver intrinsic limits.

Outline of Author's Contributions

Outline of Author's Contributions

Microstructural Evolution of Sintered Silver

In brief:

- High temperature behaviour of sintered silver under a cover-slip, acting as a die, has been examined from 200 to 400 °C
- It has also been noted that exposure to atmosphere of sintered silver stabilises the microstructure of the surface up to 400 °C.

Microstructural Evolution of Sintered Silver

• High temperature behaviour of sintered silver nanoparticles has been observed.
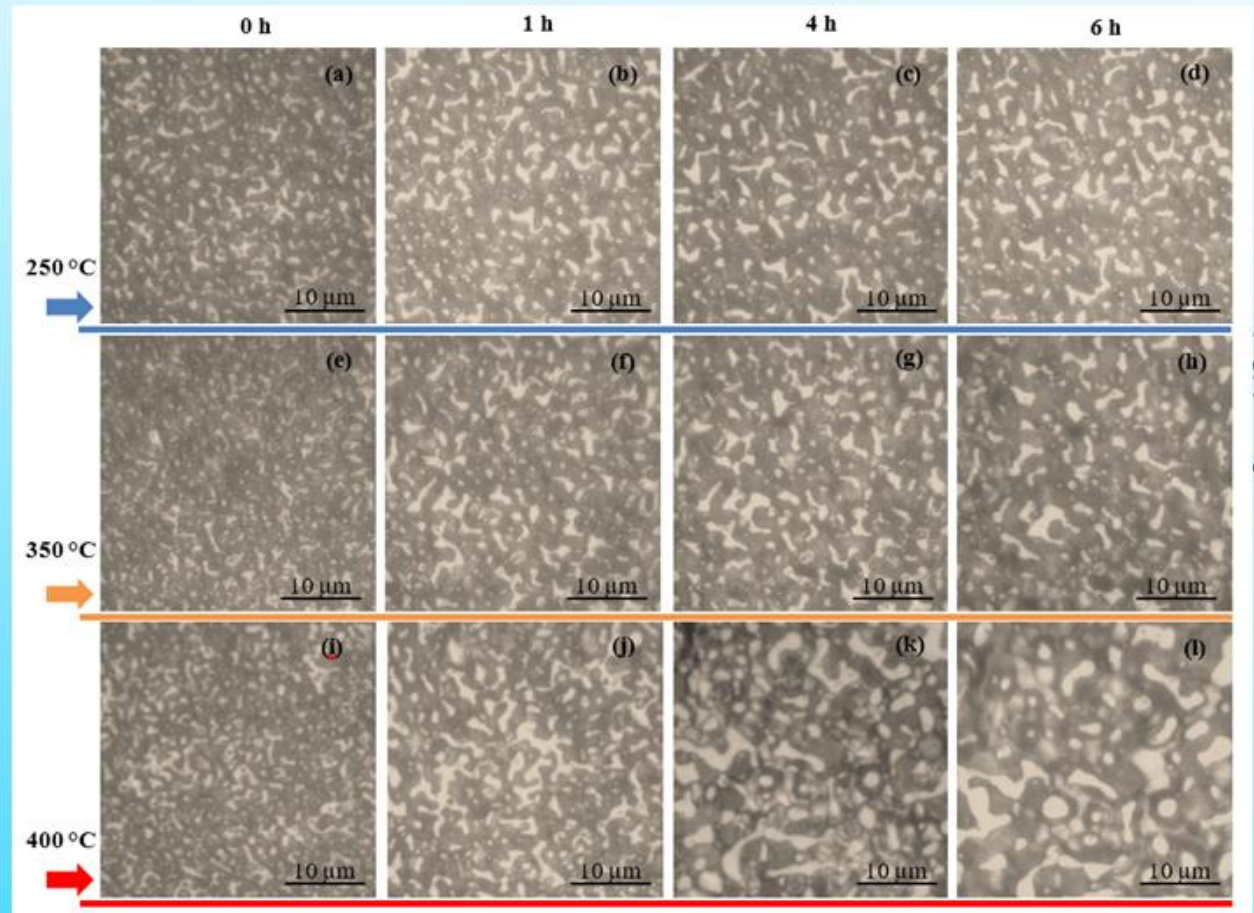
Microstructural Evolution of Sintered Silver

- This leads to unpredictability of long term reliability.
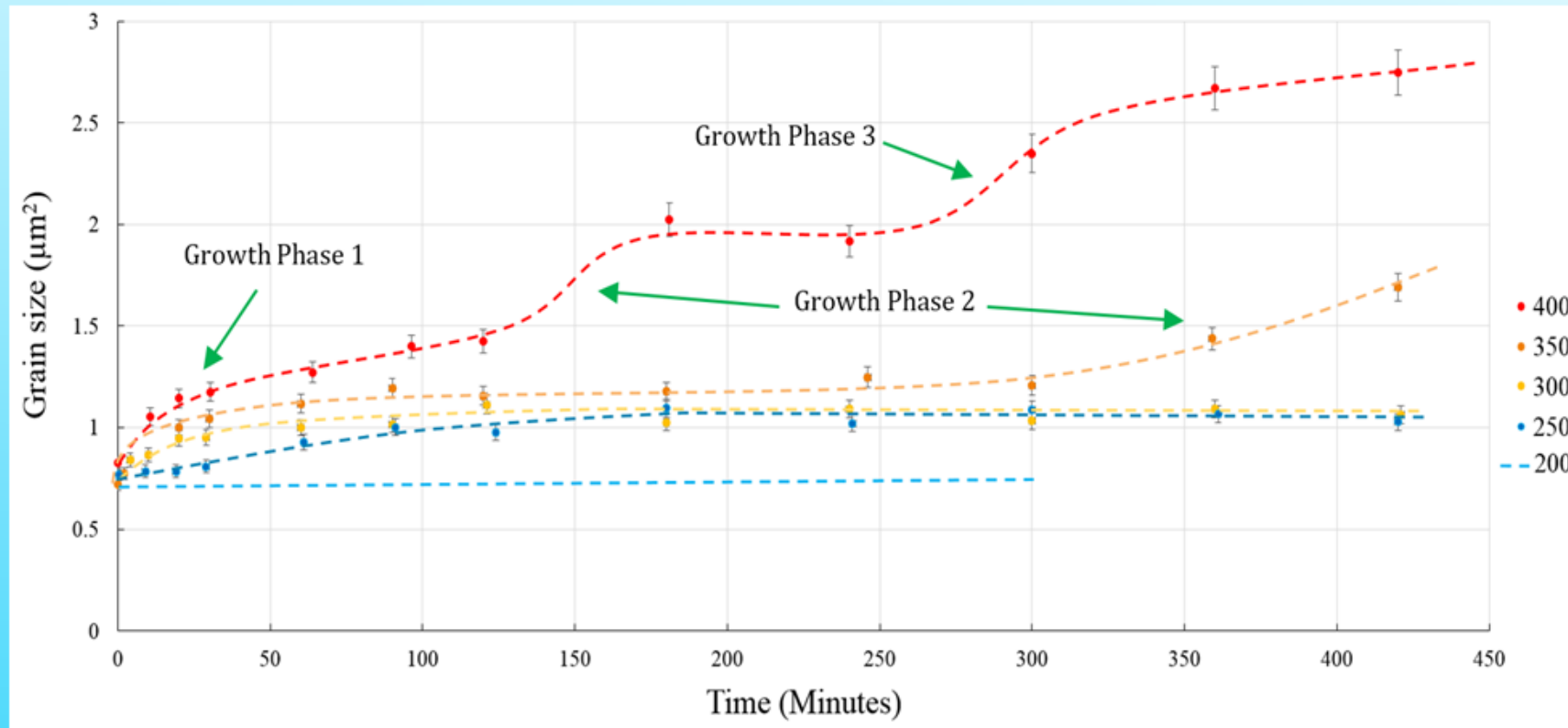
Microstructural Evolution of Sintered Silver

- Exposure to atmosphere blocks surface diffusion up to temperatures of 400 °C.

1. Control
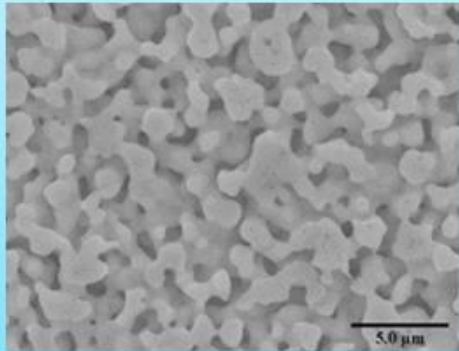
2. After storage for 24 h at 300 °C
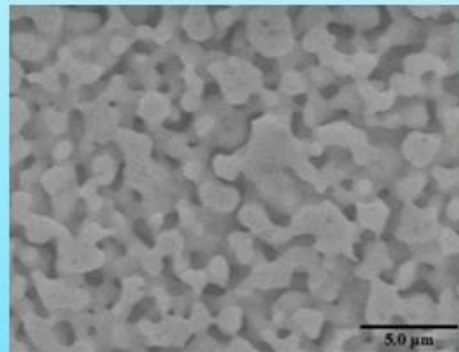
3. Additional 16 h at 300 °C and 66 h at 400 °C in vacuum
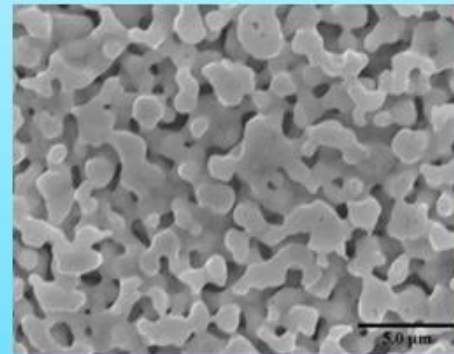
4. Additional 24 h at 500 °C

162
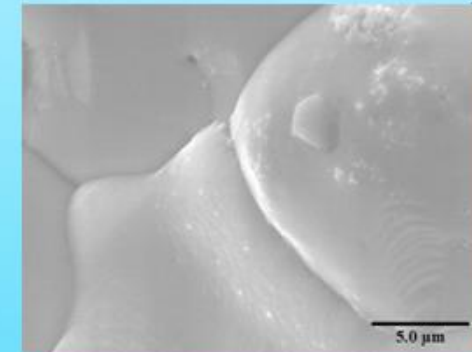
Outline of Author's Contributions

Solution for Evolution: Oxidation Treatment

In brief:
- Addition of a processing step has been tested and proven to stabilise the internal microstructure of sintered silver to 400 °C

Solution for Evolution: Oxidation Treatment

- Simple processing step to increase thermal stability of sintered silver die attach

Processing Steps
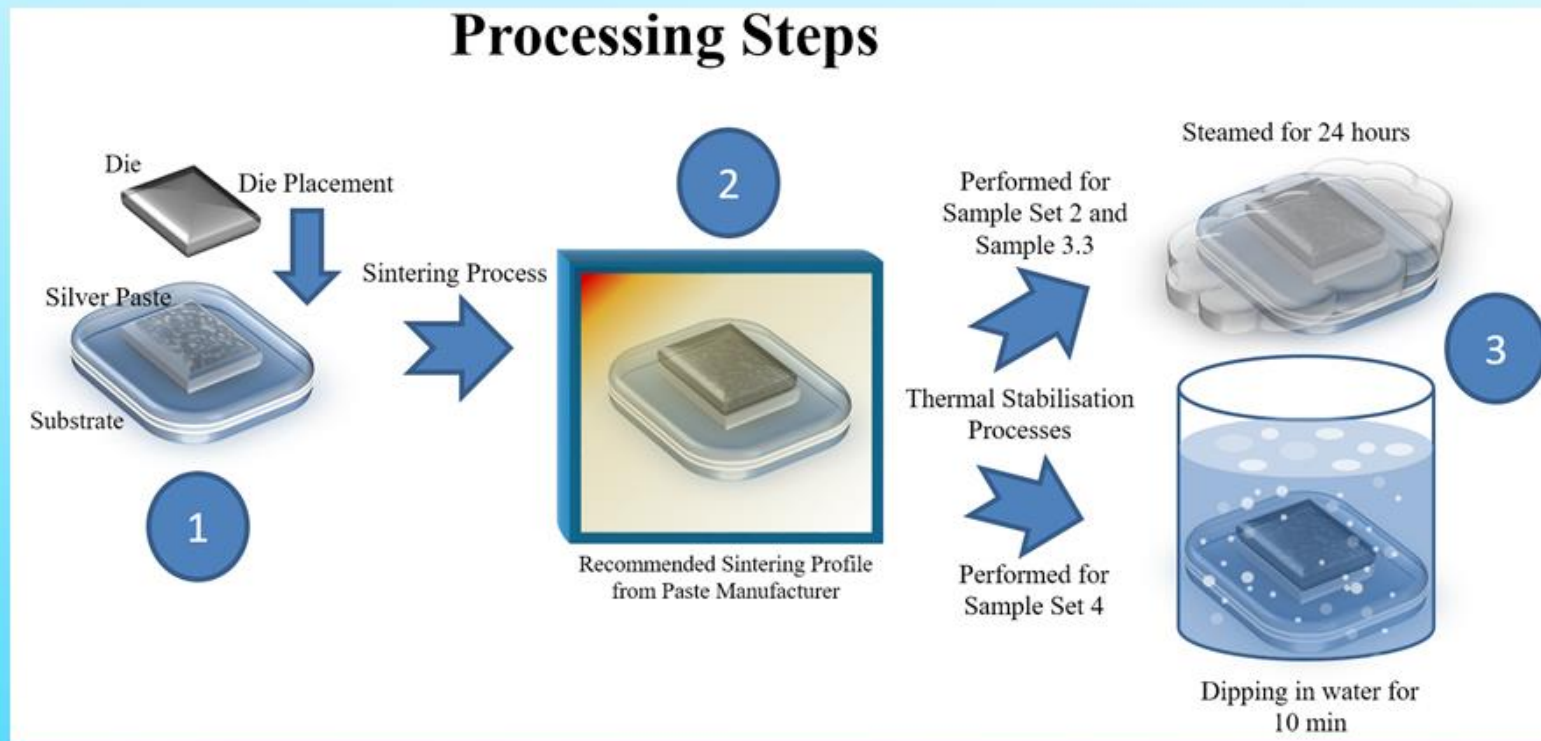
Solution for Evolution: Oxidation Treatment

- The thermal stability increased from 200 °C of conventional sintered silver to 400 °C
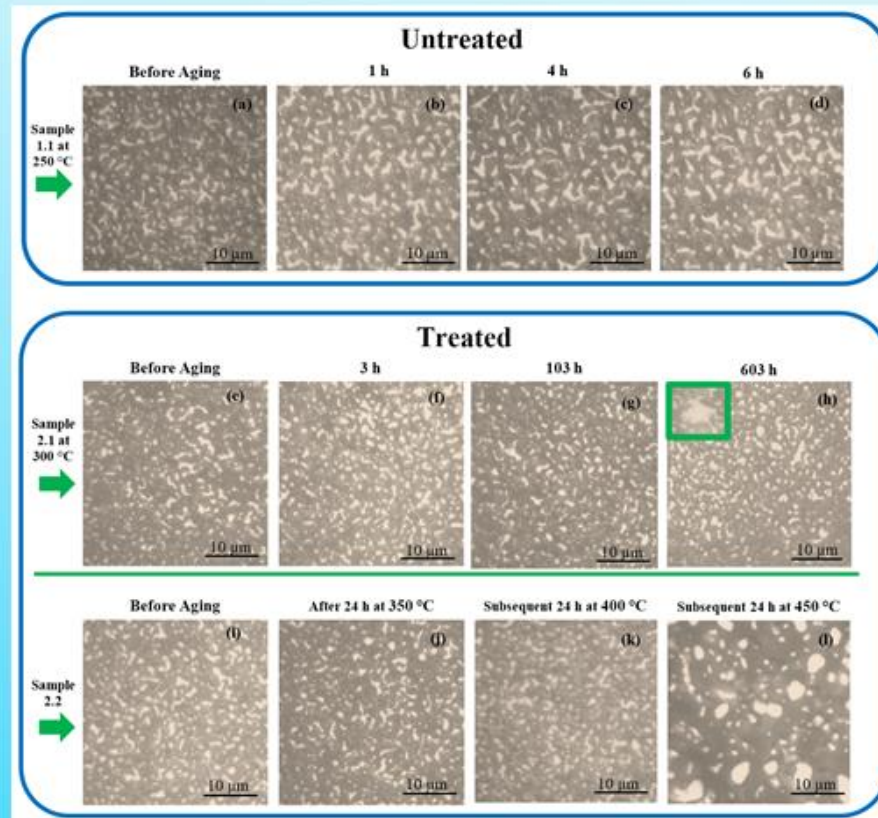
The experimental data of the treated sintered silver was generated by Mr Khalid Khtatba

166

Solution for Evolution: Oxidation Treatment

- Oxidation of silver surfaces is known as the main cause of this stabilisation
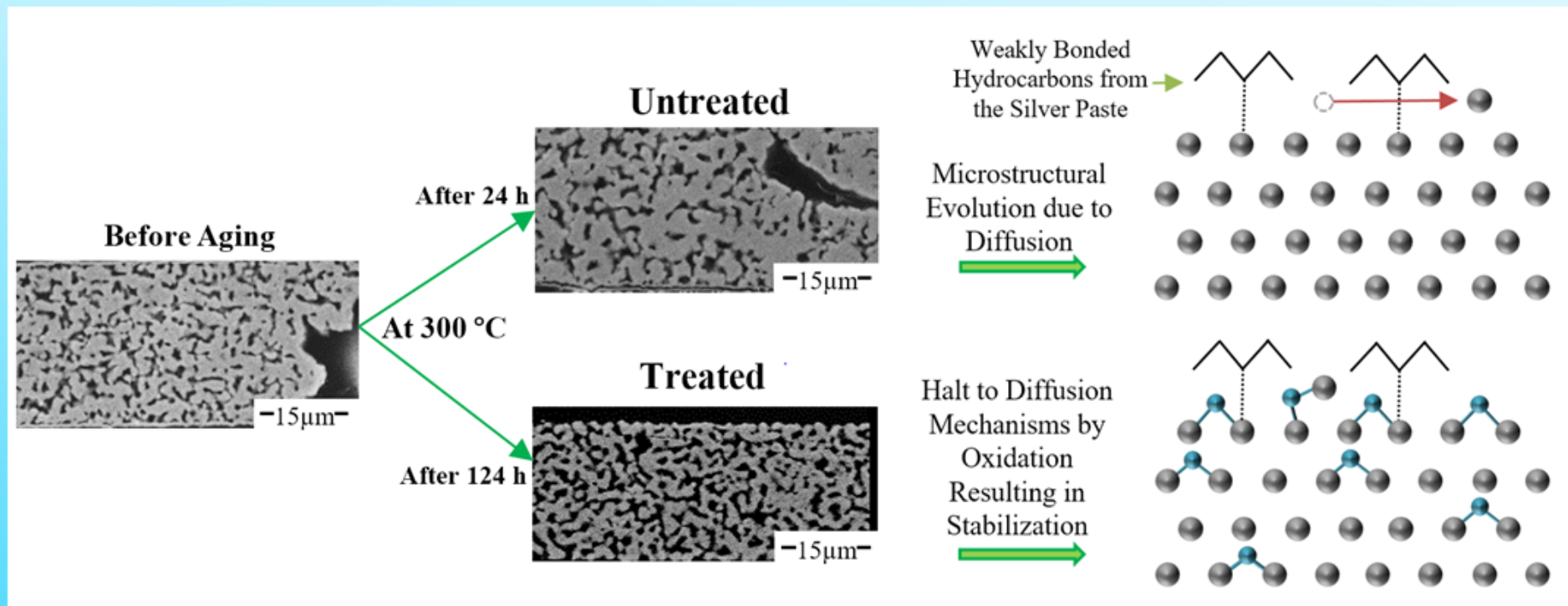
The untreated sintered silver samples and their SEM images were produced by Prof. Samjid Mannan, and the treated sintered silver by Mr Khalid Khtatba

Outline of Author's Contributions

Interactions with Two Common Metallisations

In brief:
- Interactions and shear strength of sintered silver over two substrate metallisations, silver and gold, have been observed
- Detailed investigations of interactions amongst sintered silver and gold substrate indicated fast migration of gold atoms inside the die attach and vice versa.

Interactions with Two Common Metallisations

- Rapid collapse of void number density after 24 h ageing in the sintered Ag layer on **Au substrate**.
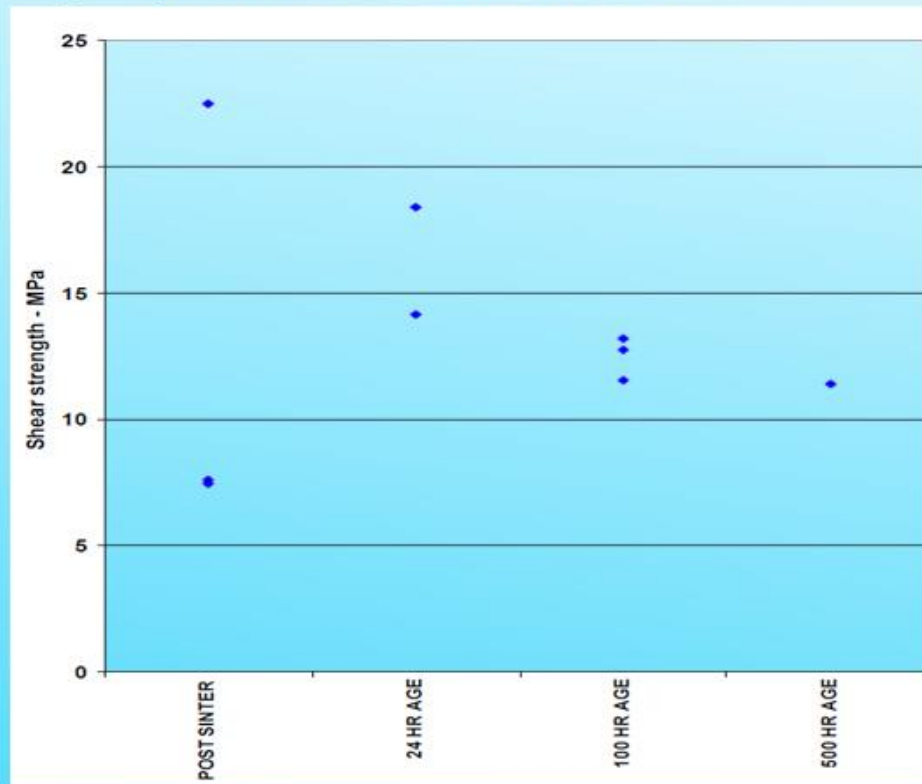
The samples and their associated shear strength data were generated by Eltek Semiconductors

Interactions with Two Common Metallisations

- Shear strength of pressure-free sintered Ag decreases during ageing at 300 °C due to high porosity layer growth
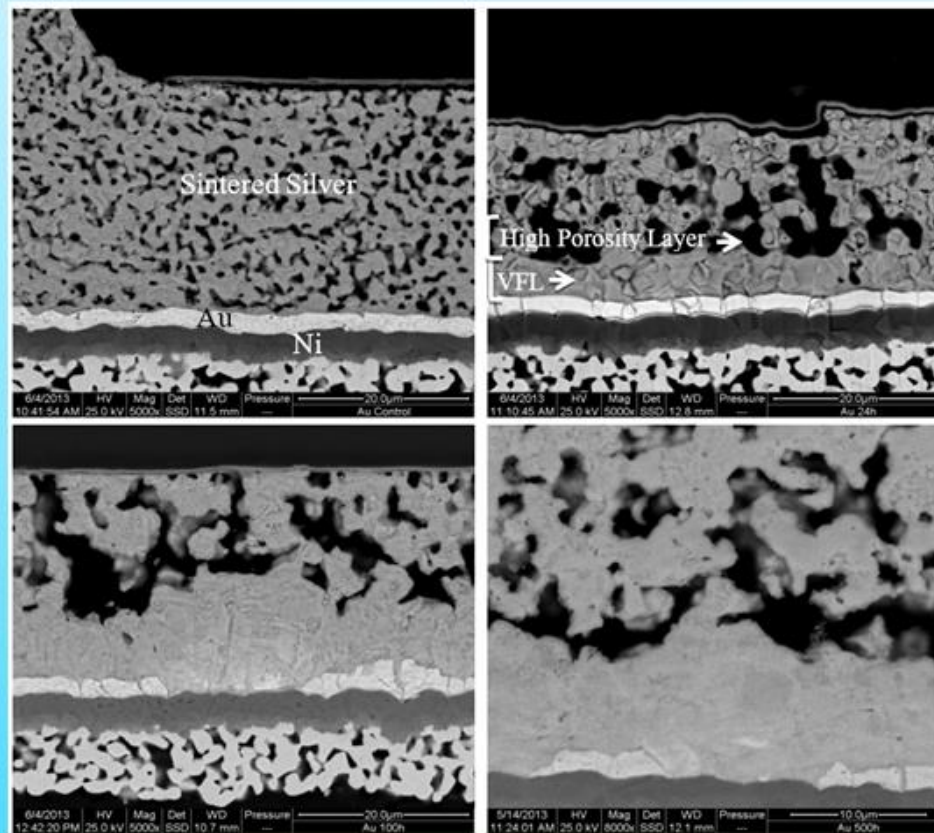
Control — Sintered Silver, High Porosity Layer, VFL, Au, Ni
After 24 h at 300 °C
After 100 h at 300 °C
After 500 h at 300 °C

Interactions with Two Common Metallisations

- Void free layer and high porosity layer growth explained in terms of atomic diffusion and grain boundary migration.
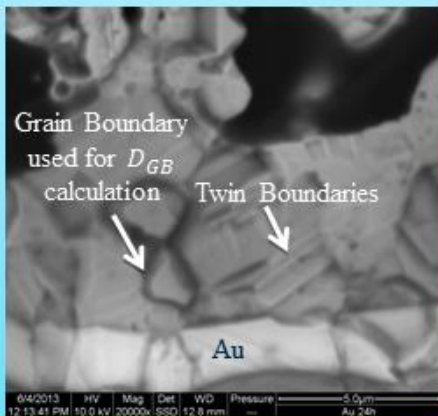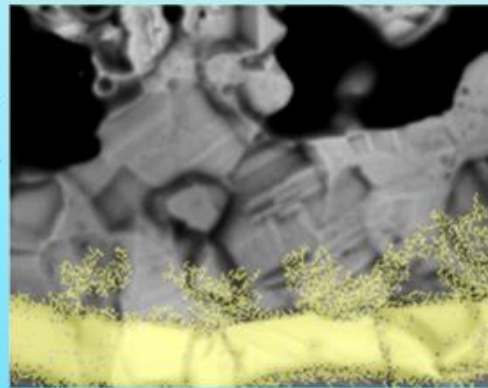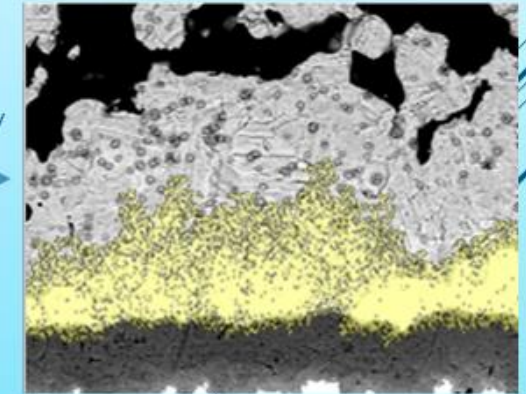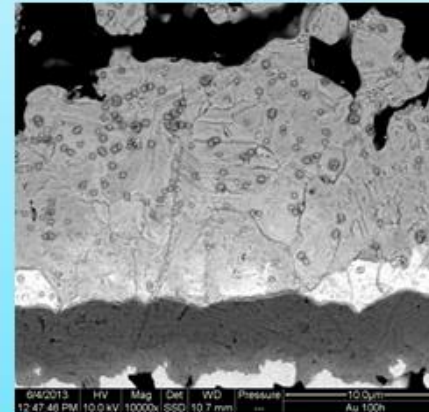
After 24 h at 300 °C

After 100 h at 300 °C

Outline of Author's Contributions

Solution for Interactions: Mesh Placement

In brief:
- Interactions between sintered silver and gold metallisation has been used to produce a thermally stable die attach by placing a mesh interposer between two gold metallisations on die and substrate and filling mesh gaps with silver nanoparticle paste.
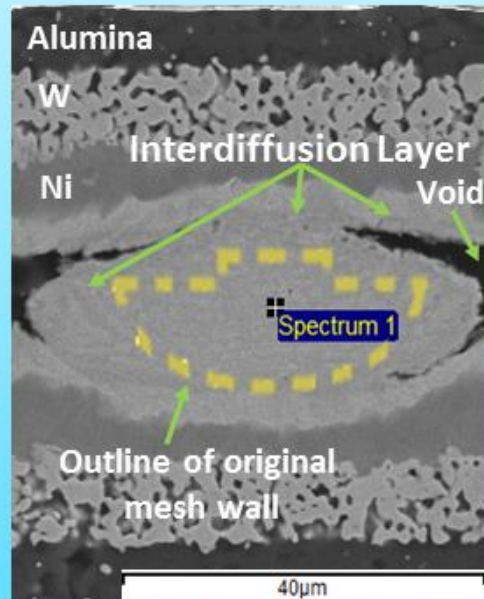
Solution for Interactions: Mesh Placement

• Material interdiffusion previously identified as a problem is utilized positively.
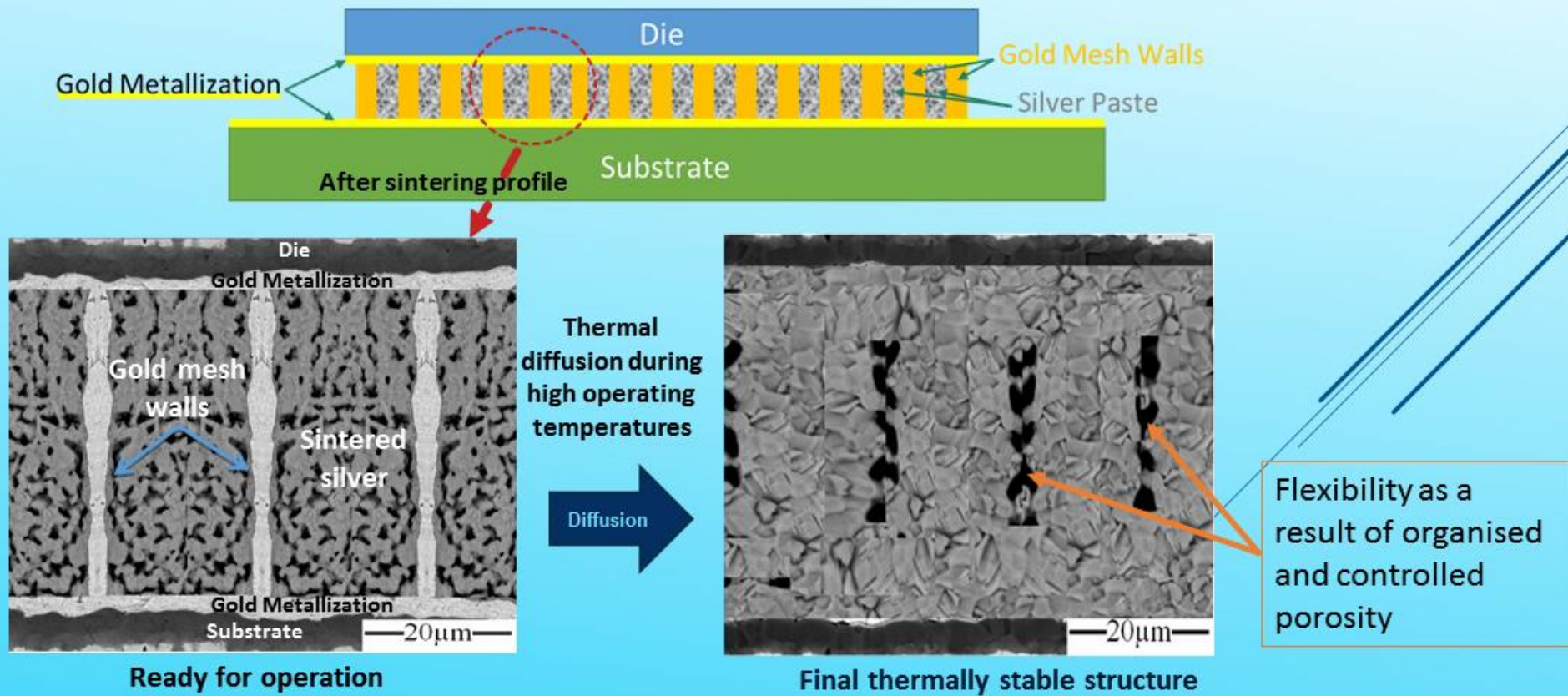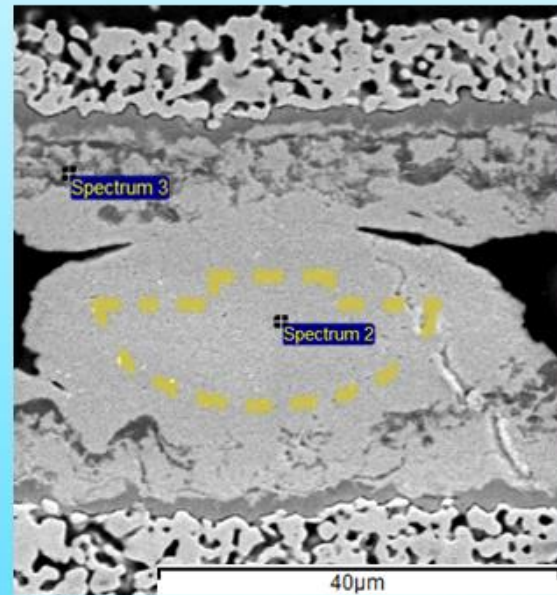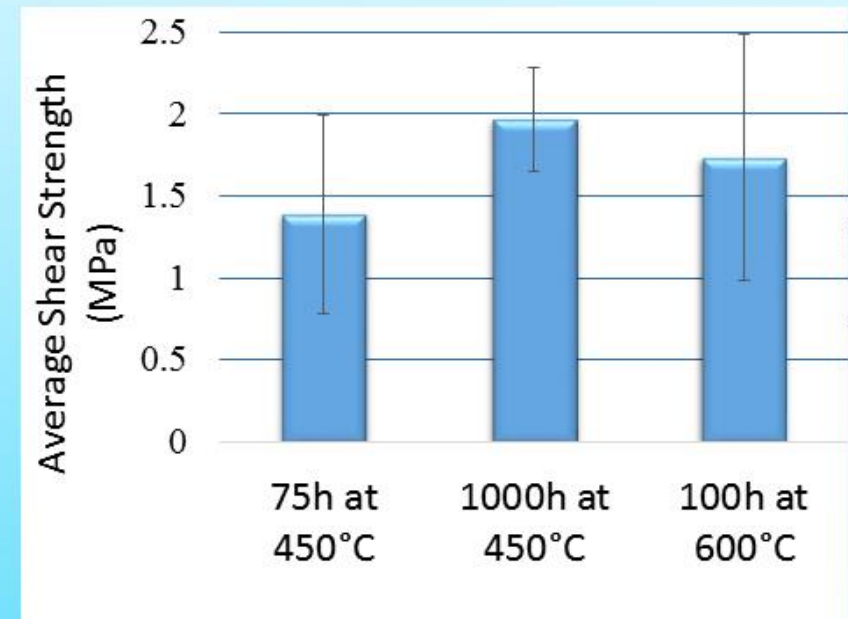
Solution for Interactions: Mesh Placement

• Retention of mechanical strength at high temperatures and microstructural stability.
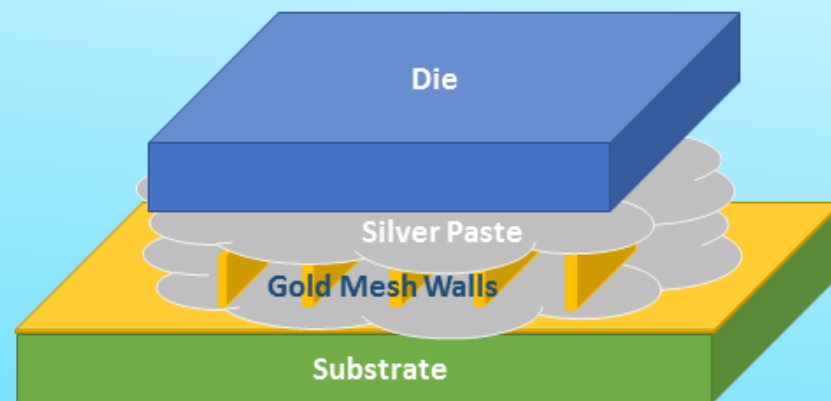

Stored for 24 h at 450 °C

Stored for 1000 h at 450 °C

The shear strength data was produced by Dr Yohan Noh

Solution for Interactions: Mesh Placement

- Processing is easy and requires no expensive new tooling or processing pressure.

Conclusions and Recommendations on Future Work

- Sintered silver microstructural changes significant above 250 °C

- Surface oxidation stops microstructural changes up to 400 °C

- Engineering the oxidation effect to stabilise internal structure
  - Mechanical tests after aging of oxidisation treated sample

- Gold and silver interdiffusion significant at the interface

- This interaction was used to establish a novel die attach
  - Mechanical tests on this die attach using improved mesh designs

Reference List and Publications

Journal Publications:

- Paknejad, S.A., Mansourian, A., Noh, Y., Khtatba, K. and Mannan, S.H., 2016. Thermally stable high temperature die attach solution. *Materials & Design, 89*, pp.1310-1314.

- Paknejad, S.A., Dumas, G., West, G., Lewis, G. and Mannan, S.H., 2014. Microstructure evolution during 300° C storage of sintered Ag nanoparticles on Ag and Au substrates. *Journal of Alloys and Compounds, 617*, pp.994-1001.

- Paknejad, S.A., Mansourian, A., Greenberg, J., Khtatba, K., Van Parijs, L. and Mannan, S.H., 2016. Microstructural evolution of sintered silver at elevated temperatures. *Microelectronics Reliability, 63*, pp.125-133.

- Paknejad, S.A. and Mannan, S.H., 2017. Review of silver nanoparticle based die attach materials for high power/temperature applications. *Microelectronics Reliability*.

Further Publication and Patents

Conference Publication:

- Paknejad, S.A., Mansourian, A., Noh, Y., Khtatba, K., Van Parijs, L. and Mannan, S.H., 2015. Factors influencing microstructural evolution in nanoparticle sintered Ag die attach. Additional Papers and Presentations, 2015(HiTEN), pp.50-58.

Patents:

- Method and apparatus for creating a bond between objects based on formation of inter-diffusion layers, patent pending: 15/176,567
- Increasing stability of porous silver to at least 400 °c, Patent Pending: 62/448,240